UNIVERSITY OF CALIFORNIA
RIVERSIDE

Explorations in Heterocyclic Chemistry: Applications in Hydrogen Storage and in Small Drug Molecules

A Dissertation submitted in partial satisfaction
of the requirements for the degree of

Doctor of Philosophy

in

Chemistry

by

Jay-Ar Bendo

June 2016

Dissertation Committee:
Dr. Thomas H. Morton, Chairperson
Dr. Michael Pirrung
Dr. Christopher Switzer

The Dissertation of Jay-Ar Bendo is approved:

Committee Chairperson

University of California, Riverside

Acknowledgement

It has been six years since I started my graduate school journey and I have met some of the most fascinating and intelligent people I would come across to at University of California, Riverside. One of those people is Dr. Thomas Hellman Morton. Don't let the middle name fool you, he is one of the most approachable and caring professors at UCR. I don't think I would be the person or chemist I am today without his guidance. I want to thank him for all the time, patience, and knowledge that he was willing to spare, not just to me, but to all the former and current graduate students, along with the undergraduate students, in his lab. I have learned so much from him, not just academically but also lessons about life, such as: if you want to get out of jury duty, wear a bow tie; that way, they will dismiss you, since they would think you are an odd individual….or a chemist.

I would also want to thank the staff and faculty of UCR such as Dr. Dan Borchardt who is always willing to help me with either NMR or Raman; Dr. Kondrat for teaching me mass spectrometry; Dr. Jos Oomens, Dr. Giel Berden and the staff and students formally at FOM Institute for Plasma Physics at The Netherlands for IR multiple photon dissociation experiments; and Dr. Luke Daeman for all his help with Inelastic Neutron Scattering experiments. The trip to Netherlands was quite an experience.

I would like to thank the graduate students who have come and left and are still currently at UCR (mostly 4th floor Chemical Sciences). We all have

experienced the failures and disappointments of how research is, and that is why we are able to bear it since we all can relate to each other and support each other. I want to thank Dr. Aaron Moehlig and Dr. Michael (Miguel) Young for the help and guidance they gave us as we were still first year students. I want to thank my lab mates, who without, my six years of graduate school would have been dull, boring, and unbearable. You guys made everyday fun, Dr. Hou Ung, Dr. Yoojin Ghang, Dr. Omar Hamdy, Erik Romero, Mark Hilado, Eric Commendatore, Taylor Le, Carroll Hy, Katie Houston, the rest of undergrads, the Hooley group, and the Larsen group.

Finally, I would like to thank my family. I am so glad I chose to stay around in Southern California, since I can be around my family more. Even though we may have drifted away a bit as we started got older and got busy with our own lives, the short times we spend together during get-togethers are moments I enjoy and value.

Finally, I want to give my ate Mira a big thank you. Ever since my nanay passed away, she has been my guardian and my second mom. I know she had her own family to take care of, but she still made sure that there is a roof over my head and that I always have something to eat, especially when I get home after a long day at work. I would also like to mention my kuya Toto, as we siblings have supported each other during the sad times in our lives.

I would like to dedicate all these hard work to my nanay. As a single mother, she made a darn good job raising the three of us by herself. She always

made sure that we never left home hungry and that we would always step outside looking our best in our iron-pressed elementary school uniforms. By the time I realized it, I was pursuing a higher education while attending undergraduate college. That is when I also realized that she was my inspiration for all my hard work and that I wanted her to see me walk up that stage as I graduate from college. Once she passed away, I thought I lost that reason and inspiration, but instead she was replaced by my nieces and nephew. I know it might seem like it's impossible, but I want to set an example for you guys so that you can try to, not just follow, but do better than me, Jaymie, Zyra, Jayden, and Zayn. If your uncle Jay can do it, I believe you guys can also. And I guess that also applies to my future kids.

Lastly, I would like to thank my beautiful better half, Kanica. You have been very patient and have waited all these years for me. You have experienced my frustration, depression, and stress from research and school first hand, yet you are still around. You were always there to cheer me up and tell me to man up when I needed some scolding. There has been no one else that has done so much for me as you have. And I plan to do the same thing for you, as I look forward to spending the rest of my life with you.

ABSTRACT OF THE DISSERTATION

Explorations in Heterocyclic Chemistry:
Applications in Hydrogen Storage and in Small Drug Molecules

by

Jay-Ar Bendo

Doctor of Philosophy, Graduate Program in Chemistry
University of California, Riverside, June 2016
Dr. Thomas H. Morton, Chairperson

Heterocyclic have been utilized in a variety of applications ranging from simple solvents to anti-cancer drugs. This dissertation prepares and analyzes new heterocyclic rings with a view toward their application for hydrogen storage or pharmaceutical uses.

Previous studies of ethylene diaminoborane have shown its potential as a hydrogen storage molecule. Using a different purification method from the published literature, a sample of ethylene diaminoborane having a slight impurity was achieved. Analysis of the impurity verified that it is $[B_3H_8]^-$ anion, and its effect on the properties of ethylene diaminoborane, such as dehydrogenation, was investigated. The resulting end product upon dehydrogenation of ethylene diaminoborane was characterized as polymers of its heterocycle rings.

Ethylene diaminoborane is a derivative of ammonia borane, a widely studied hydrogen storage molecule. Two molecules of ammonia borane can isomerize to form diammoniate of diborane. By tethering the two molecules of ammonia borane and allowing isomerization to happen in the gas phase, different charged heterocycles can form. Investigation of these heterocyclic cations in the gas phase show their potential as hydrogen storage compounds.

One field which heterocycles are widely used is in pharmaceutical agents. Using established experience with hydrogen bonding between base pairs, a new heterocycle structure has been designed and synthesized. This molecule was designed to bind to a specific secondary structure, known as *i*-motif, of single-stranded DNA, which might possibly be found in oncogenes. The synthetic pathway of the target molecule is outlined in this dissertation. Preliminary studies of this molecule show potential binding to its deprotonated form and also to some DNA strands that form the *i*-motif.

Table of Contents

List of Figures

List of Tables

List of Schemes

List of Equations

Chapter I:

Is Hydrogen Evolution Catalyzed by 2-Bora-1,3-Diazacyclopentanium Ion in the Solid Phase?

Introduction:

Coal mining and its use in homes marked the start of harvesting and using fossil fuel as a source of energy.[1] With the Chinese discovering and refining oil and natural gas, and with the later discovery of petroleum in 1859 in the United States, the use of a variety of fossil fuels entered a new stage. Originally used for illumination, petroleum's biggest impact has been in its use for internal combustion engine at the start of the 20th century, when it was proved to surpass steam or electricity as a source of energy. To this day, the use of fossil fuel, both for transportation and for electric power generation, has made modern life possible, for the advancement of technology would have been naught without it. In the United States alone, 82% of the energy demand is met by fossil fuel.[2] Globally, about 65% of refined petroleum is used in transportation of people and goods and is expected to rise as countries continue to develop and expand their transportation infrastructure.[3]

By the end of 2014, proven world oil reserves totaled 1655 billion barrels and more oil reserves are being discovered.[4] The US. Energy Information Administration predicts that by 2030, assuming present trends, perhaps as much as half of the oil reserves will be exhausted.

Aside from the possible depletion of fossil fuel in the near future, another problem rises from the products of fossil fuel use. The combustion of fossil fuel produces volatile organic compounds, particulate matter, sulfur dioxide (acid rain), nitrogen oxides (smog and acid rain), and carbon oxides (global warming).[5]

The most devastating of all these products is the long term effect of the accumulated carbon oxides in the atmosphere. A study published in *Science* magazine predicted how continued use of fossil fuel and addition of carbon emissions to the atmosphere can affect the rise of sea levels.[6] They predict that with about 10,000 gigatonnes of carbon emission per year, Antartica is projected to become almost ice-free and contribute a rise of 3 meters of sea-level per century during the next millennium.

In order to address the twin problems of dwindling supply and the pernicious effect of combustion products, the use of fossil fuel has to be decreased. However, the expansion of technology will not stop, and the demand for energy will continue to increase. The only solution to this would be to decrease the dependency on fossil fuel, and energy will have to come from another source. One of the most promising alternative means of storing energy is hydrogen. Hydrogen can be produced from renewable energy sources such as biomass, wind, solar, geothermal, and hydro-electric power.[7,8] Aside from its very high abundance, hydrogen burnt with oxygen produces only water vapor as its product. This is not completely environmentally benign: if hydrogen is burnt with air, for lean mixtures of gases have to be used to prevent formation of nitrogen oxides.[8]

Compared to battery-powered automobiles, a hydrogen-powered vehicle has a greater driving range per full tank and, in principle, can be charged/refueled faster. For bigger automobiles, such as buses and trucks, the

fuel cell used for hydrogen can also be scaled up. This is a more practical approach compared to increasing the battery size, which would add weight and volume, to give the same energy output needed for these vehicles.[10]

One of the biggest problems of turning to hydrogen economy as fuel in moving vehicles lies in its transportation and storage. If hydrogen is going to replace fossil fuel (and would be the number one source of energy in the future), a vehicular hydrogen storage approach has to be found. The most simple method of storing and transporting hydrogen would be as compressed gas in cylinders. Different kinds of tanks for hydrogen storage have been designed, which include carbon-fibre-reinforced and hydrogen-inert aluminum tanks.[8] The main problem with this approach are that only 4% of the weight of the system is hydrogen. Also, tanks tend to leak hydrogen (which results to fuel and efficiency loss). Overpressuring also poses dangerous situations (especially while traveling).[8] An addition to this, tanks available through current technology lack the capacity to travel more than 500 km.[9]

Chemical storage of hydrogen offers another way to transport hydrogen. One way to do this is through the use of nanoporous materials such as carbon nanotubes. However, the drawback with this method is that, at present, hydrogen adsorption and storage has to be at the temperature of liquid nitrogen.[11,12] Other nanoporous materials, such as zeolite and activated carbons, are still being improved and studied.[13] Metal hydrides can also provide chemical storage for hydrogen. Even though elemental hydrides may not be suitable due to high

pressure and high temperature, intermetallic metal (alloy) hydrides, such as $LaNi_5H_6$, show a promising hydrogen storage property.[14] However, metal hydrides have a low H_2 mass density, which do not meet the Department of Energy (**DOE**) targets for onboard vehicle ($LaNi_5H_6$ has below 2% H_2 mass, DOE target is 6.5%) and require high temperature and pressure to desorb hydrogen.[15-17]

The most promising compound for chemical storage of hydrogen seems to be ammonia borane (**AB**), as shown in **Figure 1.1**. **AB**, with a low molecular weight (30.7 $g \cdot mol^{-1}$) and high gravimetric hydrogen capacity (19.6 wt %), has opened a whole new different field of hydrogen storage materials.[18]

Background:

The two major drawbacks with **AB** come from the detrimental properties of the depleted product to the fuel cell and rehydrogenation of these depleted products. After multiple, consecutive hydrogen releases, **AB** polymerizes and forms as an end product borazine, a compound that poisons the catalyst and will eventually kill the fuel cells, as well as an intractable polymer.[19] Borazine is known to polymerize to form a gummy residue known as polyborazine. This polymerization eliminates the harmful property of borazine to the catalyst; however, recycling of polyborazine back to **AB** presents another problem. The expulsion of 2.5 equivalents of hydrogen from **AB** to form polyborazine, as shown in **Figure 1.1**, liberates -57.7 $kJ \cdot mol^{-1}$.[20] With such a large exothermicity

during dehydrogenation, regeneration of the spent fuel will require a substantial energy input. Sutton *et al*. used hydrazine, a chemical used as rocket fuel, to generate spent **AB**.[20] This approach seems inefficient, since hydrazine is a compound that can be utilized as a fuel itself.

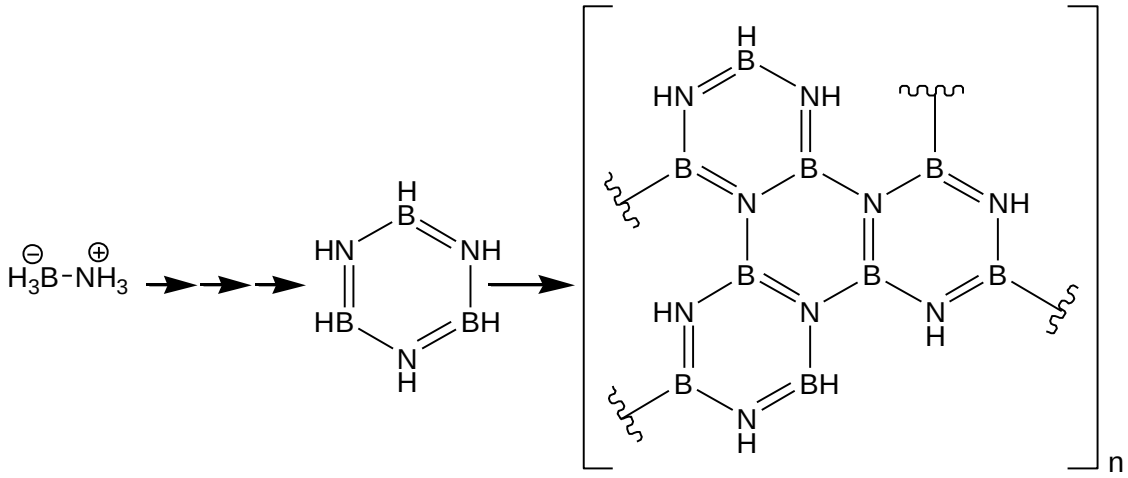

Figure 1.1[19]: Dehydrogenation of ammonia borane leads to formation of borazine and eventually borazine polymerizes to from polyborazine.

One way to solve this problem of **AB** is to look at different derivatives. One such derivative is shown in **Figure 1.2**, in which 2 molecules of **AB** are tethered to each other using an ethylene chain.[21] Neiner *et al.* and other workers have noted that by replacing one of the amino hydrogens with methylene chain, expulsion of ammonia gas and other gases due to decomposition is avoided.[22,23]

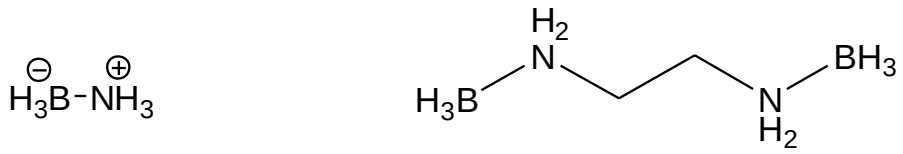

Ammonia Borane

Ethylene Diaminoborane

Figure 1.2: Ammonia borane and one of its derivative(ethylene diaminoborane) which is composed of **AB** molecules tethered to each other via an ethylene chain.

Other studies in the hydrogen storage field includes looking at catalysts that can promote dehydrogenation in lower temperatures and faster rates. Acid or base treatment, catalysts, or ionic liquids are some examples used for dehydrogenation catalysis.[24-26] Using a metal-free catalyst as shown in **Figure 1.3**(**A**), Lu *et al.* was able to stimulate dehydrogenation of **AB**.[27] Their catalyst takes advantage of its high Lewis acidity, which, based on density functional theory (**DFT**) computations, provides an intramolecular stabilization of the initial three-center-two-electron complex between the catalyst and **AB**. Using ionic liquids such as 1-ethyl-3-methylimidazolium([EMIM][OAc]), shown in **Figure 1.3**(**B**), Banerjee *et al.* concluded that the dehydrogenation of **EDAB** in the presence of the ionic liquid happens under milder condition compared to just pure **EDAB**. This decrease in temperature is due to the combined effect of an intermediate carbene formation from the ionic liquid cation and the presence of a basic acetate ionic liquid anion, which together lower the LUMO energy significantly.[28]

A) **B)**

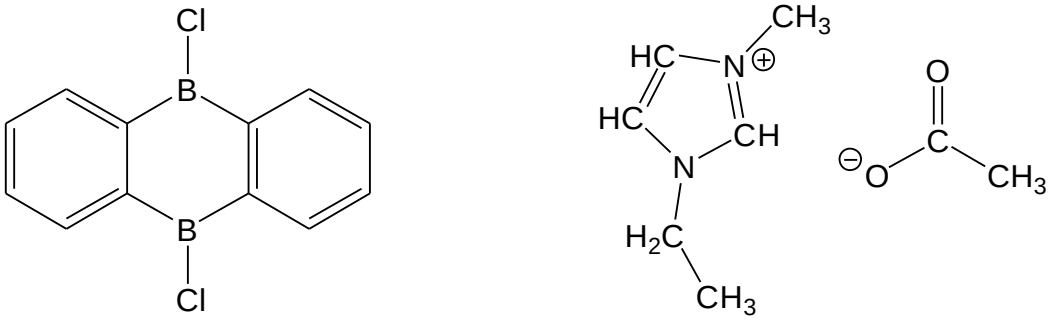

Figure 1.3: A) A metal-free catalyst and B) ionic liquid which have been shown to promote dehydrogenation of **AB**.

This chapter goes over the characterization and dehydrogenation of **EDAB**. Using a different purification from the one published by Edwards and Kelly[29] in their synthesis of pure **EDAB**, we were able to isolate **EDAB** containing a specific impurity. Upon closer inspection using NMR spectroscopy, we have identified this impurity. We now raise the question of whether this impurity might be responsible for catalysis of hydrogen release from **EDAB**.

Experimental:

I. General

Dry THF was obtained from a solvent purification system (<5ppm of water). Several lots of borane in dimethyl sulfide were purchased from Aldrich which came in Acro-sealed bottles and were kept in the freezer after opening. Ethylene diamine was purchased from MP Biomedicals and kept sealed after

opening. The acetonitrile-d_3 used for NMR analysis was purchased from Cambridge Isotope Laboratories and kept sealed after opening.

II. Synthesis:

Ethylene diaminodiborane (**EDAB**) was synthesized,with minor modifications, based on Edwards and Kelly's procedure in which they were able to get the same compound.[29] In a typical procedure, the glassware, spin vanes, and syringes were oven dried before use. A 50 ml round bottom flask was dried in an oven and purged with nitrogen gas while cooling back to room temperature, followed by attaching a septum cap and a balloon via hypodermic needle. The balloon was inflated with nitrogen gas to make sure that the whole system is kept under inert atmosphere. The round bottom was then cooled in an ice-bath and dry THF (18 ml) introduced using a glass syringe. The flask and solvent were maintained at 0°C and $BH_3{\cdot}Me_2S$ (1.76 ml, 18.6 mmol) was added. Ethylene diamine (0.50 ml, 7.4 mmol) was then added dropwise via a glass syringe while stirring and cooling. The reaction was stirred overnight and left to warm up to room temperature. The THF and Me_2S solvents were removed under vacuum to give a crude white powder.

III. Purification:

Edwards and Kelly's purification (**EDAB A**):

The crude white powder was placed in a round bottom flask and cooled in an ice-bath. Cold water (about 3.3 ml to 500 mg of the powder) was added and the slurry was stirred for 10 minutes at 0ºC. The slurry was filtered and the white

solid washed with cold water before drying under vacuum overnight. The same spectra for the analysis of the compound acquired from this purification was included in the paper by Edwards and Kelly.

Silica elution purification (**EDAB B**):

The crude white powder was dissolved in the minimum amount of acetonitrile and passed through a silica column using ethyl acetate as eluent (approximately 200 ml of ethyl acetate was used). The eluent was collected and the solvent removed under vacuum to yield a white powder.

IV. Characterization and Dehydrogenation Analysis:

400 MHz ^{1}H NMR spectra were recorded using Varian Inova 400 (2 channel Z axis gradient spectrometer). 96 MHz ^{11}B NMR spectra were recorded using Bruker Avance 300 (2 channel Z axis gradient spectrometer).

Inelastic neutron scattering (**INS**) spectroscopy has been described in detail elsewhere.[30,31] In a brief description, the neutron source is generated from collision of accelerated protons against a heavy-metal target (*i.e.* tungsten). The specific instrument used for the samples is called the Filter Difference Spectrometer (FDS) in which the neutron beam collides with the sample and pass through filters as they exit. The neutrons interact with the sample, scattered and then sorted by their time of flight (**TOF**) which is based from the time they interact with the sample to when they reach the detector. As the incoming neutron interacts with the sample, some of the neutron's energy is lost and transferred in the form of molecular vibration; this loss of energy of the neutron is

related to and can be measure by the TOF. INS data were acquired at Los Alamos Neutron Scattering Center (LANSCE) in Los Alamos, New Mexico with assistance of Dr. Luke Daemen. A schematic diagram of the FDS is shown in **Figure 1.4**.

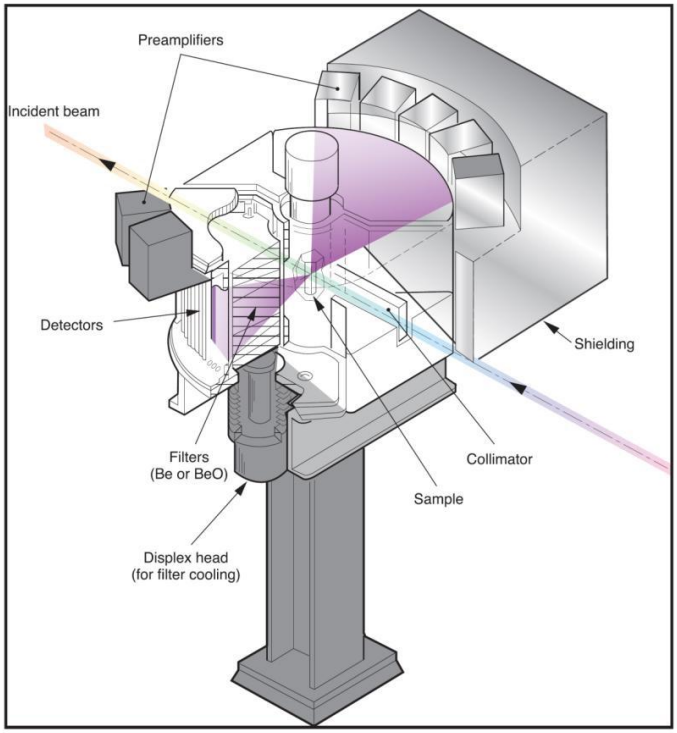

Figure 1.4: Schematic diagram of the Inelastic Neutron Scattering instrument. Image was taken from "http://lansce.lanl.gov/lujan/instruments/FDS.shtml".

In a typical INS experiment, about 0.4-1.5grams of solid sample are packed in an aluminum sample container in a glovebox. The sample is cooled to 10 K and irradiated for 10-12 hours at constant temperature in the FDS.

Thermogravimetric analysis (TGA) was performed by Dr. Chengyu Mao on a TGA Q500 analyzer (TA Instrument). Samples were heated at a 0.5°C ramp under constant N_2 flow during the analysis. The onset dehydrogenation temperature of the sample was determined to be 103.0 °C.

Gas evolution from the diaminediborane compounds were measured by Dr. Mao using a home-built gas analysis system consisting of a gas line coupled with a Hiden quadrupole mass spectrometer (MS, Model HALO 201) equipped with a Faraday detector, as shown in **Figure 1.5**. The detector of the mass spectrometer was mounted on a reducing Tee (**Figure 1.6**) specifically designed as a chamber for ultra-high vacuum systems through the first flange, and the tip of the detector was placed inside the Tee chamber. The second flange of the Tee was connected to a Turbo pump station (HiCube 80 Eco, Pfeiffer Vacuum) controlled by a DCU002 unit. The ultimate pressure can reach lower than 10^{-7} mbar within the chamber. The third flange of the Tee was connected to the outlet of a breakable leak valve (Kurt J. Lesker, **Figure 1.7**), which can control the flow of gas into a vacuum system from an external source. The inlet pressure of the leak valve can be adjusted by a graduated indexing. All of the connections mentioned above are sealed by ConFlat flanges composed of a copper gasket and knife-edge gland. Argon was used as a carrier gas and the flow rate was set as constant by a Mass flow controller (MFC). Target gas was carried by Ar flow and fed into the vacuum chamber through the inlet of the leak valve. All gas lines were made of Teflon tubing (1/8”, 1/16”) and interconnected through Swagelok fittings with suitable size. The MS was running in the multiple ion detection mode detecting ion peaks at *m/z* 2 (H_2).

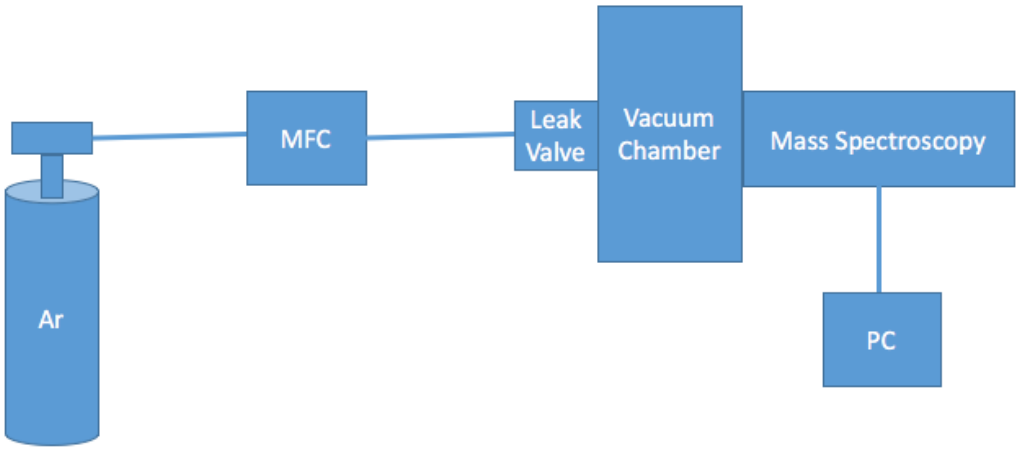

Figure 1.5: Schematic diagram of the gas analysis system used to analyze the dehydrogenation of **EDAB**.

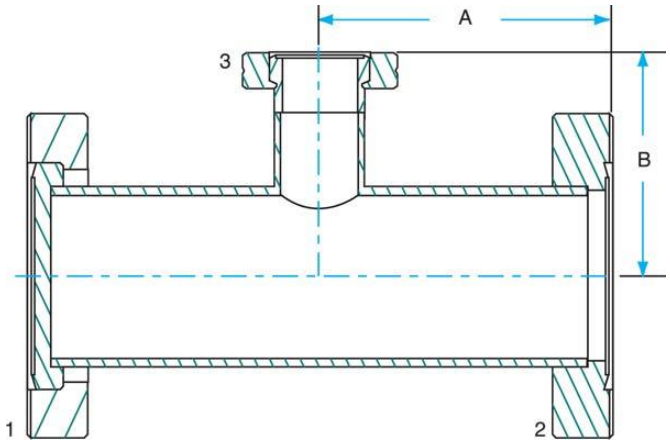

Figure 1.6: A diagram of the detector of the mass spectrometer mounted on a reducing Tee. Image was taken from “http://www.lesker.com/newweb/flanges/fittings_cf_tees.cfm?pgid=reducertee”.

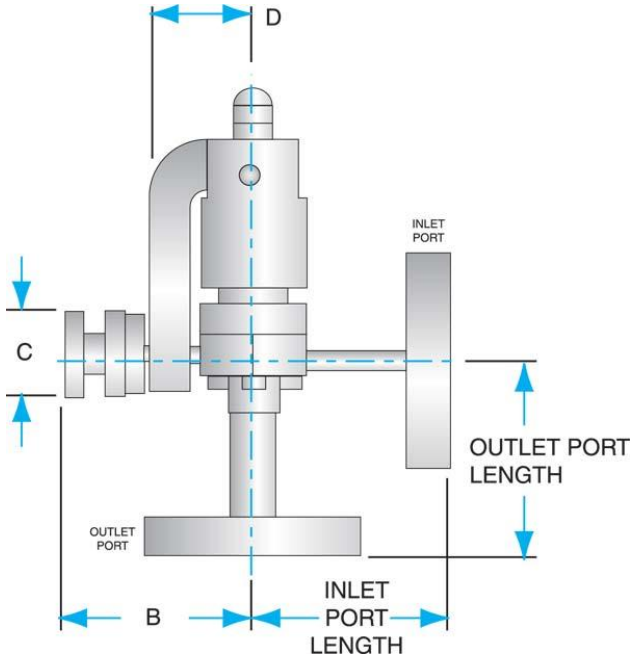

Figure 1.7: Diagram of the third flange of the Tee which can control the flow of gas into a vacuum system from an external source. Image was taken from "http://www.lesker.com/newweb/valves/allmetalvalves_leak_lvm.cfm?pgid=cf".

In a typical dehydrogenation analysis experiment, a specific amount of the sample was introduced into a three-necked round bottom flask to act as the reactor. The reactor was fixed on a metal stand and the middle opening was capped with a glass stopper. The other two openings are fitted with glass valve adapters so that a gas line can be attached via 1/8" Vincon tubings (**Figure 1.8**). All glass junctions were sealed by vacuum grease to make sure a tight seal. The whole system was then purged with Ar until all gases in the system has been evacuated and only trace amounts of O_2 and N_2 can be detected by the MS. The glass valves were then closed and the reactor flask immersed into the oil bath. The reactor was kept at a constant temperature for several hours until all the

compounds were decomposed. The valves were then opened and the generated hydrogen gas within the reactor was carried by Ar flow into the MS for analysis.

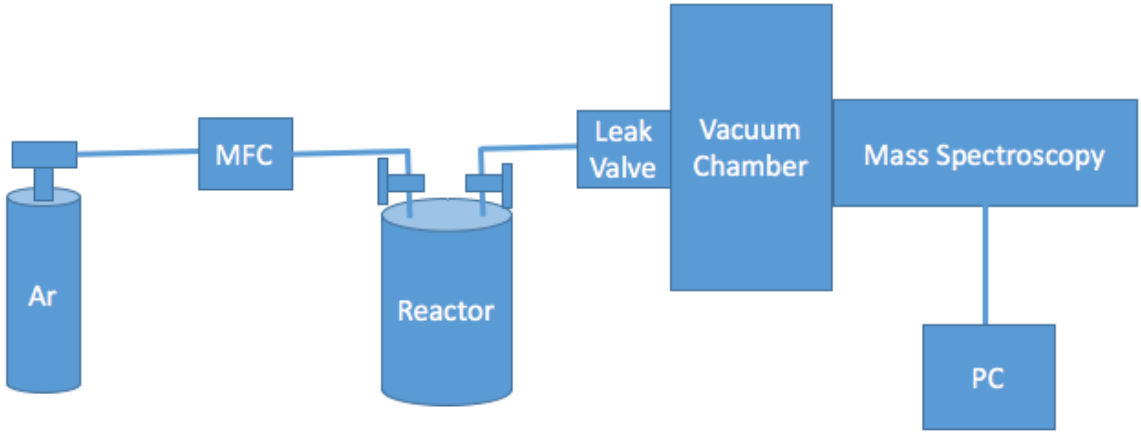

Figure 1.8: A schematic diagram of a typical experiment using the gas analysis system.

V: Low Temperature Pyrolyses:

Samples were also sealed in breakseal ampoules and heated in a 85°C oven for more than a week, for comparison with the aforementioned hydrogen release experiments. The breakseal ampoules were opened with a loud pop, indicating evolution of gas, but no quantitation was attempted.

Liquid Chromatography/Time of Flight Mass Spectrometry analyses in positive ion mode were done using Agilent 6210 LC/Tof. In a typical experiment, a small amount of the spent compound from hydrogen liberation (~1-2mg) was dissolved in 1.5 ml of methanol. The instrument is operated in the “Multimode” and optimizes both electrospray ionization (**ESI**) and atmospheric pressure chemical ionization (**APCI**) parameters.

Results:

Characterization of fully hydrogenated **EDAB**:

The synthesis of **EDAB** yielded a crude white powder. Analysis of the powder showed that along with the desired compound, impurities were also present in the sample. Using ^{1}H and ^{11}B NMR, one of these impurities was characterized as $[BH_4]^-$ ion. In the ^{1}H NMR shown in **Figure 1.9**(**A**), the $[BH_4]^-$ ion shows up as a quartet and septet at δ = -0.56 to 0.051 ppm due to the ^{11}B and ^{10}B coupling to hydrogens, respectively. The ^{11}B NMR, displayed in **Figure 1.9**(**B**), shows the $[BH_4]^-$ anion at δ = -38.12 ppm. $[BH_4]^-$ anions have been recorded to show up at in the negative regions due to their anionic character[32] with the same quartet and septet coupling in the ^{1}H NMR. The coupling pattern of borohydride in the ^{1}H NMR can be explained by the equation *1.1* below, in which *n* is the number of the specific nucleus present and *I* is the spin quantum number of that coupled nucleus.[33]

$$\text{Multiplicity} = 2nI+1 \qquad (1.1)$$

Since ^{11}B and ^{10}B have spin quantum numbers of 3/2 and 3, respectively, their coupling to protons would be quartet and septet based on the equation. Aside from the $[BH_4]^-$ anion, a closer look at the ^{11}B NMR shows other boron-containing impurities. While the peak at δ = -38.1 ppm corresponds to the

$[BH4]^-$ counterion and the peak at δ = -19.2 ppm for the BH3 terminal groups of **EDAB**, the rest of the peaks are unaccounted for.

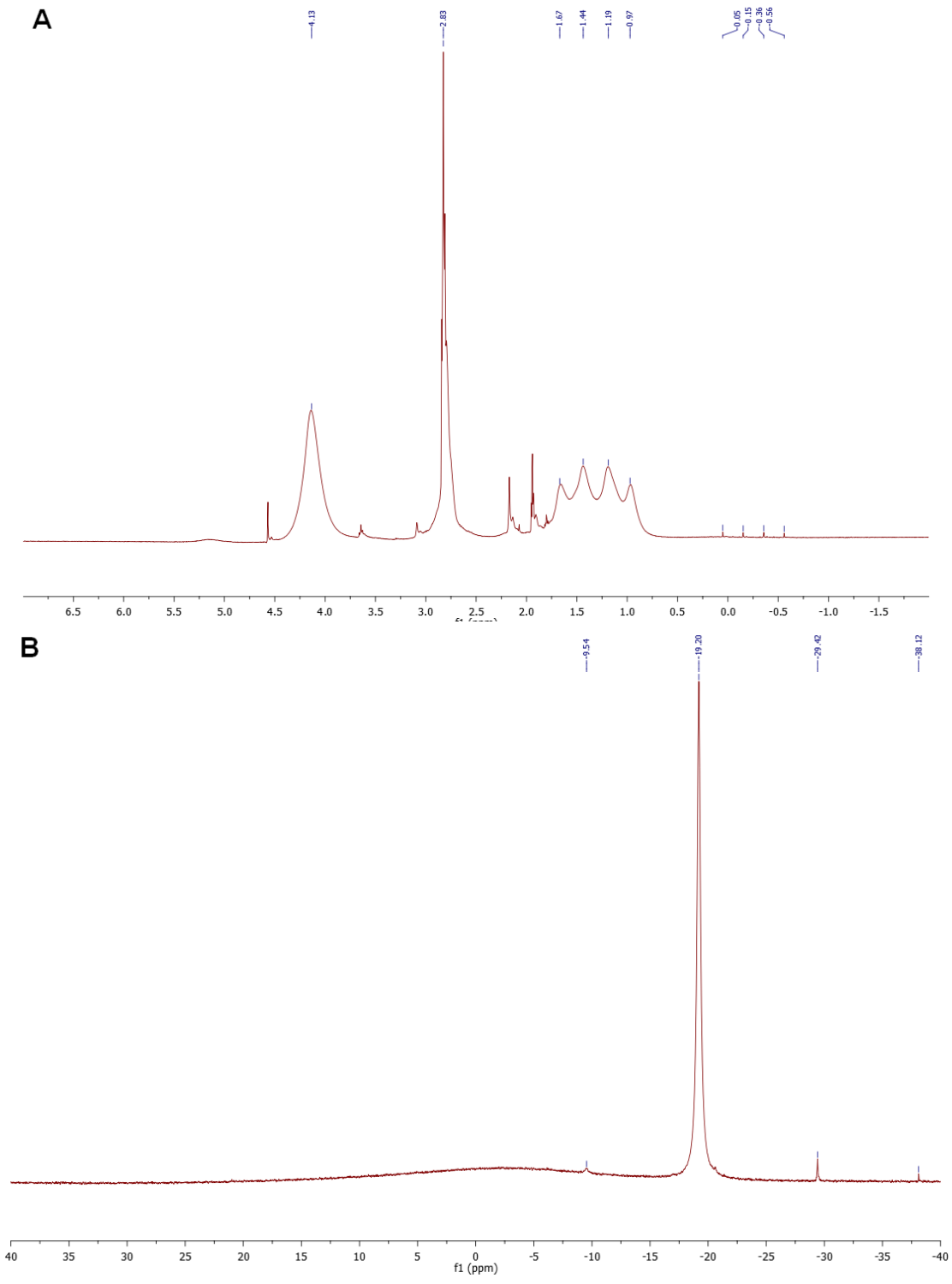

Figure 1.9: (**A**) ^{1}H and (**B**) ^{11}B NMR analysis of the crude sample of **EDAB** which shows boron containing impurities.

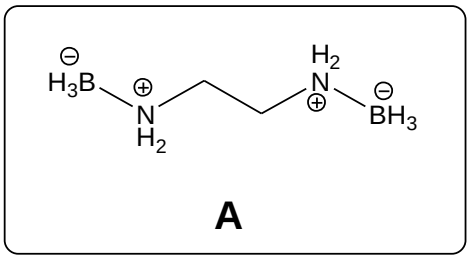

A

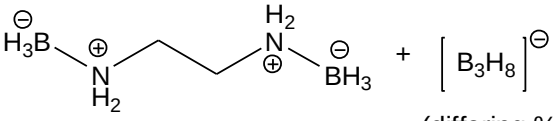

(differing %)

B

Using Edward and Kelly's procedure of washing the crude material with water, a pure **EDAB A** was acquired.[24] Analysis using ^{1}H and ^{11}B NMR shows that only peaks corresponding to pure **EDAB** are present and all the impurities are gone. The broad quartet shown in ^{1}H in **Figure 1.10**(**A**) is characteristic of the B-H coupling of the BH_3 groups of **EDAB**.

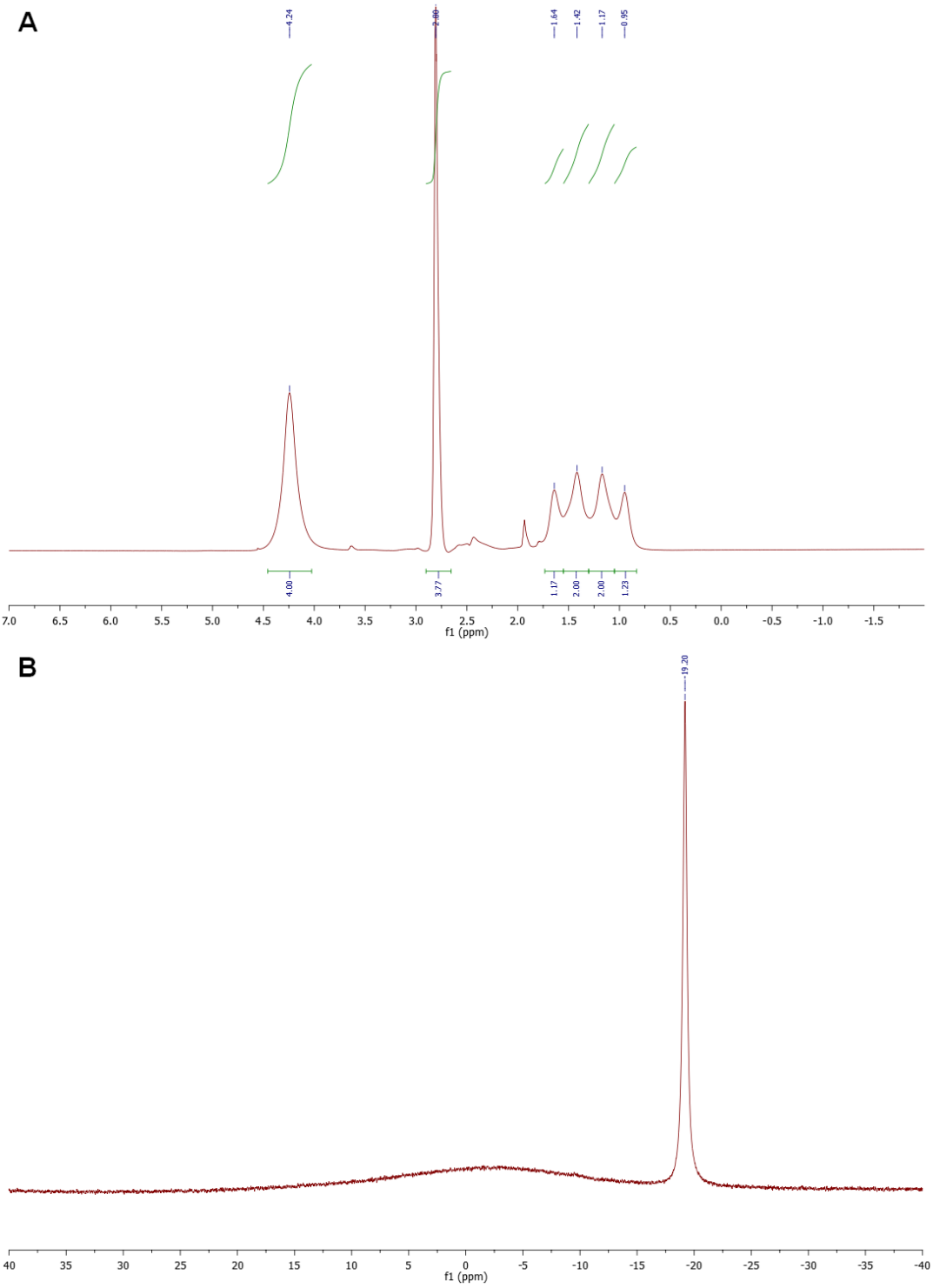

Figure 1.10: (**A**)^{1}H and (**B**)^{11}B NMR analysis of the pure **EDAB A** purified using Edwards and Kelly's procedure and shows the absence of any counterion.

In this project, a different purification method was used by dissolving the crude material in acetonitrile and eluting it through silica using ethyl acetate. Unlike the pure sample that Edwards and Kelly collected, the sample acquired from this method retained one of the impurities that was initially present in the crude sample. Analysis of that impurity using NMR spectroscopy identifies that impurity (eluted along with the pure compound) is the $[B_3H_8]^-$ ion, which gives the sample **B** above.

Using equation *1*, the B-H coupling of $[B_3H_8]^-$ ion should show a dectet for ^1H NMR. **Figure 1.11**(**A**) shows a set of peaks at δ = -0.23 to 0.51 ppm which are small but which does follow the trend. The ^{11}B NMR, presented in **Figure 1.11**(**B**), shows the impurity peak at δ = -29.39 ppm. Similar chemical shifts for the $[B_3H_8]^-$ have been recorded using ammonium octahydrotriborate, which gave the same dectet peak for ^1H NMR at δ = 0.2 ppm and ^{11}B NMR peak at δ = -30 ppm.[34]

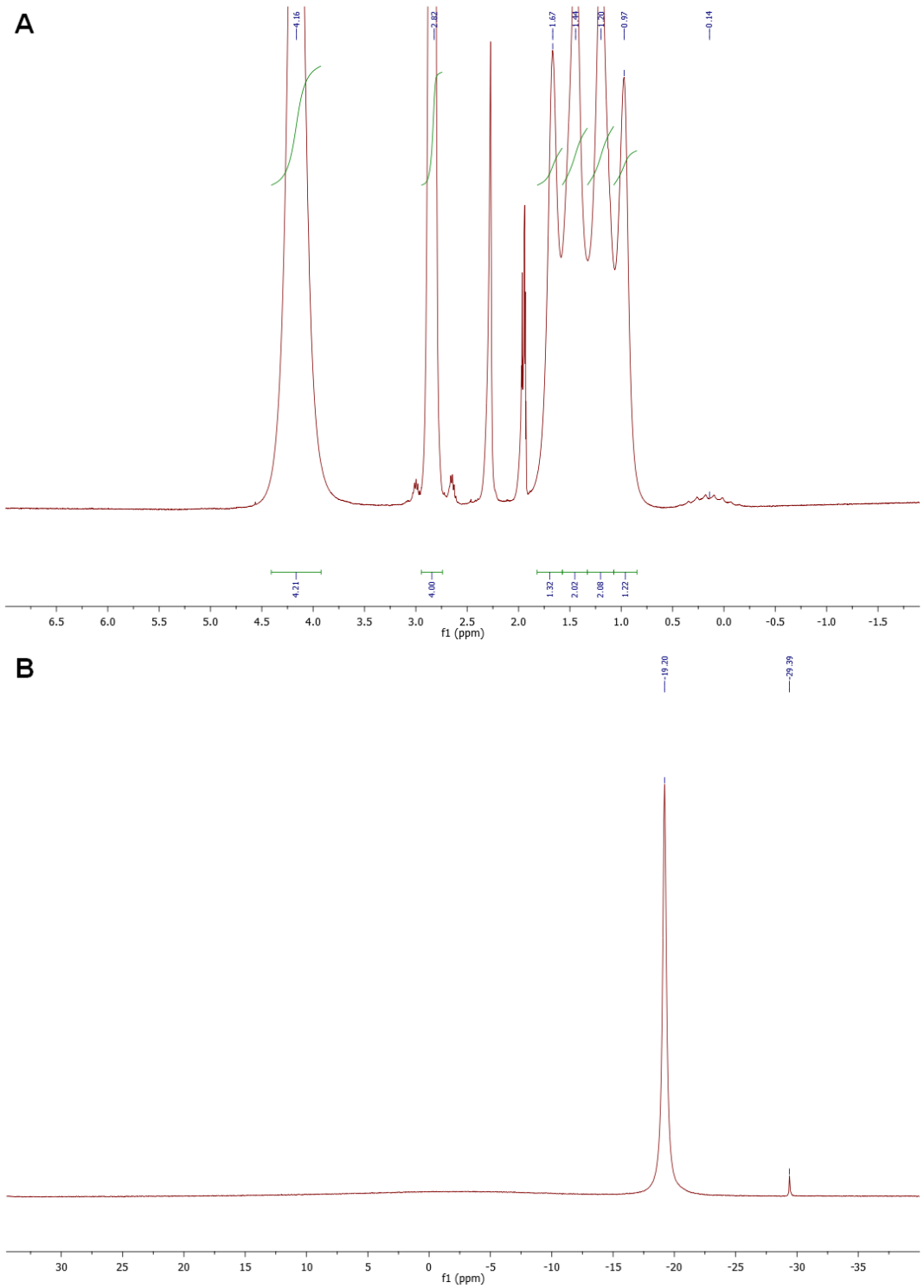

Figure 1.11: (**A**) ^{1}H NMR of the silica-purified **EDAB B** which shows the dectet set of peaks as the most upfield peak corresponding to the B-H coupling of $[B_3H_8]^-$. (**B**) ^{11}B NMR of **B** which shows the impurity at δ = -29.39 ppm.

Washing **B** with water, just as in the Edwards and Kelly's purification, gets rid of the $[B_3H_8]^-$ impurity. It was also found that grinding the solid sample of **B** using a mortar and pestle also decreases the quantity of the $[B_3H_8]^-$ ion. This indicates that the $[B_3H_8]^-$ ion is not stable enough when excessive kinetic energy is applied to it.

Further analysis included Inelastic Neutron Scattering (**INS**) which showed much the same spectral data between **A** and **B**. The comparison in **Figure 1.12** shows that both sample have an identical structure characterization and confirms that majority of **B** is composed of the same pure **EDAB** as **A**. The bands (perhaps 3 peaks) around 550 cm^{-1} in the sample prepared according to Edwards and Kelly's procedure shows that even this sample contains impurities, which are removed by chromatography. However, this impurity was not identified.

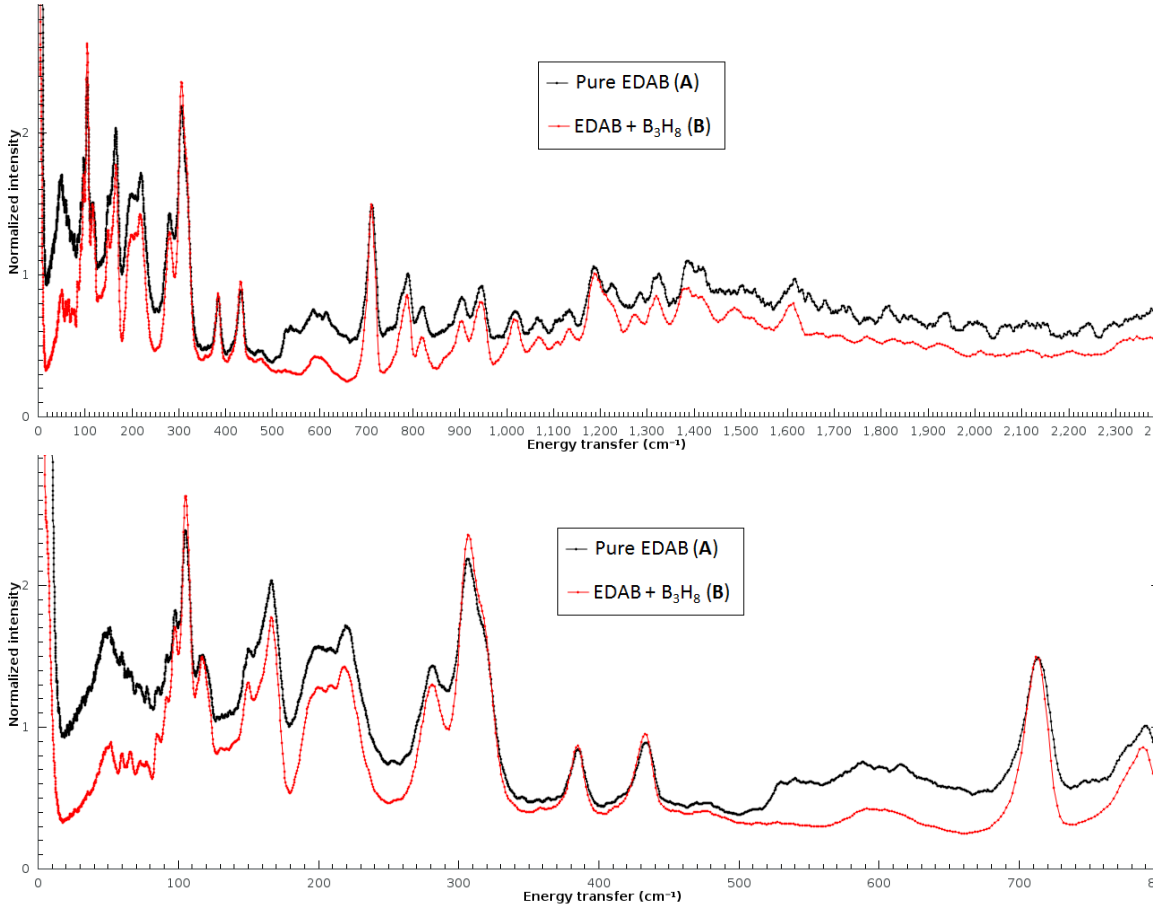

Figure 1.12: INS spectra from 0 to 2400 cm^{-1} (top) and 0 to 800 cm^{-1} (bottom) which shows the same structural characterization of **A** and **B**.

Hydrogen Desorption:

One of the questions that arose, after confirming the presence of $[B_3H_8]^-$ ion, is whether it can affect the properties of **EDAB**, specifically its hydrogen expulsion. Since $[B_3H_8]^-$ is anionic, electric charge balance requires a cationic counterion, which we believe to be the 2-bora-1,3-diazacycloalkanium ions described in Chapter 2 of this thesis. In order to address the issue of catalysis, dehydrogenation analyses of **A** and **B** were performed and compared.

Thermogravimetric analysis (**TGA**) run of **A** (**Figure 1.13**) shows that hydrogen desorption happens at 110°C. This is consistent with what Neiner *et al.* and Leardini *et al.* observed with their pure compound requiring a temperature of at least 120°C for dehydrogenation to occur.[22,23] For **B**, which contains $[B_3H_8]^-$, the dehydrogenation happens at 104°C with a decrease in % weight of ~3.5%. The presence of the $[B_3H_8]^-$ ion correlates not only with lowering the dehydrogenation temperature (by about 6°C) but also affects the amount of hydrogen expelled.

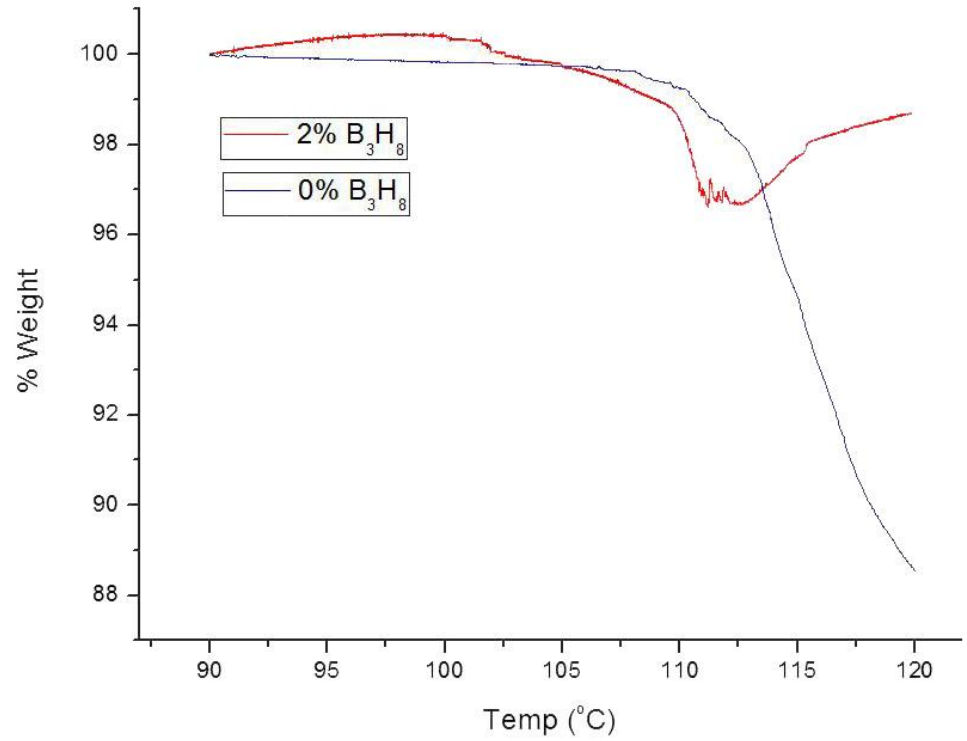

Figure 1.13: Thermogravimetric analysis (TGA) of **A** (0% B_3H_8) and **B** (2% B_3H_8) showing a difference in dehydrogenation temperature between the two samples of about 6°C.

Because catalysis was observed for B, we explored whether this would correlate quantitatively with the fractional abundance of $[B_3H_8]^-$. Using the dehydrogenation temperature acquired from the TGA experiment, hydrogen desorption mass spectrometry analysis were performed to study the rate of dehydrogenation for **A** and **B** (with different loadings of $[B_3H_8]^-$, as ascertained by NMR). Just as Neiner *et al*. and Leardini *et al*. noted, no impurities such as NH_3 or borazine were detected upon heating of either sample. Only pure hydrogen gas was observed. The purity of expelled gas is important for fuel cell application because other volatile compounds, such as the ones mentioned above, can harm or disable a fuel cell catalyst.[20] Other probable impurities include diborane gas and ethylene diamine, which were also not observed. The presence of these compounds can be attributed to the decomposition of **EDAB**, meaning that dehydrogenation chemistry dominates over the decomposition pathway.[22]

Even though both **A** and **B** show pure H_2 as product, the rate of dehydrogenation between them is quite different. **Figure 1.14** shows the mass spectrometry dehydrogenation runs for **A** and **B** at isothermal heating at 100°C. Just as Neiner *et al*. observed, no induction period was observed for either samples in the beginning. However, **B** starts showing an induction period after about two hours of heating. Even though **B** does go through an induction period, it is followed by a pronounced expulsion of hydrogen, as shown by the mound at three to eight hours of heating. On one hand, after nine hours, the quantity of

hydrogen expelled by **B** is lower than the quantity expelled by **A**. On the other hand, **A** shows a constant rate of H_2 release throughout the whole run. Both runs were not allowed to go to full exhaustion and the dip at the end corresponds to closing the system to the detector and returning back to the baseline signal. This baseline value was used to integrate of the area underneath the peaks (cut off at 22 hours) and showed that the average expelled hydrogen quantity is almost the same for both samples (**A** with $3.95e^{-6}$ and **B** with $3.66e^{-6}$). Even though both samples release the same amount of hydrogen, one thing to note is that **B** shows a faster rate of dehydrogenation (shown by the mound in the beginning of the run) compared to **A.** Even at the end of the run, the quantity of H_2 being released by **B** is about half of the amount as being released by **A**.

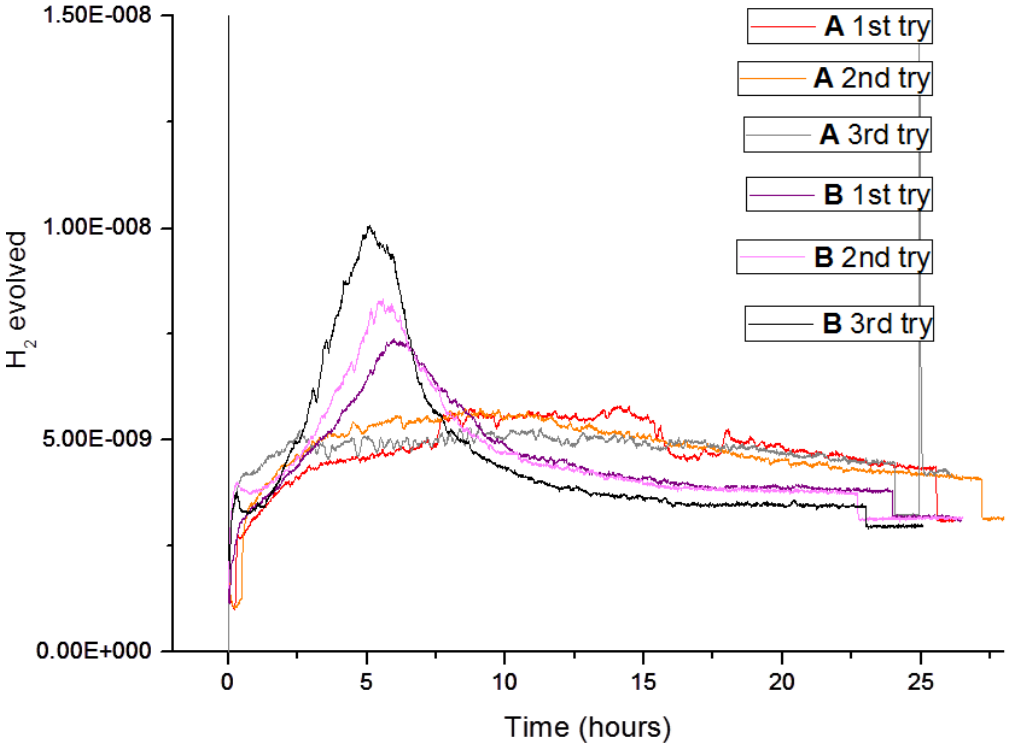

Figure 1.14: Mass spec dehydrogenation runs comparing samples **A** and **B**. Sample B shows a pronounced expulsion of hydrogen in the beginning.

Two samples of **B**, with differing $[B_3H_8]^-$ concentrations, were prepared to investigate if the ion and its cationic counterion possess some catalytic properties. Since chemical distributors have a very general quality control procedures, different lots of borane-methyl sulfide can differ in their purity. This was utilized to synthesize 3.5% $[B_3H_8]^-$ **B** and 2% $[B_3H_8]^-$ **B** samples. The percentages were calculated by integration of the peaks of the ^{11}B NMR and dividing each by their corresponding number of borons. Using the same parameters in the mass spec dehydrogenation analysis, the comparisons of the runs for each sample are shown in **Figure 1.15**. The runs for 3.5% $[B_3H_8]^-$ show

an average of the maximum peak at about 7.5 hours while for 2% $[B_3H_8]^-$ at about 5 hours. Integration of the area underneath the peaks for 3.5% **B** shows that the average amount of expelled hydrogen is about the same as the 2% **B** (3.5% **B** with $4.18e^{-6}$). However, since it takes a longer time for dehydrogenation to happen with a higher loading of the $[B_3H_8]^-$ ion, it can be inferred that neither the $[B_3H_8]^-$ ion (nor its counterion) is directly participating on the catalysis of **EDAB** dehydrogenation. In other words, catalysis of H_2 elimination from **EDAB** does take place, but the catalytic species remains unknown.

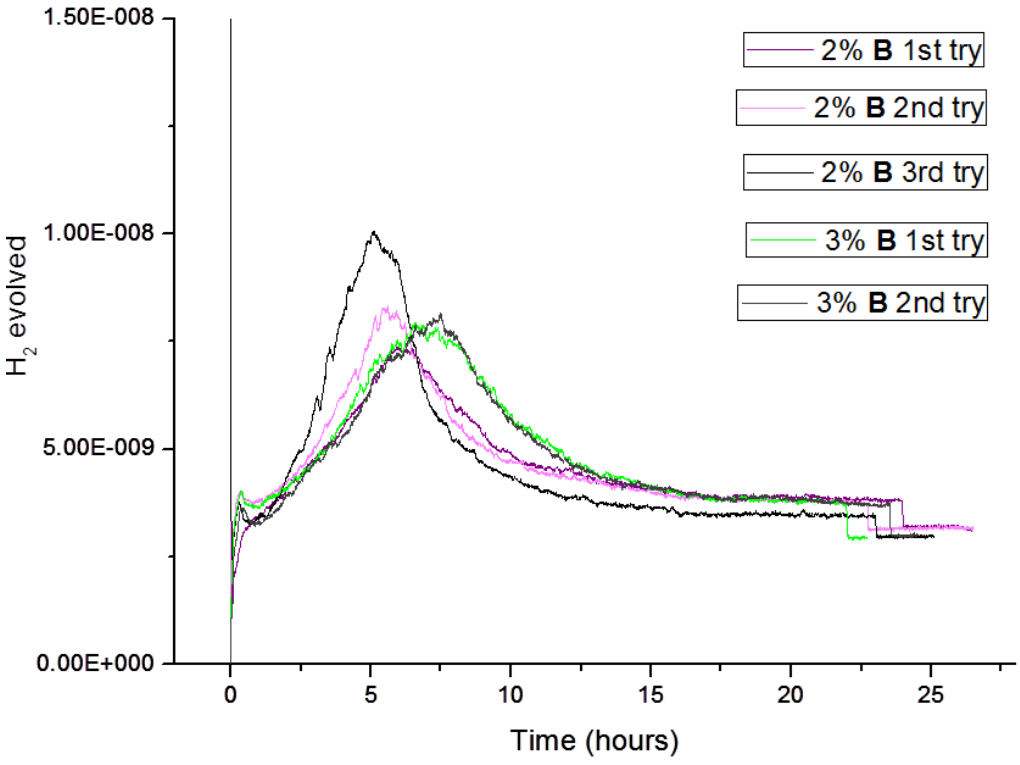

Figure 1.15: Mass spec dehydrogenation runs for B with different percentages of the $[B_3H_8]^-$ ion. The sample with a higher quantity of the ion shows a slower dehydrogenation rate which is contradicts the prediction that the $[B_3H_8]^-$ ion or its counterion being the direct catalyst.

We have identified the $[B_3H_8]^-$ anion as an impurity in the **EDAB** that is purified by column chromatography. In Chapter 2 of this thesis, we assert that the positively charged ion associated with this anion is 1,3-diaza-2-boracyclopentanium ion. Inelastic neutron scattering shows that a sample purified using Edwards and Kelly's procedure also has an impurity, as yet unidentified. The material purified by column chromatography shows an accelerated rate of hydrogen release relative to the same material purified by Edwards and Kelly's methods. Before discussing the characterization of the 1,3-diaza-2-boracyclopentanium ion, however, we present an analysis of the material left after dehydrogenation.

Characterization of spent ethylene diaminoborane:

Neiner *et al*. has mentioned that they heated **EDAB** at 85°C for 33 hours and observed no thermal or dehydrogenation events. However, in our hands, prolonged heating of **A** and **B** at 85°C for longer times show that some dehydrogenation does occur. About 100mg of **A** and **B** were sealed in separate ampoules and left in a 85°C oven for about 72 days. After cooling, the ampoules were opened, and the loud popping sound that followed was evidence for gas evolution inside. After weighing the difference in mass, **A** lost 0.4% while **B** lost 3.9% of its weight, which can attributed to H_2 evolution. Since these % weights are lower than what was observed for the mass spec experiments, it can be

presumed that the leftover white powders are compounds resulting from the preliminary dehydrogenation.

This presumption was further proven by analyzing the powder of oven-pyrolyzed **EDAB** using ^{1}H and ^{11}B NMR, which still shows the same peaks corresponding to **EDAB** but with additional peaks. **Figure 1.16**(**A**) shows the ^{1}H NMR and the presence of a $[BH_4]^-$ ion but absence of the $[B_3H_8]^-$ ion. The appearance of $[BH_4]^-$ ion, which is evident at δ = -39 ppm in the ^{11}BNMR in **Figure 1.16**(**B**), was also observed by Neiner *et al*. as the first peak to appear in their *in situ* MAS ^{11}B NMR experiment of heating **EDAB**.[22] This can be thought of as parallel to the formation of diammoniate of diborane (**DADB**, $[NH_3BH_2NH_3]^-$ $[BH_4]^+$) which is observed as a precursor to **AB** dehydrogenation.

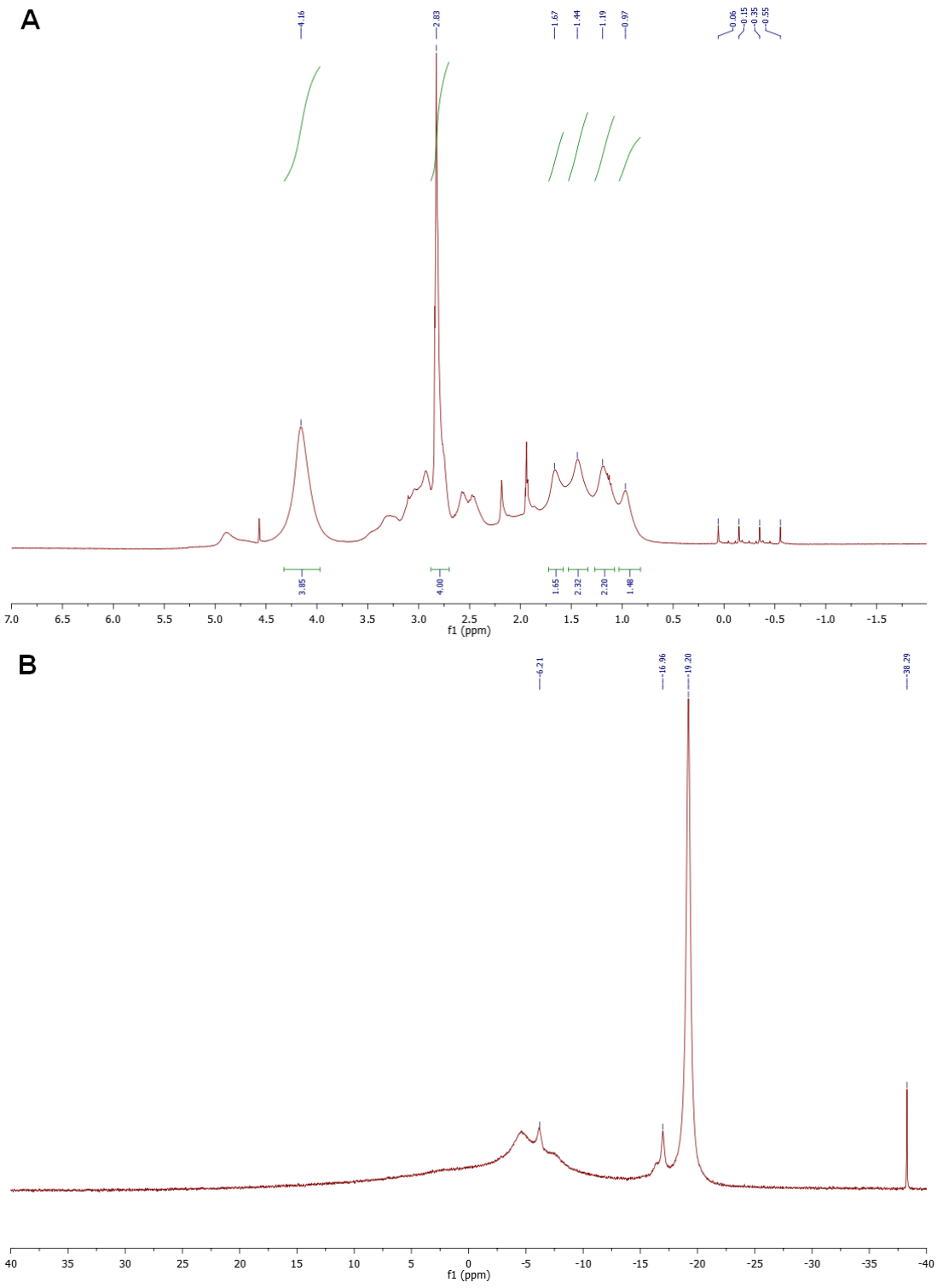

Figure 1.16: (**A**) ^{1}H and (**B**) ^{11}B NMR of the spent **EDAB** after preliminary dehydrogenation by isothermal oven heating at 85°C.

As far as the isothermal mass spec dehydrogenation analysis is concerned, **Figure 1.17**(**A**) shows the ^{1}H NMR of the spent **EDAB** still has a small amount of the $[BH_4]^-$ ion at δ = 0.57 to 0.05ppm. However, the quantity of this ion is so small that it cannot be observed in the ^{11}B NMR in **Figure 1.17**(**B**). The complete disappearance of the ^{11}B NMR δ = -19ppm peak, which corresponds to the BH_3 groups of **EDAB**, means that all the fully hydrogenated material is gone. The appearance of new resonances at δ = -5ppm and δ = -18ppm indicates the formation of an sp^3 BH and a BH_3 in a different environment from the starting **EDAB**, respectively. Neiner *et al*. observed the same changes and peak appearances and have noted that the new peaks became more broad as dehydrogenation proceeded.[22]

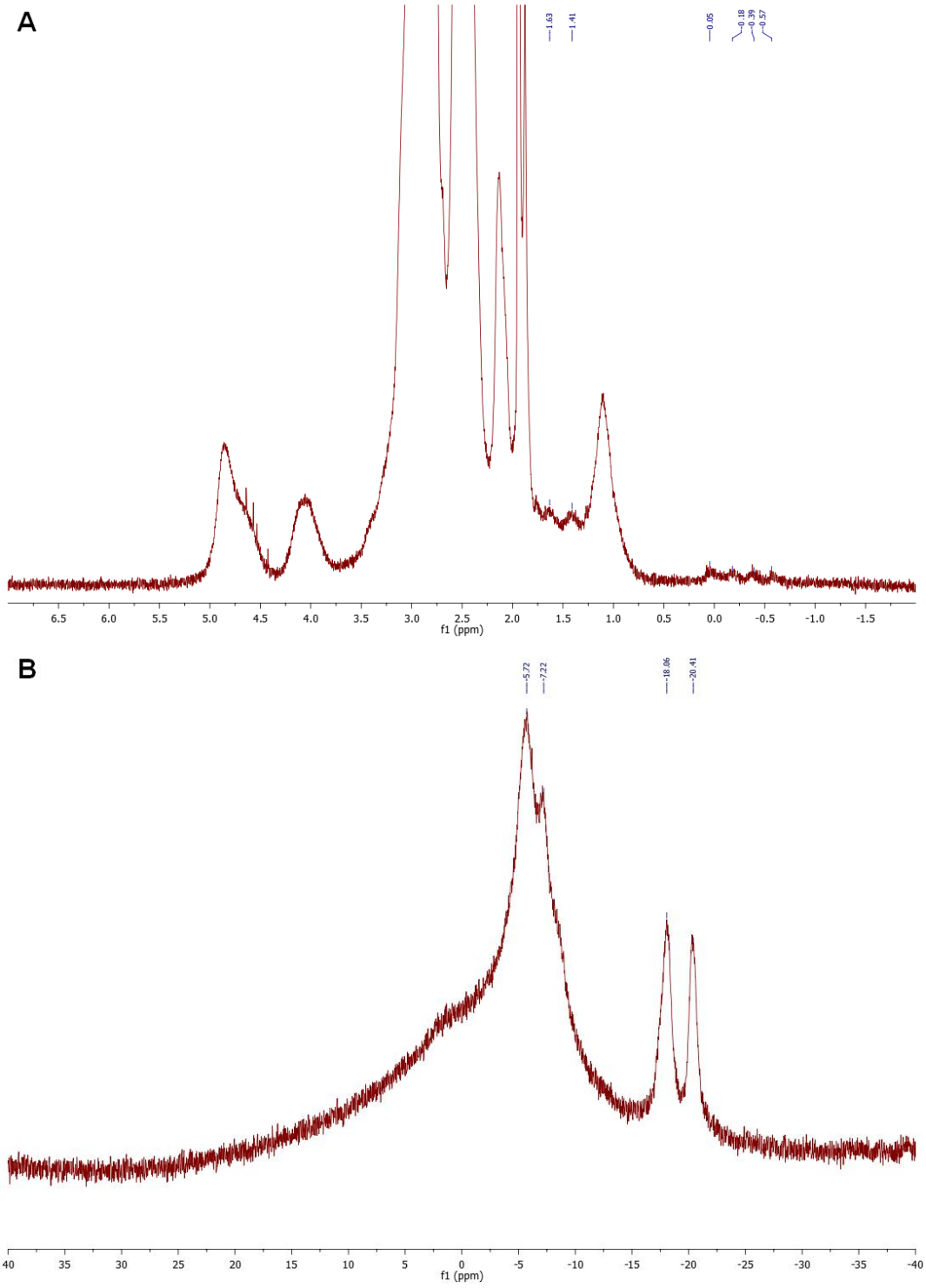

Figure 1.17: (**A**) ^{1}H and (**B**) ^{11}B NMR of the spent **EDAB** after dehydrogenation using isothermal heating at 100°C for mass spec analysis.

Using Neiner *et. al*'s ^{11}B MAS NMR data and their *in situ* temperature-programmed IR and operando Raman-MS measurements, Leardini *et al*. were able to come up with a mechanism, shown in **Scheme 1.1**, for the dehydrogenation of **EDAB**. They proposed that, based on the crystal structure of **EDAB** showing that the molecules have the linear and not the cyclic conformation (as also shown by the single crystal X-ray study[35]), the relevant moieties are closer for an intermolecular reaction.[22,23] The first step involves an isomerization, which gives a borohydride analogous to the formation of **DADB** from **AB**. The first release of hydrogen from this borohydride analogue leads to the formation of an **EDAB** dimer, and further hydrogen release gives oligomers.

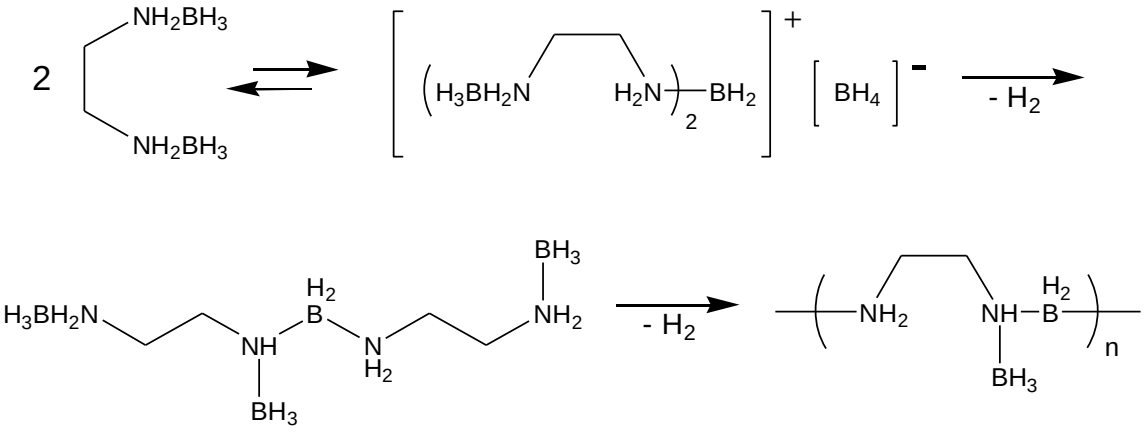

Scheme 1.1[22]: Proposed mechanism by Neiner *et al.* on the dehydrogenation of **EDAB** which first initially isomerizes to form a borohydride followed by release of hydrogen via oligomerization .

Since the proposed end product of Neiner *et al*. and Leardini *et al*. is a neutral molecule, it would be impossible to see it using mass spectrometry.

However, Liquid Chromatography Mass Spectrometry-Electrospray Ionization(+)(**LCMS-ESI**) analysis of the spent powder shows almost the same structure but with a slight difference. For the molecule to be charged, a loss of a proton leading to intramolecular cyclization of the **EDAB** monomers within the oligomer should happen, as portrayed in **Scheme 1.2**.

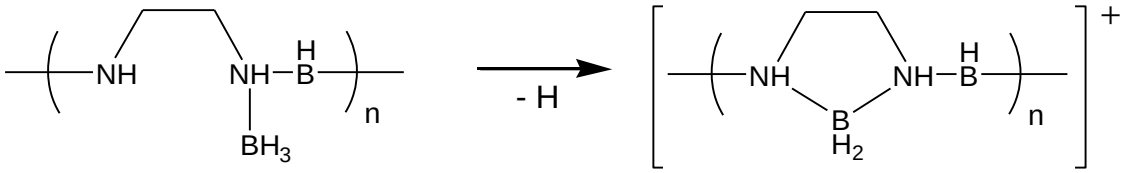

Scheme 1.2: Intramolecular cyclization of the **EDAB** monomers within the oligomer to form charged species which can be detected by LCMS-ESI.

Characterization of spent ethylene diaminoborane:

Figure 1.18 shows the spectrum recorded by LCMS-ESI of the oven pyrolyzed sample. The resulting charged oligomers range in size from trimer to dodecamer. The theoretical isotopic distribution spectrum for each oligomer was calculated and compared with the experimental spectrum. **Figure 1.19** shows some of these comparisons, which also suggest that further dehydrogenation occurred after polymerization and intramolecular cyclization.

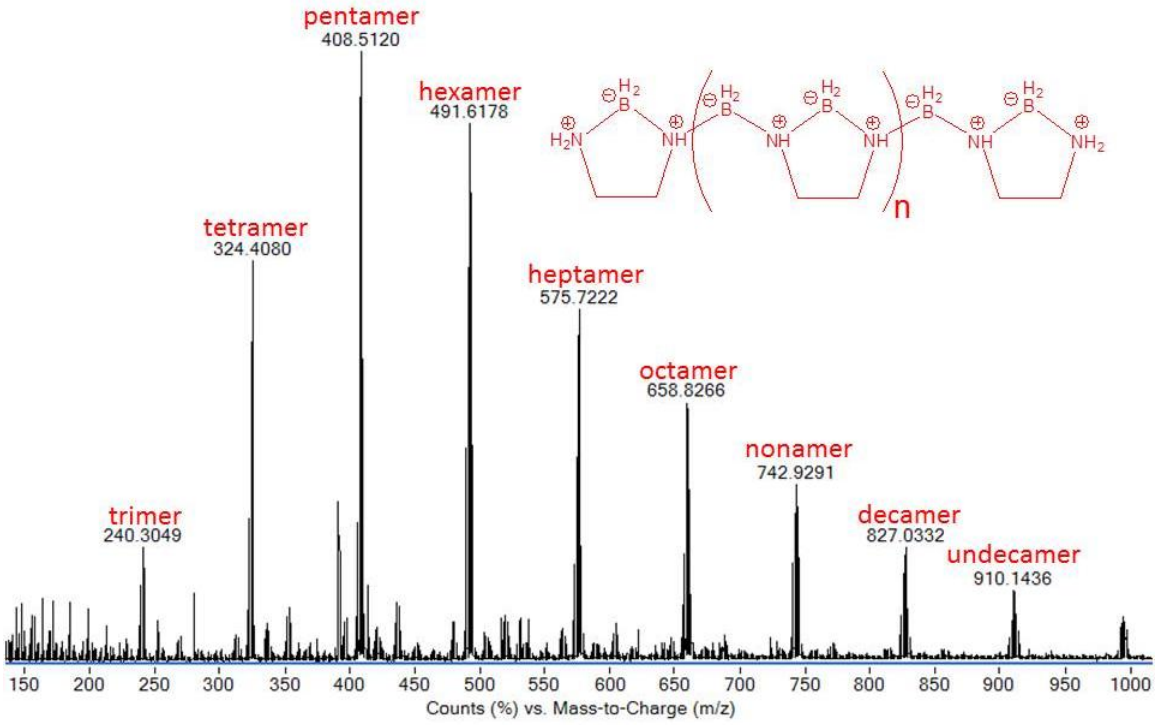

Figure 1.18: LCMS-ESI spectrum of oven pyrolyzed **EDAB** which shows different oligomer lengths ranging from trimer to dodecamer.

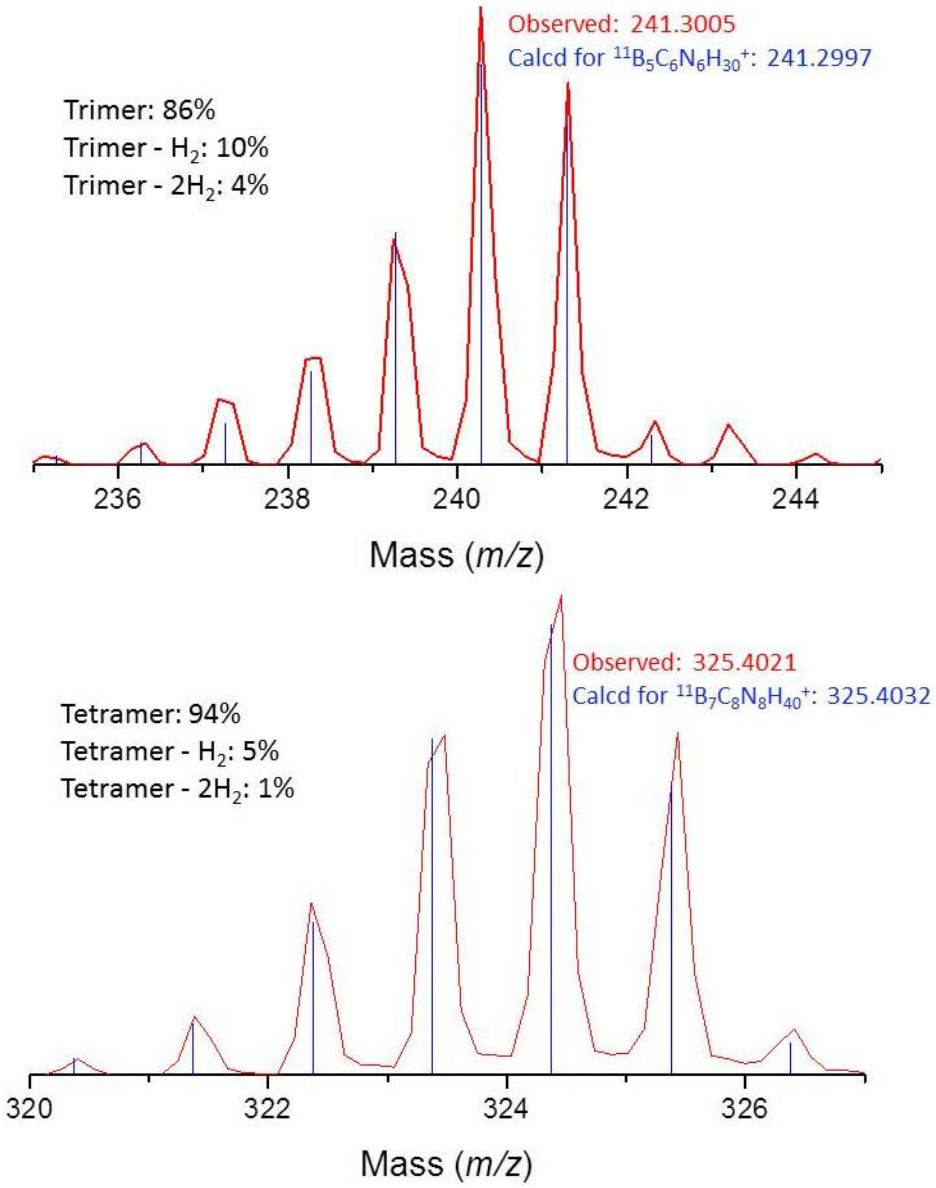

Figure 1.19: Isotopic distribution comparison between the experimental spectrum (red line) and calculated spectrum (blue drop-down lines) of the trimer(top) and tetramer(bottom) oligomers of spent **EDAB** via oven heating.

Based on the comparison, 86% of the trimer is the fully hydrogenated trimer while 10% and 4% of it are trimers after losing one and two equivalents of H_2, respectively. As for the tetramer, 94% of it is the fully hydrogenated tetramer

and 5% and 1% are after a loss of H_2 and $2H_2$, respectively. This further release of H_2 may be coming from dehydrogenation from the B-N bond linking the cyclic rings[23] , as shown in **SchemeR3**.

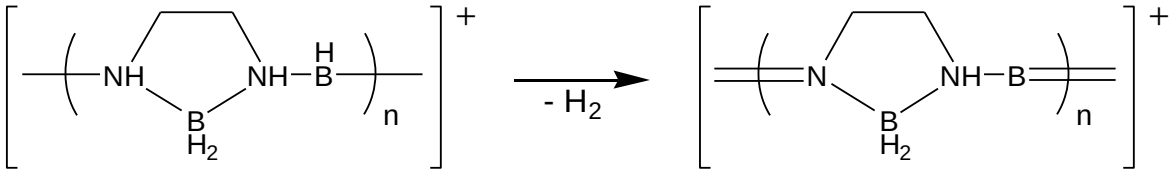

Scheme 1.3: Possible dehydrogenation pathway which releases more hydrogen after oligomer formation and intramolecular cyclization.

Considering the mechanism that has been proposed and what was observed using isotopic distribution comparison, equation *(1.2)* can be used to find out the hydrogen % weight that can be expelled from **EDAB**.

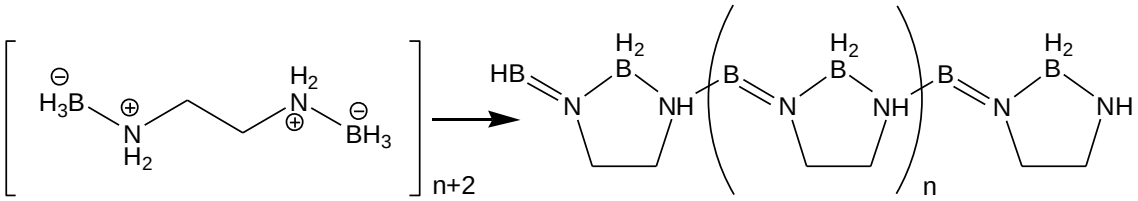

$$\lim_{n \to \infty} \frac{An + B}{Cn + D}$$

A = MW of H released per subunit
B = MW of H released in dimer
C = MW of charged subunit
D = MW of charged dimer

(1.2)

Neiner *et al*. and Leardini *et al*. observed a loss of 10.3 and 9.4 weight % H_2 released after heating **EDAB** to 200°C, respectively. Using equation *2*, as the oligomer size approaches infinity, the hydrogen % weight released limit is about 8.63%, which surpasses the hydrogen % weight requirement of Department of Energy (**DOE**) standard for hydrogen storage molecules.

Conclusion:

Two different samples of **EDAB** were prepared through two different purification methods. The $[B_3H_8]^-$ ion, which can be considered an impurity that co-elutes with pure **EDAB** through silica, is found in the column-purified sample, but destroyed by grinding and is not found in samples purified by washing with water. The column-purified sample turns out to have some catalytic property with regard to H_2 elimination, but this catalysis does not correlate with the abundance of $[B_3H_8]^-$. This catalytic property was observed when a sample of pure **EDAB**(**A**) was compared with the silica-purified **EDAB**(**B**) using TGA, mass spec dehydrogenation, and oven pyrolysis. The latter sample, expelling the same quantity of hydrogen as the primary sample, showed a lower temperature and faster rate of hydrogen release. Since the experiments in this report were only done at temperatures of the first dehydrogenation event (and the second dehydrogenation happens at about 169°C[22,23]), the recorded % of hydrogen in the TGA analysis is only half of the weight that can be ultimately expelled. A study of the spent **EDAB** (including confirmation of the expected isotopic distribution) supports the fact that the hydrogen % weight expelled is higher than what was expected and satisfies the DOE standards.

References:

1: Institute for Energy Research “Encyclopedia Entry: Fossil Fuels” <http://instituteforenergyresearch.org/topics/encyclopedia/fossil-fuels/>

2: Energy Information Administration, Monthly Energy Review, March 2015, <http://www.eia.doe.gov/emeu/mer/pdf/pages/sec1_7.pdf>

3: Greene D. L. “Fuel Choice for Multi-fuel Vehicles” *Contemp. Pol. Issues*, **1990**, *8*, 118-137.

4: Energy Information Administration, Monthly Energy Review, March 2015 <http://www.eia.doe.gov/emeu/mer/pdf/pages/sec7_5.pdf>

5: Journalist’s Resource “The Health Effects and Costs of Air Pollution: Research Roundup” Dec. 7, 2015. <http://journalistsresource.org/studies/environment/pollution-environment/health-effects-costs-air-pollution-research-roundup>

6: Winkelmann, R.; Levermann, A.; Ridgwell, A.; Caldeira, K. “Combustion of Available Fossil Fuel Resources Sufficient to Eliminate the Antarctic Ice Sheet” *Science Advances*, **2015**, *1.* DOI:10.1126/sciadv.1500589. <http://advances.sciencemag.org/content/1/8/e1500589.full>

7: Office of Energy Efficiency & Renewable Energy “Hydrogen Production” <http://energy.gov/eere/fuelcells/hydrogen-production>

8: Schlapbach, L.; Zuttel, A. “Hydrogen-storage materials for mobile application” *Nature*, **2001**, *414*, 353-358.

9: Aceves, S. M.; Berry, G. D.; Martinez-Frias, J.; Espinosa-Loza, F. “Vehicular Storage of Hydrogen in Insulated Pressure Vessels” *Int. J. Hydrogen Energy*, **2006**, *31*, 2274–2283

10: Treehugger “Toyota on Hydrogen fuel cell technology:’Simply a Better Battery’” <http://www.treehugger.com/cars/toyota-hydrogen-fuel-cell-technology-simply-better-battery.html>

11: Dillon, A. C.; Gennett, T.; Alleman, J. L.; Jones, K. M.; Parilla, P. A.; Heben, M. J. “Carbon Nanotube Materials for Hydrogen Storage” *Proceedings of the 2000 DOE/NREL Hydrogen Program Review*, **2000**.
< http://www1.eere.energy.gov/hydrogenandfuelcells/pdfs/28890kkk.pdf>

12: Dillon, A. C.; Jones, K. M.; Bekkedahl, T. A.; Kiang, C. H.; Bethune, D. S.; Heben, M. J. “Storage of Hydrogen in Single-walled Carbon Nanotubes” *Nature*, **1997**, *386*, 377-379.

13: Nijkamp, M. G.; Raaymakers, J. E. M. J.; Van Dillen, A. J.; De Jong, K. P. “Hydrogen Storage Using Physisorption - Materials Demands” *Appl. Phys. A*, **2001**, *72*, 619-623.

14: Sandrock, G.; Thomas, G. “The IEA/DOC/SNL On-line Hydride Databases” *Appl. Phys. A*, **2001**, *72*, 153-155.

15: Schlapbach, L.; Meli, F.; Züttel, A.; Westbrook, J. H; Fleischer, R. L. In: *Intermetallic Compounds: Principles and Practice*, **1994**, *2*, Ch. 22.

16: Zaluska, A.; Zaluski, L.; Stroem-Olsen, J. O. “Structure, catalysis and atomic reactions on the nano-scale: a systematic approach to metal hydrides for hydrogen storage” *Appl. Phys. A,* **2001**, *72*, 157-165.

17: Yvon, K. “Complex Transition-metal Hydrides” *Chimia,* **1998***,* 52, 613-619.

18: Stephens, F. H.; Pons, V.; Baker, R. T. “Ammonia-borane: the hydrogen source *par excellence*?” *Dalton Trans*, **2007**, 2613-2626.

19: Conley, B. L.; Guess, D.; Williams, T.; “A Robust, Air-Stable, Reusable Ruthenium Catalyst for Dehydrogenation of Ammonia Borane” *J. Am. Chem. Soc.*, **2011**, *133*, 14212-14215.

20: Sutton, A. D.; Burrell, A. K.; Dixon, Garner III, E. B.; Gordon, J. C.; Nakagawa, T.; Ott, K. C.; Robinson, J. P.; Vasiliu, M. “Regeneration of Ammonia Borane Spent Fuel by Direct Reaction with Hydrazine and Liquid Ammonia” *Science*, **2011**, *331*, *6023*, 1426-1429.

21: Zhao, Q.; Li, J.; Hamilton, E. J.; Chen, X. “The Continuing Story of Diammoniate of Diborane” *Journal of Organomettalic Chemistry*, **2015**, *798*, 24-29.

22: Neiner, D.; Karkamkar, A.; Bowden, M.; Choi, Y. J.; Luedtke, A.; Holladay, J.; Fisher, A.; Szymczak, N.; Autrey, T. “Kinetic and Thermodynamic Investigation of Hydrogen Release From Ethane 1,2-di-amineborane” *Energy Environ. Sci.*, **2011**, *4*, 4187-4193.

23: Leardini, F.; Valero-Pedraza, M. J.; Perez-Mayoral, E.; Cantelli, R.; Banares, M. A. “Thermolytic Decomposition of Ethane 1,2-Diamineborane Investigated by Thermoanalytical Methods and in Situ Vibrational Spectroscopy” *J. Phys. Chem. C*, **2014**, *118*, 17221-17230.

24: Bluhm, M. E.; Bradley, M. G.; Butterick III, R.; Kusari, U.; Sneddon, L. G. “Amineborane-based Chemical Hydrogen Storage: Enhanced Ammonia Borane Dehydrogenation in Ionic Liquids” *J. Am. Chem. Soc.*, **2006**, *128*, 7748-7749.

25: Denney, M. C.; Pons, V.; Hebden, T. J.; Heinekey, D. M.; Goldberg, K. I. “Efficient Catalysis of Ammonia Borane Dehydrogenation” *J. Am. Chem. Soc.*, **2006**, *128*, 12048-12049.

26: Keaton, R. J.; Blacquiere, J. M.; Baker, R. T. “Base Metal Catalyzed Dehydrogenation of Ammonia-borane for Chemical Hydrogen Storage” *J. Am. Chem. Soc.*, **2007**, *129*, 1844-1845.

27: Lu, Z.; Schweighauser, L.; Hausmann, H.; Wegner, H. A. “Metal-Free Ammonia-Borane Dehydrogenation Catalyzed by a Bis(borane) Lewis Acid”, *Angew. Chem. Int. Ed.*, **2015**, *54*, 15556-15559.

28: Banerjee, B.; Kundu, D.; Pugazhenthi, G.; Banerjee, T. “Quantum Chemical and Experimental Insights for the Ionic Liquid Facilitated Thermal Dehydrogenation of Ethylene Diamine *Bis*borane” *RSC Adv.*, **2015**, *5*, 85280-85290.

29: Edwards, J. O.; Kelly, H.C. “Ethane 1,2-Diamineborane” *J. Am. Chem. Soc.* **1960**, *82*, 4842-4846.

30: Eckert, J.; Sewell, T. D.; Kress, J. D.; Kober, E. M.; Wang, L.; Olah, G. “Vibrational Analysis of Inelastic Neutron Scattering Spectrum of Tetramethylammonium Borohydride by Molecular Dynamics Simulations and Electronic Structure Calculations” *J. Phys. Chem. A*, **2004**, *108*, 11369-11374.

31: Hartman, M. R.; Rush, J. J.; Udovic, T. J.; Bowman Jr, R. C.; Hwang, S. J. “Structure and Vibrational Dynamics of Isotopically Labeled Lithium Borohydride Using Neutron Diffraction and Spectroscopy” *J. Solid State Chem.*, **2007**, *180*, 1298-1305.

32: Lingam, H. K.; Chen, X.; Zhao, J.; Shore, S. G. “A Convenient Synthesis and a NMR Study of the Diammoniate of Diborane” *Chemistry*, **2012**, *18 (12)*, 3490-3492.

33: Shaler, T. A. “Generalization of Pascal’s Triangle to Nuclei of Any Spin” *J. Chem. Ed.,* **1991**, *68(10)*, 853.

34: Huang, Z.; Chen, X.; Yisgedu, T.; Meyers, E. A.; Shore, S. “Ammonium Octahydrotriborate (NH4B3H8): New Synthesis, Structure, and Hydrolytic Hydrogen Release” *Inorganic Chemistry*, **2011**, *50*(*8*), 3738-3742.

35: Ting, H. Y.; Watson, W. H.; Kelly, H. C. “Molecular and Crystal Structure of Ethylenediamine-*bis*borane, C2H14B2N3” *Inorg. Chem.*, **1972**, *11(2)*, 374-377.

Chapter II:

2-Bora-1,3-Diazacycloalkanium Ions in the Gas Phase

Introduction:

The search for an efficient, safe, and inexpensive storage system for hydrogen has led to studies of different varieties of materials. These include tanks of compressed gas, nanoporous materials, metal hydrides, and boron-nitrogen compounds.[1-4] Boron-nitrogen compounds show a tremendous amount of potential as hydrogen storage compound due to their high hydrogen content, thermal stability, and hydrogen release kinetics.

Department of Energy's (DOE) target for onboard hydrogen system by the year 2020 includes that it should have at least 5.5% of its weight as hydrogen.[5] Ammonium borohydride (**ABH_2**, H_4NBH_4) has the highest hydrogen content (24%) of solid state materials and meets the DOE standard. At temperatures below 160°C, **ABH_2** can release 18% of its weight as hydrogen. The dehydrogenation of **ABH_2** was studied by Nielsen *et al.* and observed that it happens in three distinct exothermic steps, as shown in **Scheme 2.1**. The first stage of **ABH_2** decomposition, Eqn (1), takes place at 50°C, but, over the long term, **ABH_2** has to be stored at -40°C.[6]

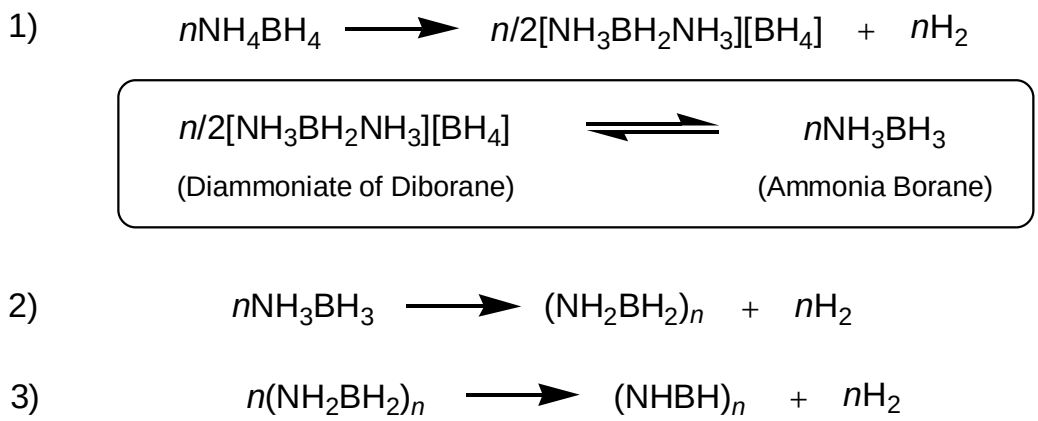

Scheme 2.1[6]: The dehydrogenation of **ABH_2** happens in three exothermic steps. An isomerization between diammoniate of diborane and ammonia borane (box) happens before the second dehydrogenation.

Even though this property of **ABH_2** may appear desirable for hydrogen storage, these exothermic releases lead to a thermal energy runaway that makes it nearly impossible to reverse the process. This problem of regeneration of spent **ABH_2** is one of its biggest drawbacks. In fact, one of the reasons that **ABH_2** can release a huge amount of H_2 under 100°C (12% wt) can be attributed to its instability. If stored in ambient temperature, **ABH_2** has a half-life of 6 hours and slowly decomposes to give hydrogen and diammoniate of diborane (**DADB**, $[H_3NBH_2NH_3]^+[BH_4]^-$). This instability of **ABH_2** makes it hard to handle and study, which hinders its potential as a hydrogen storage candidate.

As stated in the previous chapter, the stability of ammonia borane (**AB**, H_3NBH_3) makes it a more attractive as well as the most studied hydrogen storage molecule. Even though **AB** has a lower hydrogen capacity (19.6% wt) than **ABH_2**, it still satisfies the DOE requirements. One way to synthesize **AB** is reacting gaseous borane (B_2H_6) with ammonia. Using this method, the cleavage

of the gaseous borane can occur symmetrically to give **AB** or unsymmetrically to give **DADB**.[4] **AB** contains both hydridic B-H and protic N-H bonds with a strong B-N bond which, under most conditions, favors hydrogen loss over dissociation. Such conditions include heating **AB** at either a temperature increase of <1°C min^{-1} rate or isothermal heating at ≤90°C.[7,8] At higher rates of temperature increase or at higher temperature heating, thermal decomposition happens in which **AB** produces polyaminoborane ($(H_2NBH_2)_n$), borazine ($B_3N_3H_6$), diborane (B_2H_6), and hydrogen.[9] As discussed in the previous chapter, borazine and diborane are harmful to the fuel cell catalyst.[10] Along with these problems, the regeneration of spent **AB** pose the biggest hurdle on using **AB** as a hydrogen storage molecule.

In order to solve these problems of **AB**, different alterations of **AB** have been studied. One of these modifications is to substitute one of the H in the NH_3 group with a more electron-donating element. This approach is assumed not only to lower the dehydrogenation temperature but also to prevent decomposition of **AB** through B-N bond dissociation.[11] This is probably due to the electron-donating element making the **AB** B-H richer, thus, depressing, the emission of NH_3.

Metals can be considered as electron-donating elements due to their Lewis base properties. Xiong *et. al.* was able to synthesize metal amidoboranes by ball milling 1:1 molar ratios of **AB** with the corresponding alkali-metal hydrides.[11] The resulting products $LiNH_2BH_3$ (**LiAB**) and $NaNH_2BH_3$ (**NaAB**)

have 14% and 9% wt hydrogen, respectively. When heated, both metal amidoboranes immediately released hydrogen and have a dehydrogenation peak at around 89-92°C. No borazine was detected for either dehydrogenation and 8% wt and 6% wt of hydrogen release were observed for **LiAB** and **NaAB**, respectively, within the first hour of heating at ~91°C. Heating at this temperature up to 19 hours gave 11% wt and 7% wt for **LiAB** and **NaAB**, respectively, to give fully desorbed end products. Based on X-ray and ^{11}B NMR analysis, the dehydrogenated products of metal amidoboranes consist of borazine-like or poly-borazine-like compounds, a similar phenomenon as observed for **AB** dehydrogenation. Several problems are associated with metal amidoboranes. Along with the lack of facile reversibility, the purity of the hydrogen released was later found to suffer from simultaneous formation of ammonia and the $[NH2BH3]^{-}$ anion.

Replacement of H with an alkyl group can also increase the electron density on **AB**. Another **AB** modification includes methyl derivatives such as $MeNH_2BH_3$ (**MeAB**). **MeAB** might have a lower H% wt of 18% compared to **AB**, but its dehydrogenation happens at a lower temperature of ~80°C (**AB** is ≤90°C).[12,13] **Scheme 2.2**(**A**) shows the dehydrogenation pathway of **MeAB** in which a **DADB** analogue is initially formed and gives the cyclic end product *N*-trimethylcyclotriborazane. This end product is analogous to the borazine end product of **AB** dehydrogenation. According to TGA and mass spec studies by Bowden *et al.*, a volatile compound was observed during dehydrogenation of

MeAB and was identified to be the *N*-trimethylcyclotriborazane end product.[13,14] They found that the volatility of *N*-trimethylcyclotriborazane is affected by the rate of heating of **MeAB**. Just like the borazine, this borazine-like compound resulting from dehydrogenation of MEAB is an undesired end product that is detrimental to the fuel cell catalyst. At slower rates, such as 0.5°Cmin^{-1} rather than 2°Cmin^{-1}, the cyclic molecule can crosslink to another molecule to form an amorphous solid, which prevents further mass loss due to sublimation as shown in **Scheme 2.2**(**B**). This non-volatile amorphous solid can be related to the observed crosslinked product of borazine which possess rehydrogenation issues.

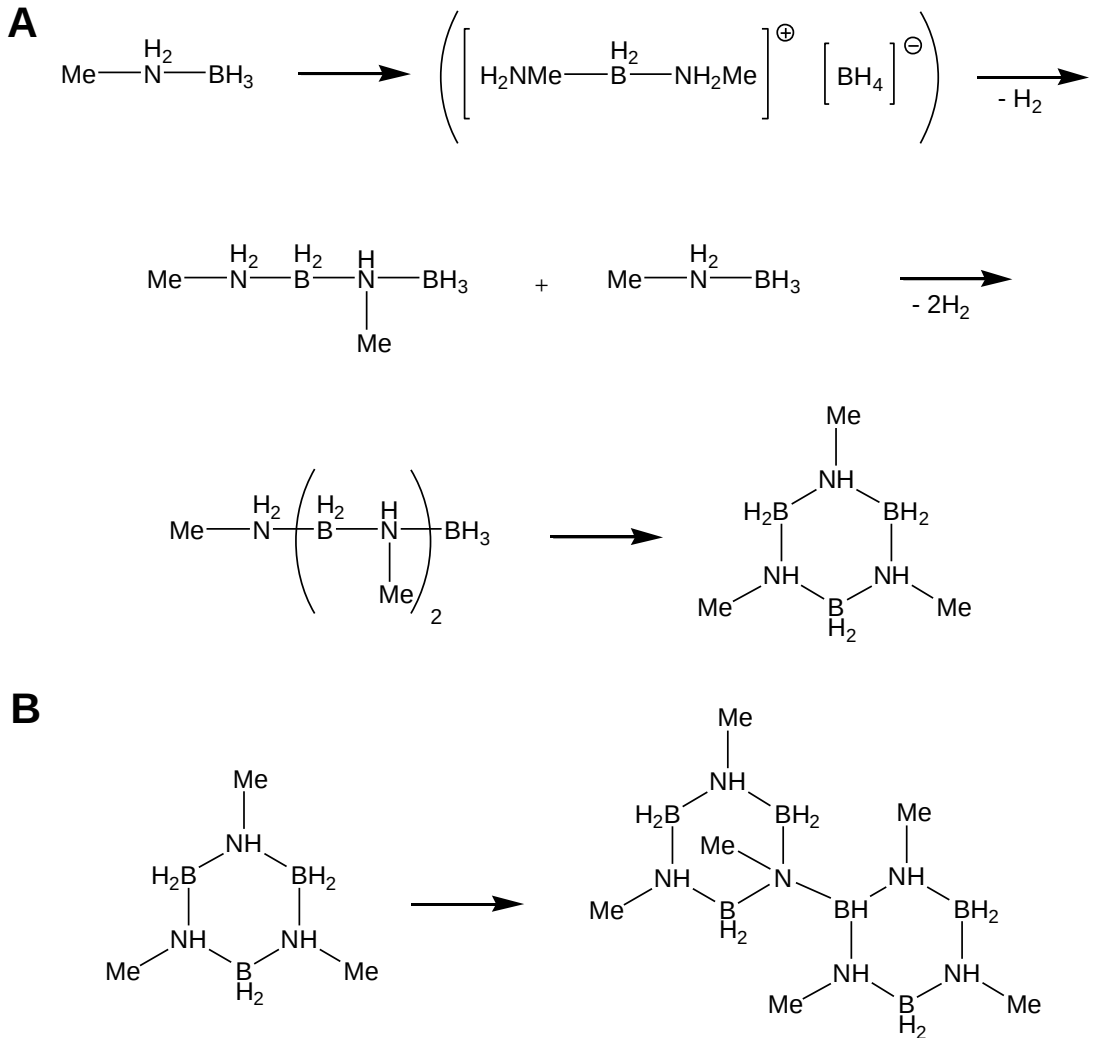

Scheme 2.2[13]: (**A**) The dehydrogenation of **MeAB** which forms a diammoniate of diborane analogue before forming a trimer and eventually the *N*-trimethylcyclotriborazane end product. (**B**) Two molecules of *N*-trimethylcyclotriborazane can cross-link and for an amorphous solid.

Another **AB** modification include tethering two molecules of **AB** with different alkyl chain lengths. Li *et al.* synthesized their compounds 1,2-di-aminopropane borane (**1,2-TMDAB**) and 1,3-di-aminopropane borane (**1,3-TMDAB)**, shown in **Figure 2.1**, using BH_3·THF and 1,2-diaminopropane and 1,3-diaminopropane, respectively.[15]

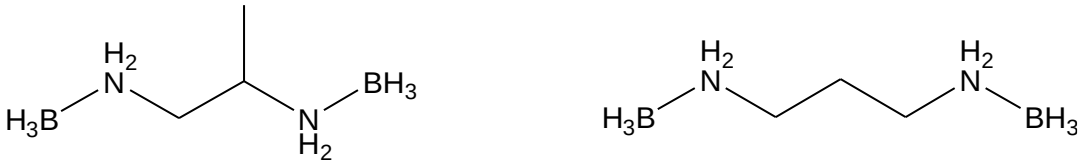

1,2-TMDAB 1,3-TMDAB

Figure 2.1: Derivatives in which two molecules of **AB** are tethered together using different alkyl chains.

Both their compounds possess 15.6% wt hydrogen and release hydrogen at two different temperatures. **1,2-TMDAB** expels hydrogen at 125°C and 185°C while **1,3-TMDAB** is at 150°C and 194°C. No impurities such as borazine, NH_3, or B_2H_6 were detected during dehydrogenation and only pure hydrogen was expelled. The recorded hydrogen release for **1,2-TMDAB** and **1,3-TMDAB** were 7.4% and 6.3% wt hydrogen, respectively. Using ^{11}B NMR, it was assumed that dehydrogenation of their compounds form C-B-N polymers, similar to **AB** and other **AB** derivatives.

Luo *et al*. approached the alkylation of **AB** using a different method of incorporating the molecule as part of a ring, as shown in **Figure 2.2**.[17] Their 1,2-BN cyclohexane (**1,2-BNCyc**) is isoelectronic and isostructural to cyclohexane and has a 9.4% wt hydrogen. After heating **1,2-BNCyc** in toluene for two hours at 150°C, one equivalent of H_2 per molecule was observed to be released. This 4.7% wt H_2 release leads to a formation of the trimer in **Figure 2.2**, which is quite different from the oligomer/polymer formation as end products of previous **AB**

derivatives. Some disadvantages of **1,2-BNCyc** include its more intricate synthesis and isolation procedures along with the low hydrogen % wt release.

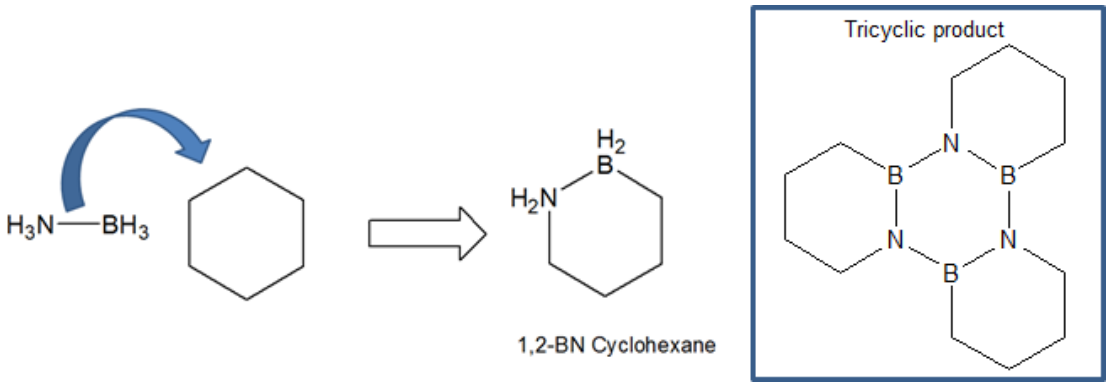

Figure 2.2: Incorporation of **AB** as part of the ring makes a new derivative which is isoelectronic and isostructural as cyclohexane. The tricyclic product resulting from dehydrogenation of 1,2-BN Cyclohexane.

Background:

Considering the concurrent problems with **AB** and its derivatives, it may be wise to consider molecules that are derived from another parent model compound rather than **AB**. Diammoniate of diborane (**DADB**, $[H_3NBH_2NH_3]^+[BH_4]^-$) has the same hydrogen % content as **AB**. The formation of **DADB** has been evident as a product of $\mathbf{ABH_2}$ decomposition, an alternative product in **AB** synthesis, and an intermediate of **AB** dehydrogenation. [4,6-8] **DADB** analogues are also formed in the dehydrogenation of **MeAB** and metal amidoboranes.[10,13]

In its initial discovery, it took several years of dispute to finally assign the correct molecular structure of **DADB**. The first proposed structure was

$[H_3BNH_2BH_3]^-[NH_4]^+$, which was then corrected by ^{11}B NMR, Raman, X-ray crystal structure, and calculation studies to the $[H_3NBH_2NH_3]^+[BH_4]^-$ structure.[4,18]

As an isomer of two molecules of **AB**, **DADB** has the same hydrogen % wt of 19.6%. However, because the two have identical empirical formulas, **DADB** suffers from the same dehydrogenation impurities and regeneration problems as its isomer. Just like **AB**, modifications of **DADB** may solve these problems and provide a completely new collection of hydrogen storage molecules.

Using the same strategy as Luo *et. al.*[17], **DADB** can also be incorporated in a ring by tethering its amine groups with different alkyl chain lengths. When Li *et al.*'s **1,3-TMDAB** derivative was synthesized and introduced in the gas phase using a mass spectrometer, the cyclic ion, shown in **Figure 2.3**, was observed. This may be due to the fact that the **1,3-TMDAB** is a neutral linear compound which is undetectable in the mass spectrometer while the cyclic structure alone is an ion. Other ring homologues were also observed in the mass spectrometer from compounds synthesized using different alkyl chain lengths. Even though it has not been purified in the condensed phase, mass spectrometry gives the chance to isolate these cyclic cations and study their dehydrogenation properties in the gas phase. This chapter describes the gas phase study of these **DADB** derivatives, their dehydrogenation, and their products. Using other spectroscopic methods, it has been possible to characterize these novel cation derivatives along with their daughter fragments. Using all this information, it can be claimed

that these **DADB** cation derivatives show some potential as hydrogen storage candidates.

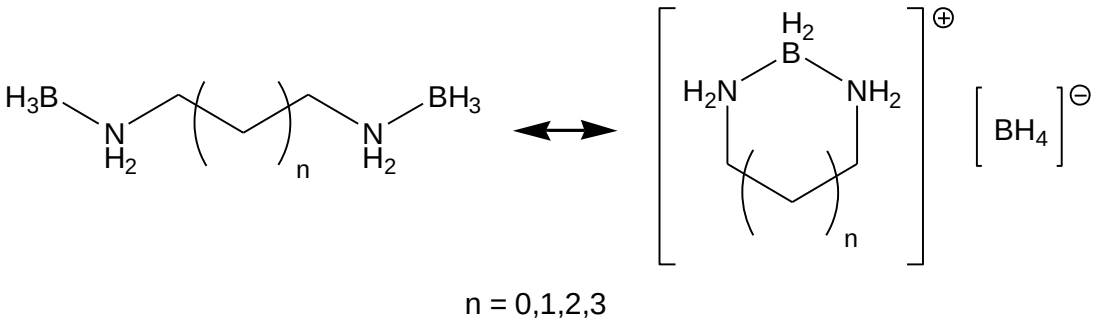

n = 0,1,2,3

Figure 2.3: A **DADB** derivative cyclic ion which was observed in the gas phase via mass spectrometer which is an isomer of the neutral linear compound.

Experimental:

I. General

Borane in dimethyl sulfide was purchased from Aldrich. The chemical was stored in an acro-sealed bottle and kept in the freezer after opening. 1,3-diaminopropane and putrescine were acquired from Acros Organics and cadaverine was from Tokyo Chemical Industry. All diaminoalkane starting materials were kept sealed after opening. The NMR solvent (acetonitrile-d_3) and borane-d_3 in dimethyl sulfide were purchased from Cambridge Isotope Laboratories and kept sealed after opening.

II. Synthesis

The synthesis of 1,3-di-amino propane was followed, with some slight modification, from a previously published procedure by Li *et al.* in which they

were able to acquire the same compound.[15] The same spectra for the analysis of 1,3-diaminopropane was included as part of Li *et al.*'s publication. The synthesis of ethylene diaminoborane was followed, with some slight modification, from a previously published procedure of Edwards and Kelly in which they were able to get the same compound.[19] The same spectra for the characterization of ethylene diaminoborane was included in Edwards and Kelly's paper. The glassware, spin vanes, and syringes were oven dried before use. Nitrogen gas was purged into a 50 ml round bottom flask as it is cooled down to room temperature. After cooling, a septum cap was affixed and a N_2-filled balloon was attached via a hypodermic needle, with the balloon kept inflated with nitrogen to make sure that the whole system is under inert atmosphere. The round bottom was cooled in an ice-bath, charged with 18ml of dry THF, and the solution was allowed to cool to 0°C. BH3.Me2S (18.6mmol) was added, allowed to cool, and followed by the dropwise addition of the diaminoalkane starting material (7.4mmol) while stirring and cooling. The reaction was allowed to warm up to room temperature overnight and the solvents removed under vacuum to give a crude white powder. Purification of the crude product consisted of dissolving the solid in a minimum amount of acetonitrile and passing it through a silica column using ethyl acetate as eluent. About 250-300 ml of the eluent solvent was used. The eluent collected was concentrated *in vacuo* to give a white powder.

The dideuterated samples were prepared by substituting the borane starting material with borane-d_3 in dimethylsulfide. As for the tetradeuterated

samples for the mass spectrometry, the purified compound were dissolved in ethanol-OD in which the amine protons are exchanged to deuteria and the solution is directly injected into the instrument.

III. Characterization

400 MHz ^{1}H NMR spectra were recorded using Varian Inova 400 (2 channel Z axis gradient spectrometer). 96 MHz ^{11}B NMR spectra were recorded using Bruker Avance 300 (2 channel Z axis gradient spectrometer).

Density functional theory (**DFT**) calculations were used to predict the most stable conformation of the molecules along with their gas phase infrared spectra (both normal modes and, where appropriate, anharmonic frequencies). Comparison between the predicted and experimental infrared spectra confirmed the structures of the molecules.

Infrared Multiple Photon Dissociation (IRMPD) spectroscopy was conducted at the FOM Institute for Plasma Physics at Rijnhuizen in the city of Nieuwegein, The Netherlands (a suburb of Utrecht). The ions were generated and introduced to the FT-Ion Cyclotron Resonance mass spectrometer via electrospray ionization (**ESI**) source. The ions were isolated *in vacuo* for several seconds, mass selected, and subsequently irradiated for several seconds with pulses generated from the infrared laser. Three different kinds of laser were utilized: a fixed frequency CO_2 laser used to study ion dissociation, as well as two tunable lasers for characterization. The free electron laser for infrared

experiments (FELIX) is a tunable IR source that recorded the fingerprint domain from 300 – 1800 cm^{-1} region while the Nd:YAG laser pumped Optical Parametric Oscillator tunable laser recorded the IR in the domain 2350-3900cm^{-1}. Experimental IRMPD spectra were obtained *via* action spectroscopy where the abundance of a selected daughter ion is plotted as a function of the FELIX laser frequency.[20-22] **Figure 2.4** shows a schematic representation of the FELIX interface with an ICR.

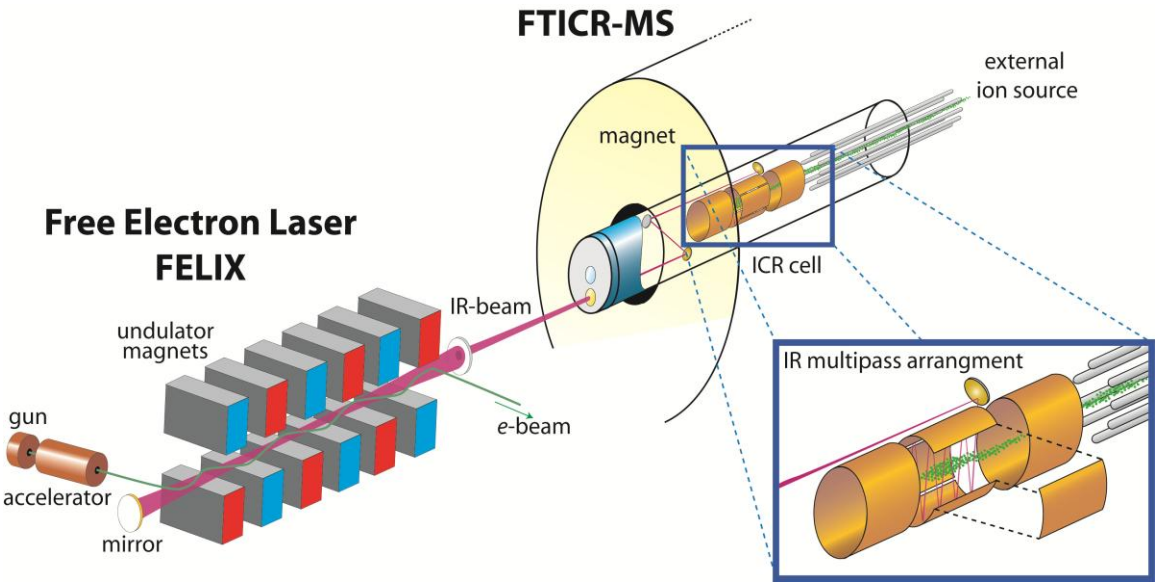

Figure 2.4[20]: A schematic representation of FELIX which uses tunable lasers to obtain an IRMPD spectra of gaseous ions in the gas phase. Image was taken from the Polfer *et al.*'s paper, Figure 1.

Inelastic neutron scattering (**INS**) spectroscopy has been described in detail elsewhere[23,24] and briefly described in the previous chapter. In a typical INS experiment, preparation of the sample involved packing about 0.4-1.5 grams of the solid compound in an inert atmosphere. The sample was cooled to 10 K

and irradiated at constant temperature for 10-12 hours in the Filter Difference Spectrometer (**FDS**) at the Lujan Neutron Center situated at the Los Alamos National Lab. The assistance of Dr. Luke Daemen is gratefully acknowledged.

IV. Decomposition

A linear triple quadruple mass spectrometer was utilized to do tandem MS/MS experiments. Lab frame energies of 4 to 20V were used with Ar as collision gas for these experiments at the Faculté de Pharmacie, Université Paris-Sud XI, Châtenay-Malabry. The linear quadrupole consists of three linear quadroples: Q1, q2, and Q3. In Q1, alternating AC and DC electric fields isolate an ion with a specific mass-to-charge ratio. In q2, only rf is used for axialization and collision, where the isolated ions collide with the Ar gas. Q3 then uses AC and DC electric fields, just like Q1, to scan all the resulting fragment ions.

In a FT-ICR dissociation experiment, a specific ion was isolated and irradiated with CO2 laser for several milliseconds to promote dissociation. The isolated ion can either be the parent ion or a resulting daughter ion. By isolating the daughter ion and further dissociating it with the laser, MS/MS experiments can be performed.

Mass spectrometric analysis of spent molecules was done using Agilent 6210 LC-Tof. About 1-2mg of the sample was dissolved in 1.5mL of methanol and introduced to the instrument operating in the “Multimode”, which optimizes both ESI and atmospheric pressure chemical ionization (**APCI**) parameters.

VI. Theory/Calculation

Geometry optimization and anharmonic vibrational frequencies were calculated for the cyclic cations using the Gaussian 09 program suite at the B3LYP/aug-CC-PVTZ level. DFT calculations were used to confirm and characterize the formation of these cations.

Results:

Characterization:

The different cyclic ions that were prepared and studied included 2-bora-1,3-diazacyclooctanium ion (**BDACOct**), 2-bora-1,3-diazacycloheptanium ion (**BDACHept**), 2-bora-1,3-diazacyclohexanium ion (**BDACHex**), and 2-bora-1,3-diazacyclopentanium ion (**BDACPent**) and shown in **Figure 2.5**.

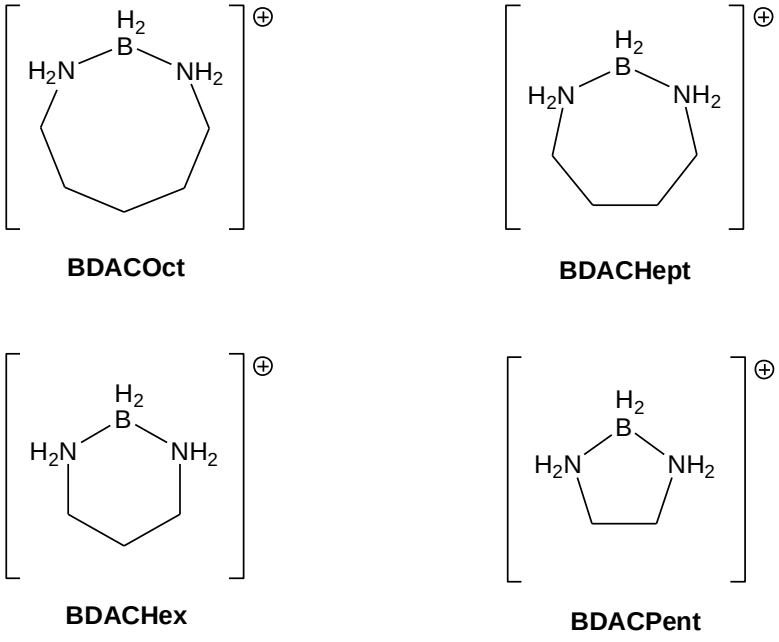

Figure 2.5: 2-bora-1,3-diazacycloalkanium ions isolated in the gas phase via mass spectrometry. Each ion is isoelectronic to the corresponding cycloalkane hydrocarbon counterpart.

These cyclic ions have a similar structure as **DADB** and contain only sp^3 centers, which makes them isoelectronic (and very similar in structure) to the corresponding hydrocarbons. **BDACPent** has a hydrogen % weight of 13.7%, **BDACHex** 13.8 %, **BDACHept** 13.9%, and **BDACOct** 13.9%. All of these cyclic ions satisfy the DOE requirement for hydrogen storage molecule. As stated above, the formation of these cyclic ions arises from the introduction of their neutral *bis*bora-diazaalkane linear compounds into the gas phase. To make sure that the right cyclic ions are formed upon gas phase injection, the corresponding linear compounds were first characterized based on their structure and purity. **Figure 2.6** shows the NMR spectra in solution (acetonitrile-d_6) of each of the linear compounds.

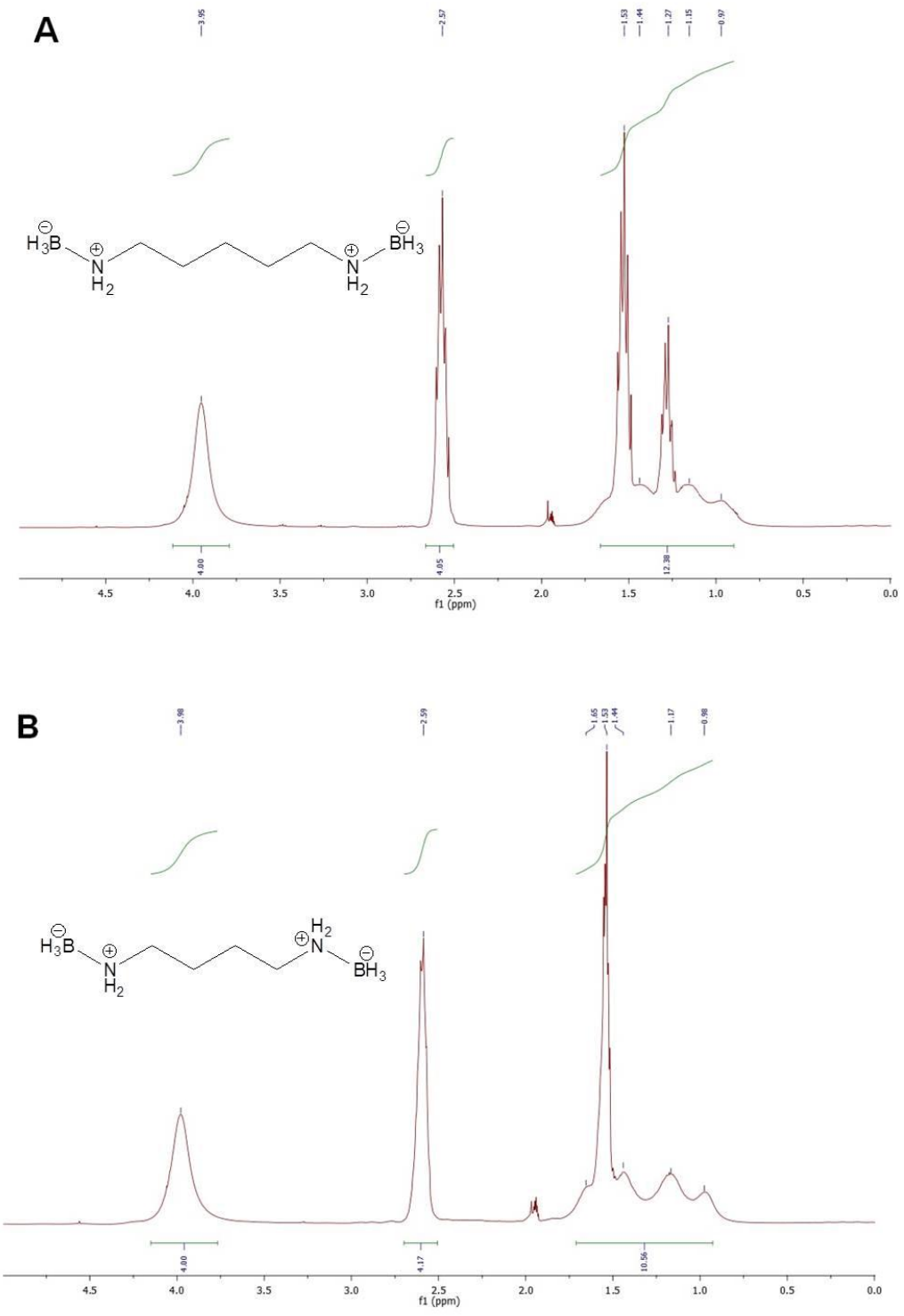

Figure 2.6.1: ^{1}H NMR (300 MHz) spectra of neutral linear compounds (**A**) *bis*-bora -N,N'-1,7-diazaheptane and (**B**) *bis*-bora-N,N'-1,6-diazahexane.

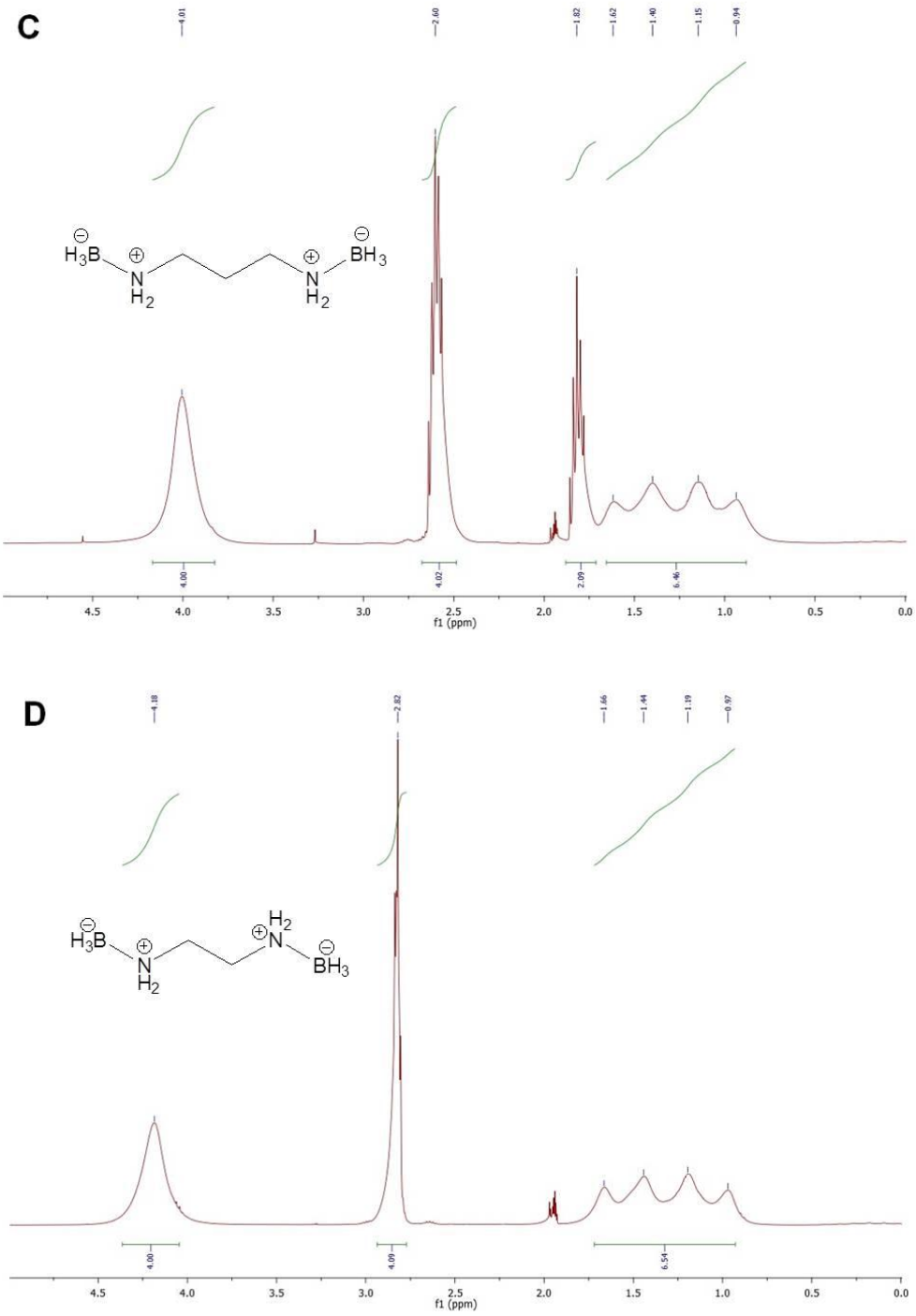

Figure 2.6.2: ^{1}H NMR (300 MHz) spectra of neutral linear compounds (**C**) *bis*-bora-N,N'-1,5-diazapentane and (**D**) *bis*-bora-N,N'-1,4-diazabutane.

The broad quartet at δ = 0.75 to 1.75 ppm and broad peak at δ = 3.75 to 4.5 ppm are characteristic of the BH_3 and NH_2 groups for each compound, respectively. The longer the methylene chain is, the more sets of peaks are present in the alkane region. The INS profiles for the neutral linear compounds in solid phase were recorded and are reproduced in **Figure 2.7**.

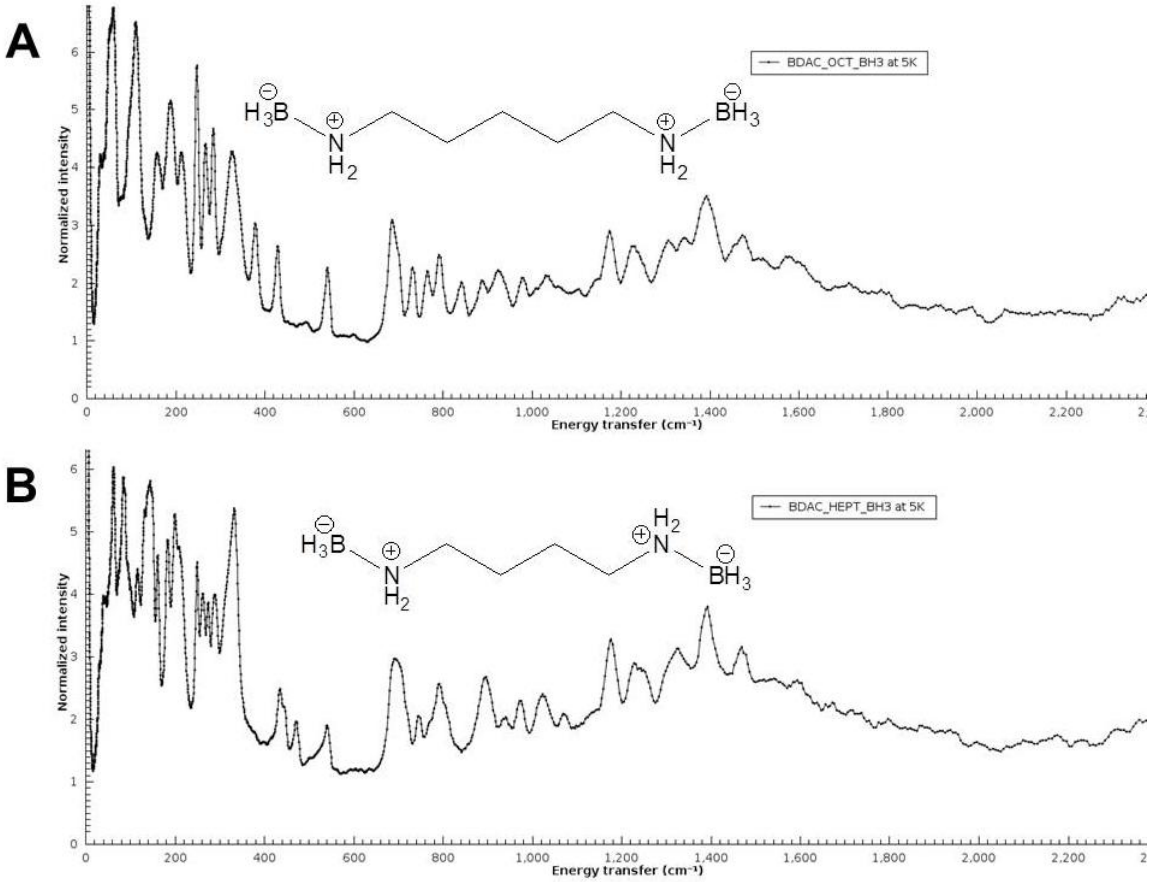

Figure 2.7.1: INS spectra of neutral linear compounds (**A**) N,N'-*bis*bora-1,5-diazapentane and (**B**) N,N'-*bis*bora-1,4-diazabutane.

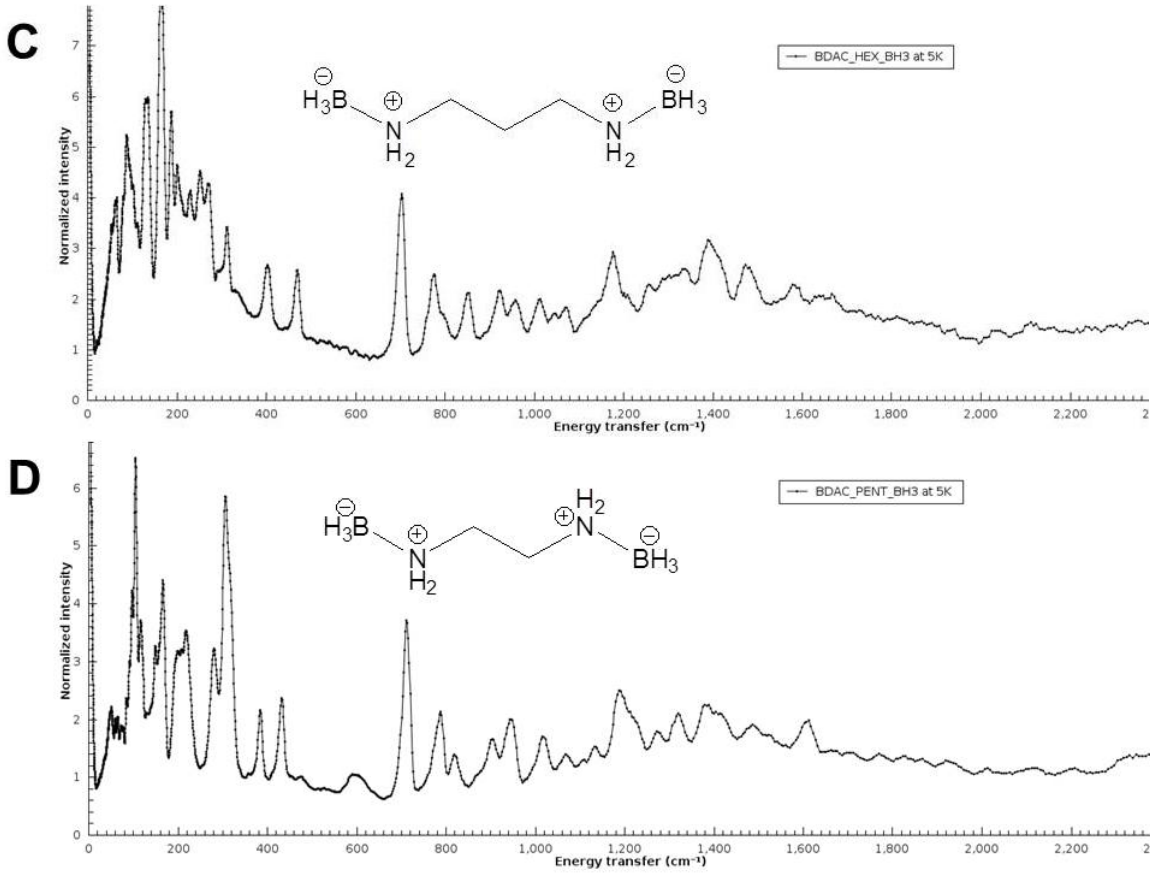

Figure 2.7.2: INS spectra of neutral linear compounds (**C**) N,N'-*bis*bora-1,3-diazapropane and (**D**) N,N'-*bis*bora-1,2-diazaethane.

After introduction of the linear compounds to the gas phase via mass spectrometry, the cyclic ions were formed and isolated. The experimental IR spectra of the isolated parent ions (with an exception of **BDACPent**) were acquired by IRMPD spectroscopy in collaboration with Dr. Jos Oomens and are shown as blue silhouettes in **Figure 2.8**. Density functional theory (**DFT**) calculations were utilized to predict theoretical IR spectra, shown as red solid lines in the foreground, for each compound which was compared to the corresponding experimental spectrum. The comparisons between the

experimental and theoretical spectra show good fits, confirming the formation and presence of the cyclic ions in the gas phase. The cause of the peak mismatch in the 1800 to 2000 cm^{-1} region for **BDACHept** and **BDACHex** (two peaks of equal intensity predicted, but only a single peak observed) are still unknown and under investigation. It is also important to note that because DFT calculations are based on IR absorptions while IRMPD acquires a spectrum through "action spectroscopy"[22] following the absorption of many IR photons, the intensity differences between theoretical and observed bands can be neglected, only the positions of the peaks are important.

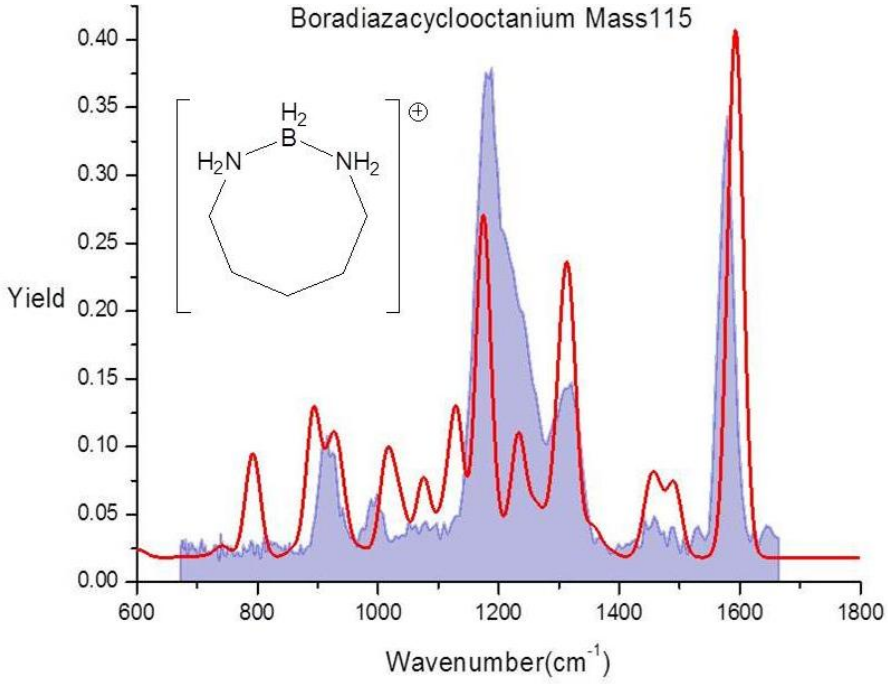

Figure 2.8.1: Comparison between the experimental IRMPD spectra (blue silhouette) and theoretical DFT spectra (red solid line) for **BDACOct** confirming the presence of the cyclic cations in the gas phase.

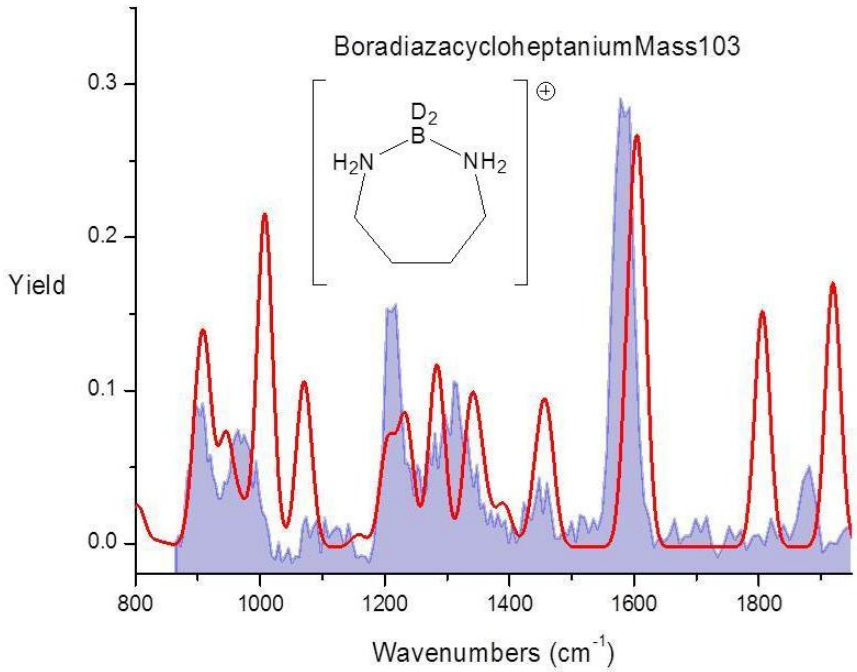

Figure 2.8.2: Comparison between the experimental IRMPD spectra (blue silhouette) and theoretical DFT spectra (red solid line) for **BDACHept-d_2** confirming the presence of the cyclic cations in the gas phase..

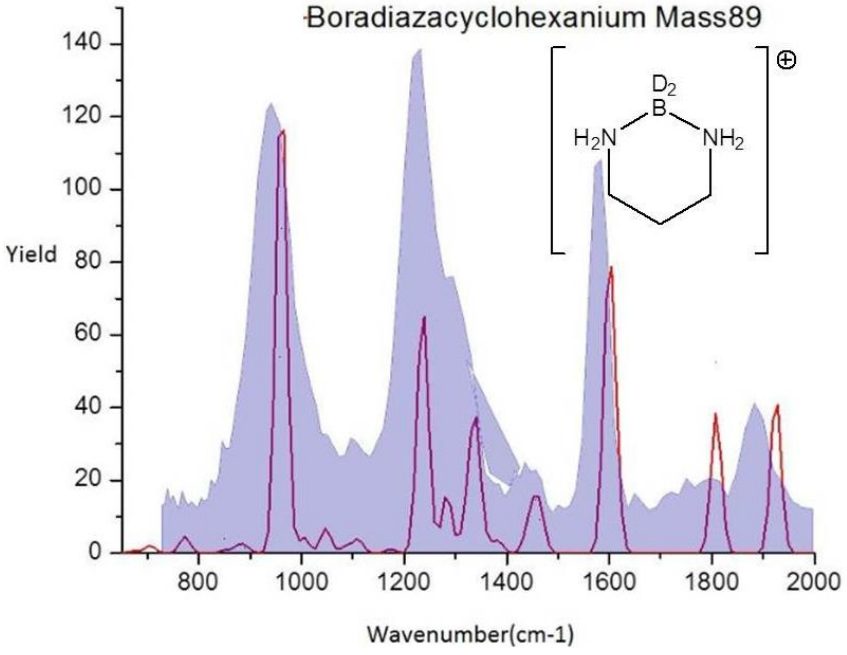

Figure 2.8.3: Comparisons between the experimental IRMPD spectra (blue silhouette) and theoretical DFT spectra (red solid line) for **BDACHex-d_2** confirming the presence of the cyclic cations in the gas phase.

Hydrogen Desorption and Decomposition:

Two different kinds of mass spectrometer were used to study the dehydrogenation of the cyclic ions. In a triple quad mass spectrometer (**TQMS**), **BDACOct** was isolated (principal ion at *m/z* 115) and subjected to collisionally activated dissociation (**CAD**) as shown in **Figure 2.9**(**A**). The activation leads to a loss of 2 moles of H_2 to give *m/z* 113 and then *m/z* 111 daughter ions. Along with dehydrogenation, prominent peaks from loss of neutral molecules with combined mass of 19 and of 47 were observed to give *m/z* 96 and *m/z* 68. One possible pathway that would give loss of 19 atomic mass units (**amu**) is expulsion of an ammonia molecule followed by H_2 expulsion (or *vice versa*). (**BDACHex** dehydrogenation/decomposition below explains this more in detail.) Loss of 47 amu can be attributed to loss of 19 amu followed by loss of ethylene (28 amu).

Using the ion cyclotron resonance (**ICR**) mass spectrometer in **Figure 2.9**(**B**), CO_2 laser activation of the *m/z* 115 parent ion revealed the same decomposition pathway observed from TQMS, as well as peaks at *m/z* 86 and *m/z* 84. We speculate that these latter ions come from loss of ethyl radical or from loss of the elements of BNH_4 (29 amu) and ethyl radical (or BNH_4) plus H_2, respectively. **Figure 2.10** shows the confirmation of the structure of the daughter ion *m/z* 113 by IRMPD and the calculated spectroscopic comparison. The dehydrogenated *m/z* 113 daughter ion was activated by the CO_2 laser to give peaks *m/z* 96 (a loss of ammonia), *m/z* 68 (a loss of an ethylamine), and *m/z* 57 (a loss of butene).

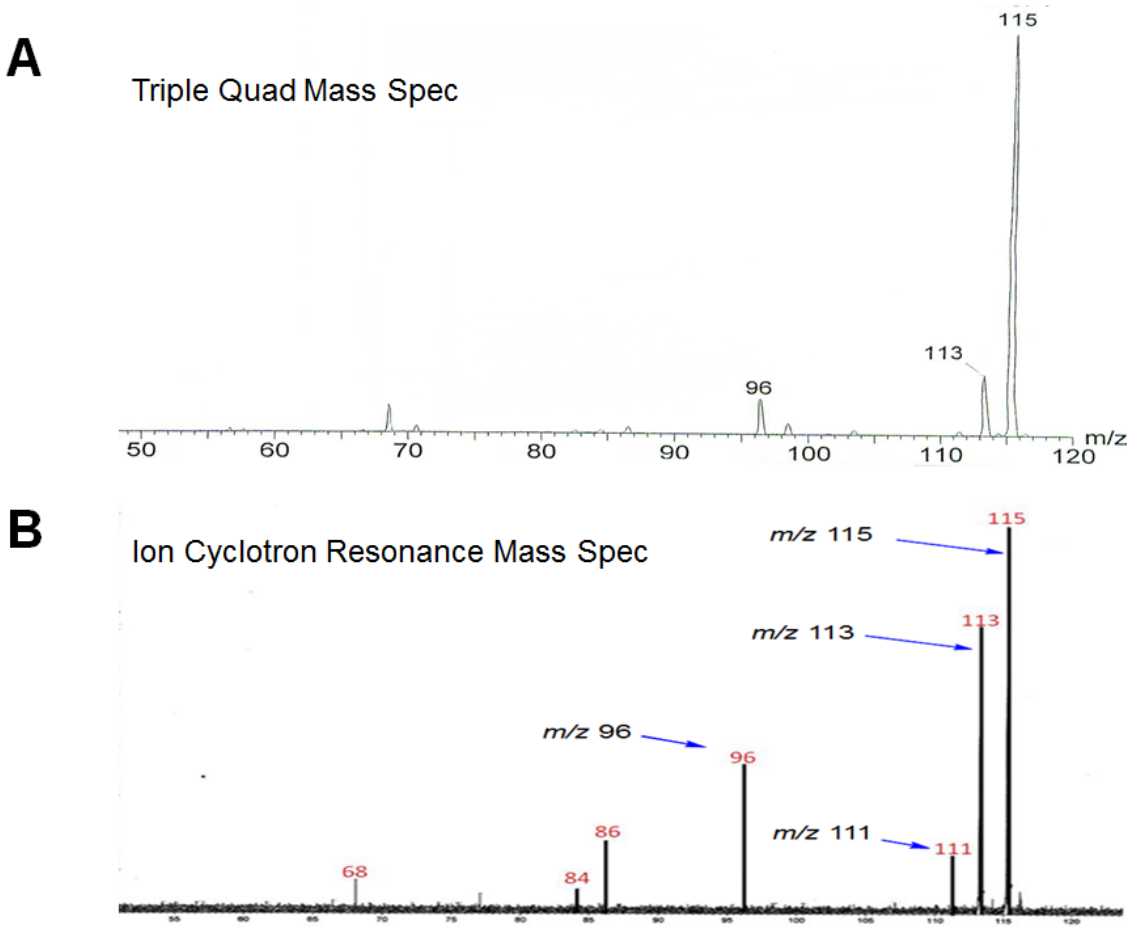

Figure 2.9: Analysis of **BDACOct** using (**A**) TQMS and (**B**) ICR mass spectrometers showing expulsion of hydrogen and also decomposition.

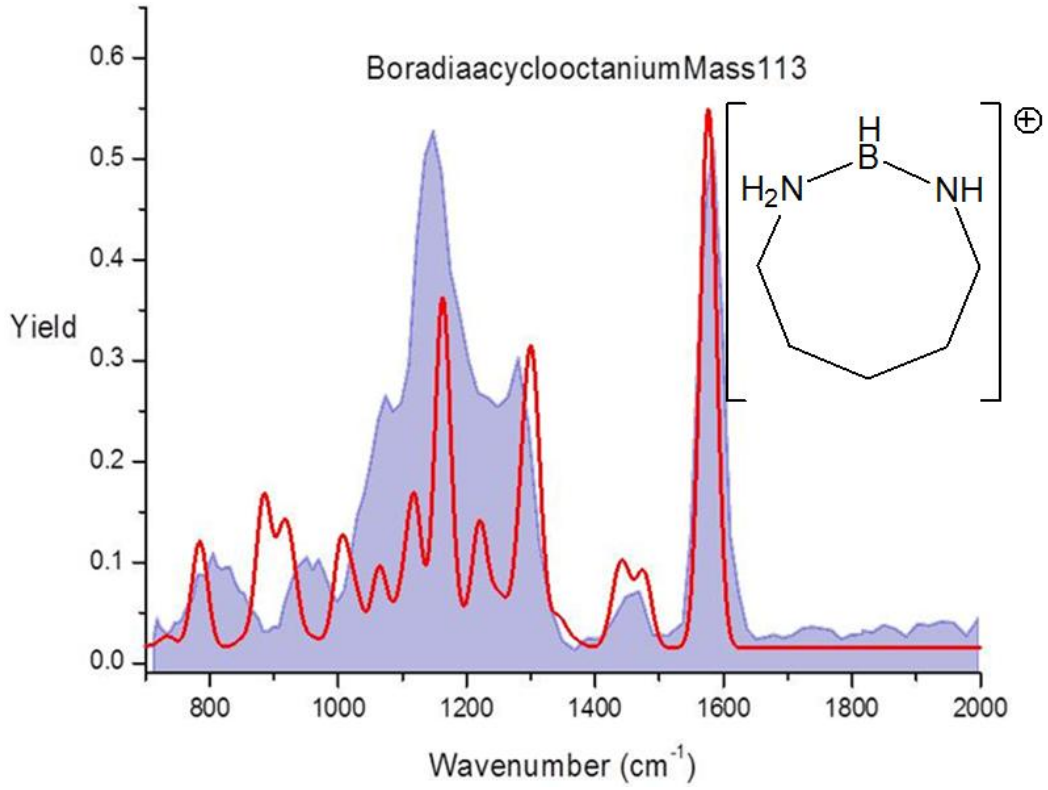

Figure 2.10: Experimental IRMPD and DFT calculated spectra comparison that confirms the structure of the *m/z* 113 daughter ion.

Figure 2.11(**A**) shows the mass spectrum of **BDACHept** (principal ion at *m/z* 101) after CAD using TQMS. Unlike the bigger ring homologue **BDACOct**, this cyclic ion releases only one equivalent of H_2 to give *m/z* 99. Expulsion of ammonia gave the *m/z* 84 daughter ion. ICR mass spectrometry analysis, depicted in **Figure 2.11**(**B**), showed the same dehydrogenation and decomposition pathways but with further expulsion of a propene molecule from the *m/z* 99 daughter ion. The structure of the m/z 57 daughter ion was confirmed by IRMPD and calculated spectra comparison shown in **Figure 2.12**.

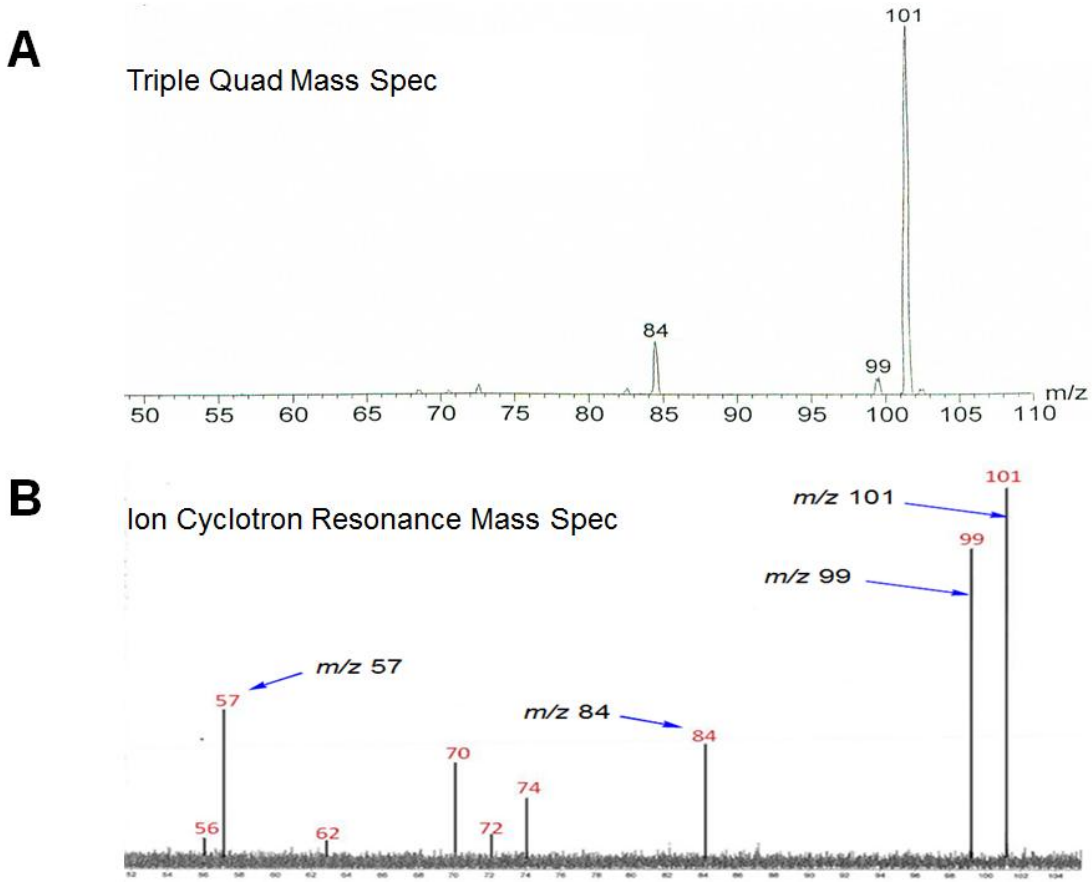

Figure 2.11: **BDACHept** was subjected to (**A**) TQMS and (**B**) ICR mass spectrometers analysis and showed release of one equivalent of H_2. Other fragments were formed during activation.

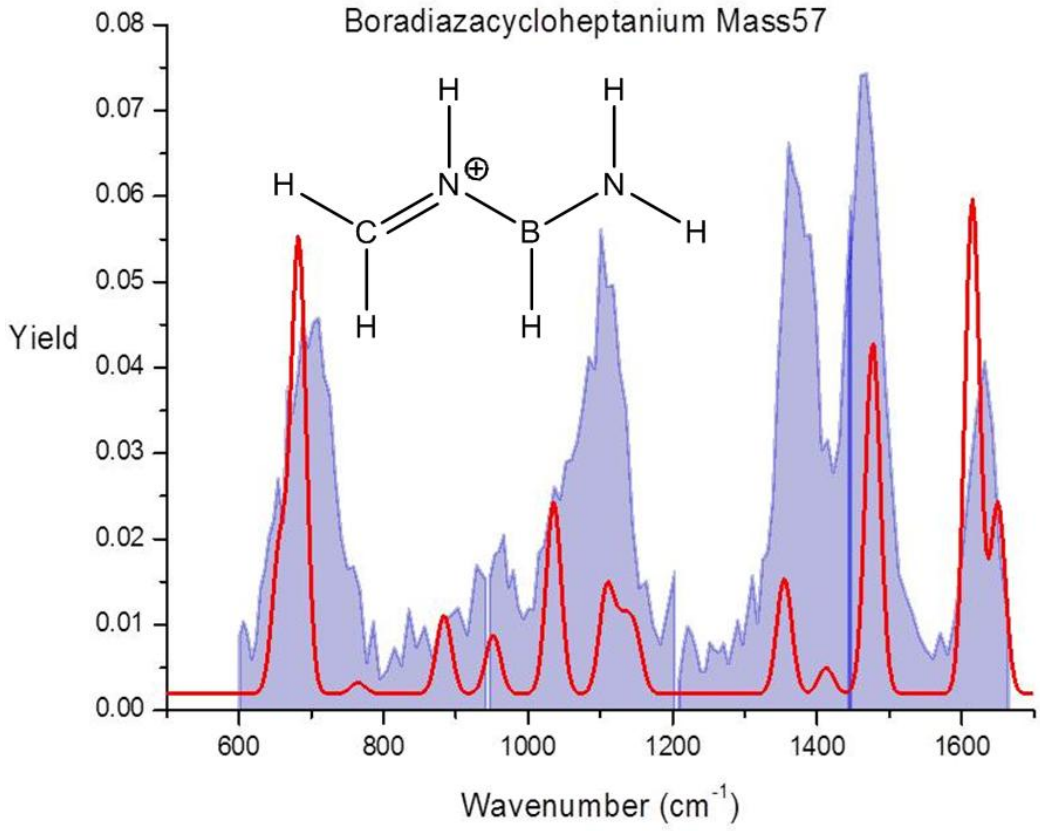

Figure 2.12: Comparison of the experimental IRMPD spectrum with the theoretical spectrum confirms the structure of the daughter ion after successive expulsion of hydrogen and propene molecules from **BDACHept**.

BDACHex (principal ion at *m/z* 87) was isolated in TQMS and CAD gave a loss of H_2 to give *m/z* 85 in **Figure 2.13**. From *m/z* 85, a loss of an ethene molecule gave a daughter ion *m/z* 57, a daughter ion with a similar structure to **BDACHept**'s *m/z* 57 daughter ion above. The parent ion also successively expelled ammonia followed by H_2 (or vice versa) to give *m/z* 68, the same decomposition behavior as seen with **BDACOct**. This pathway was confirmed by isolation of the daughter ion *m/z* 85 which unimolecularly *does* not give *m/z* 68

after activation as shown in **Figure 2.14**, proving that *m/z* 68 directly comes from the parent ion and strongly suggesting that NH_3 loss precedes H_2 loss.

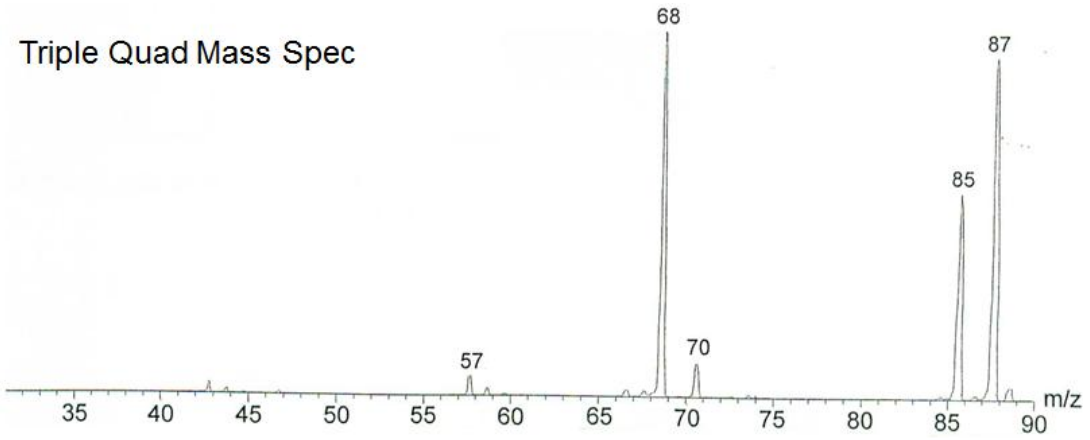

Figure 2.13: TQMS of **BDACHex** which goes through dehydrogenation and decomposition give the daughter fragments shown above.

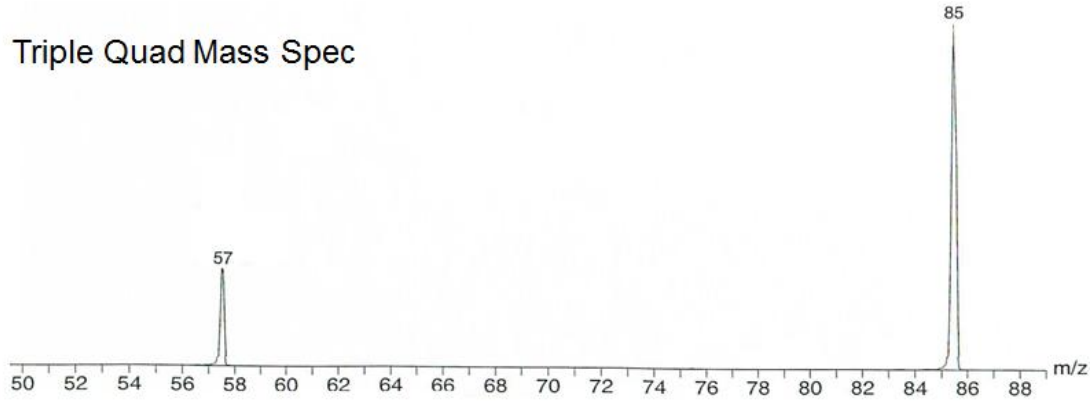

Figure 2.14: Isolation and fragmentation of daughter ion *m/z* 85 proved that hydrogen is first expelled before ammonia from the parent ion.

BDACPent (principal ion at *m/z* 73) was isolated in the gas phase using TQMS, as shown in **Figure 2.15**, and expelled an H_2 molecule to give *m/z* 71 or an ammonia molecule to give *m/z* 56. When the *m/z* 71 daughter ion was isolated and activated by CAD in **Figure 2.16**, additional loss of H_2 was observed

to give *m/z* 69. Also, *m/z* 71 expelled an ammonia and a hydrogen cyanide molecule to give daughter ions *m/z* 54 and *m/z* 44, respectively.

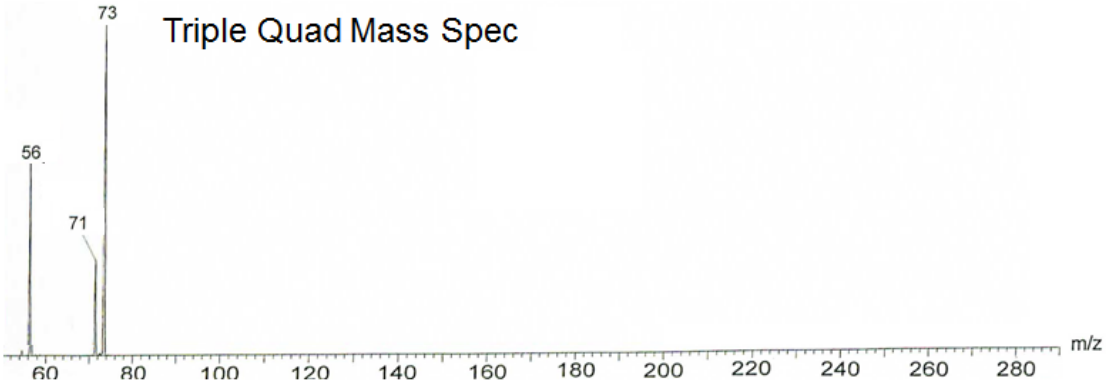

Figure 2.15: **BDACPent** was isolated and activated to release hydrogen along with ammonia.

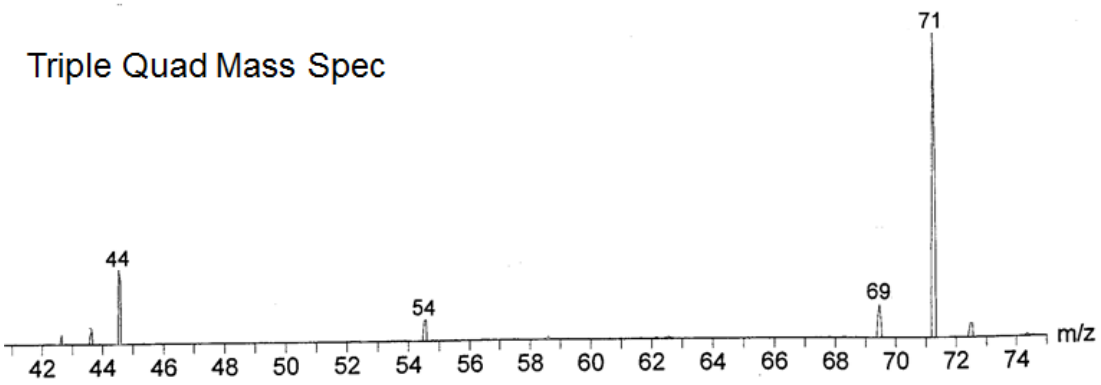

Figure 2.16: Further activation of the isolated daughter ion *m/z* 71 showed that another molecule of H_2 can be released.

Out of all the four samples, only the 8-membered ring gives rise to loss of two H_2 molecules (**BDACPent** loss of two H_2 molecules is very small). Does this represent loss of two hydrogen atoms from nitrogen (one from each nitrogen atom) and two from boron, as **Scheme 2.3** illustrates? Because the ion from the double H_2 loss did not have sufficient intensity for IRMPD spectroscopy, a mass

spectrometric labeling experiment answers that question. Deuterated analogues that were prepared included **BDACOct-*d*$_4$**, **BDACHex-*d*$_4$**, **BDACHex-*d*$_2$**, and **BDACPent-*d*$_4$**. **Figure 2.17** depicts the ICR mass spectrum of **BDACOct-*d*$_4$** (*m/z* 119) showing a loss of HD plus H_2 as the exclusive pathway for double dehydrogenation. Since the N-B-N linkage contains only two hydrogens (and four deuteria), the product ion must result from loss of at least one hydrogen atom from the carbon chain. Hence, **Scheme 2.3** does not occur. The sets of peaks at *m/z* 97 and *m/z* 87 are due to isotopomers of the fragments which includes different combinations of the amounts of hydrogen and deuterium.

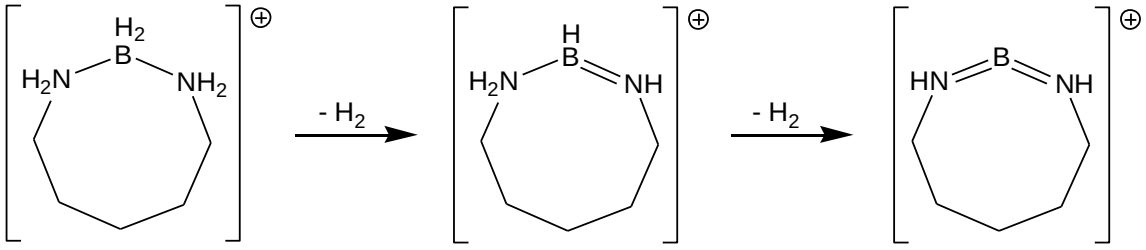

Scheme 2.3: A possible double dehydrogenation pathway for **BDACOct**. Mass spectrometric labeling studies shows disproves this pathway and suggests that the methylene chain may be participating in the dehydrogenation.

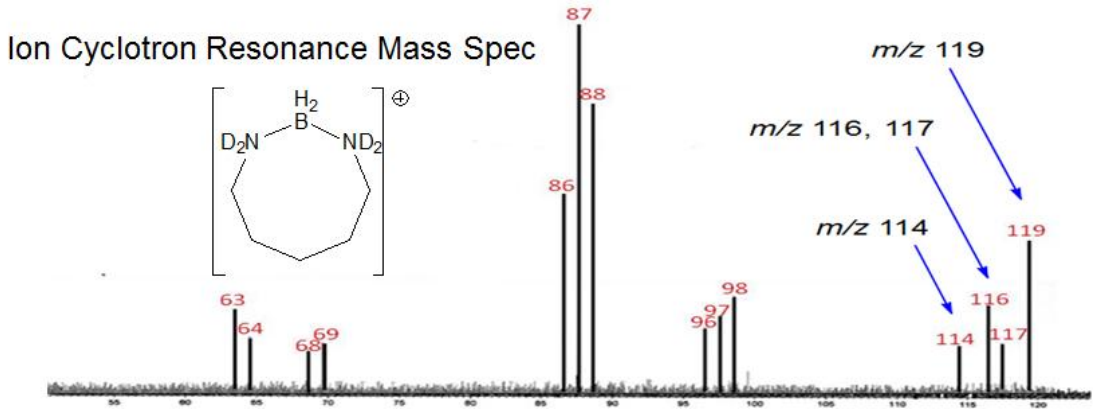

Figure 2.17: ICR analysis of tetradeuterated **BDACOct** which showed expulsion of isotopomers of hydrogen, as well as loss of H2 plus HD (*m/z* 114). The triplet sets of peaks at lower *m/z* also correspond to expulsion of isotopomer fragments.

As for the tetradeuterated **BDACHex** (principal ion at *m/z* 91) isolated and activated using TQMS in **Figure 2.18**(**A**), a loss of H_2 and HD molecules give *m/z* 89 and *m/z* 88, respectively, in a 1 to 5 ratio. A loss of isotopomers of ammonia followed by hydrogen from the parent ion gave daughter ion *m/z* 69. ICR was used to analyze the dideuterated **BDACHex** in **Figure 2.18**(**B**) and showed release of H_2 and HD to give *m/z* 87 and *m/z* 86, respectively, in almost the same quantity (both ^{10}B and ^{11}B isotopomers were present, which accounts for *m/z* 88, most of *m/z* 85, and *m/z* 57). The isotopomer *m/z* 58 daughter ion (*m/z* 57 in the undeuterated analogue) was also observed from expulsion of a neutral ethene molecule from the dehydrogenated daughter ion.

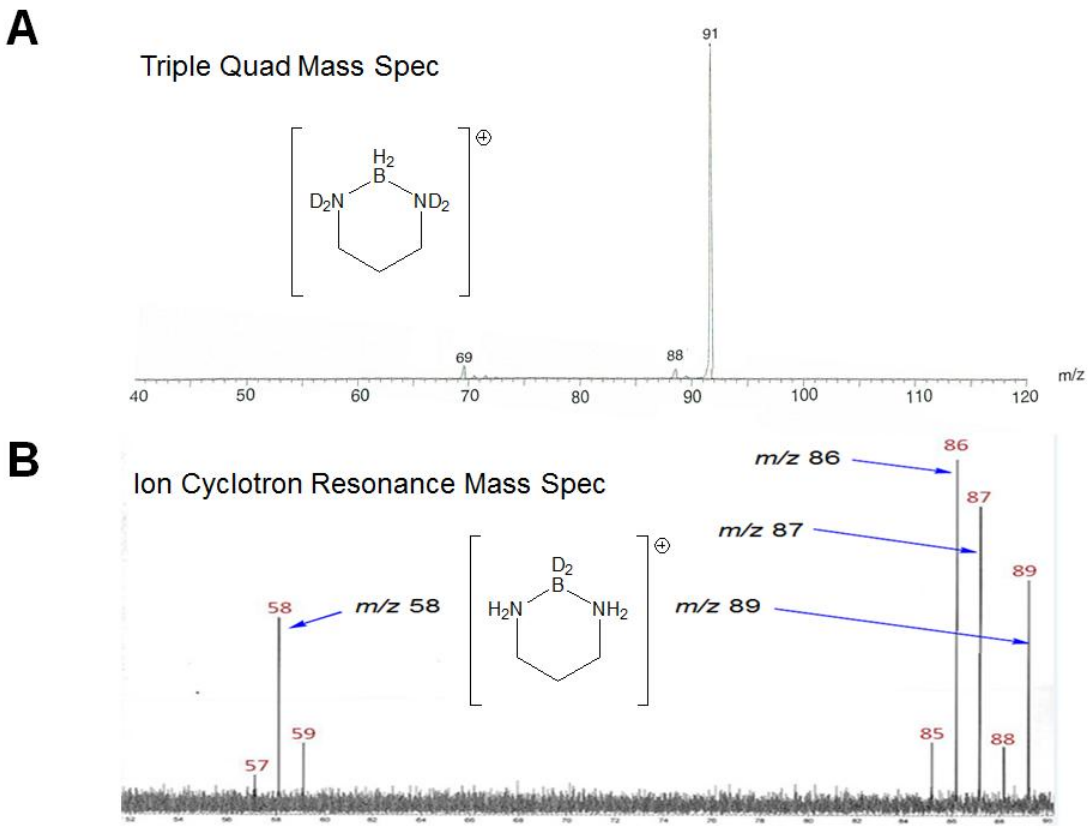

Figure 2.18: Mass Spectrometry analysis of (**A**) tetradeuterated **BDACHex** and (**B**) dideuterated **BDACHex** using TQMS and ICR, respectively. Both ^{10}B and ^{11}B isotopomers were present in the ICR spectrum. The dehydrogenation/ decomposition of the deuterated analogues follow the same pathway as the undeuterated ions.

Figure 2.19 illustrates the isolation of tetradeuterated **BDACPent** in TQMS and showing a loss of HD, D_2, and ND_3 to give *m/z* 74, *m/z* 73, and *m/z* 57, respectively.

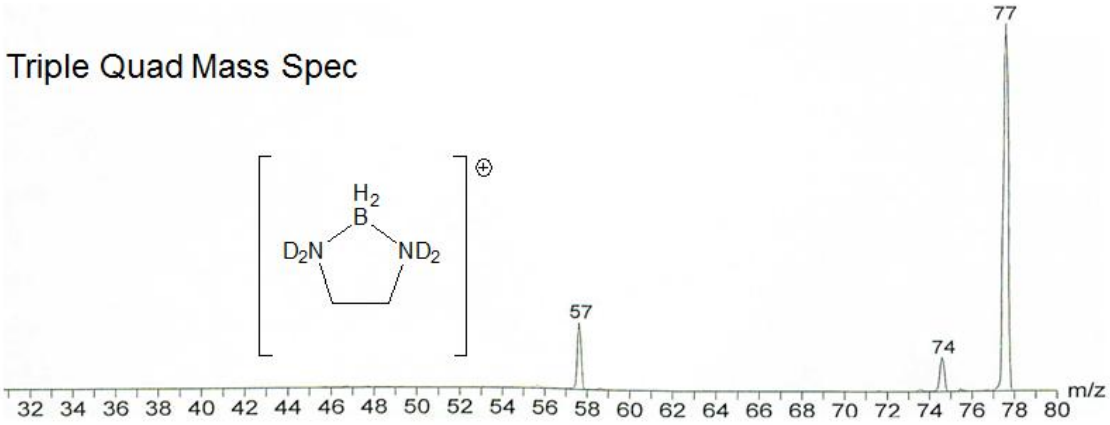

Figure 2.19: TQMS of tetradeuterated **BDACPent** which shows expulsion of HD, D_2, and ND_3.

Table 2.1 summarizes the dehydrogenation and decomposition of the 2-bora-1,3-diazacycloalkanium ions, along with their deuterated analogues, using the two different mass spectrometers. Only **BDACOct** and **BDACPent** released 2 equivalents of H_2 while **BDACHept** and **BDACHex** only released 1 molecule. Aside from dehydrogenation, all of these ions are also prone to decomposition, expelling ammonia and alkene molecules. The deuterated analogues for each ion follows the same dehydrogenation and decomposition pathways (mutatis mutandis) as their corresponding undeuterated counterparts.

Table 2.1: Mass spectrometry (TQMS and ICR) analysis of the dehydrogenation and decomposition of each 2-bora-1,3-diazacycloalkanium ions.

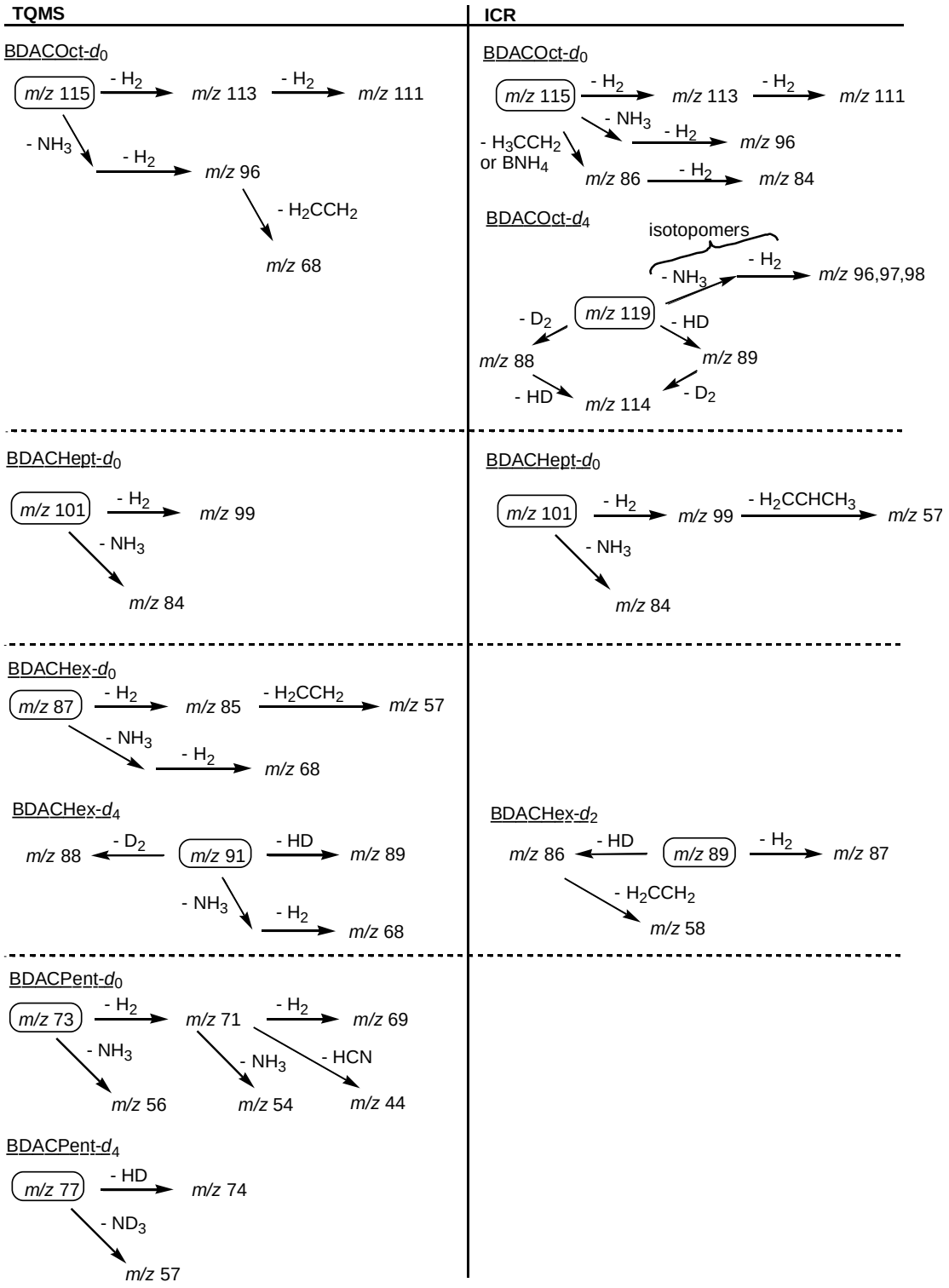

Along with the possibility of the methylene chain participating in dehydrogenation as shown by **BDACOct-*d*$_4$**, one other interesting observation that should be noted is the deuterium discrepancy from dehydrogenation of the deuterated analogues. The expulsion of H_2 and HD together raises a question, considering that only HD molecules should be eliminated if the first dehydrogenation is happening from the N-B-N branch of the ions. One explanation can be the possibility of scrambling of the protons of the N-B-N branch, either as a consequence of electrospray ionization or after activation by absorption of IR photons. In other words, does the scrambling happen before laser activation or is IR activation completely responsible for it? Using the dideuterated **BDACHex** as the example, scrambling of the protons in the N-B-N branch would give the isotopomers given in **Figure 2.20**.

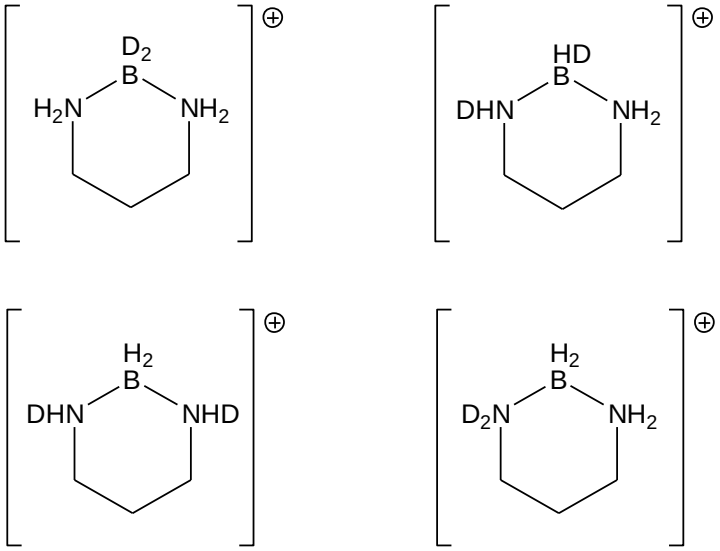

Figure 2.20: Isomers of dideuterated **BDACHex** if scrambling is happening with the protons in the N-B-N branch.

Optimization and frequency calculations were performed for these isotopomers, the calculated frequency intensities were weighted based on their ratios, and all four spectra were put together to give a new theoretical spectrum. **Figure 2.21** compares the new theoretical spectrum with the experimental spectrum acquired using IRMPD. The new calculated spectrum shows additional bands that are not present in the experimental IRMPD spectrum making the comparison between the experimental IRMPD spectrum and the static isotopomer (in which the two deuteria are stuck on the boron atom) in **Figure 2.8**(**C**) a better fit. This analysis suggests that if scrambling is indeed happening before laser excitation, only a very small amount of the sample is experiencing it. That is to say, the experimental data in hand indicate that isotopic scrambling (if it occurs) takes place after activation.

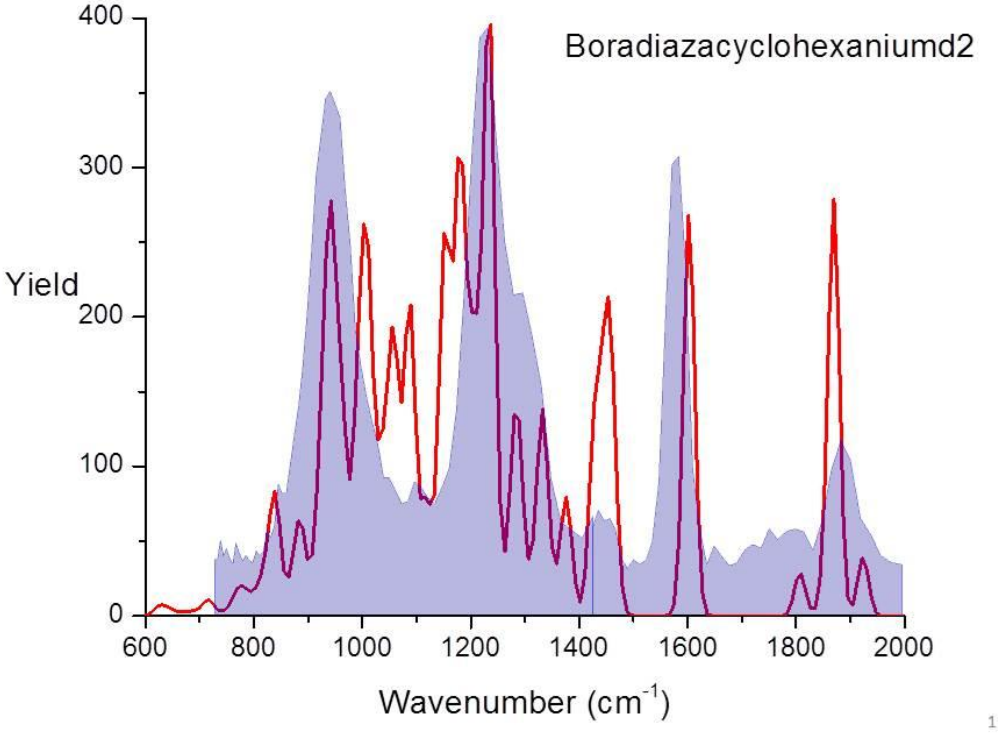

Figure 2.21: Comparison of the experimental IRMPD spectrum (blue silhouette) against the total theoretical spectrum (red solid line) of the isotopomers of dideuterated **BDACHex**. Additional peaks are present on the calculated spectrum which is absent in the IRMPD spectrum.

The simultaneous occurrence of both H_2 and HD expulsion during dehydrogenation (assuming complete scrambling after activation) can be quantified in terms of an isotope effect. This deuterium isotope effect may be concealed for the tetradeuterated **BDACOct**, **BDACHex**, and **BDACPent** samples due to their high deuterium content. However, the similar abundances of H_2 and HD expulsion from the dideuterated **BDACHex** (**Figure 2.18** (**B**)) show a more obvious isotope effect. Using the concepts of a possible scrambling to form different isotopomers and the observed H_2:HD expulsion ratio from **BDACHex-**

***d*$_2$**, the magnitude of a kinetic isotope effect can be estimated. **Table 2.2** shows the isotopomers, their weighted ratios, their weighted molecule expulsions, and the calculation of the kinetic isotope effect equation. Using the total equation derived from the table and the observed expulsion of about 8% D_2 (which includes ^{10}B isotopomer, as well), 48% HD, and 44% H_2 in the ICR analysis of **BDACHex-*d*$_2$** in **Figure 2.18**(**B**), the kinetic isotope effect is calculated to be roughly 1.4. The intensity of *m/z* 85 (which corresponds, in part, to D_2 loss) appears greater than expected, since this experiment did not remove the ^{10}B natural abundance ion, which has the same nominal mass.

Table 2.2: Calculation of the kinetic isotope effect for **BDACHex-*d*$_2$** which accounts for the different isotopomers and their weighted properties.

Isotopomers	Weighted ratio	Weighted molecule expulsion			Equation
		D_2	HD	H_2	
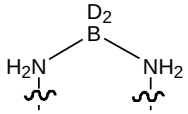	1	0	1	0	$(1)(0)D_2(kie^2) + (1)(1)HD(kie) + (1)(0)H_2$
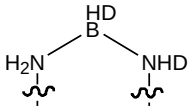	4	$^1/_8$	$^4/_8$	$^3/_8$	$(4)(^1/_8)D_2(kie^2) + (4)(^4/_8)HD(kie) + (4)(^3/_8)H_2$
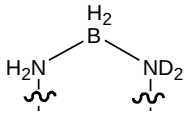	1	0	$^4/_8$	$^4/_8$	$(1)(0)D_2(kie^2) + (1)(^4/_8)HD(kie) + (1)(^4/_8)H_2$
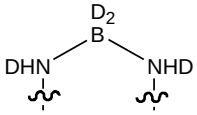	2	0	$^4/_8$	$^4/_8$	$(2)(0)D_2(kie^2) + (2)(^4/_8)HD(kie) + (2)(^4/_8)H_2$
				Total Equation:	$^1/_2(kie^2) + 4^1/_2(kie) + 3H_2$

Conclusion:

Utilizing gas phase and mass spectrometry, it was possible to isolate and study the dehydrogenation of the 2-bora-1,3-diazacycloalkanium ions. From the gas phase analysis, it has been shown that it is possible for these ions to release hydrogen. Together with a hydrogen % weight of ~14%, they can be considered as candidates for H_2 storage. Additional information from this study included the discovery of the isotope effect's influence to retard hydrogen expulsion. One practical problem that needs to be addressed is the expulsion of volatile

ammonia and alkene byproducts, as these can damage the fuel cell catalyst and system. If this drawback can be addressed, these cyclic ions can provide models for novel hydrogen storage molecules.

References:

1: Schlapbach, L.; Zuttel, A. “Hydrogen-storage Materials for Mobile Application” *Nature*, **2001**, *414*, 353-358.

2: Nijkamp, M. G., Raaymakers, J. E. M. J., Van Dillen, A. J.; De Jong, K. P. “Hydrogen Storage Using Physisorption--materials Demands” *Appl. Phys. A*, **2001**, *72*, 619-623.

3: Sandrock, G.; Thomas, G. “The IEA/DOC/SNL On-line Hydride Databases” *Appl. Phys. A*, **2001**, *72*, 153-155.

4: Stephens, F. H.; Pons, V.; Baker, R. T. “Ammonia-borane: the hydrogen source *par excellence*?” *Dalton Trans*, **2007**, *25*, 2613-2626.

5: Office of Energy Efficiency & Renewable Energy “Hydrogen Production” <http://energy.gov/eere/fuelcells/hydrogen-production>

6: Nielsen, T. K.; Karkamkar, A.; Besenbacher, F.; Jensen, T. R.; Autrey, T. “Methods to stabilize and destabilize ammonium borohydride” *Dalton Trans.*, **2013**, *42*, 680-687.

7: Baitalow, F.; Baumann, J.; Wolf, G.; Jaenicke-Robler, K.; Leitner, G. “Thermal Decomposition of B-N-H Compounds Investigated by Using Combined Thermoanalytical Methods” *Thermochimica Acta*, **2002**, *391*, 159-168.

8: Wolf, G.; Baumann, J.; Baitalow, F.; Hoffmann, F. P. “Calometric Process Monitoring of Thermal Decomposition of B-N-H Compounds” *Thermochimica Acta*, **2000**, *343*, 19-25.

9: Baumann, J.; Baitalow, F.; Wolf, G. “Thermal Decomposition of Polymeric Aminoborane $(H_2BNH_2)_x$ Under Hydrogen Release” *Thermochimica Acta*, **2005**, *430*, 9-14.

10: Conley, B. L.; Guess, D.; Williams, T.; “A Robust, Air-Stable, Reusable Ruthenium Catalyst for Dehydrogenation of Ammonia Borane” *J. Am. Chem. Soc.*, **2011**, *133*, 14212-14215.

11: Xiong, Z.; Yong, C. K.; Wu, G; Chen, P.; Shaw, W.; Karkamkar, A.; Autrey, T.; Jones, M. O.; Johnson, S. R.; Edwards; P. P.; David, W. I. F. “High-capacity Hydrogen Storage in Lithium and Sodium Amidoboranes” *Nature Materials*, **2007**, *7*, 138-141.

12: Sun, C.; Yao, X.; Du, A.; Li, L.; Smith, S.; Lu, G. “Computational Study of Methyl Derivatives of Ammonia Borane for Hydrogen Storage” *Phys. Chem. Chem. Phys.*, **2008**, *10*, 6104-6106.

13: Bowden, M. E.; Brown, I. W.; Gainsford, G. J.; Wong, H. “Structure and Thermal Decomposition of Methylamine Borane” *Inorganica Chimica Acta*, **2008**, *361*, 2147-2153.

14: Beachley, O. T. “Intermediates in the Formation of N-Methylaminoborane Trimer and N,N-Dimethylaminoborane Dimer” *Inorganic Chem.*, **1967**, *6*, 870-874.

15: Li, L.; Gu, Q.; Tang, Z.; Chen, X.; Tan, Y.; Li, Q.; Yu, X. “Two Novel Derivatives of Ammonia Borane for Hydrogen Storage: Synthesis, Structure, and Hydrogen Desorption Investigation” *J. Mater. Chem. A*, **2013**, *1*, 12263-12269.

16: Fijalkowski, K. J.; Grochala, W. “Substantial Emission of NH_3 During Thermal Decomposition of Sodium Amidoborane, $NaNH_2BH_3$” *J. Mater. Chem.*, **2009**, *19*, 2043-2050.

17: Luo, W.; Zakharov, L. N.; Liu, S. “1,2-BN Cyclohexane: Synthesis, Structure, Dynamics, and Reactivity” *J. Am. Chem. Soc.*, **2011**, *133*, 13006-13009.

18: Schlesinger, H. J.; Burg, A. B. “Hydrides of Boron. VII. The Structure of the Diammoniate of Diborane and its Relation to the Structure of Diborane” *J. Am. Chem. Soc.*, **1938**, *60*, 290-299.

19: Edwards, J. O.; Kelly, H.C. “Ethane 1,2-Diamineborane” *J. Am. Chem. Soc.* **1960**, *82*, 4842-4846.

20: Polfer, N. C.; Oomens, J. “Reaction Products in Mass Spectrometry Elucidated with Infrared Spectroscopy” *Phys. Chem. Chem. Phys.*, **2007**, *9*, 3804-3817.

21: Oepts, D.; van de Meer, A. F. G.; van Amersfoort, P. W. “The Free-Electron-Laser user facility FELIX” *Infrared Phys. Technol.*, **1995**, *36*, 297-308.

22: Polfer, N. C. “Infrared Multiple Photon Dissociation Spectroscopy of Trapped Ions” *Chem. Soc. Rev.*, **2010**, *40*, 2211-2221.

23: Eckert, J.; Sewell, T. D.; Kress, J. D.; Kober, E. M.; Wang, L.; Olah, G. “Vibrational Analysis of Inelastic Neutron Scattering Spectrum of Tetramethylammonium Borohydride by Molecular Dynamics Simulations and Electronic Structure Calculations” *J. Phys. Chem. A*, **2004**, *108*, 11369-11374.

24: Hartman, M. R.; Rush, J. J.; Udovic, T. J.; Bowman Jr, R. C.; Hwang, S. J. “Structure and Vibrational Dynamics of Isotopically Labeled Lithium Borohydride Using Neutron Diffraction and Spectroscopy” *J. Solid State Chem.*, **2007**, *180*, 1298-1305.

Chapter III:

Synthesis of 8-Amino-4-Trifluoromethyl-1H,9H-Pyrido[2,3-*f*]Quinazoline-2,10-Dione

Introduction:

Cancer is the second leading cause of death in the United States.[1] For 2016, an estimated 1,685,000 new cancer cases will be diagnosed and approximately 595,70 deaths will be due to cancer.[2]

One of the functions of the human body is regulate cells, however, cancer cells can avoid the regulatory steps and often lead to uncontrolled cell growth.[3] The capabilities of cancer cells include self-produced growth signals, insensitivity to anti-growth signals, angiogenesis (the process in which new blood vessels can form from pre-existing ones), evasion of apoptosis (the self-destruction of cells), limitless reproductive potential, and invasion of healthy tissues which leads to metastasis.[4]

Every living organism has hereditary information in each cell coded by DNA. The DNA encodes, among other messages, the ability for a cell to repair or replicate itself. Many natural DNA repair mechanisns have been discovered (including replacement of incorporated ribonucleotides instead of deoxyribonucleotides[5]), since variations in the DNA sequence can cause cancer.

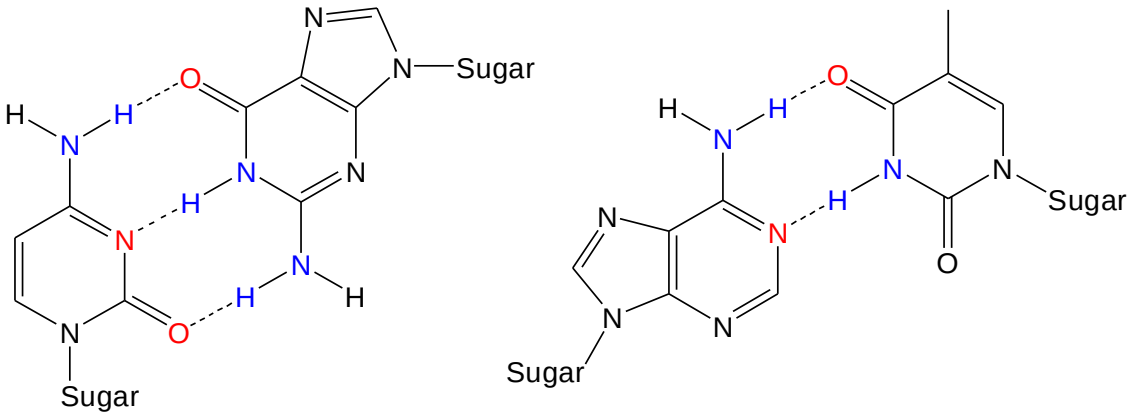

Figure 3.1: Nucleobase pairings which make up the DNA sequence: cytosine with guanine and adenine with thymine. The hydrogen bonding interaction between the bases are made up of hydrogen donors (**D**, blue) and hydrogen acceptors (**A**, red).

The DNA sequence is comprised of complementary base pairs of nucleobases: guanine to cytosine and adenine to thymine, as shown in **Figure 3.1**.[6] These complementary base pairs interact with each other through hydrogen-bonds as shown by the dashed lines in **Figure 3.1**. Unlike the rest of the nucleobases, guanine has been observed to hydrogen bond both at the Hoogsteen face and at the Watson-Crick face, as shown in **Figure 3.2**(**A**). Using this Hoogsteen face interaction, four guanine nucleobases can interact with each other to form a tetrad, as shown in **Figure 3.2**(**B**).[2,7,8,9] Two or more layers of tetrad layered on each other forms a DNA secondary structure called a G-quadruplex.[10]

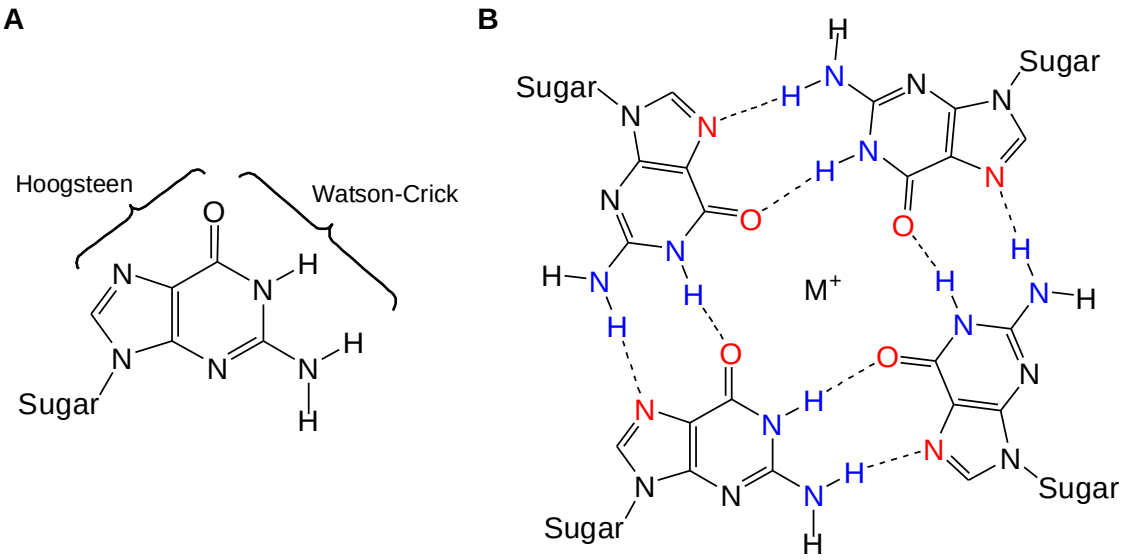

Figure 3.2: **A**) Guanine nucleobase which can use either the Hoogsteen face or the Watson-Crick face for hydrogen bonding. **B**) Four guanine nucleobases interacting with each other to form a secondary structure known as G-quadruplex. The metal cation in the middle, usually potassium, serves as a template.

There is evidence that G-quadruplexes can form in the middle of the DNA, not only at the ends of chromosomes (where they are known as telomeres). G-quadruplexes can be classified into four different classes.[4] These classes are based on the number of bases on the loop regions (segments of DNA that connect one set of a 3 guanine series to the other, it is composed of unbound nucleobases), number of tetrads that form at one time, the length of base chains between the tetrads, and their folding pattern. G-quadruplex notation is read starting at the 5'-end, where each integer separated by a colon represents a loop, and ending at the 3'-end; so that a 5'-[1:2:1]-3' notation represents a G-quadruplex starting at the 5'-end, having one base on the first loop, two bases on the second loop, one base on the third loop, and ending at the 3'-end. The

different G-quadruplex classes are shown in **Figure 3.3**. Class I is the simplest form in which one single G-quadruplex predominates, but due to loop isomers, different loop sizes can form. Class II forms two different G-quadruplexes that are independent of each other and separated by three turns of DNA. Class III is the same as Class II as two G-quadruplexes are formed, however, they form tandem to each other. This tandem formation adds stabilization to their secondary structures and also makes it possible for an intermolecular interaction between the two G-quadruplexes. Class IV, just like Class I, forms only one G-quadruplex, but can exist as different combinations of G-quadruplex at a time due to the excess of the guanine bases on the strand. G-quadruplexes can form in parallel (Class I and II) and anti-parallel (Class III and IV) DNA strand orientations.

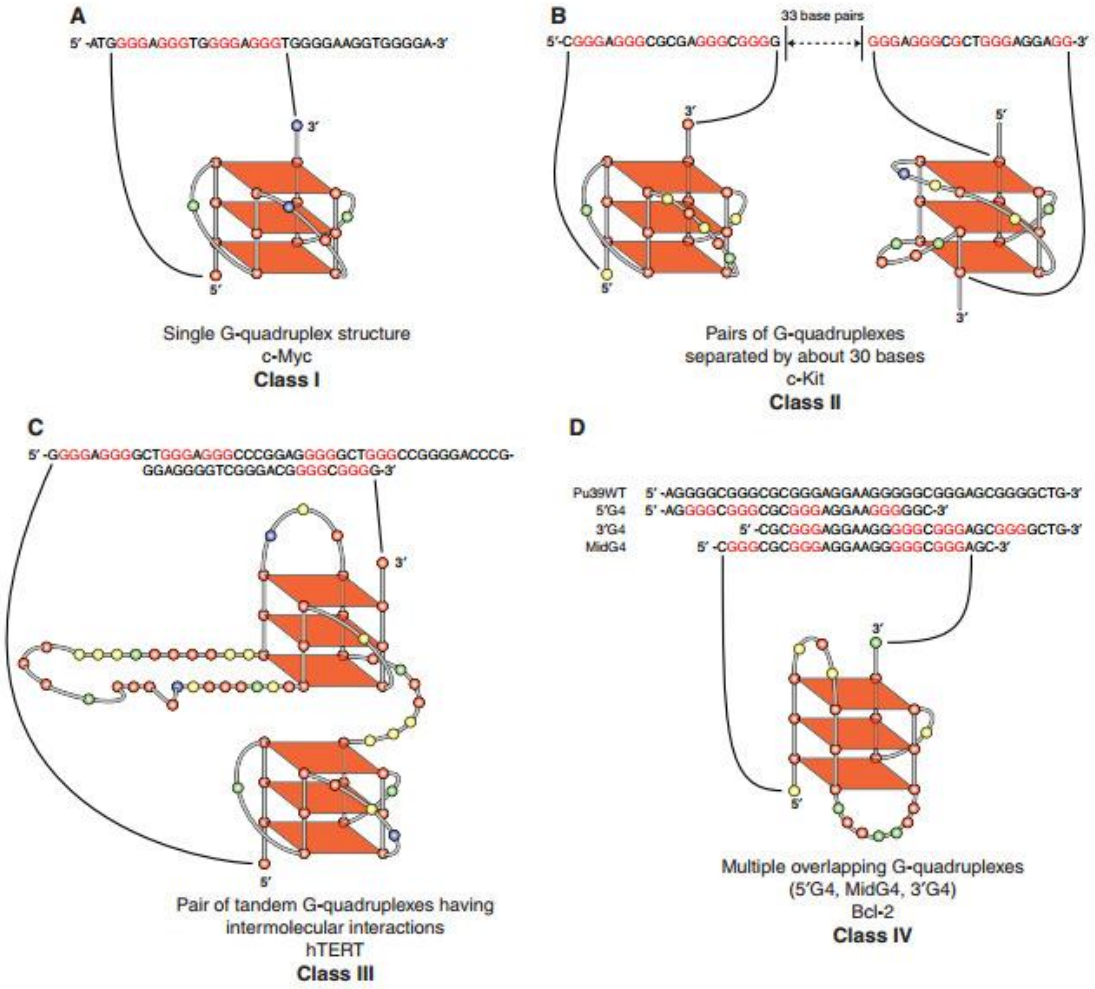

Figure 3.3[4]: The four different classes of G-quadruplex within several oncogene sequences: **A**) Class I within C-Myc, **B**) Class II within c-Kit , **C**) Class III within hTERT, and **D**) Class IV. Image was taken from Brooks *et al.*'s paper, Figure 2.

These secondary structures form on DNA single strands that are guanine-rich. Telomeres, located at the end of eukaryotic chromosomes, are made up of repeating sequences of guanine-rich single strand regions that overhang duplex DNA. One function of telomeres is to protect the genetic material of a chromosome during replication. After many replication cycles, the telomeres are prone to deteriorate making the chromosome unable to replicate. However, an

enzyme known as telomerase has been known to extend the life of telomeres. Many cancer cells overexpress this enzyme.[11]

Formation of G-quadruplexes by single-strand self-association has been detected in guanine-rich regions located in the middle of DNA.[6] The guanine-rich NHE-III sequence is located in the c-Myc promoter region and "silenced" by the formation of G-quadruplex and *i*-motif. Stabilizing these secondary structures inhibits the activation of the enzyme NM23-H2, the protein necessary to unfold the G-quadruplex and *i*-motif, thus disabling the transcription of c-Myc.[12]

Background:

Complementary to the guanine-rich sequence in duplex DNA is a cytosine-rich sequence. The guanine rich single strand forming G-quadruplex is precedented, while the cytosine-rich single strand forms a secondary structure known as *i*-motif at low pH. Since the pKa of cytosine is 4.3, it is still unclear whether the *i*-motif can form at physiological pH (7.3).

The *i*-motif consists of at least 6 proton bound dimers (**PBD**) of cytosine nucleobases, which consist, in turn, of a neutral and protonated cytosine, as shown in **Figure 3.4**(**B**). This hemiprotonated cytosine dimer has two ordinary and one ionic hydrogen bonds.[13] These PBDs are intercalated such that the middle PBD is oriented 90° in respect to the PBD above and below, as shown in **Figure 3.4**(**A**).[14,15,16] Since one of the cytosines has to be protonated in each dimer so as to form PBD, the *i*-motif forms below pH 6 *in vitro* and has not yet been observed *in vivo*.[13]

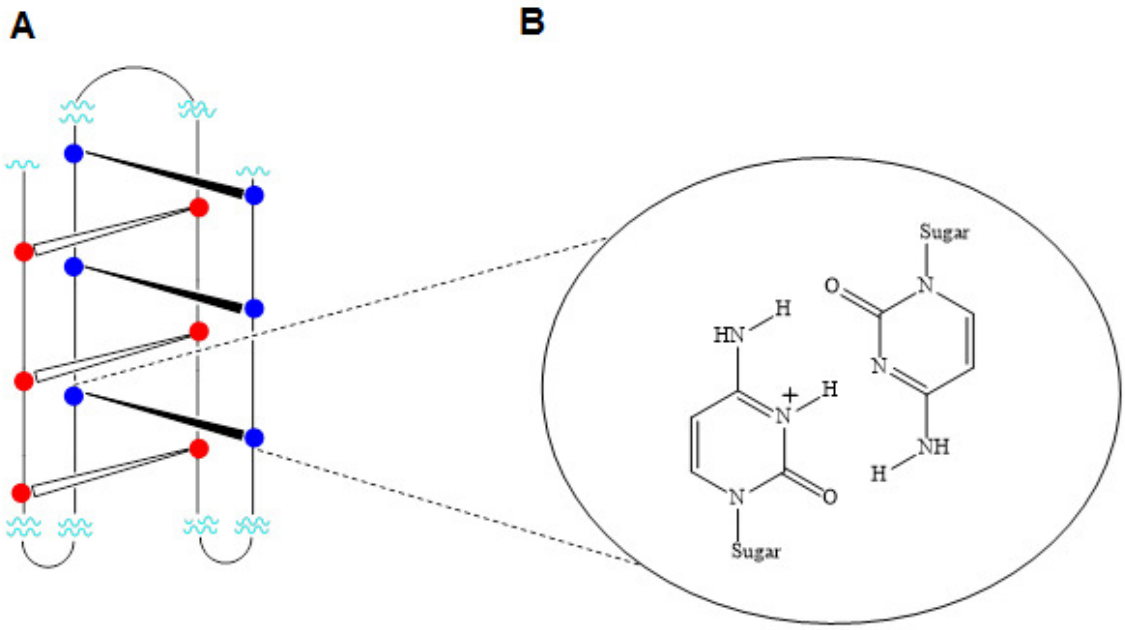

Figure 3.4: **A**) A schematic representation of the i-motif with each of the white and black wedges representing a PBD. **B**) A protonated and neutral cytosine forming a PBD through two ordinary and one ionic hydrogen bondings.

Just as G-quadruplexes, *i*-motifs can be categorized into two classes: Class I and Class II *i*-motifs are separated by the small and large number of bases in their loop regions, respectively (**Figure 3.5**).[4]

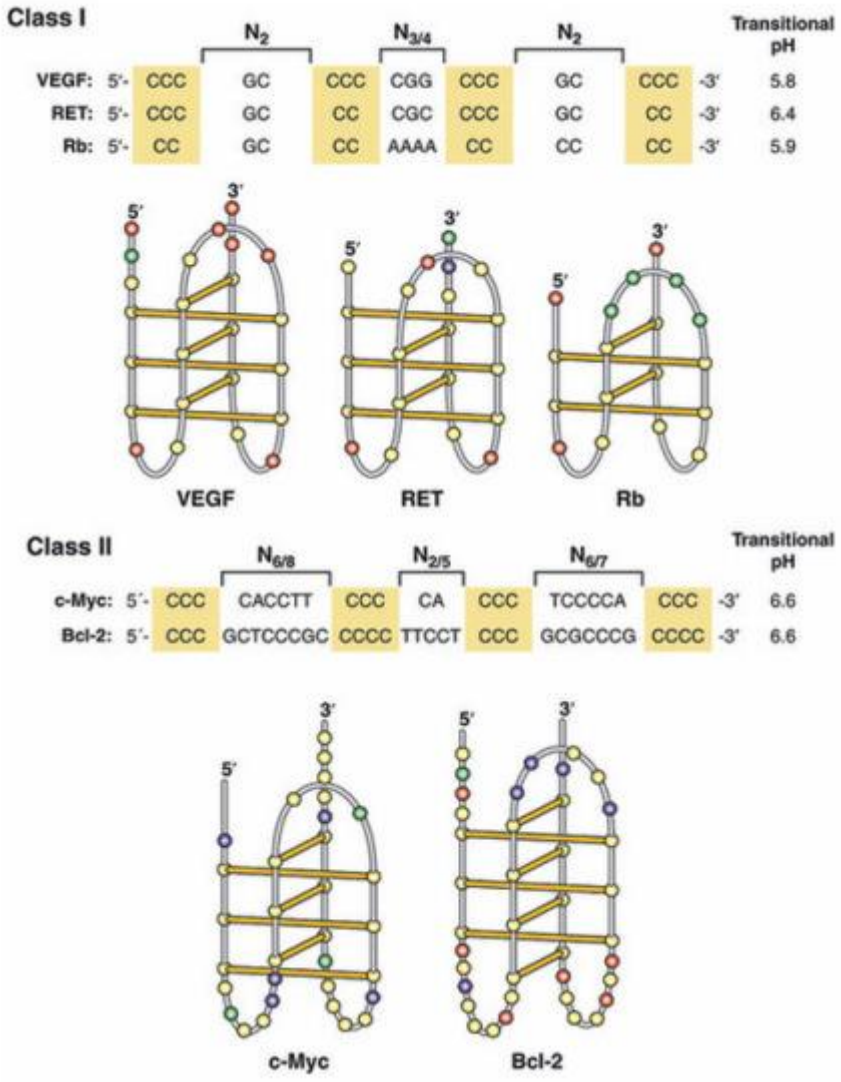

Figure 3.5[4]: The two classes of *i*-motifs that are found within several oncogenes promoter sequences. Class I has a small number of nucleobases in the loop region while Class II has a larger number of nucleobases. Image was taken from Brooks *et al.*'s paper, Figure 3.

Because one of the cytosines is protonated, each base pair forming the *i*-motif is charged. Repulsion between successive base pairs add to the instability of the *i*-motif.[17] Theoretically, there are different ways to stabilize the *i*-motif: ligand binding of the cytosine^{+}-cytosine of the top and bottom base pairs, ligand

binding to the loop regions, or ligand binding to the phosphate backbone.[18] Even though ligand binding to the G-quadruplex and its effect to down-regulate the expression of cancer cells has been observed, ligand binding to the *i*-motif has not been widely studied.[19]

Different ligands that can bind and stabilize the i-motif have been investigated in the past. One example is tetraammonium porphyrin (**$TMPyP_4$**), as shown in **Figure 3.6**(**A**), by the Hurley group.[13] As a more generic model for the *i*-motif, a complex formed from four strands of 5'-dAACCCC sequence was used, shown in **Figure 3.6**(**B**).[20] They found that overnight incubation of 5'-dAACCCC with increasing concentrations of $TMPyP_4$ enhanced the yield of the aggregated (*i*-motif) form of the strands. They believe that the $TMPyP_4$, having a high density of positive charge, quenches the electronic repulsion of the phosphate backbones in the narrow grooves. However, since $TMPyP_4$ had no effect on the melting point, it was assumed that it functions only as a facilitator for *i*-motif formation and not as a stabilizer.[21]

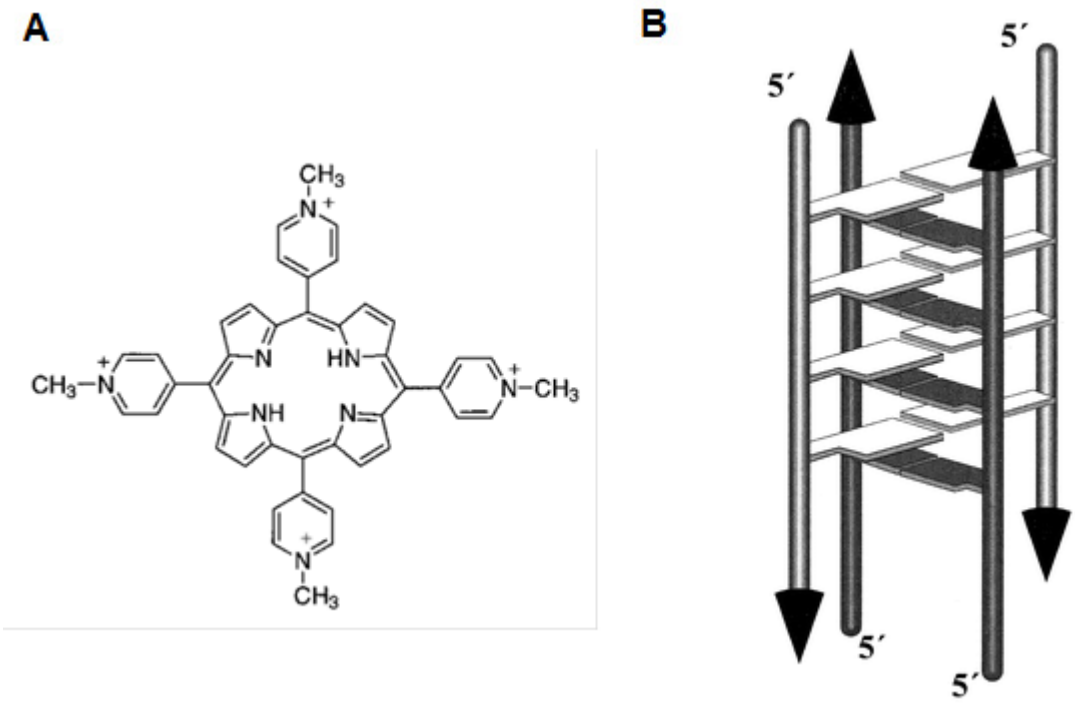

Figure 3.6[21]: **A**) A ligand used by the Hurley group and believed to bind the *i*-motif via the phosphate backbone in the narrow groove. **B**) The generic *i*-motif model used by the Hurley group which is formed by four strands of 5'-dAACCCC. Image was taken from Hurley *et al.*'s paper, Figure 1.

Another ligand that Hurley *et al.* looked at is IMC-48, shown in **Figure 3.7**(**A**), and they have tested it on bcl-2. Bcl-2 is an oncogene that promotes growth of cancer cells as it disrupts the cell's apoptotic function. This oncogene has been shown to exist in equilibrium between hairpin and *i*-motif structure.[22] IMC-48 stabilizes the *i*-motif formation by interacting with the thymine bases in the loop region, as shown in **Figure 3.7**(**B**). On the other hand, the IMC-76 ligand destabilizes the *i*-motif formation and favors the hairpin structure of bcl-2.

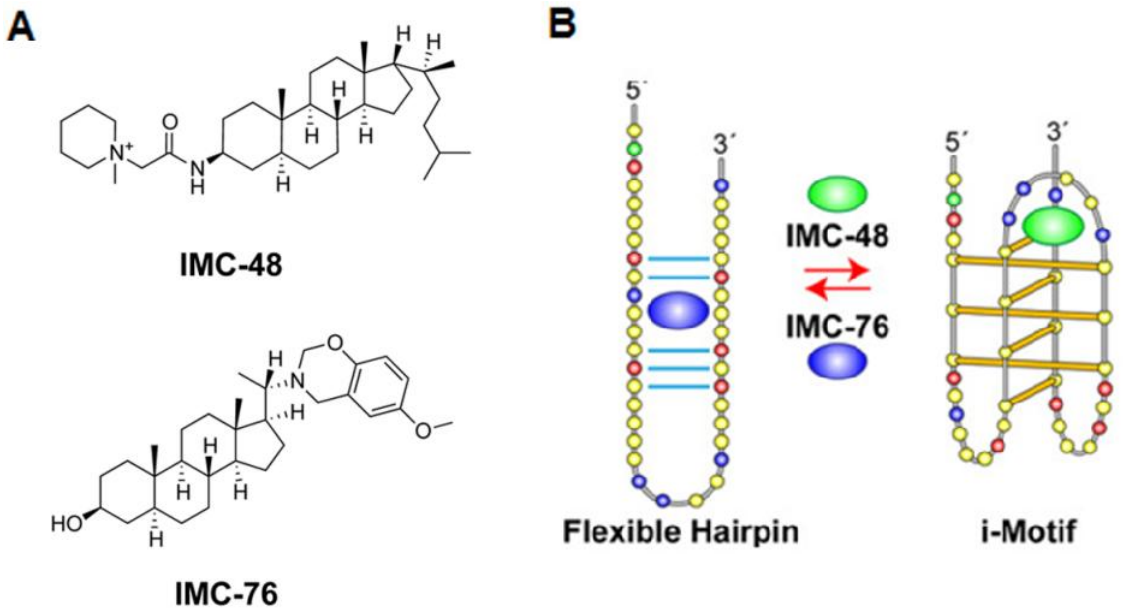

Figure 3.7[22]: **A**) The two ligands, studied by the Hurley group, that have been found to affect the *i*-motif stability. **B**) IMC-48 ligand favored the formation of the *i*-motif while IMC-76 preferred the hairpin structure. Image was taken from Hurley *et al.*'s paper, Figure 2 and Figure 3.

Goal:

This chapter presents a molecule that has the potential to act a ligand to bind to the *i*-motif. Our target molecule consists of an electron-rich carbostyril/quinoline backbone and an isocytosine moiety that can interact with the nucleobases on the strand. Since a protonated isocytosine moiety can bind only to a neutral cytosine of the *i*-motif, we assume that our target molecule can stabilize the secondary structure by binding on the cytosines on the loop region. It may also be possible for the target molecule to bind to exposed neutral cytosine residue in a situation when the *i*-motif flips due to charge repulsion between the PBDs. Just like in the case of IMC-48, binding interactions on the

loop region may stabilize and even promote *i*-motif formation which can lead to the inhibition of cell expression.

Experimental:

Many of the procedures below do not give an isolable yield of the desired product but are included so as to direct future investigators as to what has already been attempted.

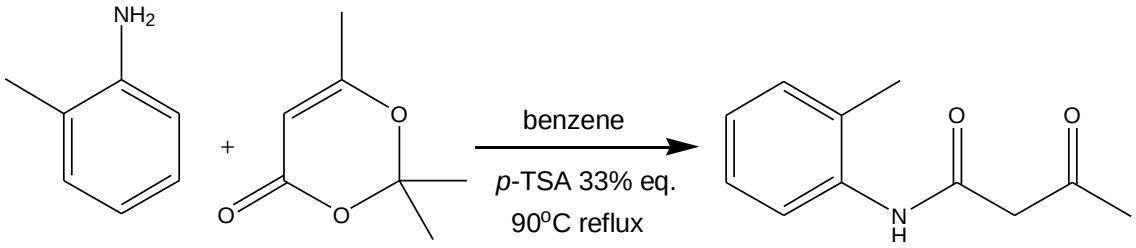

Scheme 3.1.1[23]: Synthesis of 2-methyl-*N*-arylacetoacetamide.

The compound 2-methyl-N-arylacetoacetamide was previously synthesized by Kaslow *et al.* and they were able to get the same compound.[23] A mixture of 1.72 g (10 mmol) *p*-TSA, 3.21 ml (30 mmol) of *o*-toluidine and 10 ml of benzene was warmed to 50°C in an inert flask. 4.25 ml (32 mmol) of 2,2,6-trimethyl-4H-1,3-dioxin-4-one (diketene-acetone complex) was added slowly into the warm solution. The solution was heated to 90°C and refluxed overnight. After reaction, the solution was cooled to room temperature and then stored in the freezer for 3 hours. The resulting solid was then filtered and washed with cold mixture of 2:1 benzene:ligroin (25 ml) to give the crude product. Analysis of the crude material showed some impurities. The crude material was recrystallized by dissolving it in a hot solution of 1:1 ethanol:water. Cooling the solution gave

crystals with a yield of 28%. The same spectra for the analysis of the compound were included in the paper published by Kaslow *et al.*.

APCI-ESI MS: MH^+: 192.1020 (calc. 191.1019)

^{1}H NMR (400 MHz, $CDCl_3$): δ 2.34 (3H, s), δ 2.35 (3H, s), δ 3.65 (2H, s), δ 7.08 (1H, t, J = 8 Hz), δ 7.20 (2H, d, J = 8 Hz), δ 7.94 (1H, d, J = 12 Hz), δ 9.17 (1H, br s)

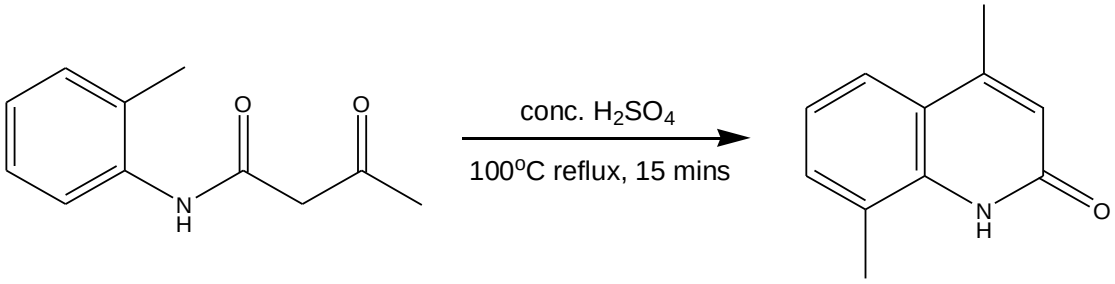

Scheme 3.1.2[23]: Synthesis of 4,8-dimethylcarbostyril.

The compound 4,8-dimethylcarbostyril was previously synthesized by Kaslow *et al.* and they were able to get the same compound.[23] *N*-arylacetoacetamide (1.6 g, 8.4 mmol) was added, in 2-3 portions, to 2.3 ml of hot concentrated sulfuric acid, maintaining the temperature at 85°C.After addition, the solution was heated and stirred at 100°C for 15 minutes, then cooled to 60°C, and then poured into 12 ml of ice-water. More ice was added to the mixture, followed by treatment with concentrated NaOH until no more further precipitate formed. The cream colored suspension was filtered to obtain a white solid which was washed with 2 ml water, 2 ml 2% sodium bicarbonate, and 2 ml water. The solid was dried under vacuum, transferred and spread out in a beaker, and oven dried (~70°C) over 2 days. 1.053 g (72%) of the product was obtained. The same

spectra for the analysis of the compound were included in the paper published by Kaslow *et al.*.

APCI-ESI MS: MH^+: 174.0919 (calc. 174.0913)

^{1}H NMR (400 MHz, $CDCl_3$): δ 2.50 (6H, s), δ 6.55 (1H, s), δ 7.15 (1H, t), δ 7.35 (1H, d, J = 10 Hz), δ 7.55 (1H, d, J = 12 Hz), δ 9.37 (1H, br s)

IR:

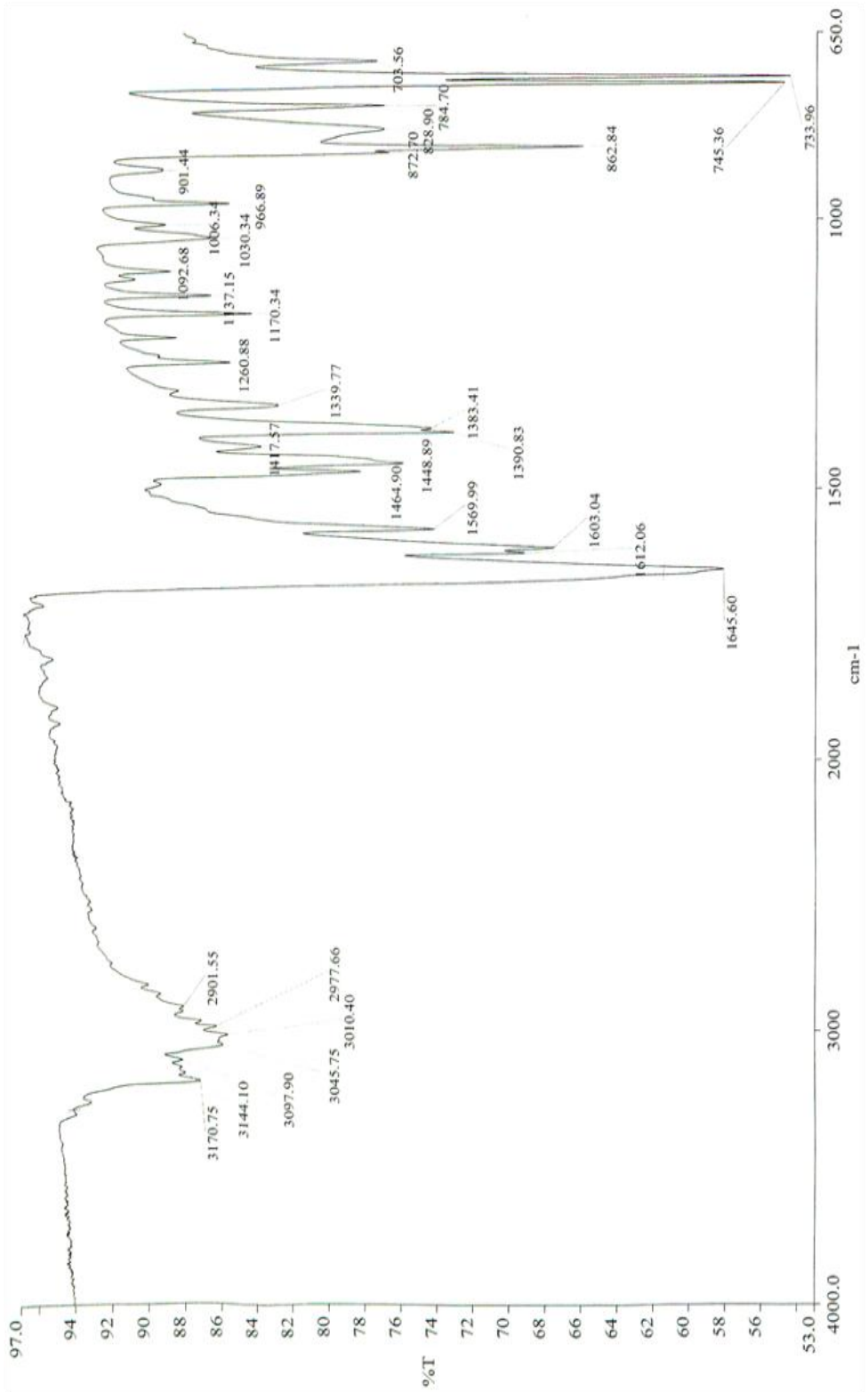
%T
cm-1
4000.0
3000
2000
1500
1000
650.0
97.0
53.0
3170.75
3144.10
3097.90
3045.75
3010.40
2977.66
2901.55
1645.60
1612.06
1603.04
1569.99
1464.90
1448.89
1390.83
1383.41
1339.77
1260.88
1170.34
1137.15
1092.68
1030.34
1006.34
966.89
901.44
872.70
862.84
828.90
784.70
745.36
733.96
705.56

Attempted Nitration with nitric acid/sulfuric acid

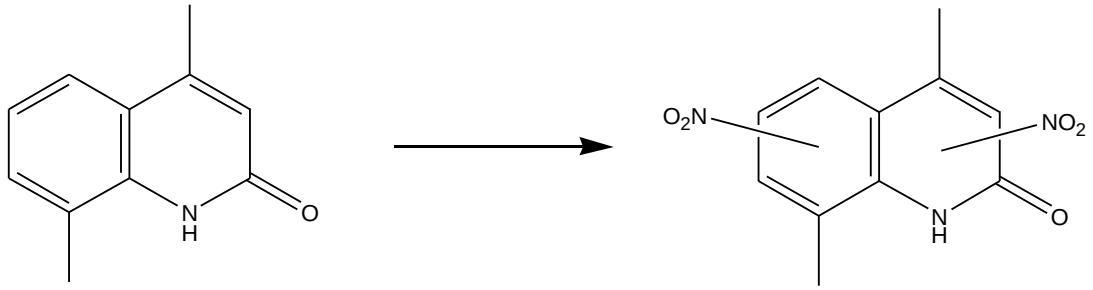

Scheme 3.1.3[24]: Nitration of 4,8-dimethylcarbostyril using concentrated nitric acid and concentrated sulfuric acid.

The nitration of 4,8-dimethylcarbostyril was followed from a previous nitration procedure that was published by Malhotra *et. al*..[24] 230 mg (1.3 mmol) of the 4,8-dimethylcarbostyril was introduced into a 25ml flask and cooled in an ice-bath. 3ml of concentrated sulfuric acid was added to the flask and cooled. 2 ml of 1:1 concentrated sulfuric acid:concentrated nitric acid mixture was added dropwise via an addition funnel to the flask while in ice-bath over 8 minutes. After addition, the addition funnel was replaced with an air condenser and the solution was heated slowly. The heat was started at 25°C and increased by 10°C per seven minutes up to 72°C. The solution was heated at 72°C for 1.5 hours and then cooled to room temperature. The cooled solution was then added to 35 ml of ice resulting in precipitation of solid. The yellow solid was filtered and washed with cold water. After drying under vacuum, 203 mg of the crude material was acquired. Analysis showed only the 4,8-dimethylcarbostyril starting material.

Chlorination

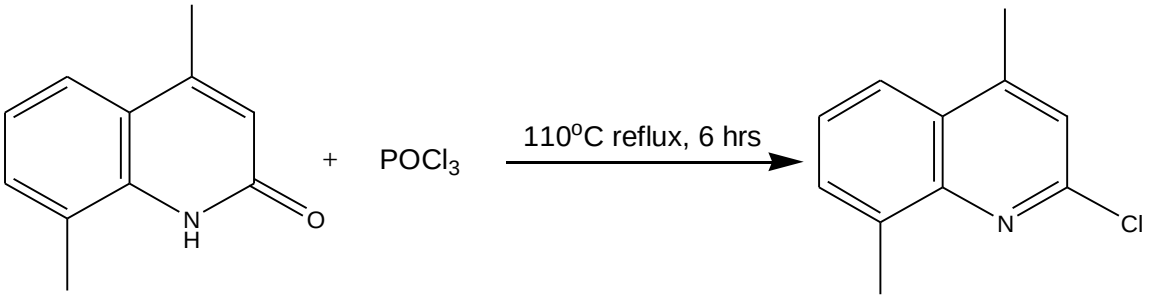

Scheme 3.2.1[25]: Chlorination of the carboxyl group of 4,8-dimethylcarbostyril using phosphoryl chloride.

The compound 2-chloro-4,8-dimethylquinoline was previously synthesized by Heitbaum *et al.* and they were able to get the same compound.[25] Chlorination of 4,8-dimethylcarbostyril was started by introducing 5 ml (53.6 mmol) phosphoryl chloride into a 25 ml flask. 500 mg of carbostyril was added to the flask and completely dissolved after heating. An additional 430 mg (5.37 mmol total) carbostyril was added to the solution and the heating was continued. The solution was refluxed for 6 hours and the excess phosphoryl chloride was distilled off. Ice was slowly added to the reaction flask to quench the reaction. After the reaction had cooled to room temperature, the aqueous layer was extracted with 3 x 30 ml of chloroform. The combined organic layers were dried with sodium sulfate and the decanted solution was concentrated *in vacuo*. 847 mg (83%) of the product was achieved. The same spectra for the analysis of the compound were included in the paper published by Heitbaum *et al.*.

APCI-ESI MS: MH^+: 192.0569 (calc. 192.0575)

^{1}H NMR (400 MHz, $CDCl_3$): δ 2.68 (3H, s), δ 2.78 (3H, s), δ 7.24 (1H, s), δ 7.46 (1H, t, J = 10 Hz), δ 7.58 (1H, d, J = 8 Hz), δ 7.81 (1H, d, J = 12 Hz)

IR:

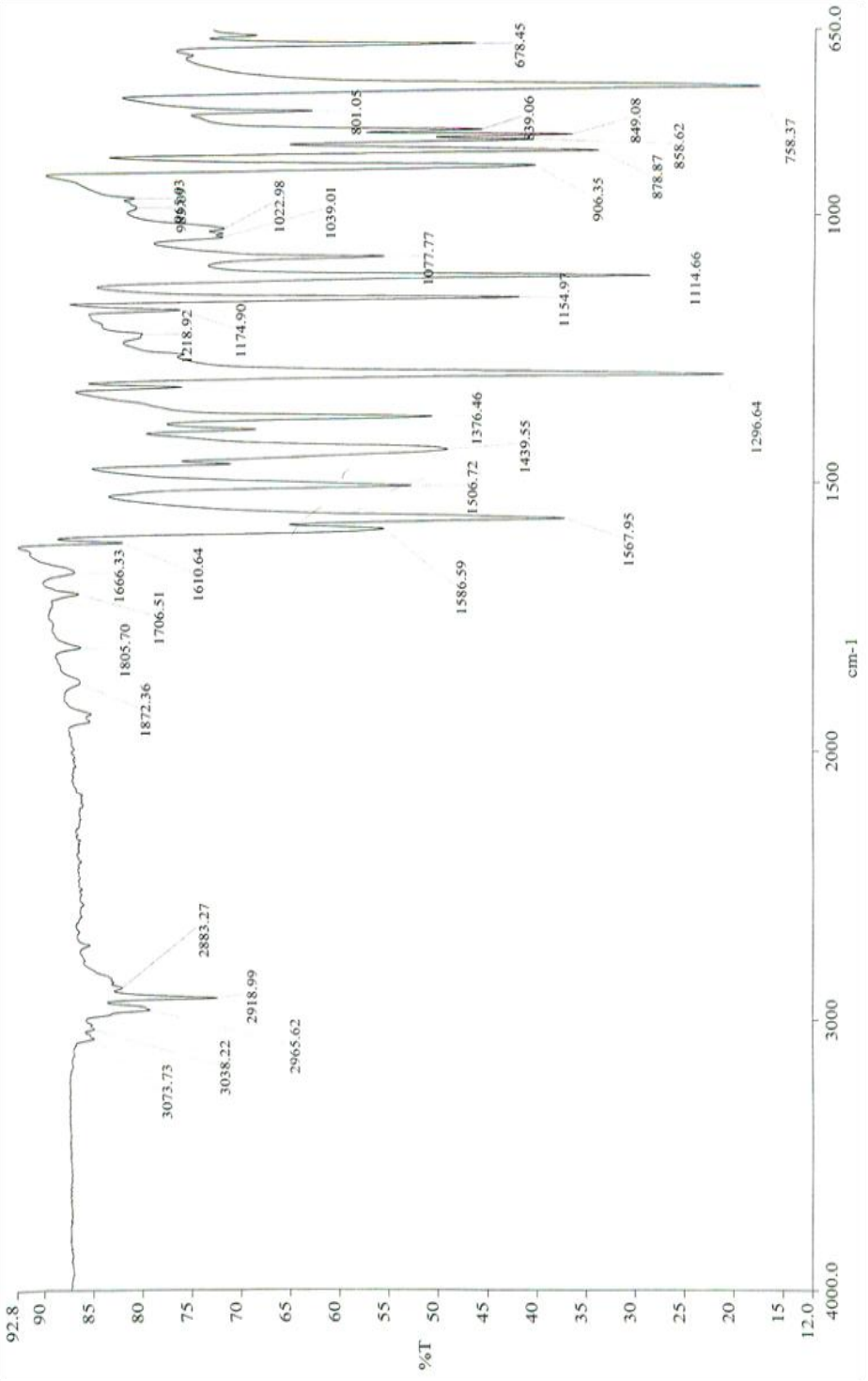

Nitration with fuming nitric acid of 2-chloro-3,8-dimethylquinoline

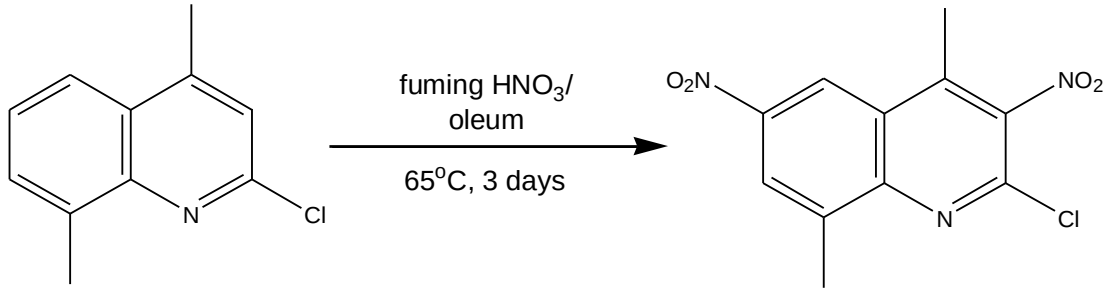

Scheme 3.2.2[26]: Aromatic nitration of 2-chloro-4,8-dimethylquinoline using fuming nitric acid and oleum.

The procedure for the nitration of 2-chloro-4,8-dimethylquinoline was adapted, with slight modification, from a previously published procedure by Hill *et al.*.[26] 3.7 ml of fuming nitric acid was added to a dry 25 ml flask and cooled in an ice-bath. 4.2 ml of oleum was added slowly over a period of time at 0°C. 2-Chloro-4,8-dinitroquinolone (650 mg, 3.4 mmol) was added in small portions at 0°C. After the addition, the mixture was warmed to room temperature and then slowly heated at a rate of 1°C per 3 minutes until 65°C. The solution was stirred at 65°C for 3 days. After cooling to room temperature, the flask was further cooled in an ice-bath and 20 ml of ice-cold water added. The resulting solid was filtered, washed with ice-cold water, and dried under vacuum. The crude material was dissolved in hot isopropanol, allowed to cool to room temperature, then left in the refrigerator overnight . The off-yellow crystals were filtered, washed with cold isopropanol, and dried under vacuum to give 212 mg (22%).

APCI-ESI MS: MH^+: 282.0272 (calc. 282.0276)

^{1}H NMR (400 MHz, $CDCl_3$): δ 2.59 (3H, s), δ 3.06 (3H, s), δ 7.52 (1H, s), δ 8.20 (1H, s)

Attempted oxidation of 2-chloro-3,6-dinitro-4,8-dimethylquinoline

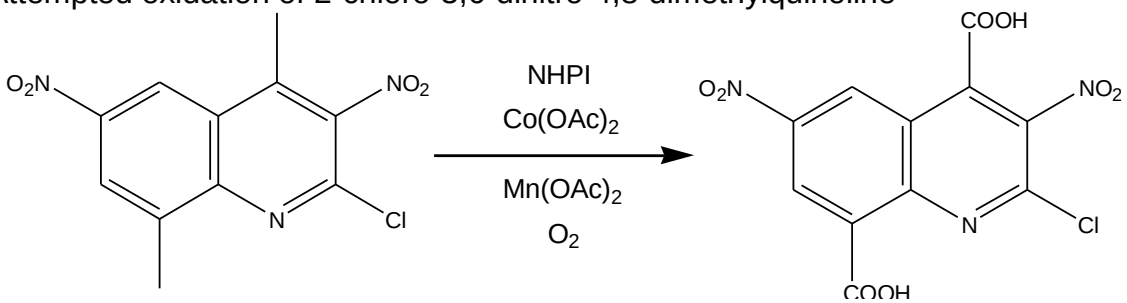

Scheme 3.2.3[27]: Attempted oxidation of the methyl groups of 2-chloro-4,8-dimethyl-3,6-dinitroquinoline.

The oxidation procedure of 2-chloro-3,6-dinitro-4,8-dimethylquinoline was adapted, with slight modification, from a previously published procedure from a patent produced by Du Pont de Nemours and Co.[27] 2-Chloro-4,8-dimethyl-3,6-dinitroquinolone (100 mg, 0.356 mmol), along with 12 mg (0.074 mmol) *N*-hydroxyphthalimide (NHPI), 2 mg (8 μmol) cobalt(II) acetate, and 2 mg (7 μmol) manganese(II) acetate, were added to a pyrex tube. 5 ml of acetic acid was added and the sides of the tube was wiped dry with a kimwipe. The tube was then sealed and placed in a 70°C oven for a week. The oxygen inside the tube was calculated to be about 0.134 mmol since the tube was opened to the atmosphere prior to sealing. Only starting material was recovered.

Attempted synthesis of *N*-oxide of 2-chloro-4,8-dimethylquinoline

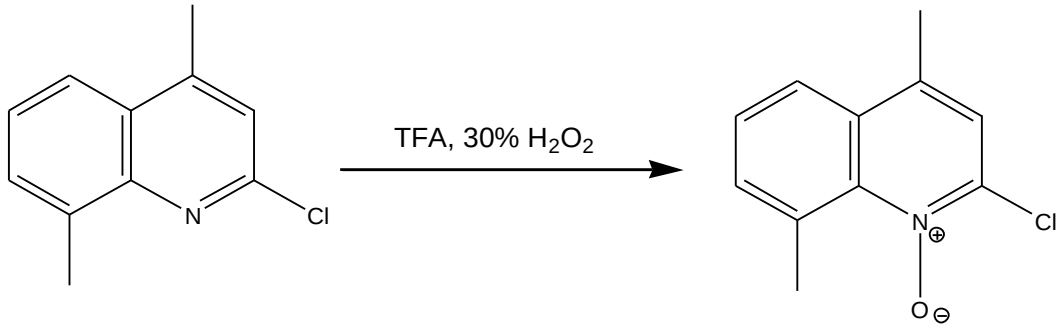

Scheme 3.2.4[28]: Attempted synthesis of N-oxide-2-chloro-4,8-dimethylquinoline.

The synthesis of N-oxide-2-chloro-4,8-dimethylquinoline was adapted, with a slight modification, from a previously published procedure by Liotta *et al.*.[28] 200 mg (1.05 mmol) of 2-chloro-4,8-dimethylquinoline was added to a 10 ml flask and cooled in an ice-bath. 0.785 ml (10.3 mmol) of trifluoroacetic acid was used to dissolve the sample while in the ice-bath, followed by drop-wise addition of 30% hydrogen peroxide. The solution was taken off the ice-bath, allowed to warm to room temperature, and stirred for 2 hours. Chloroform was added to the reaction and the resulting solution washed with 6M aqueous sodium hydroxide (3 x 5 ml). The combined aqueous washes were then back extracted with dichloromethane (4 x 10 ml). The combined organic layers were dried over anhydrous magnesium sulfate. Concentration of the solution gave a solid product which was analyzed to be pure starting material.

Synthesis of 4-hydroxy-2-methyl-*N*-arylacetoacetamide

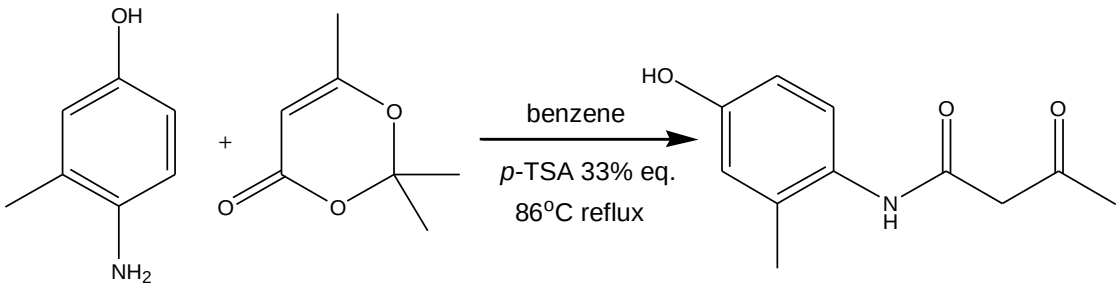

Scheme 3.3.1[23]: Synthesis of 4-hydroxy-2-methyl-*N*-arylacetoacetamide.

The synthesis of 4-hydroxy-2-methyl-N-arylacetoacetamide was adapted, with a slight modification, from a previously published procedure by Kaslow *et al.*.[23] 2.33 g (13.5 mmol) *p*-Toluenesulfonic acid and 5 g (40.6 mmol) 4-amino-*m*-cresol were added into a 50 ml round-bottom flask and purged with nitrogen. 40 ml of benzene was added and the mixture heated to 50°C. 8.1 ml (60.9 mmol) of 2,2,6-trimethyl-4H-1,3-dioxin-4-one (diketene-acetone complex) was added dropwise, a reflux condenser attached, repurged with N_2, and the solution refluxed at 86°C for 24 hours to give clear brown solution with black tar at the bottom. The tarry solid was collected and dissolved in isopropanol. Stripping off the isopropanol gave a tar which was extracted with ethyl acetate (3 x 100 ml). The organic layer from extraction was concentrated to give a crude oil. The oil was purified through a silica gel column using 3:7 hexane:ethyl acetate. 749 mg (31%) of the product was obtained. A similar spectrum for the analysis of the compound were included in the paper published by Kaslow *et al.*.

APCI-ESI MS: MH^+: 208.1006 (calc. 208.0968)

^{1}H NMR (400 MHz, $CDCl_3$): δ 2.25 (3H, s), δ 2.35 (3H, s), δ 3.63 (2H, s), δ 6.63 (1H, dd, J_1 = 8 Hz, J_2 = 4 Hz), δ 6.66 (1H, d, J = 4 Hz), δ 7.54 (1H, d, J = 12 Hz), δ 8.88 (1H, br s)

Synthesis of 6-hydroxy-4,8-dimethylcarbostyril

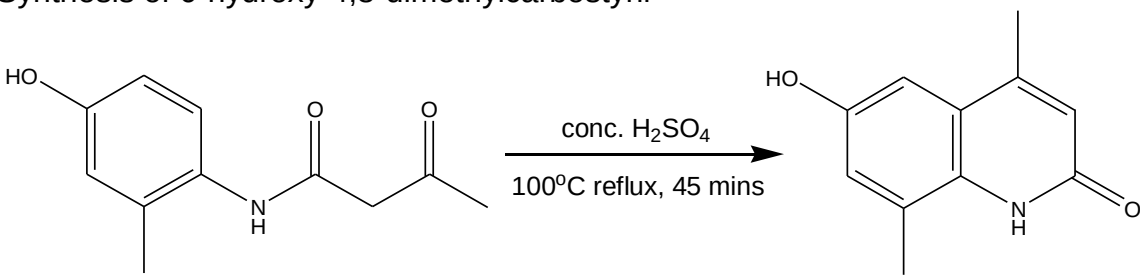

Scheme 3.3.2[23]: Synthesis of 6-hydroxy-4,8-dimethylcarbostyril.

The synthesis of 6-hydroxy-4,8-dimethylcarbostyril was adapted, with a slight modification, from a previously published procedure by Kaslow *et al.*.[23] 1.5 ml of concentrated sulfuric acid was heated to 85°C and slowly added to a 85°C preheated flask containing 1.1 g of 4-hydroxy-2-methyl-*N*-arylacetoacetamide. After addition, the solution was heated and stirred at 100°C for 2 days. The reaction was cooled down and 8 ml of cold ethanol was added. Sodium ethoxide was added dropwise until the reaction mixture was pH 7. ^{1}H NMR and mass spectrometry of the solid product showed some desired product along with a lot of impurities.

APCI-ESI MS: MH^+: 190.0870 (calc. 190.0863)

Synthesis of 4-methoxy-*N*-arylacetoacetamide

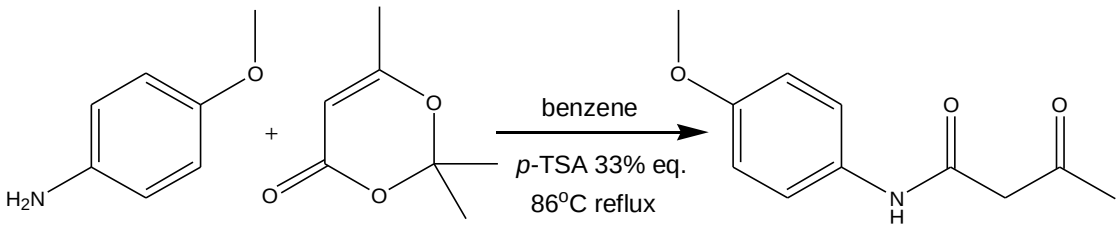

Scheme 3.4.1[23]: Synthesis of 4-methoxy-*N*-arylacetoacetamide.

The synthesis of 6-hydroxy-4,8-dimethylcarbostyril was adapted, with a slight modification, from a previously published procedure by Kaslow *et al.*.[23] 660 mg (3.83 mmol) of *p*-toluenesulfonic acid and 1.42 g (11.5 mmol) of *p*-anisidine was introduced into a 25 ml flask, capped, and purged under nitrogen. 12 ml of benzene was added and then heated to 50°C. While the solution was kept at 50°C, 2.55 ml (17.3 mmol) of 2,2,6-trimethyl-4H-1,3-dioxin-4-one (diketene-acetone complex) was added. A reflux condenser was attached to the flask, the whole system was purged under nitrogen, and then refluxed at 85°C overnight. The solution was cooled to room temperature, then refrigerated for 2 hours. The yellow solid which precipitated was filtered and recrystallized with isopropanol. The solid was filtered, washed with cold ligroin, and dried under vacuum for 2 hours. The solid contained a mixture of starting material and product, with starting material in greater abundance. A similar spectrum for the analysis of the compound were included in the paper published by Kaslow *et al.*.

APCI-ESI MS: MH^+: 208.0979 (calc. 208.0968)

^{1}H NMR (400 MHz, $CDCl_3$): δ 2.31 (3H, s), δ 3.63 (2H, s), δ 3.77 (3H, s), δ 6.73 (2H, d, J = 12 Hz), δ 7.04 (2H, d, J = 8 Hz), δ 7.32 (2H, d, J = 12 Hz), δ 7.62 (2H, d, J = 8 Hz), δ 9.87 (1H, br s)

Attempted synthesis of 6-methoxy-4-methylcarbostyril

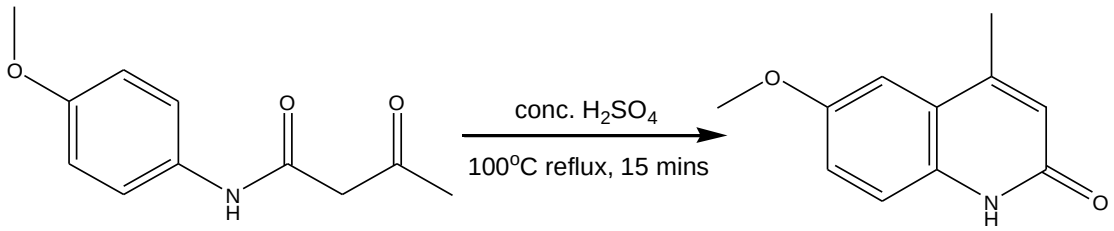

Scheme 3.4.2[23]: Attempted synthesis of 6-methoxy-4-methylcarbostyril.

The synthesis of 6-hydroxy-4,8-dimethylcarbostyril was adapted, with a slight modification, from a previously published procedure by Kaslow *et al.*.[23] 0.5 ml of concentrated sulfuric acid was heated at 85°C in a 10 ml flask. 370 mg (1.79 mmol) of 4-methoxy-*N*-arylacetoacetamide was added in increments to the hot sulfuric acid to keep the temperature at 85°C. After addition, the solution was heated and stirred at 100°C. The reaction was monitored by TLC by observing the disappearance of the starting material and any presence of carbostyril blue spot under fluorescence. After 15 minutes, the reaction was quenched by cooling the flask to room temperature, then in an ice-bath, and diluted with methanol. The off-white precipitate that formed was filtered and analyzed with TLC, mass spectrometry, and ^{1}H NMR. No product was observed.

Attempted synthesis of 6-hydroxy-4-methylhydroxyquinoline

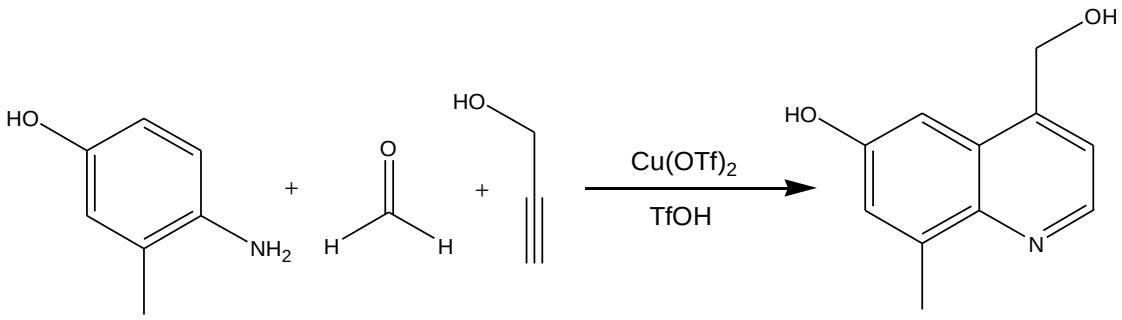

Scheme 3.5.1[29]: Attempted one-pot synthesis of 6-hydroxy-4-methylhydroxyquinoline via copper click chemistry.

The one-pot synthesis of 6-hydroxy-4,8-methylhydroxyquinoline was adapted, with a slight modification, from a previously published procedure by Meyet *et al.*.[29] 147 mg (0.41 mmol) of copper(II) triflate was placed in a thick-wall scintillation vial, followed by 0.5 g (4.06 mmol) 4-amino-*m*-cresol, 0.23 ml (4.87 mmol) propargyl alcohol, and 0.18 ml (4.87 mmol) formaldehyde. 0.04 ml (0.4 mmol) of trifluoromethanesulfonic acid was added before capping the vial and securing it with an electric tape. The reaction was heated and stirred at 100°C for 24 hours. The reaction was cooled and the crude solution was analyzed by TLC to look for the distinctive blue fluorescent spot which is characteristic of quinolines. No product was observed from the TLC analysis and mass spectrometry showed amide/iminol intermediate instead.

APCI-ESI MS: amide/iminol intermediate + H^+: 152.0706 (calc. 152.0706)

Another attempted synthesis of 6-hydroxy-4-methylhydroxyquinoline

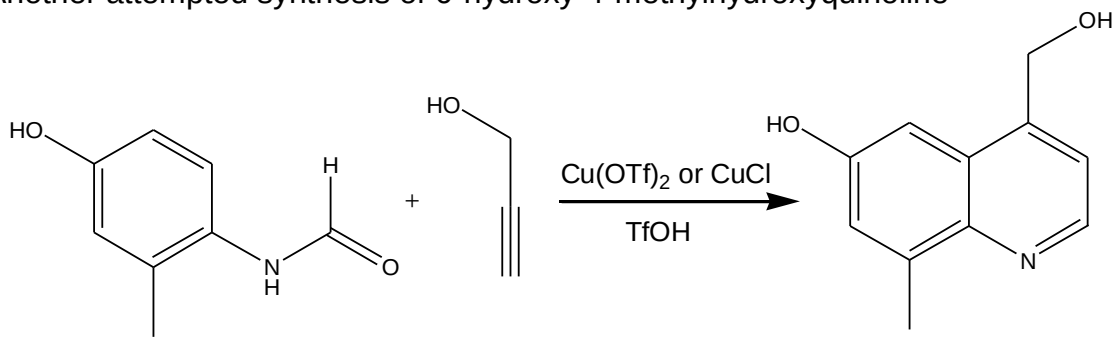

Scheme 3.5.2[30]: Attempted two-pot synthesis of 6-hydroxy-4-methylhydroxyquinoline via copper click chemistry.

The two-pot synthesis of 4-hydroxy-6-methoxyquinoline was adapted, with slight modification, from a previously published procedure by Peshkov *et al.*.[30] 61 mg (0.41 mmol) of the amide/iminol intermediate, the catalyst ($Cu(OTf)_2$ 15 mg, 0.041 mmol or CuCl 12 mg, 0.12 mmol), and propargyl alcohol were added in a thick-wall scintillation vial and capped with a septum. 0.004 ml (0.041 mmol) of trifluoromethylsulfonic acid was added through the septum cap via a needle. The septum cap was replaced with a plastic cap and secured with electric tape. The solution was heated and stirred at 100°C for 3 days. TLC analysis did not show any product and mass spectrometry analysis showed the starting material.

Synthesis of 7-amino-4-methylcarbostyril

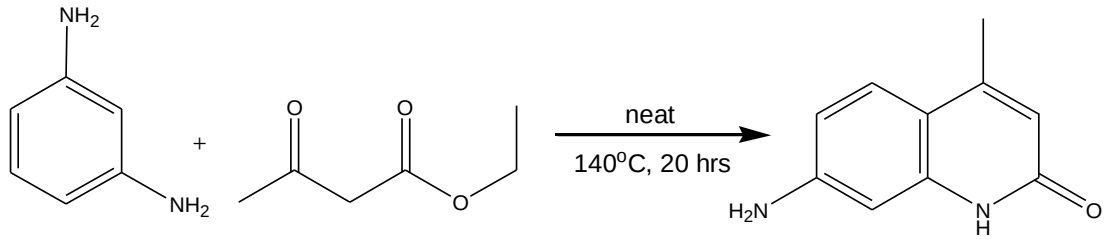

Scheme 3.6.1[31]: Synthesis of 7-amino-4-methylcarbostyril.

The compound 7-amino-4-methylcarbostyril was previously synthesized by Woods *et al.* and they were able to get the same compound.[31] 2.5 g (23.1 mmol) of *m*-phenylenediamine and 2.95 ml (23.1 mmol) of ethylacetoacetate were heated and stirred in a 25 ml flask at 140°C for 20 hours. The reaction was cooled to room temperature and 20 ml of water was added. The contents were then again heated to 110°C until the water in the solution was boiling. The mixture was then cooled again to room temperature and chilled in the refrigerator. The solid was filtered and dried under vacuum. The solid was recrystallized twice by dissolving it in hot morpholine with slow addition of heptane to give yellow solid. The solid was dried under vacuum to give 1.29 g (31%) of the product. The same spectra for the analysis of the compound were included in the paper published by Woods *et al.*.

APCI-ESI MS: MH^+: 174.0837 (calc. 174.0793)

^{1}H NMR (400 MHz, DMSO-d_6): δ 2.27 (3H, s), δ 5.72 (1H, br s), δ 5.94 (1H, s), δ 6.35 (1H, d, J = 4 Hz), δ 6.45 (1H, dd, J_1 = 12 Hz, J_2 = 4 Hz), δ 7.33 (1H, d, J = 12 Hz), δ 11.12 (1H, br s)

Melting point: 272.0-273.1°C

IR:

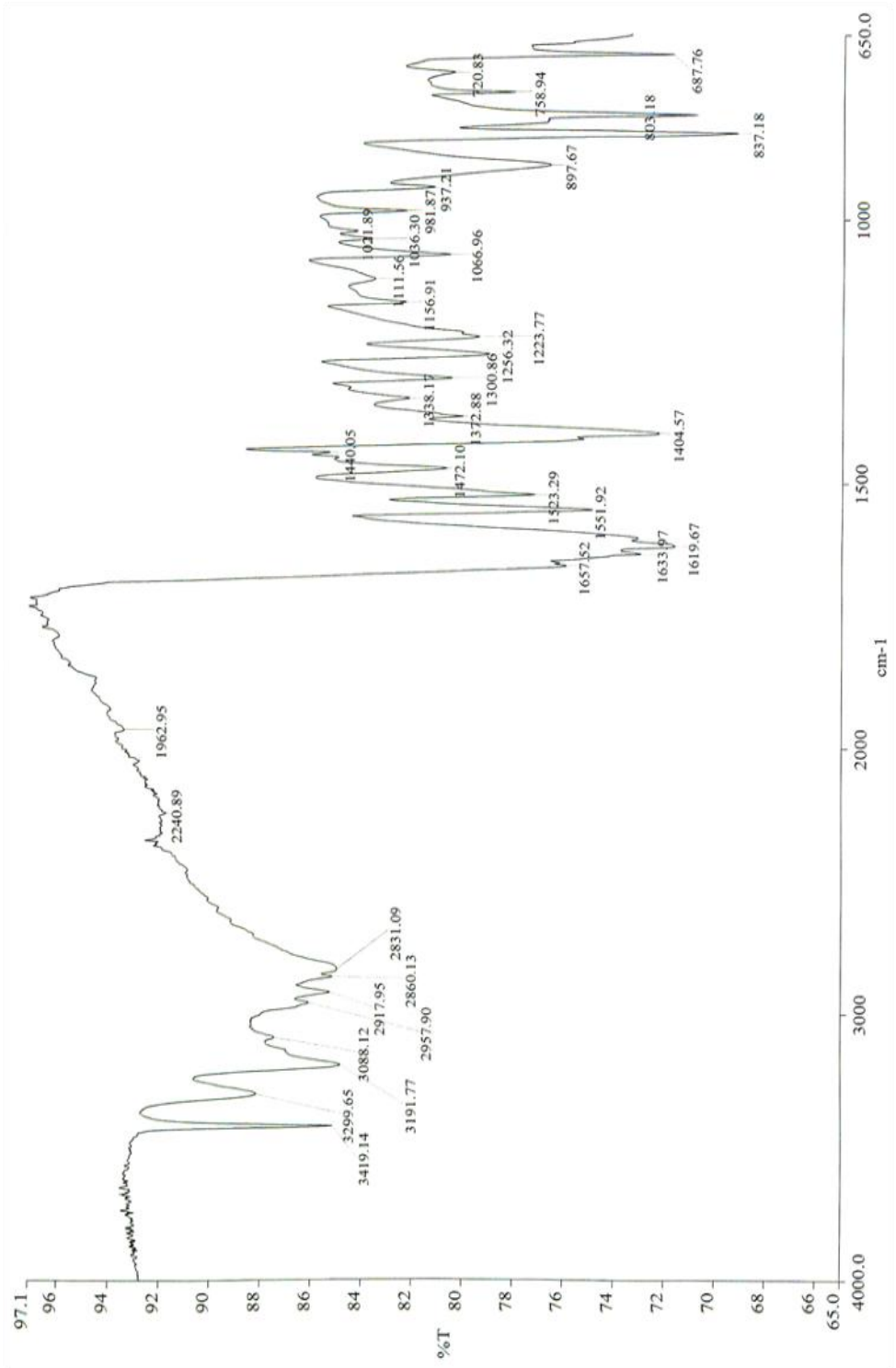
%T
cm-1
4000.0
3000
2000
1500
1000
650.0
97.1
96
94
92
90
88
86
84
82
80
78
76
74
72
70
68
66
65.0
3419.14
3299.65
3191.77
3088.12
2957.90
2917.95
2860.13
2831.09
2240.89
1962.95
1657.52
1633.97
1619.67
1551.92
1523.29
1472.10
1440.05
1404.57
1372.88
1338.17
1300.86
1256.32
1223.77
1156.91
1111.56
1071.89
1036.30
1066.96
981.87
937.21
897.67
837.18
803.18
758.94
720.83
687.76

Protection of 7-amino-4-methylcarbostyril

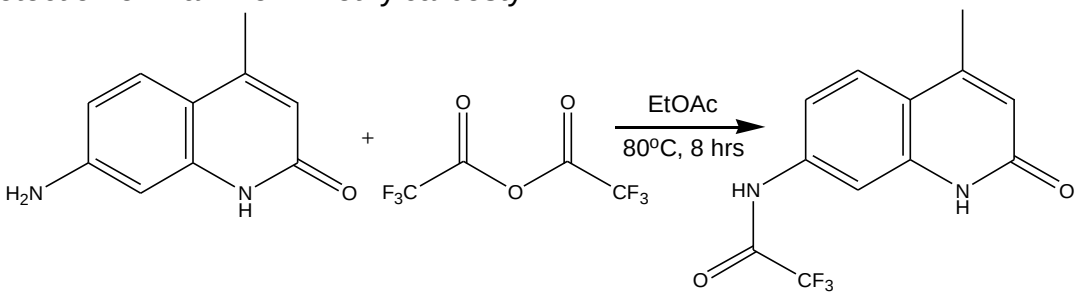

Scheme 3.6.2[32]: Protection of 7-amino-4-methylcarbostyril with trifluoroacetic anhydride.

The protection of amine group of 7-amino-4-methylcarbostyril using trifluoroacetic anhydride was adapted from a previously published procedure by Nakagawa *et al.* with slight modification.[32] 1.5 g (8.62 mmol) of 7-amino-4-methylcarbostyril and 50 ml of ethyl acetate was added into a 25 ml flask. The mixture was cooled in an ice-bath and 1.338 ml (9.48 mmol) trifluoroacetic anhydride was added dropwise. After addition, the reaction was taken off the ice-bath, warmed to room temperature, and then stirred at 80°C overnight. After cooling to room temperature, the resulting white solid was filtered and washed with cold ethyl acetate. The solid was dried under vacuum to give 1.01 g (43%) of the protected product.

APCI-ESI MS: MH^+: 271.2142 (calc. 271.2147)

^{1}H NMR (400 MHz, DMSO-*d*$_6$): δ 2.40 (3H, s), δ 6.35 (1H, s), δ 7.46 (1H, dd, J_1 = 8 Hz, J_2 = 2Hz), δ 7.73 (1H, d, J = 8 Hz), δ 7.77 (1H, d, J = 2 Hz), δ 11.50 (1H, br s), δ 11.69 (1H, br s)

^{19}F NMR (400 MHz, DMSO-*d*$_6$): δ -74.23

Chlorination of 7-trifluoroacetamido-4-methylcarbostyril

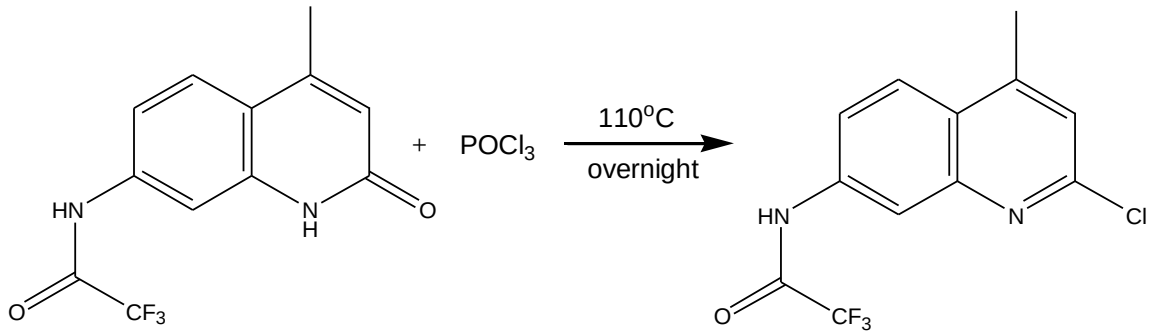

Scheme 3.6.3[25]: Chlorination of 7-trifluoroacetamide-4-methylcarbostyril.

The chlorination of 7-trifluoroacetamide-4-methylcarbostyril was adapted, with slight modification, from a previously published procedure by Heitbaum *et al.*.[25] 0.172 ml (1.85 mmol) of phosphoryl chloride was added into a 10 ml flask, followed by 50 mg (0.185 mmol) of 7-trifluoroacetamide-4-methylcarbostyril. The mixture was stirred and refluxed at 110°C overnight to give a clear brown solution. The reflux apparatus was replaced with a distillation apparatus and the excess phosphoryl chloride removed by distillation to give a brown oil. Ice water was added to quench the oil and to give a white solid. The solution was stirred to break up the solid which was then transferred to a separatory funnel. The solution was extracted with 40 ml of chloroform three times and the organic layer dried over sodium sulfate. After evaporation of the solvent, 36 mg (66%) of the product was obtained. APCI-ESI MS showed that the desired product is the most abundant yet ^{1}H and ^{19}F NMR shows a lot of impurities.

APCI-ESI MS: MH^{+}: 289.0359 (calc. 289.0350)

^{19}F NMR (400 MHz, $CDCl_3$): δ -75.97

Attempted bromination of 7-trifluoroacetamido-4-methylcarbostyril

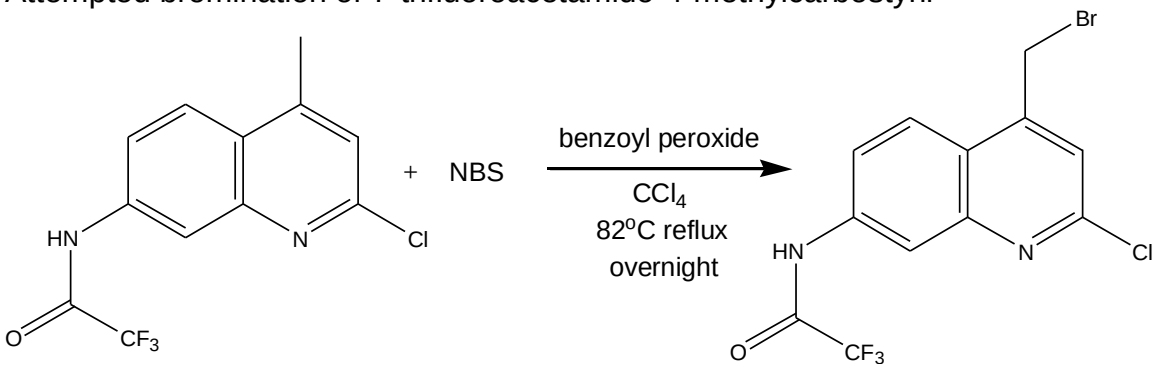

Scheme 3.6.4[33]: Attempted bromination of 7-trifuloroacetamide-4-methylcarbostyril using *N*-bromosuccinamide.

Bromination of the aromatic methyl group of the carbostyril followed a previously published procedure, with some modifications, from a patent by Hashizume *et al.*.[33] 250 mg (1.44 mmol) of 7-amino-4-methylcarbostyril and 281 mg (1.58 mmol) of *N*-bromosuccinimide were dissolved in 25 ml of carbon tetrachloride, followed by addition of 52 mg (0.215 mmol) of benzoyl peroxide. The reaction was refluxed overnight at 82°C. After cooling to room temperature, the solid was filtered and the filtrate concentrated under vacuum to give a residue. Analysis of the residue showed pure starting material.

Synthesis of 7-amino-4,8-dimethylcarbostyril

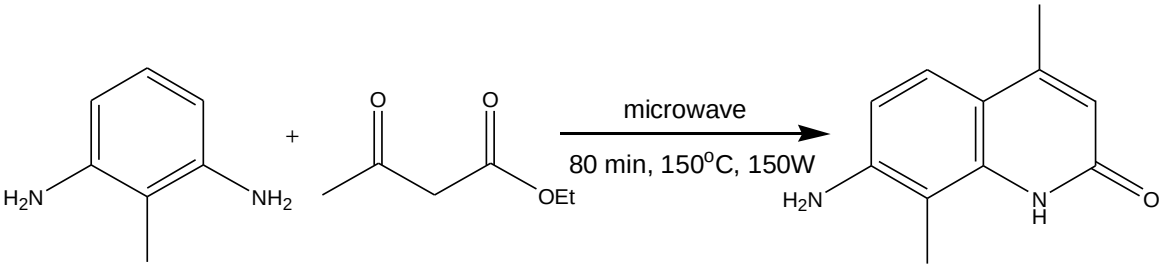

Scheme 3.7.1[34]: Synthesis of 7-amino-4,8-dimethylcarbostyril.

The compound 7-amino-4,8-dimethylcarbostyril has been synthesized by Lee *et al.* and they were able to get the same compound.[34] 244 mg (2 mmol) of 2,6-diaminotoluene, 0.255 ml (2 mmol) of ethyl acetoacetate, and 1 ml of water were placed in a 10 ml microwave glass tube with a snap-on plastic cap. The reaction was carried out in a microwave at 150°C, with 150 W radiation, for 80 minutes. After the reaction, the mixture was cooled down to room temperature and then in the freezer for 3 hours. The gray precipitate was filtered and washed with 30 ml of cold ether and 30 ml of cold water. The solid was dried under vacuum and gave 150 mg (40%) of the product. The same spectra for the analysis of the compound was included in the paper by Lee *et al.*.

APCI-ESI MS: MH^+: 189.1025 (calc. 189.1022)

^{1}H NMR (400 MHz, DMSO-d_6): δ 2.09 (3H, s), δ 2.30 (3H, s), δ 5.51 (1H, br s), δ 6.00 (1H, s), δ 6.56 (1H, d, J = 12 Hz), δ 7.27 (1H, d, J = 12 Hz), δ 10.16 (1H, br s)

IR:

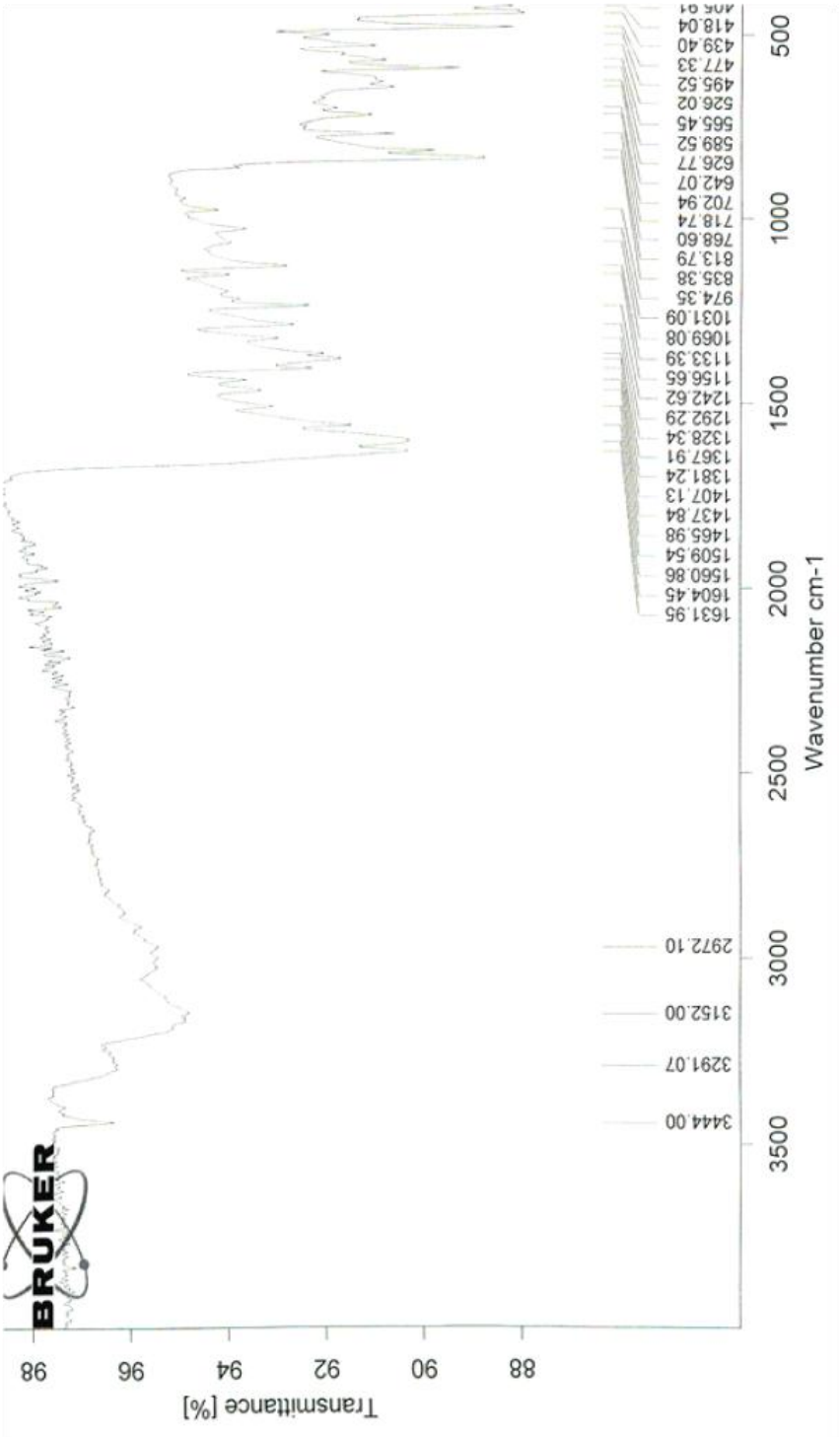
Transmittance [%]
98
96
94
92
90
88
BRUKER
3444.00
3291.07
3152.00
2972.10
1631.95
1604.45
1560.86
1509.54
1465.98
1437.84
1407.13
1381.24
1367.91
1328.34
1292.29
1242.62
1156.65
1133.39
1069.08
1031.09
974.35
835.38
813.79
768.60
718.74
702.94
642.07
626.77
589.52
565.45
526.02
495.52
477.33
439.40
418.04
Wavenumber cm-1
3500
3000
2500
2000
1500
1000
500

Attempted bromination of 2,6-diaminotoluene

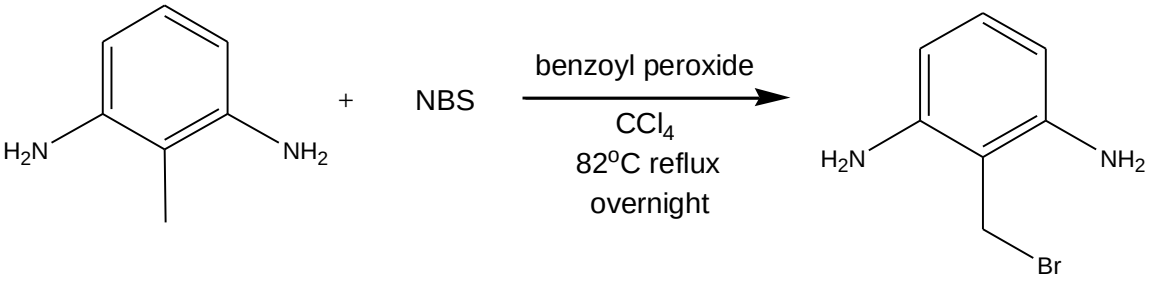

Scheme 3.7.2[33]: Attempted bromination of 2,6-diaminotoluene with *N*-bromosuccinamide..

Bromination of the methyl group of the 2,6-diaminotoluene followed a previously published procedure, with some modifications, from a patent by Hashizume *et al.*.[33] 50 mg (0.41 mmol) of 2,6-diaminotoluene and 80 mg (0.45 mmol) of *N*-bromosuccinamide were added and dissolved in 5 ml of carbon tetrachloride in a 50 ml flask. 15 mg (0.062 mmol) of benzoyl peroxide was introduced and the reaction was stirred and refluxed at 82°C overnight. The reaction was cooled to room temperature and the solid was filtered. The filtrate was washed with 20 ml saturated sodium carbonate 3 times and the organic layer dried with sodium sulfate. Analysis of the yellow solid did not show the desired product.

Protection of 7-amino-4,8-dimethylcarbostyril

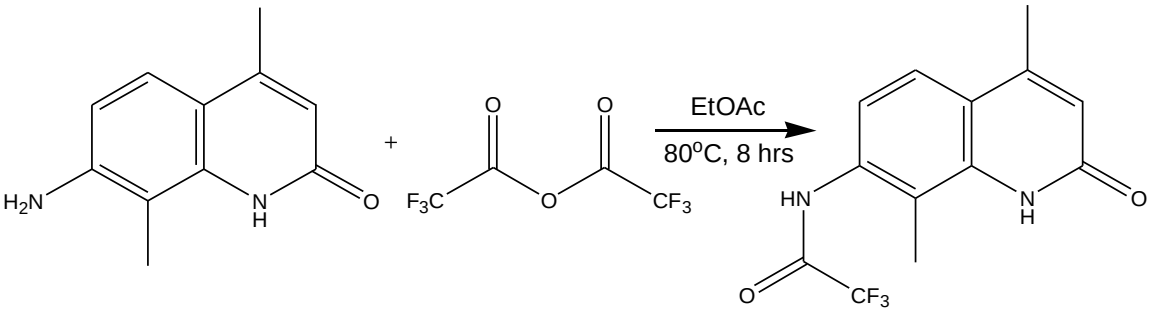

Scheme 3.7.3[32]: Protection of 7-amino-4,8-dimethylcarbostyril using trifluoroacetic anhydride.

The protection of amine group of 7-amino-4,8-dimethylcarbostyril using trifluoroacetic anhydride was adapted from a previously published procedure by Nakagawa *et al.* with slight modification.[32] 220 mg (1.17 mmol) of 7-amino-4,8-dimethylcarbostyril was added into a 25 ml flask, followed by 10 ml of ethyl acetate. The solution was cooled in an ice-bath and 0.18 ml (1.29 mmol) of trifluoroacetic anhydride was added dropwise. The reaction was stirred and refluxed overnight. The solution was cooled to room temperature, the precipitate filtered, and washed with cold ethyl acetate. The solid was dried under vacuum to give 330 mg (99%) of the product.

APCI-ESI MS: MH^+: 285.0855 (calc. 285.0845)

^{1}H NMR (400 MHz, DMSO-*d*$_6$): δ 2.25 (3H, s), δ 2.43 (3H, s), δ 6.45 (1H, s), δ 7.13 (1H, d, J = 12 Hz), δ 7.64 (1H, d, J = 12 Hz), δ 10.79 (1H, br s), δ 11.25 (1H, br s)

^{19}F NMR (400 MHz, DMSO-d6): δ -74.27 , δ -62.66

IR:

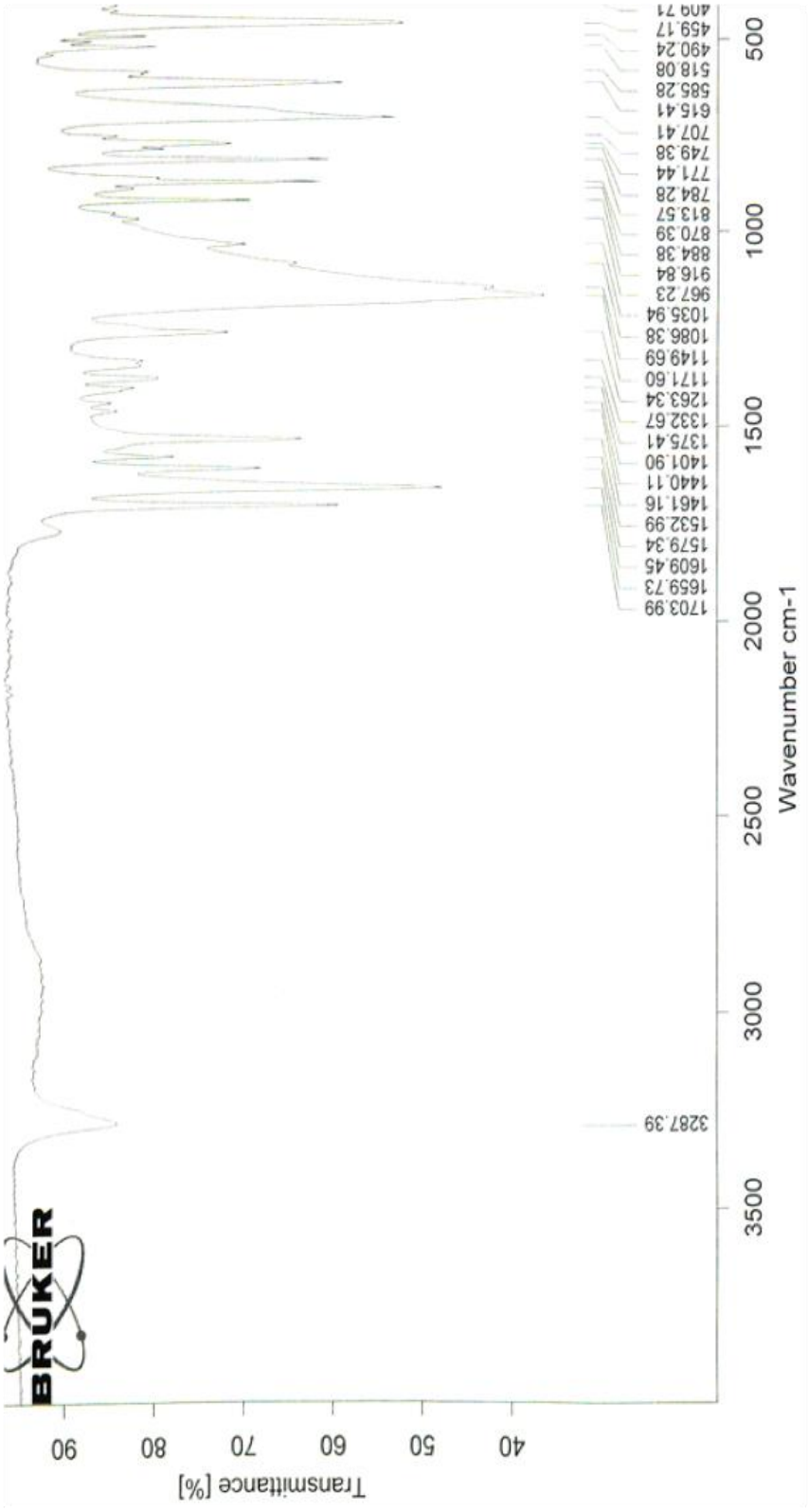
BRUKER
Transmittance [%]
90
80
70
60
50
40
Wavenumber cm-1
3500
3000
2500
2000
1500
1000
500
3287.39
1703.99
1659.73
1609.45
1579.34
1532.99
1461.16
1440.11
1401.90
1375.41
1332.67
1263.34
1171.60
1149.69
1086.38
1035.94
967.23
916.84
884.38
870.39
813.57
784.28
771.44
749.38
707.41
615.41
585.28
518.08
490.24
459.17
409.71

Attempted bromination of 7-trifluoroacetamide-4,8-dimethylcarbostyril

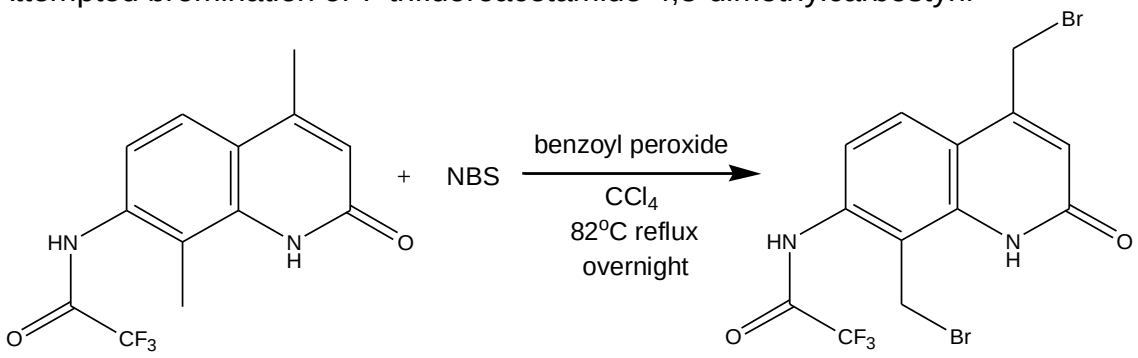

Scheme 3.7.4[33]: Attempted bromination of the aryl methyl groups of 7-trifluoroacetamide-4,8-dimethylcarbostyril using *N*-bromosuccinamide.

Bromination of the methyl group of the protected 2,6-diaminotoluene followed, with some modifications, a published procedure of Hashizume *et al.*.[33] 50 mg (0.173 mmol) of the 7-trifluoroacetamide-4,8-dimethylcarbostyril and 69 mg (0.387 mmol) of *N*-bromosuccinimide were added to a 10 ml flask. 6.4 mg (0.026 mmol) of benzoyl peroxide was added, along with 5 ml of carbon tetrachloride. The solution was stirred and refluxed at 82°C overnight and then cooled to room temperature. Precipitate formed which was filtered and analyzed, which showed pure starting material.

Synthesis of 7-amino-8-methyl-4-trifluoromethylcarbostyril

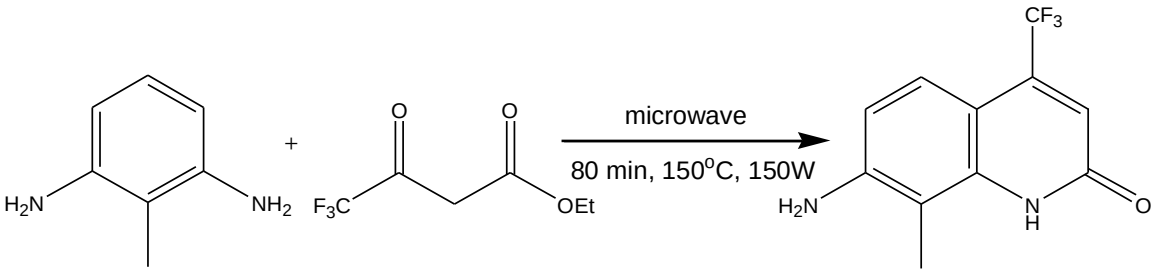

Scheme 3.8.1[34]: Synthesis of 7-amino-8-methyl-4-trifluoromethylcarbostyril.

The compound 7-amino-8-methyl-4-trifluoromethylcarbostyril has been synthesized by Lee *et al.* and they were able to get the same compound.[34] 244 mg (2 mmol) of 2,6-diaminotoluene, 0.292 ml (2 mmol) of ethyl 4,4,4-trifluoroacetoacetate, and 1 ml of water were introduced into a 10 ml microwave glass tube with a snap-on plastic cap. The reaction was carried out at 150°C for 80 minutes with 150 W of microwave irradiation. The reaction was cooled to room temperature and then in the freezer for an hour. The yellow precipitate was filtered, washed with 40 ml cold ether, washed with 40 ml cold water, and dried under vacuum. 1.86 g (96%) of the product was obtained. The same spectra for the analysis of the compound was included in the paper by Lee *et al.*.

APCI-ESI MS: MH^+: 243.0743 (calc. 243.0740)

^{1}H NMR (400 MHz, DMSO-d_6): δ 2.13 (3H, s), δ 5.93 (2H, br s), δ 6.48 (1H, s), δ 6.67 (1H, d, J = 12 Hz), δ 7.29 (1H, d, J = 12 Hz), δ 10.84 (1H, br s)

Protection of 7-amino-8-methyl-4-trifluoromethylcarbostyril

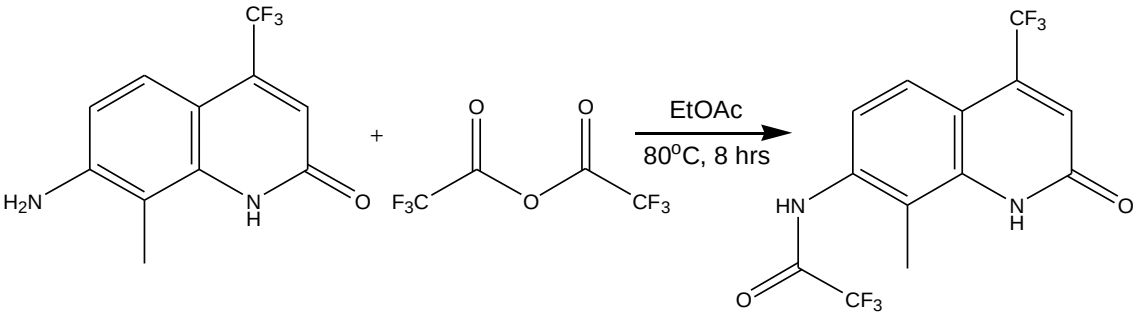

Scheme 3.8.2[32]: Protection of 7-amino-8-methyl-4-trifluoromethylcarbostyril using trifluoroacetic anhydride.

The protection of amine group of 7-amino-4,8-dimethylcarbostyril using trifluoroacetic anhydride was adapted from a previously published procedure by Nakagawa *et al.* with slight modification.[32] 500 mg (2.07 mmol) of 7-amino-8-methyl-4-trifluoromethylcarbostyril and 20 ml of ethyl acetate were added into a 50 ml flask. The solution was cooled in an ice-bath and trifluoroacetic anhydride added dropwise while cooling. The reaction was refluxed overnight and then cooled. The precipitate that formed was filtered, washed with ethyl acetate, and dried under vacuum. The protected compound obtained was 558 mg (80%).

APCI-ESI MS: MH^+: 339.0568 (calc. 339.0563)

Attempted bromination: 8-methyl-7-trifluoroacetamido-4-trifluoromethylcarbostyril

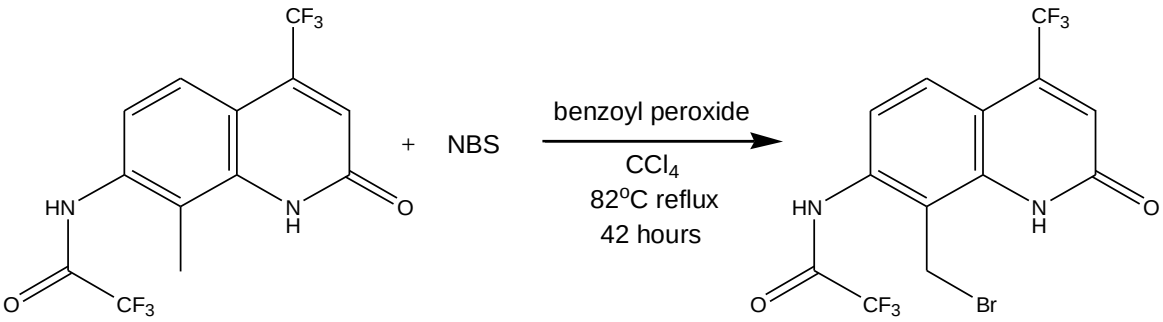

Scheme 3.8.3[33]: Attempted bromination of the methyl group of 8-methyl-7-trifluoroacetamide-4-trifluoromethylcarbostyril.

Bromination of the methyl group of the protected 8-methyl-7-trifluoroacetamide-4-trifluoromethylcarostyril followed a previously published procedure, with some modifications, Hashizume *et al.*.[33] 100 mg (0.352 mmol) of 8-methyl-7-trifluoroacetamide-4-trifluoromethylcarbostyril and 188 mg (1.06 mmol) of *N*-bromosuccinamide were added into a 50 ml flask and suspended in 10 ml of carbon tetrachloride. 13 mg (0.053 mmol) of benzoyl peroxide was added and the reaction refluxed for 42 hours. The solution was cooled to room temperature and the solid filtered and dried under vacuum. Analysis of the compound showed pure starting material.

Attempted oxidation: 8-methyl-7-trifluoroacetamide-4-trifluoromethylcarbostyril

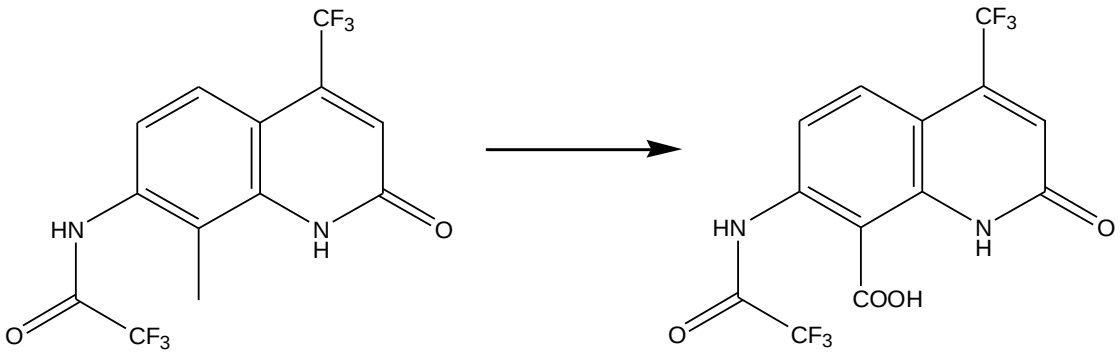

Scheme 3.8.4: Attempted oxidation of the methyl group of 8-methyl-7-trifluoroacetamide-4-trifluoromethylcarbostyril.

A) Catalytic aerobic oxidation: The catalytic aerobic oxidation of the methyl group of 8-methyl-7-trifluoroacetamide-4-trifluoromethylcarbostyril was adapted, with slight modification, from a previously published procedure by Sakaguchi *et al.*.[35] 48 mg (0.296 mmol) of *N*-hydroxyphthalimide, 15 mg (0.059 mmol) $Co(OAc)_2$, and 8 mg (0.030 mmol) $Mn(OAC)_2$ were added to a 25 ml flask and dissolved in 15 ml of acetic acid. 0.012 ml (0.30 mmol) of nitric acid was slowly added, followed by slow addition of 100 mg (2.96 mmol) of 8-methyl-7-trifluoroacetamide-4-trifluoromethylcarbostyril. A reflux condenser was attached and a balloon filled with O_2 was attached to the reflux via a needle. The solution was stirred and refluxed at 110°C for 16 hours. The solution was cooled to room temperature and the solvent evaporated under vacuum10 ml of methanol was added and the solution refluxed for 1 hour. The solution was then cooled to room temperature, then in an ice-bath. Acetonitrile was added to the chilled solution but no precipitate formed. Analysis of the liquid showed no desired product.

B) Collin's reagent oxidation: The oxidation of the methyl group of 8-methyl-7-trifluoroacetamide-4-trifluoromethylcarbostyril using Collin's reagent was followed, with some modifications, from a previously published procedure by Collins *et al.*.[36] CrO_3 was dried over NaOH and under vacuum overnight prior to using it. 300 mg (3.00 mmol) of CrO_3 was added in small portions into a stirred and cooled 2.25 ml anhydrous pyridine. The complex was washed by several decantations of petroleum ether. The solid complex was filtered and dried under vacuum. 458 mg (1.78 mmol) of the complex and 100 mg (0.296 mmol) of 8-methyl-7-trifluoroacetamide-4-trifluoromethylcarbostyril were added into a 10 ml dry flask. 5 ml of anhydrous dichloromethane was then added and the mixture was stirred in room temperature for 24 hours. TLC analysis of the crude solution showed pure starting material.

C) Pyridinium Chlorochromate oxidation: The oxidation of the methyl group of 8-methyl-7-trifluoroacetamide-4-trifluoromethylcarbostyril using PCC was followed, with some modifications, from a previously published procedure by Corey *et al.*.[37] CrO_3 was dried over NaOH and under vacuum overnight prior to using it. 300 mg (3.00 mmol) of CrO_3 was added to concentrated aqueous HCl rapidly while stirring. After 5 minutes, the homogenous solution was cooled in an ice-bath and 0.242 ml (3.00 mmol) of pyridine was added carefully over 3 minutes. The resulting solid complex was filtered, washed with petroleum ether, and dried under vacuum. 22 mg (0.102 mmol) of the complex was added into a 10 ml flask and suspended in 5 ml of dichloromethane. 23 mg (0.068 mmol) of 8-methyl-7-

trifluoroacetamide-4-trifluoromethylcarbostyril was added all at once and the mixture was stirred in room temperature for 24 hours. TLC analysis of the crude solution showed pure starting material.

D) Potassium permanganate oxidation: The oxidation of the methyl group of 8-methyl-7-trifluoroacetamide-4-trifluoromethylcarbostyril using $KMnO_4$ was followed, with some modifications, from a previously published procedure by Bogert *et al.*.[38] 100 mg (0.296 mmol) of 8-methyl-7-trifluoroacetamido-4-trifluoromethylcarbostyril, 117 mg (0.740 mmol) of $KMnO_4$, and 16 mg (0.148 mmol) of Na_2CO_3 were added into a 10 ml flask. 5 ml of water was added and the suspension refluxed at 105°C for 8 hours. The solution was cooled to room temperature and the solid separated by filtration. The filtrate was concentrated under vacuum and the resulting crude solid identified as deprotected starting material.

Protection of 2,6-diaminotoluene using trifluoroacetic anhydride

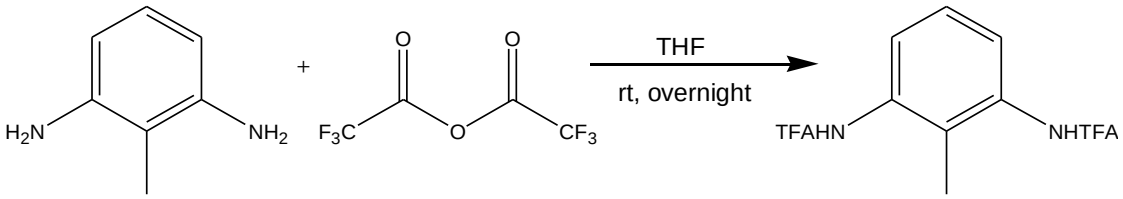

Scheme 3.9.1: Protection of 2,6-diaminotoluene using trifluoroacetic anhydride.

The protection of amine group of 2,6-diaminotoluene using trifluoroacetic anhydride was adapted from a previously published procedure by Nakagawa *et al.* with slight modification.[32] 250 mg (2.05 mmol) of 2,6-diaminotoluene was

dissolved in 5 ml of anhydrous THF and cooled in an ice-bath. 0.75 ml (5.33 mmol) of trifluoroacetic anhydride was added slowly and the solution stirred overnight in room temperature. The solvent was evaporated under vacuum to give a white powder. The solid was successively washed with water, 2% aqueous HCl, water, 4% $NaHCO_3$, and water. The crude product was recrystallized from ethyl acetate, filtered, washed with cold ethyl acetate, and dried over P_2O_5 under vacuum to afford 946 mg (37%) of the protected compound.

APCI-ESI MS: MH^+: 315.0524 (calc. 315.0563)

^{1}H NMR (400 MHz, DMSO-d_6): δ 2.02 (3H, s), δ 7.28-7.36 (3H, m, J = 8 Hz), δ 11.12 (2H, br s)

Attempted oxidation of 2,6-di(trifluoroacetamino)toluene

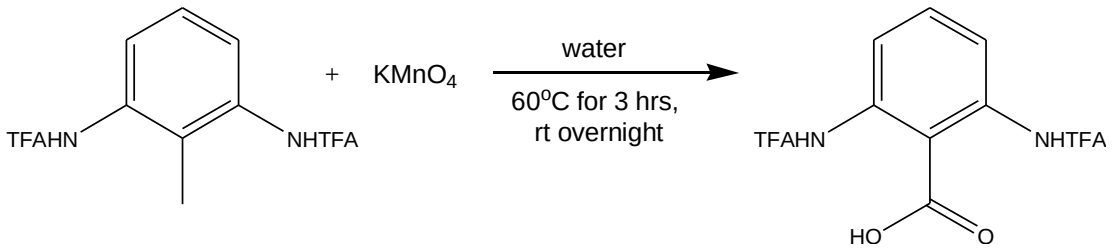

Scheme 3.9.2: Attempted oxidation of 2,6-di(trifluoroacetamido)toluene.

The oxidation of the methyl group of 2,6-di(trifluoroacetamido)toluene using $KMnO_4$ was followed, with some modifications, from a previously published procedure by Bogert *et al.*.[38] 946 mg (3.01 mmol) of 2,6-di(trifluoroacetamido)toluene, 362 mg (3.01 mmol) of $MgSO_4$, and 951 mg (6.02 mmol) of $KMnO_4$ were suspended in 45 ml of water. The mixture was heated and

stirred at 60°C for 3 hours, then stirred in room temperature overnight. The insoluble material was filtered and the filtrate was acidified with concentrated HCl. No solid formed even in acidic solution and analysis of the liquid showed starting material.

Attempted bromination of2,6-di(trifluoroacetamido)toluene

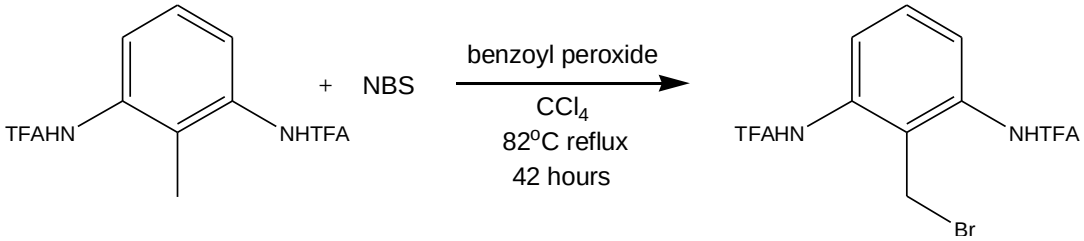

Scheme 3.9.3: Attempted bromination of 2,6-di(trifluoroacetamido)toluene.

Bromination of the methyl group of 2,6-di(trifluoroacetamido)toluene was adapted from a previously published procedure, with some modifications, by Hashizume *et al.*.[33] 100 mg (0.318 mmol) of 2,6-di(trifluoroacetamido)toluene, 125 mg (0.701 mmol) of *N*-bromosuccinimide, and 7.8 mg (0.048 mmol) of azo-*bis*-isobutyronitrile were added in a 25 ml flask and suspended in 10 ml of carbon tetrachloride. The reaction was stirred and refluxed at 83°C for 42 hours. The solution was cooled and the filtrate separated. Analysis of the crude filtrate showed no sign of the product.

Protection of 2,6-diaminotoluene using acetic anhydride

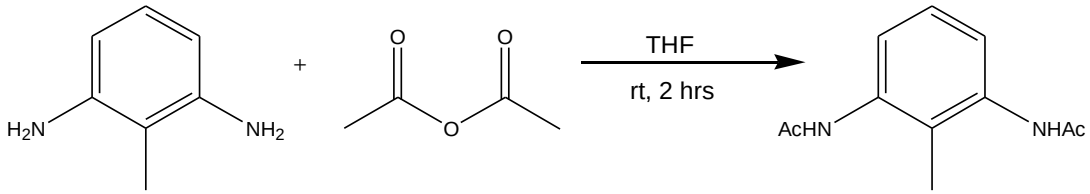

Scheme 3.10.1: Protection of 2,6-diaminotoluene using acetic anhydride.

The protection of amine group of 2,6-diaminotoluene using acetic anhydride was adapted from a previously published procedure by Nakagawa *et al.* with slight modification.[32] 200 mg (1.64 mmol) of 2,6-diaminotoluene was dissolved in 5 ml of anhydrous THF and cooled in an ice-bath. 0.403 ml (4.26 mmol) of acetic anhydride was slowly added to the mixture and stirred for 2 hours. The resulting solid was filtered, washed with water, and dried under vacuum. 300 mg (89 %) of the protected product was obtained.

APCI-ESI MS: M^-: 205.0995 (calc. 205.0986)

^{1}H NMR (400 MHz, DMSO-d_6): δ 2.04 (3H, s), δ 7.10-7.16 (3H, m, J = 8 Hz), δ 9.36 (2H, br s)

Oxidation of 2,6-di(acetamido)toluene

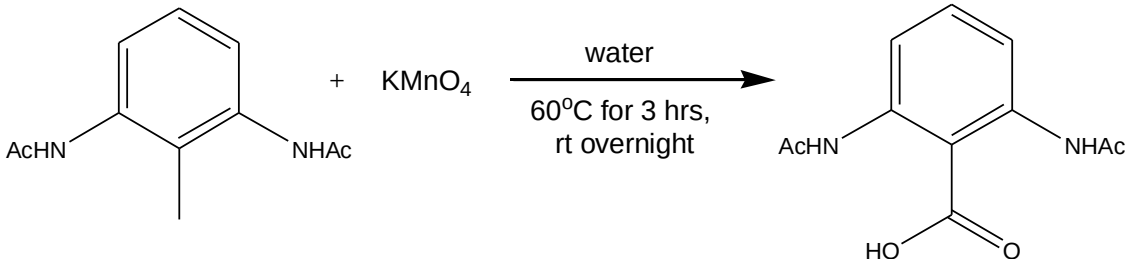

Scheme 3.10.2: Oxidation of 2,6-di(acetamido)toluene.

The oxidation of the methyl group of 2,6-di(trifluoroacetamido)toluene using $KMnO_4$ was followed, with some modifications, from a previously published procedure by Bogert *et al.*.[38] 300 mg (1.46 mmol) of 2,6-di(acetamido)toluene and 296 mg (2.46 mmol) of $MgSO_4$ were suspended in water and heated to 60°C. 1.04 g (6.56 mmol) of $KMnO_4$ was slowly added to the suspension and stirred at 60°C for 68 hours. The solution was cooled down and the solid was filtered off. The filtrate was acidified to give an off-yellow precipitate. The precipitate was filtered and dried under vacuum to give 117 mg (30%) of the product.

APCI-ESI MS: M^-: 235.0731 (calc. 235.0724)

^{1}H NMR (400 MHz, DMSO-d_6): δ 2.02 (3H, s), δ 7.39 (1H, t, J = 12 Hz), δ 7.52 (2H, d, J = 12 Hz), δ 10.00 (2H, br s)

IR:

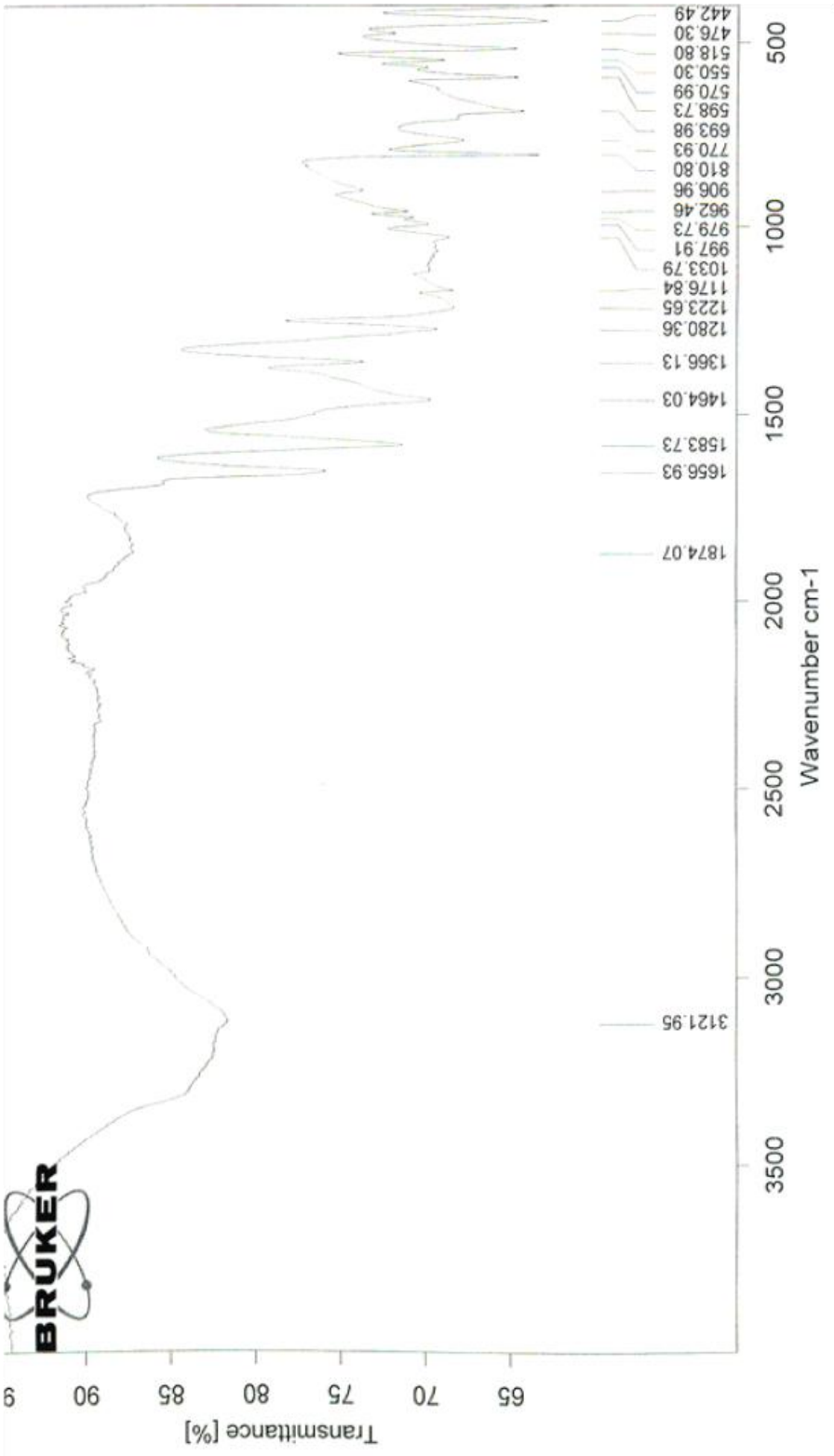
BRUKER
Transmittance [%]
65
70
75
80
85
90
9
Wavenumber cm-1
3500
3000
2500
2000
1500
1000
500
3121.95
1874.07
1656.93
1583.73
1464.03
1366.13
1280.36
1223.65
1176.84
1033.79
997.91
979.73
962.46
906.96
810.80
770.93
693.98
598.73
570.99
550.30
518.80
476.30
442.49

Deprotection of 2,6-di(acetamido)benzoic acid

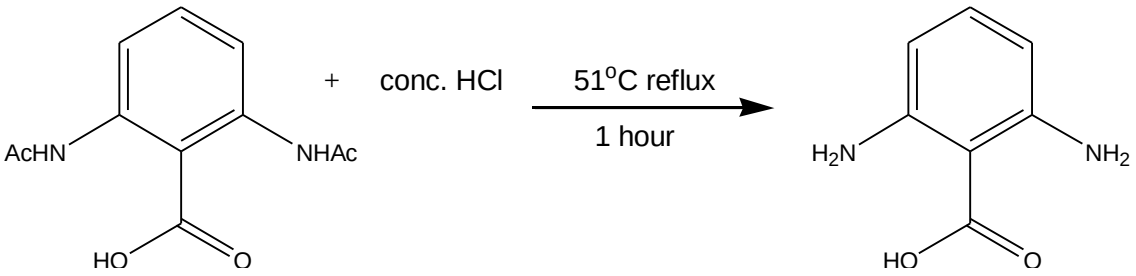

Scheme 3.10.3: Deprotection of 2,6-di(acetamido)benzoic acid.

The deprotection of 2,6-di(acetamido)benzoic acid was followed from a previously published procedure, with a slight modification, by Nakagawa *et al.*.[32] 325 mg (1.38 mmol) of 2,6-di(acetamido)benzoic acid was placed in a 25 ml flask. Concentrated HCl was added until all the solid was dissolved. The solution was refluxed at 51°C for an hour. The solution was cooled and the precipitate filtered and dried under vacuum. 260 mg (84%) of the deprotected material was obtained.

APCI-ESI MS: MH^+: 153.0644 (calc. 153.0659)

^{1}H NMR (400 MHz, DMSO-d_6): δ 4.87 (4H, br s), δ 6.69 (2H, d, J = 8 Hz), δ 7.21 (1H, t, J = 8 Hz)

Attempted synthesis of 7-amino-8-carboxy-4-trifluoromethylcarbostyril

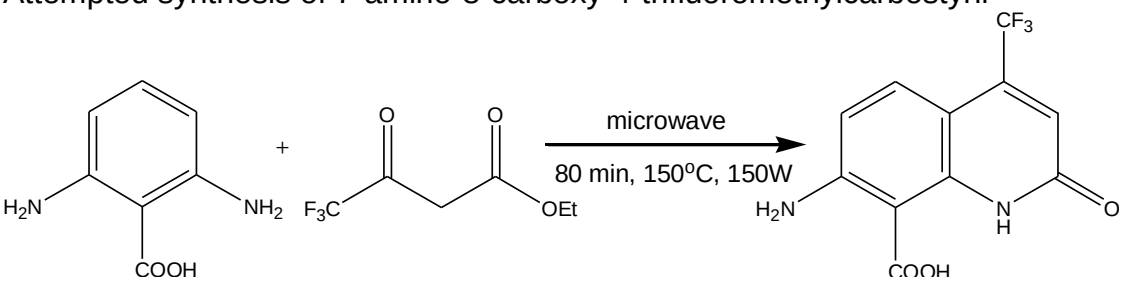

Scheme 3.10.4[34]: Attempted synthesis of 7-amino-8-carboxy-4-trifluoromethylcarbostyril.

The synthesis of compound 7-amino-8-carboxy-4-trifluoromethylcarbostyril was attempted, with some modifications, using a previously published procedure by Lee *et al.*.[34] 100 mg (0.658 mmol) of 2,6-diaminobenzoic acid, 0.096 ml (0.658 mmol) of ethyl 4,4,4-trifluoroacetoaectate, and 1 ml of water were placed in a 10 ml microwave glass tube and capped with a snap-on plastic cap. The mixture was irradiated under 150 W microwave radiation at 150°C for 80. The reaction was cooled first to room temperature and then in the freezer. The precipitate was filtered, washed with 40 ml cold ether and 40 ml cold water, and dried under vacuum to give 56 mg (31%) of the product. Analysis showed that the product is not the 7-amino-8-carboxy-4-trifluoromethylcarbostyril but instead 7-amino-4-trifluoromethylcarbostyril. The same spectrum is included for the product 7-amino-4-trifluoromethylcarbostyril in the published work of Lee *et al.*.

APCI-ESI MS: MH^+: 229.0322 (calc. 229.0583)

^{1}H NMR (400 MHz, DMSO-d_6): δ 6.15 (2H, br s), δ 6.42 (1H, d, J = 2 Hz), δ 6.45 (1H, d, J = 4 Hz), δ 6.56 (1H, dd, J_1 = 12 Hz, J_2 = 4 Hz), δ 7.34 (1H, dd, J_1 = 8 Hz, J_2 = 2 Hz), δ 11.81 (1H, br s)

^{19}F NMR (400 MHz, DMSO-d_6): δ -62.73

Attempted esterification of 2,6-di(acetamido)benzoic acid

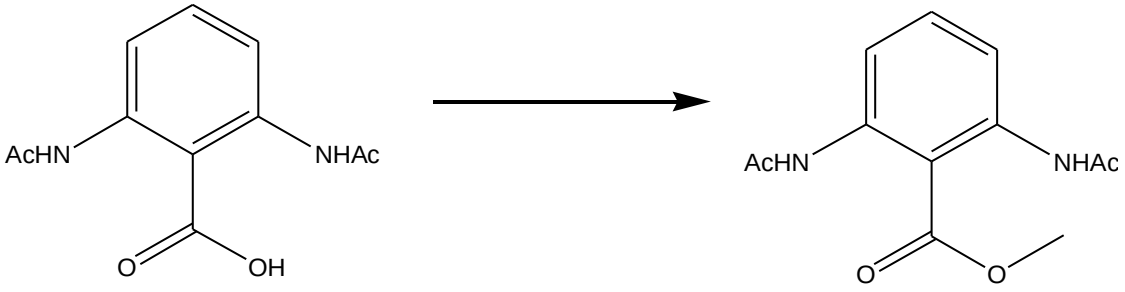

Scheme 3.11.1: Attempted esterification of the carboxyl group of 2,6-di(acetamido)benzoic acid.

A) Fischer esterification: The Fischer esterification of the carboxylic acid group of 2,6-di(acetamido)benzoic acid was adapted from a previously published procedure by Ohkata *et al.*.[39] 500 mg (1.62 mmol) of the 2,6-di(acetamido)benzoic acid was dissolved in 20 ml of methanol. The solution was cooled in an ice-bath and HCl gas (1.5 mol) was bubbled into the cooled solution while stirring for a period of 3 hours. Precipitate is observed during the reaction as the solution became cloudy. The solution was stored in the freezer overnight. The precipitate was filtered, washed with cold HCl/methanol solution, and dried under vacuum. Analysis of the solid showed deprotected starting material.

B) Esterification via acid chloride formation: The esterification through the formation of an acid chloride of the benzoic acid group of 2,6-di(acetamido)benzoic acid was followed, with some modifications, using a previously followed procedure by Lebedev *et al.*.[40] 500 mg (1.62 mmol) of the 2,6-di(acetamido)benzoic acid was dissolved in 2.76 ml of methanol and heated to 50°C. 0.238 ml (3.28 mmol) of thionyl chloride was slowly added at a rate so

that no over-boiling occurs. After all the thionyl chloride was added, the reaction was refluxed for 2 hours at 67°C in which precipitate appeared. The solid was filtered and dried under vacuum. Analysis of the solid showed unreacted starting material.

C) Esterification using methyl iodide: The esterification of the carboxylic acid group of 2,6-di(acetamido)benzoic acid using methyl idodide was followed, with some modification, from a previously published procedure by Hoorfar *et. al.*.[41] 383 mg (1.62 mmol) of 2,6-di(acetamido)benzoic acid was suspended in 20 ml of anhydrous THF. 43 mg (1.79 mmol) of NaH was slowly added at 40°C and stirred for 20 minutes. 0.111 ml (1.79 mmol) of methyl iodide was added and the mixture was refluxed at 45°C overnight. The solution was filtered to give an off-white solid. Analysis of the solid shows deprotected starting material.

D) Esterification using carbonyldiimidazole[42]: The esterification of the carboxylic acid group of 2,6-di(acetamido)benzoic acid using carbonyldiimidazole was adapted, with some modification, from a published patent procedure by GenenCor International Incorporation.[42] 250 mg (0.812 mmol) of 2,6-di(acetamido)benzoic acid and 132 mg (0.812 mmol) of carbonyldiimidazole were added in 10 ml of anhydrous dimethylformamide. The mixture was purged to keep it inert and then stirred for 1.5 hours at 40°C. 0.121 ml (0.812 mmol) of 1,8-diazabicycloundec-7-ene and 0.033 ml (0.812 mmol) of methanol added and stirred for 24 hours at 40°C. The solution was cooled,150 ml of ether was added and then acidified by adding 1.5M of HCl. The ether layer was separated and the

aqueous layer extracted with 150 ml of ether and 150 ml of ethyl acetate. The organic layers were combined and washed with water, 10% K_2CO_3, and brine. Magnesium sulfate was used to dry the organic layer. The solution was concentrated under vacuum and analysis of the resulting solid showed the starting material.

E) Esterification using dimethyl carbonate: The esterification of the carboxylic acid group of 2,6-di(acetamido)benzoic acid using dimethyl carbonate was followed, with some modification, from a previously published procedure by Rekha *et. al.*.[43] 250 mg (0.812 mmol) of 2,6-di(acetamido)benzoic acid, 0.278 ml (3.30 mmol) dimethyl carbonate, 0.0095 ml (9.32% mol) concentrated sulfuric acid, and 5 ml of anhydrous THF were mixed in a 10 ml flask, stirred, and heated to 60°C overnight. The solution was cooled and then poured into 10 ml of 10% aqueous $NaHCO_3$. The aqueous layer was extracted with 30 ml of ethyl acetate once and 30 ml of dichloromethane twice. The combined organic layers were dried with sodium sulfate. Evaporation of the solvent showed starting material.

Esterification of 2,6-di(acetamido)benzoic acid using dimethyl sulfate

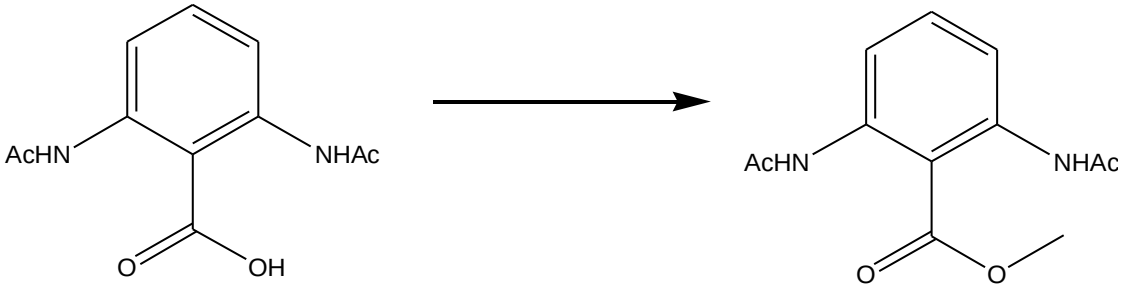

Scheme 3.11.1: Esterification of the carboxyl group of 2,6-di(acetamido)benzoic acid using dimethyl sulfate.

The esterification of the carboxylic acid group of 2,6-di(acetamido)benzoic acid using dimethyl carbonate was followed, with a slight modification, from a previously published procedure by Bose *et. al.*.[44] Esterification of the carboxyl group followed a previously published procedure.[44] 250 mg (0.812 mmol) of 2,6-di(acetamido)benzoic acid, 0.173 ml (1.82 mmol) of dimethyl sulfate, 631 mg (4.6 mmol) of potassium carbonate, and 5 ml of dry acetone were mixed in a 10 ml flask. The solution was heated and refluxed at 59°C for 3 hours. The solution was cooled and diluted with 10 ml of water followed by extraction with 10 ml of ethyl acetate three times. The combined organic layer were washed with 5 ml of brine twice and dried over sodium sulfate. The solvent was evaporated in vacuum to give a yellow solid. The solid was recrystallized in methanol to give a 55 mg (27%) of white solid.

APCI-ESI MS: MH^+: 251.1032 (calc. 251.1026)

^{1}H NMR (400 MHz, DMSO-d_6): δ 2.01 (6H, s), δ 3.73 (3H, s), δ 7.33 (2H, d, J = 8 Hz), δ 7.42 (1H, t, J = 8 Hz), δ 9.72 (2H, br s)

IR:

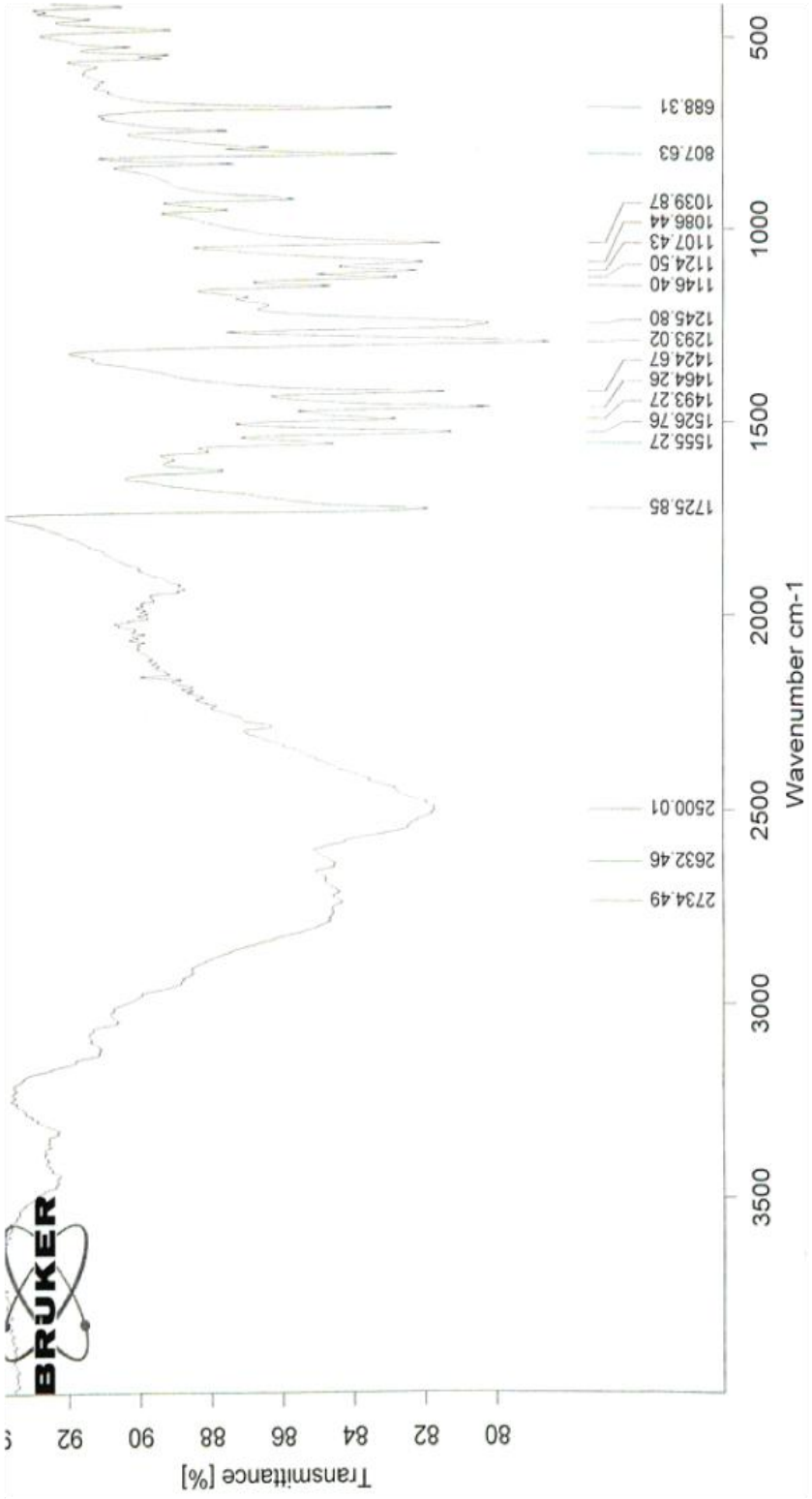
688.31
807.63
1039.87
1086.44
1107.43
1124.50
1146.40
1245.80
1293.02
1424.67
1464.26
1493.27
1526.76
1555.27
1725.85
2500.01
2632.46
2734.49
500
1000
1500
2000
2500
3000
3500
Wavenumber cm-1
80
82
84
86
88
90
92
Transmittance [%]
BRUKER

Deprotection of methyl 2,6-di(acetamido)benzoate

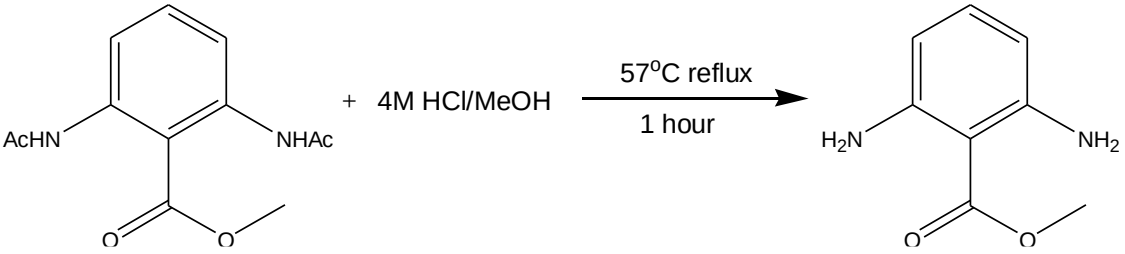

Scheme 3.11.2[38]: Deprotection of methyl 2,6-di(acetamido)benzoate.

The deprotection of methyl 2,6-di(acetamido)benzoate was followed from a previously published procedure, with a slight modification, by Nakagawa *et al.*.[32] 392 mg (1.57 mmol) of methyl 2,6-di(acetamido)benzoate was placed in a 50 ml flask and dissolved in 10 ml of 4M HCl in methanol. The solution was refluxed at 57°C for an hour, then cooled to room temperature. The white solid was filtered and dried under vacuum. 222mg (85%) of the product was recovered.

APCI-ESI MS: MH^+: 167.0822 (calc. 167.0815)

^{1}H NMR (400 MHz, DMSO-d_6): δ 3.82 (3H, s), δ 6.72 (2H, d, J = 8 Hz), δ 7.24 (1H, t, J = 8 Hz)

Synthesis of 7-amino-8-carbomethoxy-4-trifluoromethylcarbostyril

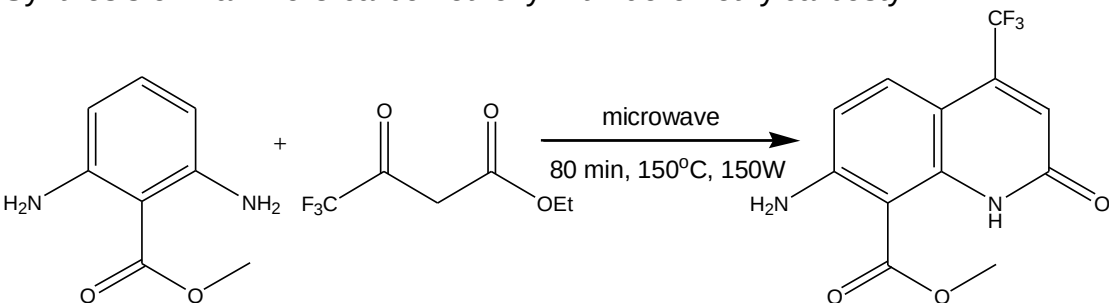

Scheme 3.11.3[33]: Synthesis of 7-amino-8-carbomethoxy-4-trifluoromethylcarbostyril.

The synthesis of compound 7-amino-8-carbomethoxy-4-trifluoromethylcarbostyril was attempted, with some modifications, using a previously published procedure by Lee *et al.*.[34] 250 mg (1.05 mmol) of methyl 2,6-diaminobenzoate, 0.154 ml (1.05 mmol) of ethyl 4,4,4-trifluoroacetoacetate, and 1 ml of water were introduced into a 10 ml microwave glass with a snap-on plastic cap. The reaction was run at 150°C for 80 minutes under 150 W microwave irradiation. The reaction was cooled to room temperature, then placed in the freezer overnight. The solid was filtered and washed with 15 ml of cold ether and 15 ml of cold water to give 78 mg (26%) of yellow solid.

Melting point: 265.3 - 266.8°C

APCI-ESI MS: MH^+: 287.0654 (calc. 287.0638)

Fluorescence: Using a published literature by Fabian *et al.*[45] (Table 4), substituents on different positions of the carbostyril affect the fluorescence maxima. Substituents on the 3- and 7-positions cause a red shift while substituents on the 4- and 8-positions do the opposite. Using Fabian *et al.*'s closest sample (sample **13**) and considering the difference on the substituents, it can be predicted that the fluorescence maxima of 7-amino-8-carbomethoxy-4-trifluoromethylcarbostyril to be about 360 nm.

^{1}H NMR (400 MHz, DMSO-d_6): δ 3.94 (3H, s), δ 6.62 (1H, s), δ 6.80 (1H, d, J = 12 Hz), δ 7.52 (2H, br s), δ 7.54 (1H, d, J = 12 Hz), δ 12.28 (1H, br s)

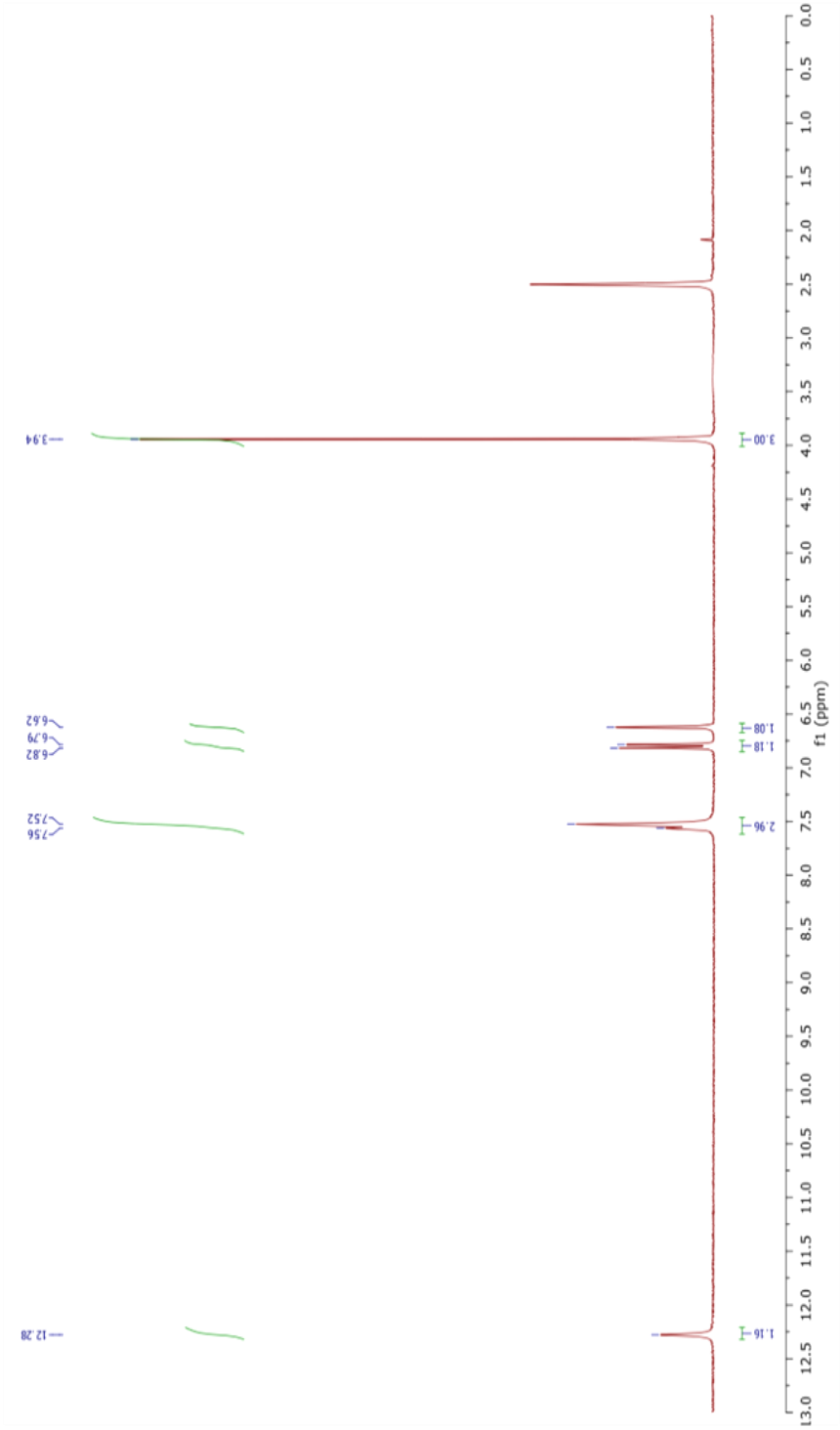

^{13}C NMR (100 MHz, DMSO-d_6): δ 53.08, δ 93.71, δ 103.63, δ 114.20, δ 114.78, δ 123.14, δ 129.88, δ 137.83, δ 143.83, δ 154.67, δ 160.48, δ 168.98

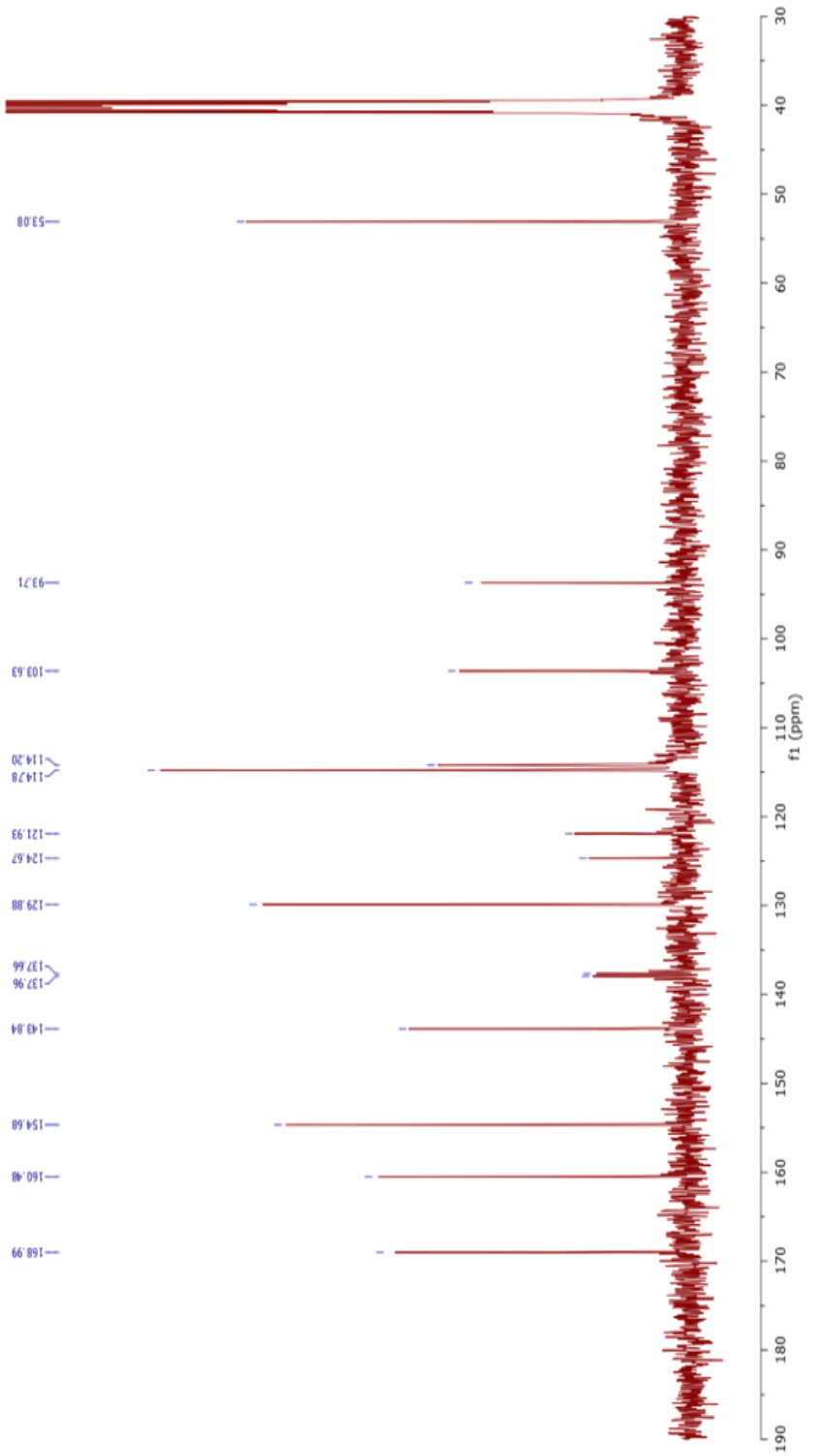

^{19}F NMR (376 MHz, DMSO-d_6): δ - 62.31 (TFA as reference at δ -76.55)

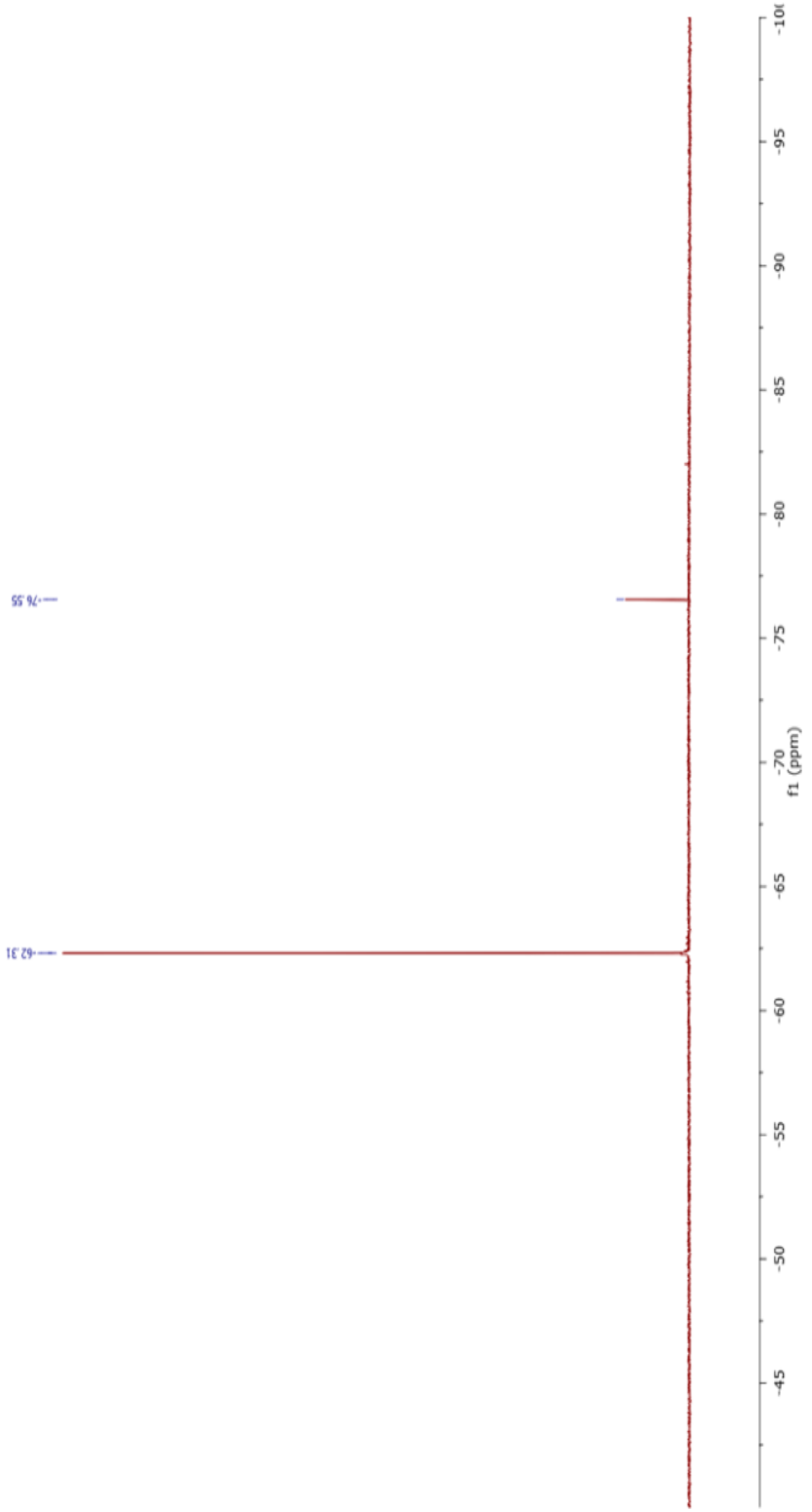

IR:

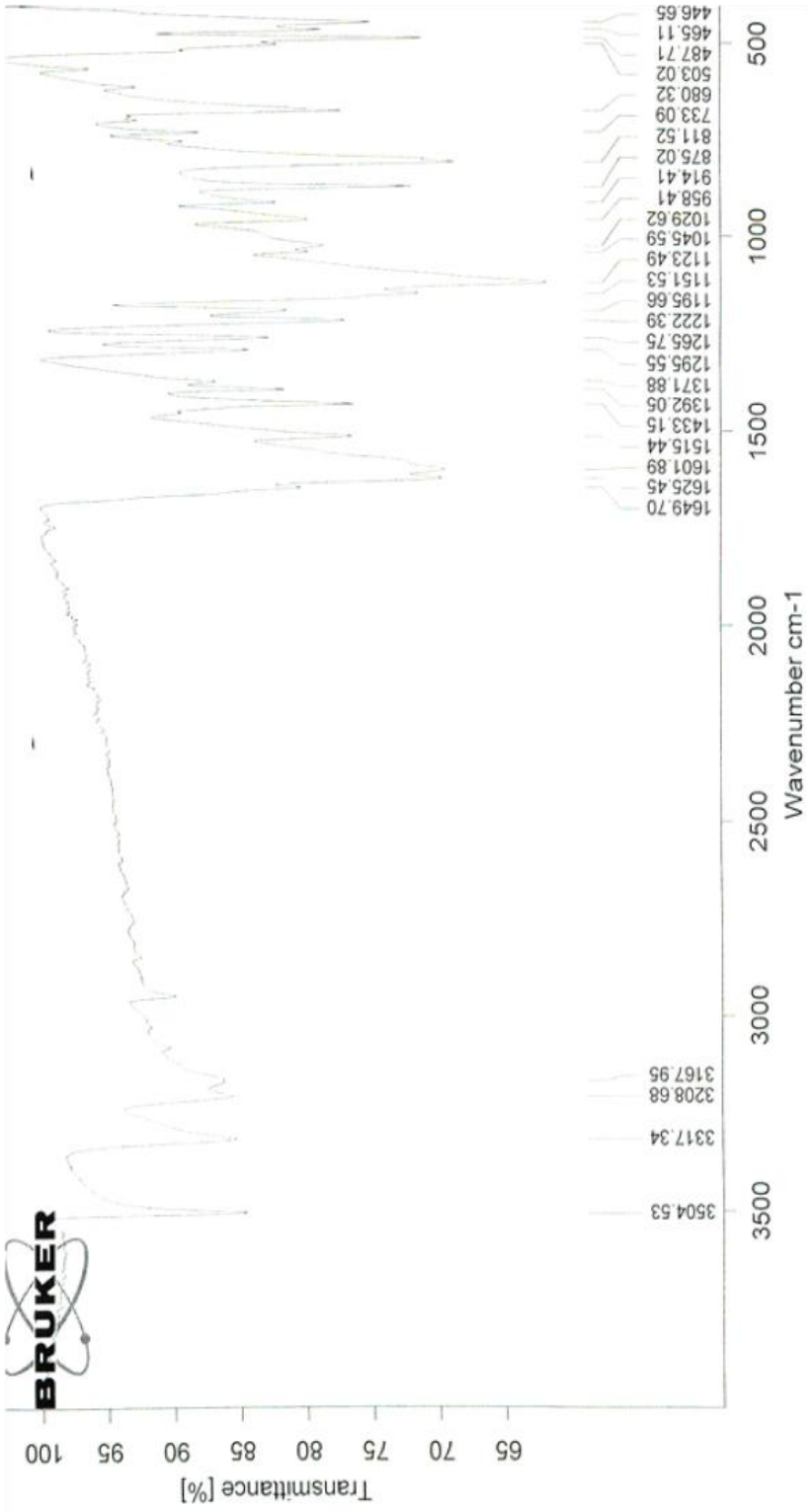
BRUKER
Transmittance [%]
100
95
90
85
80
75
70
65
Wavenumber cm-1
3500
3000
2500
2000
1500
1000
500
3504.53
3317.34
3208.68
3167.95
1649.70
1625.45
1601.89
1515.44
1433.15
1392.05
1371.88
1295.55
1265.75
1222.39
1195.66
1151.53
1123.49
1045.59
1029.62
958.41
914.41
875.02
811.52
733.09
680.32
503.02
487.71
465.11
446.65

UV:

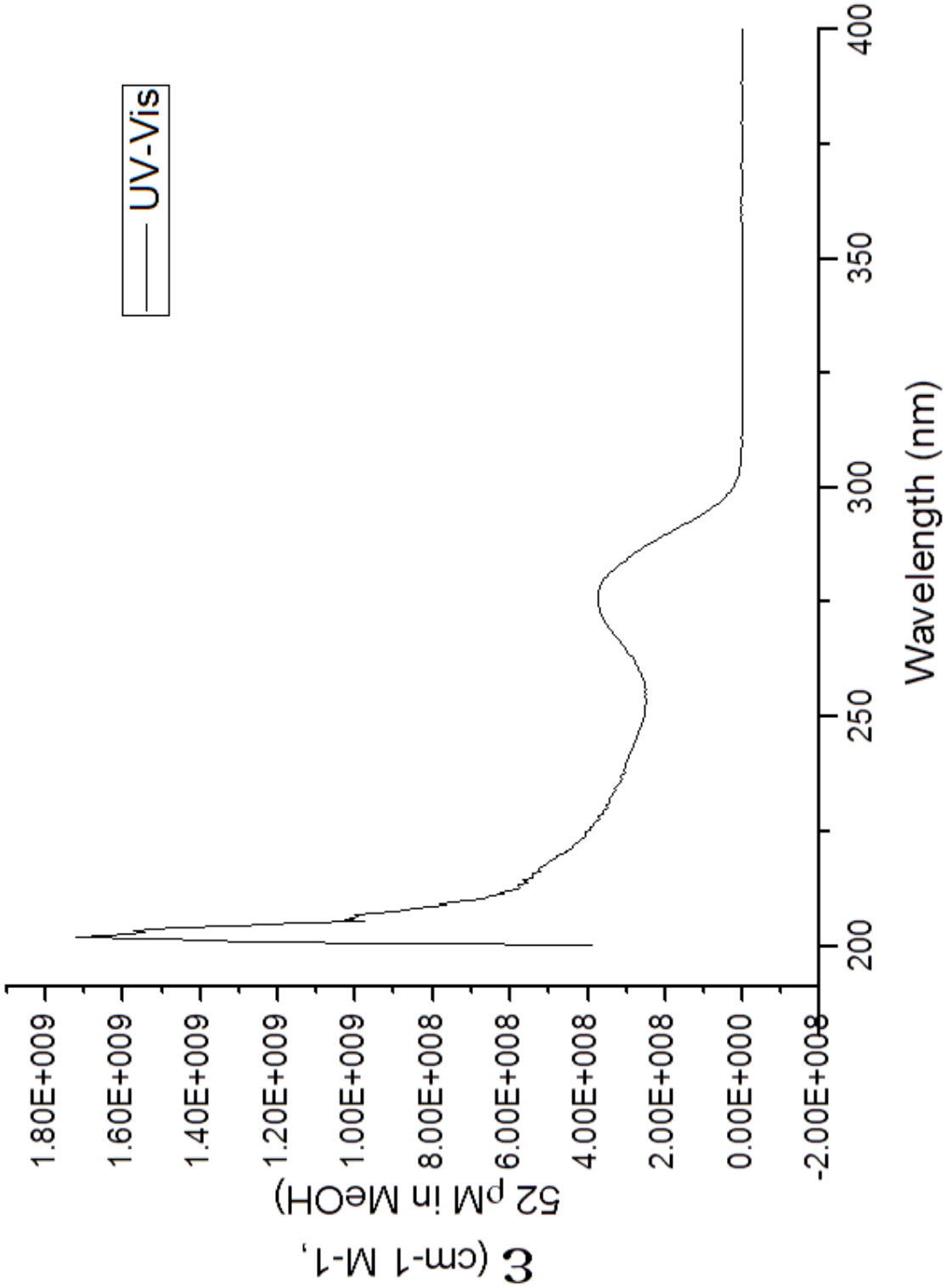
UV-Vis
ε (cm-1 M-1, 52 μM in MeOH)
1.80E+009
1.60E+009
1.40E+009
1.20E+009
1.00E+009
8.00E+008
6.00E+008
4.00E+008
2.00E+008
0.00E+000
-2.00E+008
200
250
300
350
400
Wavelength (nm)

Attempted synthesis of 7-amino-4-carboethoxy-8-carboxycarbostyril methyl ester.

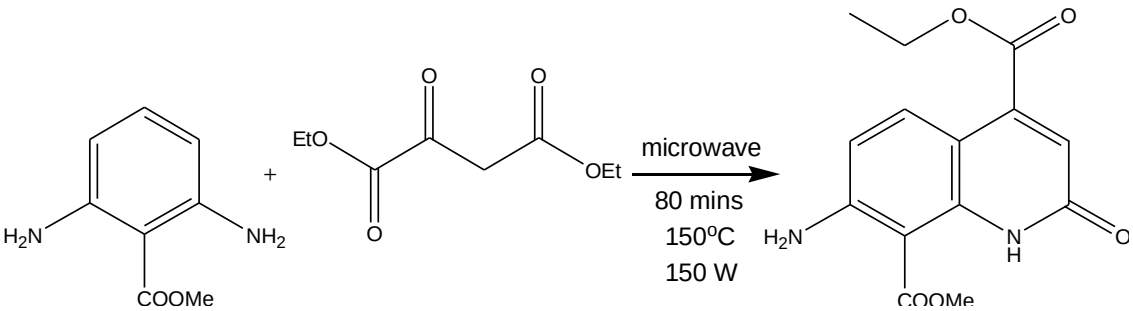

Scheme 3.11.4: Attempted synthesis of 7-amino-4-carboethoxy-8-carboxycarbostyril methyl ester.

The attempted synthesis of compound 7-amino-4-carboethoxy-8-carboxycarbostyril methyl ester was followed from a previously published procedure, with some modifications, from a patent by Pharmacia and Upjohn Company LLC.[46] 2 g (9.52 mmol) of diethyl oxaloacetate sodium salt was dissolved in 50 ml of water. 50 ml of ether was carefully placed on top of the water so that the two layers did not mix. The solution was then acidified drop-wise with 1.27 ml (23.8 mmol) of concentrated sulfuric acid to give a cloudy solution. The solution was agitated, the layers separated, and the ether layer was collected. The aqueous layer was further extracted with 50 ml of ether twice. The combined organic layer were dried over magnesium sulfate overnight. Evaporation of the solvent gave 1.48 g (82%) of the neutral diethyl oxalacetate product. 250 mg (1.05 mmol) of the methyl 2,6-diaminobenzoate, 198 mg (1.05 mmol) of neutral diethyl oxaloacetate, and 1 ml of water were placed in a 10 ml microwave glass tube and capped with a snap-on cap. The mixture was microwaved at 150°C for 80 minutes at 150 W microwave irradiation. The

reaction was cooled to room temperature, then placed in the freezer overnight. The solid was filtered, washed with 30 ml of cold ether and 30 ml of cold water, and dried under vacuum. Mass spectrometry analysis of the crude solid did not show any product.

Attempted formation of the isocytosine ring

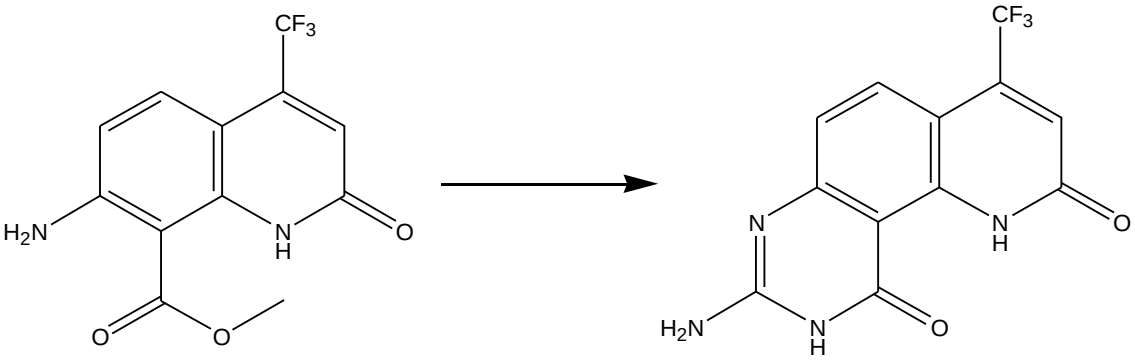

Scheme 3.12.1: Attempted formation of the isocytosine ring motif on the 7-amino-8-carbomethoxy-4-trifluoromethylcarbostyril.

A) Using chloroformamidine: The attempted formation of the third ring(isocytosine ring) on the 7-amino-8-carbomethoxy-4-trifluoromethylcarbostyril using chloroformamidine was followed from a previously published procedure, with some modifications, by Shin *et al.*.[47] 100 mg (0.350 mmol) of 7-amino-8-carbomethoxy-4-trifluoromethylcarbostyril and 60 mg (0.525 mmol) of chloroformamidine were well mixed together in a beaker. 3 g of dimethylsulfone was introduced to a 10 ml flask and heated at 125°C to melt it. The solid mixture was added slowly over the liquid dimethyl sulfone over a period of 3 minutes. The solution was stirred at 125°C for 1.5 hours and cooled to room temperature, which solidified. 8 ml of water was added and the solid was broken up to chunks.

The slurry was basified by adding about 6 ml of concentrated ammonium hydroxide and vigorously stirred for an hour. The yellow solid was filtered and dried under vacuum. Mass spectrometry and NMR analysis of the solid showed pure starting material.

B) Using Iodoformamidine: The attempted formation of the third ring(isocytosine ring) on the 7-amino-8-carbomethoxy-4-trifluoromethylcarbostyril using iodoformamidine was followed from a previously published procedure, with some modifications, by Shin *et al.*.[47] 25 mg (0.0875 mmol) of 7-amino-8-carbomethoxy-4-trifluoromethylcarbostyril and 78 mg (0.263 mmol) of iodoformamdine were well mixed together in a beaker. 500 mg of dimethyl sulfone was melted in a 5 ml flask at 125°C. The solid mixture was slowly added into the solvent over a 1 minute period and stirred at 125°C overnight. The reaction was cooled to 90°C and 1 ml of water was added. The solution was basified with ammonium hydroxide and vigorously stirred for an hour. The solution was cooled down to room temperature, the solid filtered, and the black solid was washed with ether and water. The solid was dried under vacuum overnight. Analysis of the solid showed no sign of the desired product.

C) Using thiourea/methylthiourea: The attempted formation of the third ring(isocytosine ring) on the 7-amino-8-carbomethoxy-4-trifluoromethylcarbostyril using thiourea or methylthiourea were followed from a previously published procedure, with some modifications, by Kennedy *et al.*.[48] 25 mg (0.0875 mmol) of 7-amino-8-carbomethoxy-4-trifluoromethylcarbostyril and 20 mg (0.263 mmol) of

thiourea or 57 mg of thiourea (0.263 mmol) were well mixed together. 500 mg of dimethyl sulfone was melted in a 5 ml glass vial with a cap. The vial was opened and the solid mixture was added slowly to the sulfone solvent. The solution was stirred at 125°C overnight and cooled to 100°C the next day. 1 ml of water was added, mixed, and basified with 0.5 ml of concentrated ammonium hydroxide. The solution was vigorously stirred for an hour, the solid filtered, and washed with water and ether.The solid was dried under vacuum overnight. Analysis of both products showed that loss of the carbomethoxy group happened which gave 7-amino-4-trifluoromethylcarbostyril.

Isocytosine ring formation:7-amino-8-carbomethoxy-4-trifluoromethylcarbostyril

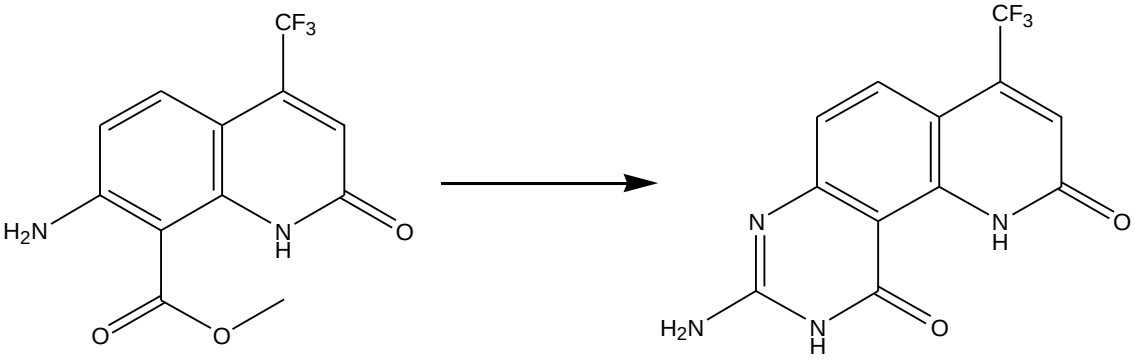

Scheme 3.12.2: Formation of the isocytosine ring motif on the 7-amino-8-carbomethoxy-4-trifluoromethylcarbostyril using free-base guanidine.

A) Conventional heating: The formation of the third ring(isocytosine ring) on the 7-amino-8-carbomethoxy-4-trifluoromethylcarbostyril using free-base guanidine and conventional heating was followed from a previously published procedure, with some modifications, from a patent by Smithkline Beecham Intercredit B. V..[49]

6 ml of ethanol was cooled and 69 mg (3.00 mmol) of sodium metal chunks were slowly added. In a separate solution of 6 ml of ethanol, 287 mg (3.00 mmol) of guanidinium chloride salt was dissolved and cooled. The guanidinium chloride solution was slowly added to the sodium solution to give a white precipitate. The solid was filtered off under nitrogen and the clear filtrate was collected. Additional filtering was done if the filtrate was not clear. The filtrate was transferred into a 25 ml flask and 100 mg (0.350 mmol) of the 7-amino-8-carbomethoxy-4-trifluoromethylcarbostyril was added. A reflux condenser was attached and the solution was refluxed for 7 days at 81°C. The solution was cooled to room temperature and the solid was filtered. The filtrate was concentrated to give a yellow residue. The residue was dissolved in minimum amount of water and acidified with glacial acetic acid. The resulting precipitate was filtered to give 5 mg (5%) an orange solid. Analysis of the compound showed a mixture of the desired compound and 7-amino-8-carboxy-4-trifluoromethylcarbostyril in approximately the same amount.

B) Microwave synthesis: The formation of the third ring(isocytosine ring) on the 7-amino-8-carbomethoxy-4-trifluoromethylcarbostyril using free-base guanidine and microwave irradiation was followed from a previously published procedure, with some modifications, from a patent by Smithkline Beecham Intercredit B. V..[49] The same quantity of free-base guanidine was acquired using the same procedure as above. After filtration of the sodium chloride salt, the filtrate was concentrated to give a cloudy oil. The free-base guanidine, 7-amino-8-

carbomethoxy-4-trifluoromethylcarbostyril, and 1 ml of ethanol were placed in a microwave glass tube and capped with a snap-on plastic cap. The reaction was performed at 120°C for 90 minutes under 150 W of microwave radiation. The resulting mixture was filtered and the filtrate was concentrated to give a yellow-brown oil. The oil was dissolved in water and acidified with glacial acetic acid to give an orange solid. Analysis of the 5 mg (5%) solid showed that the microwave procedure gives the same product (along with 7-amino-8-carboxy-4-trifluoromethylcarbostyril) as the conventional heating procedure above.

APCI-ESI MS: MH^+: 297.0589 (calc. 297.0594)

^{1}H NMR (400 MHz, DMSO-d_6): δ 6.88 (1H, s), δ 7.10 (1H, d, J = 4 Hz), δ 7.82 (1H, d, J = 12 Hz), δ 13.14 (2H, br s)
(peaks corresponding to the impurity are marked with " * ")

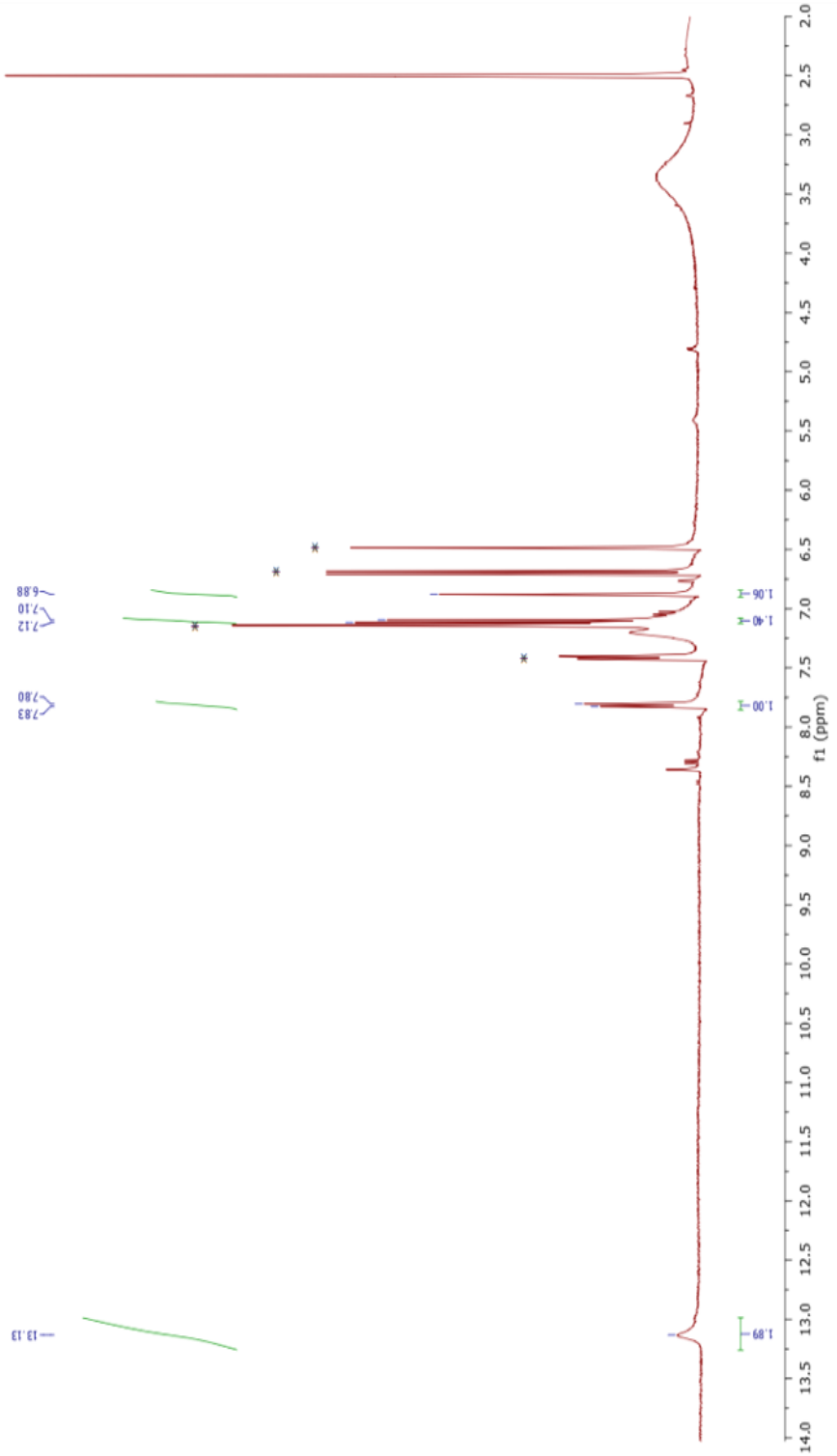

^{19}F NMR (400 MHz, DMSO-d_6): δ - 62.23

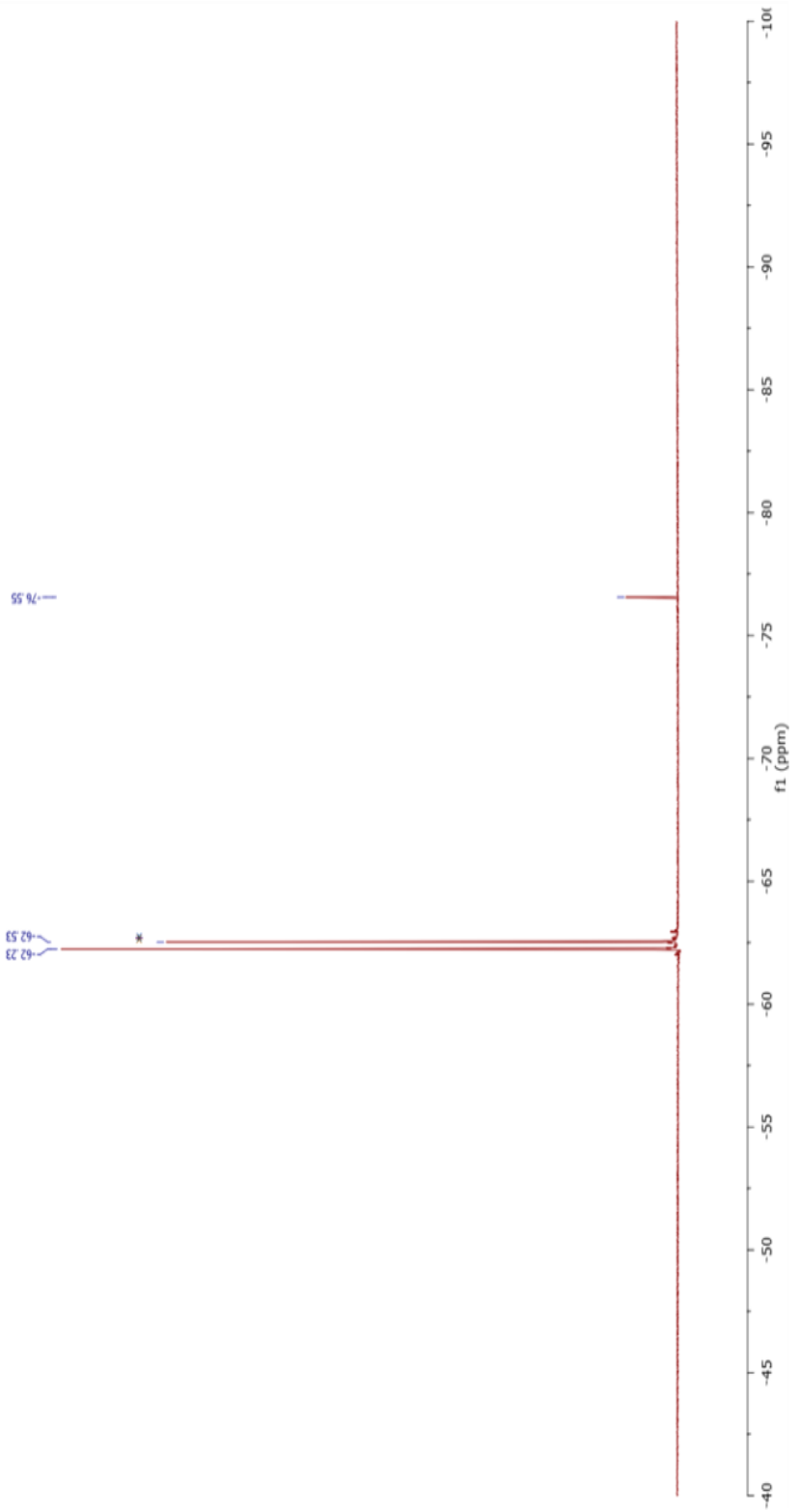

IR:

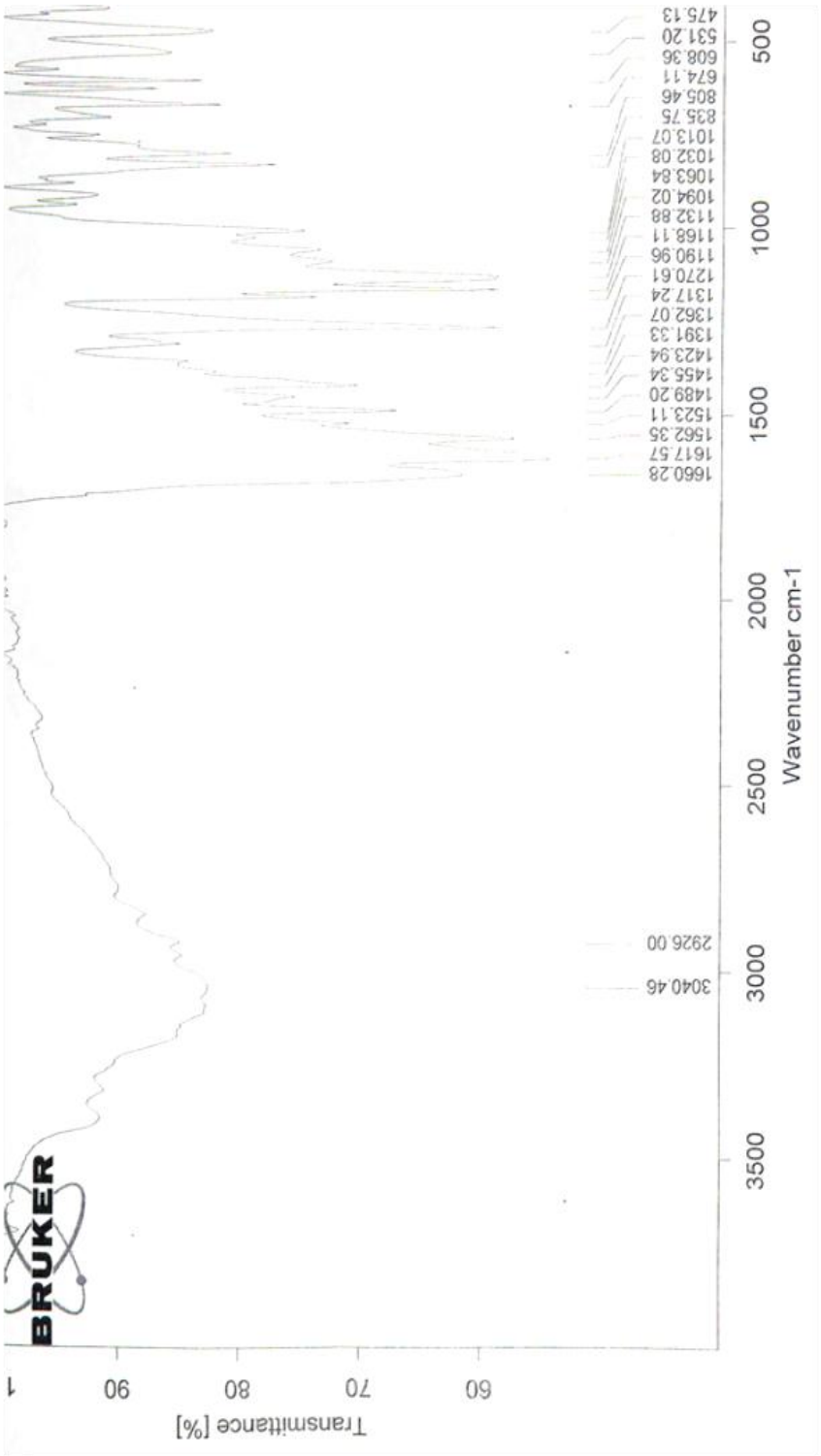
BRUKER
Transmittance [%]
100
90
80
70
60
Wavenumber cm-1
3500
3000
2500
2000
1500
1000
500
3040.46
2926.00
1660.28
1617.57
1562.35
1523.11
1489.20
1455.34
1423.94
1391.33
1362.07
1317.24
1270.61
1190.96
1168.11
1132.88
1094.02
1063.84
1032.08
1013.07
835.75
805.46
674.11
608.36
531.20
475.13

Trifluoroacetic acid salt of 7-amino-8-carbomethoxy-4-trifluoromethylcarbostyril

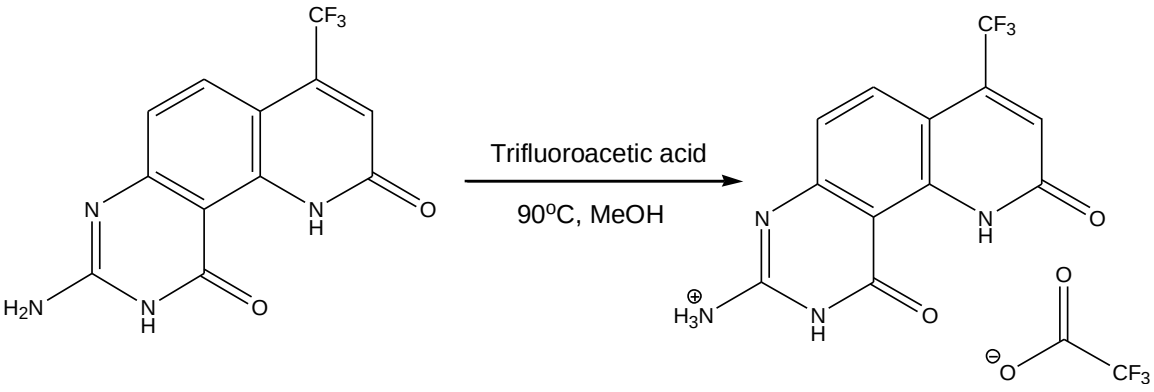

Scheme 3.12.3: Formation of **Target 1** trifluoroacetic acid salt.

66 mg of the crude 7-amino-8-carboxymethoxy-4-trifluoromethylcarbostyril (~0.1 mmol) was suspended in 20mL of boiling methanol and 1 mL of trifluoroacetic acid added to the suspension. Upon addition of the acid, the cloudy brown suspension became clear with the same color. The methanol solvent and excess trifluoroacetic acid were allowed to evaporate over the weekend to give a yellow solid.

Recrystallization:TFA salt of 7-amino-8-carbomethoxy-4-trifluoromethylcarbostyril

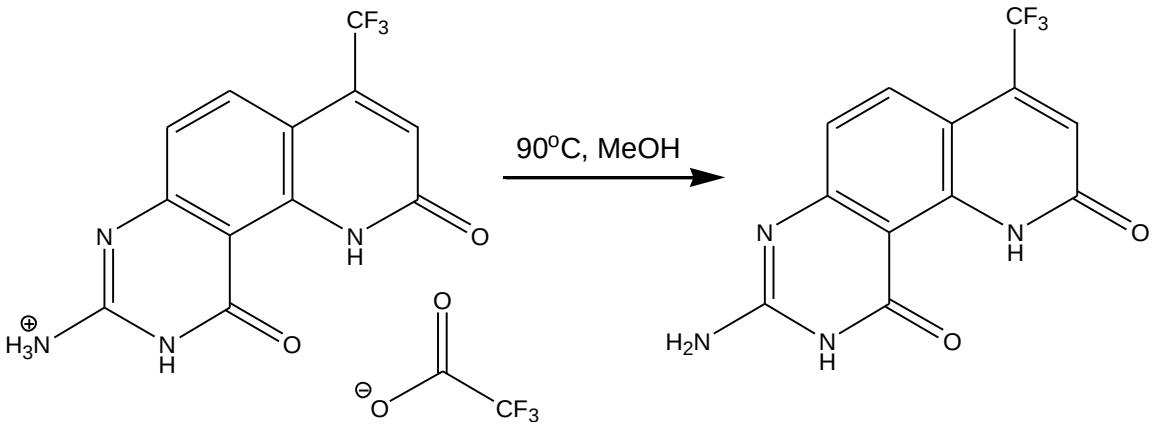

Scheme 3.12.4: Formation of the free base **Target 1** from its trifluoroacetic acid salt.

10 mg of the salt (~0.02mmol) was dissolved in boiling methanol until no more solid is present (~60mL of methanol). The solution was allowed to cool to room temperature overnight to give a precipitate. The cloudy solution was centrifuged, the supernatant was pipetted, and the solid was dried under vacuum. Analysis of the solid showed the free base of **Target 1**. A missing peak in the ^{13}C NMR may be due to N-broadening of carbon surrounded by three nitrogen atoms of the guanidine.

Melting point: >400°C (sample decomposed)

APCI-ESI MS: MH^+: 297.0589 (calc. 297.0594)
MH^-: 295.0451 (calc. 294.0448)

^{1}H NMR (400 MHz, DMSO-d_6): δ 6.89 (1H, s), δ 7.10 (1H, d, J = 8 Hz), δ 7.83 (1H, d, J = 8 Hz), δ 11.76 (1H, br s), δ 12.97 (1H, br s)

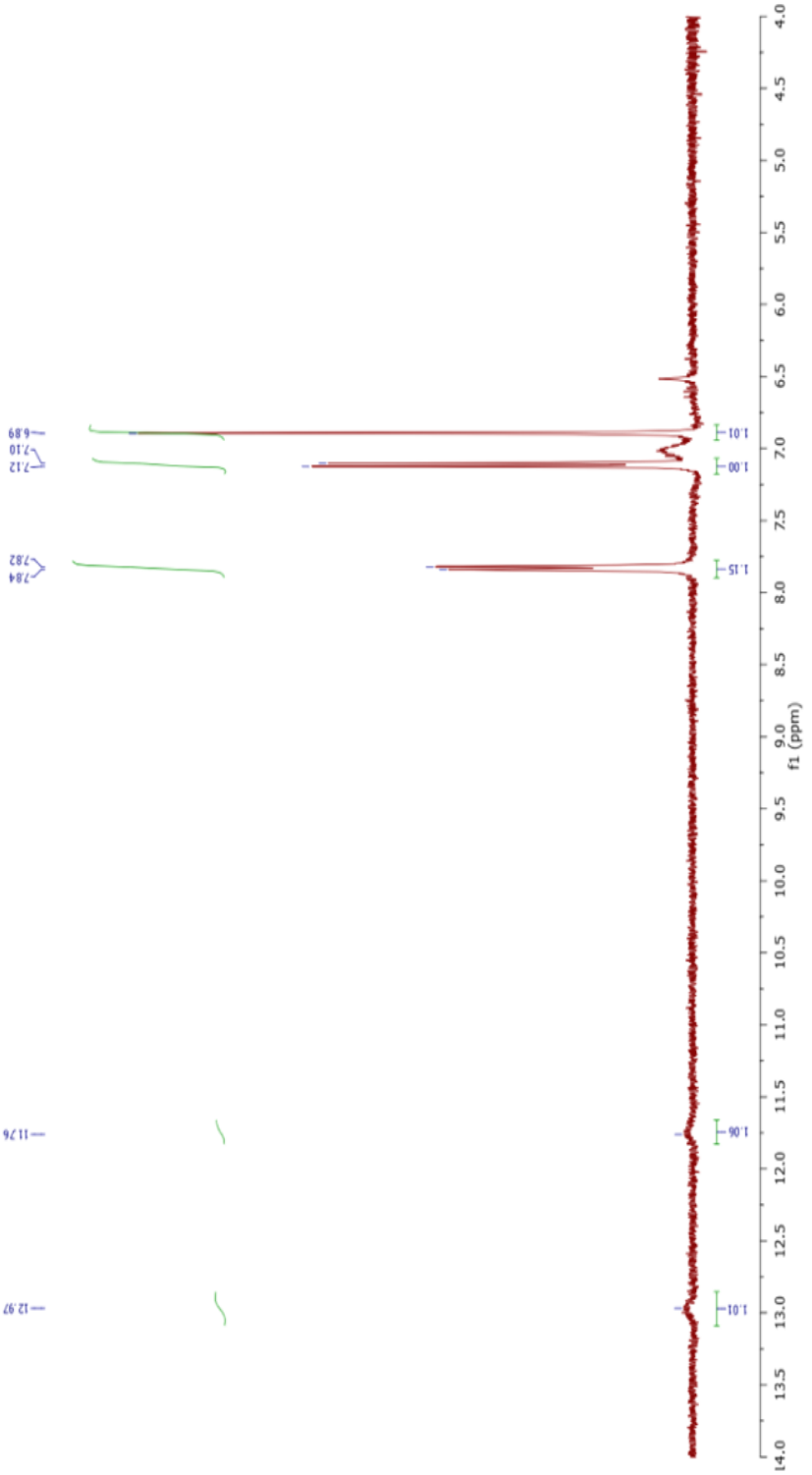

^{13}C NMR (100 MHz, DMSO-d_6): δ 100.71, δ 106.40, δ 117.62, δ 119.56, δ122.62, δ129.62, δ 136.67, δ 140.91, δ 140.95, δ 153.75, δ 159.37

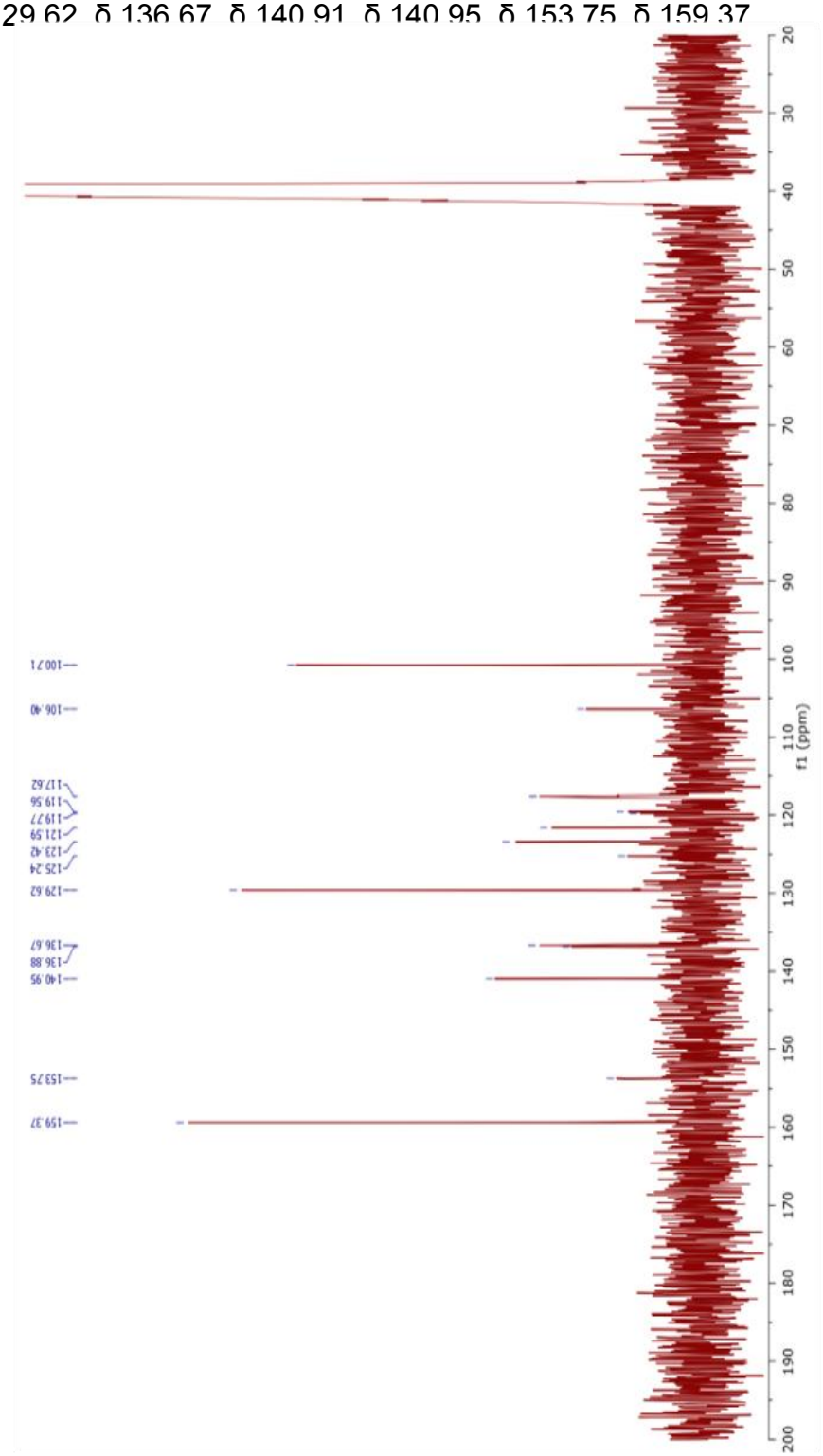

^{19}F NMR (400 MHz, DMSO-d_6): δ - 62.52

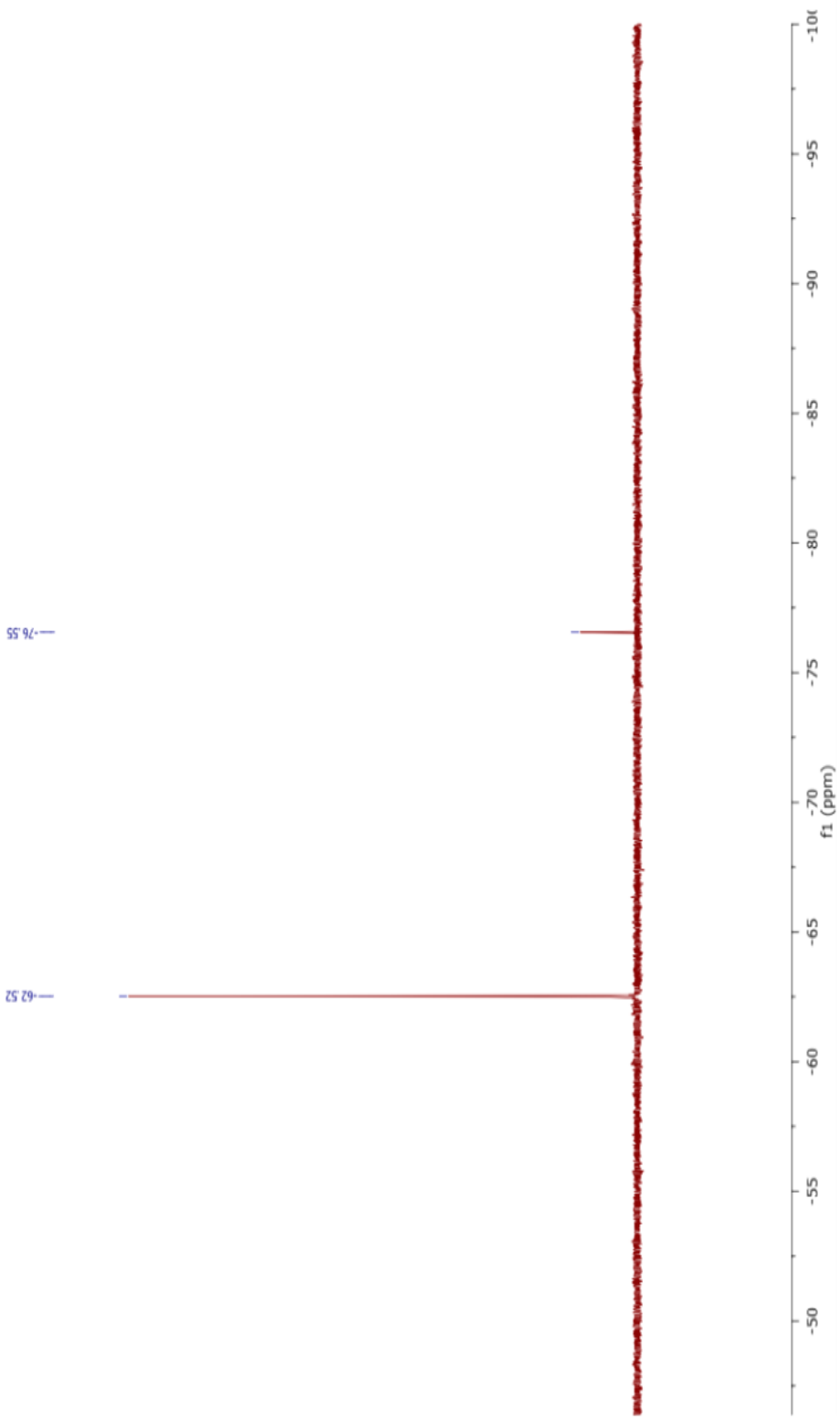

IR:

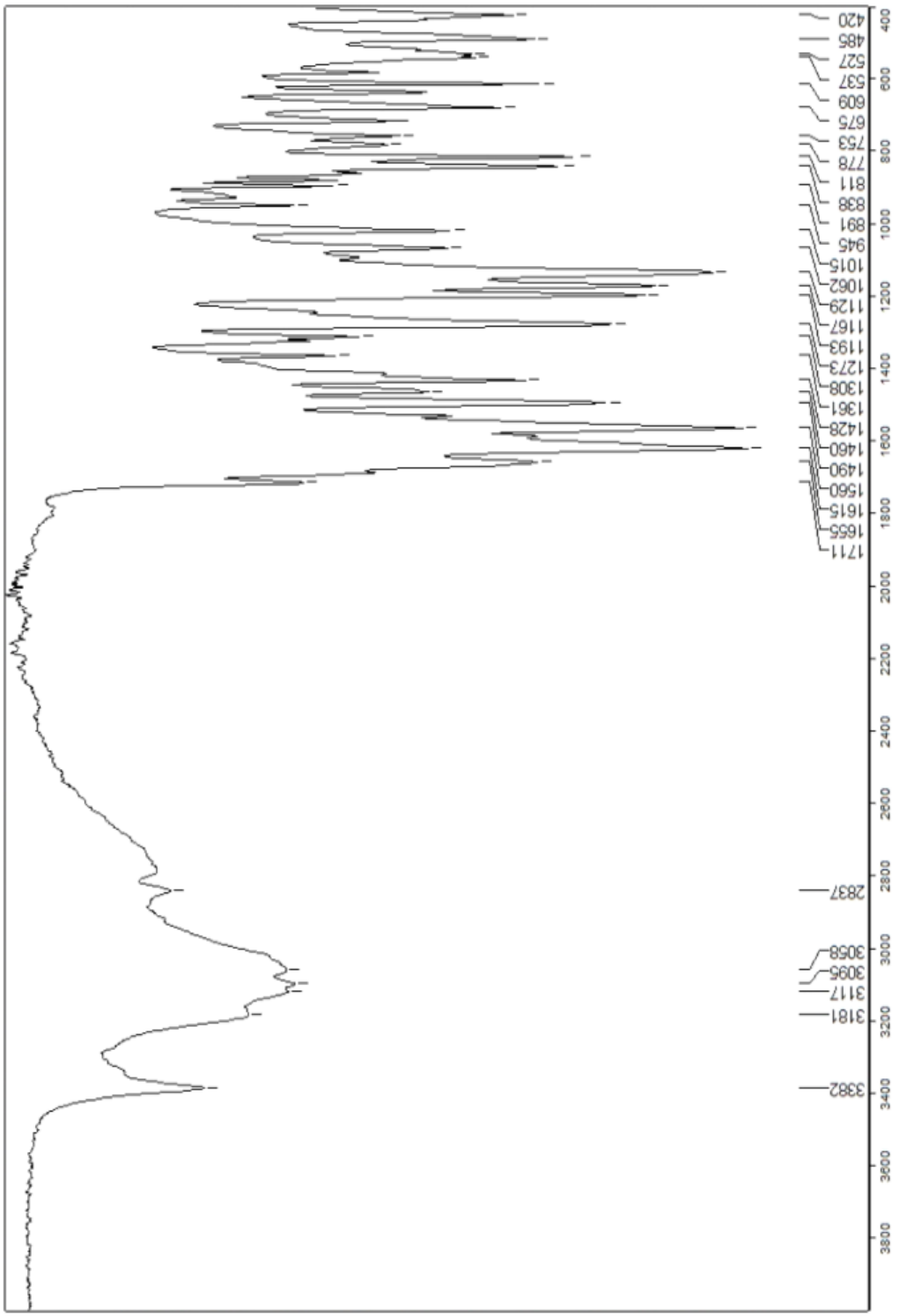
420
485
527
537
609
675
753
778
811
838
891
945
1015
1062
1129
1167
1193
1273
1308
1361
1428
1460
1490
1560
1615
1655
1711
2837
3058
3095
3117
3181
3382
400
600
800
1000
1200
1400
1600
1800
2000
2200
2400
2600
2800
3000
3200
3400
3600
3800

IR (Fingerprint region):

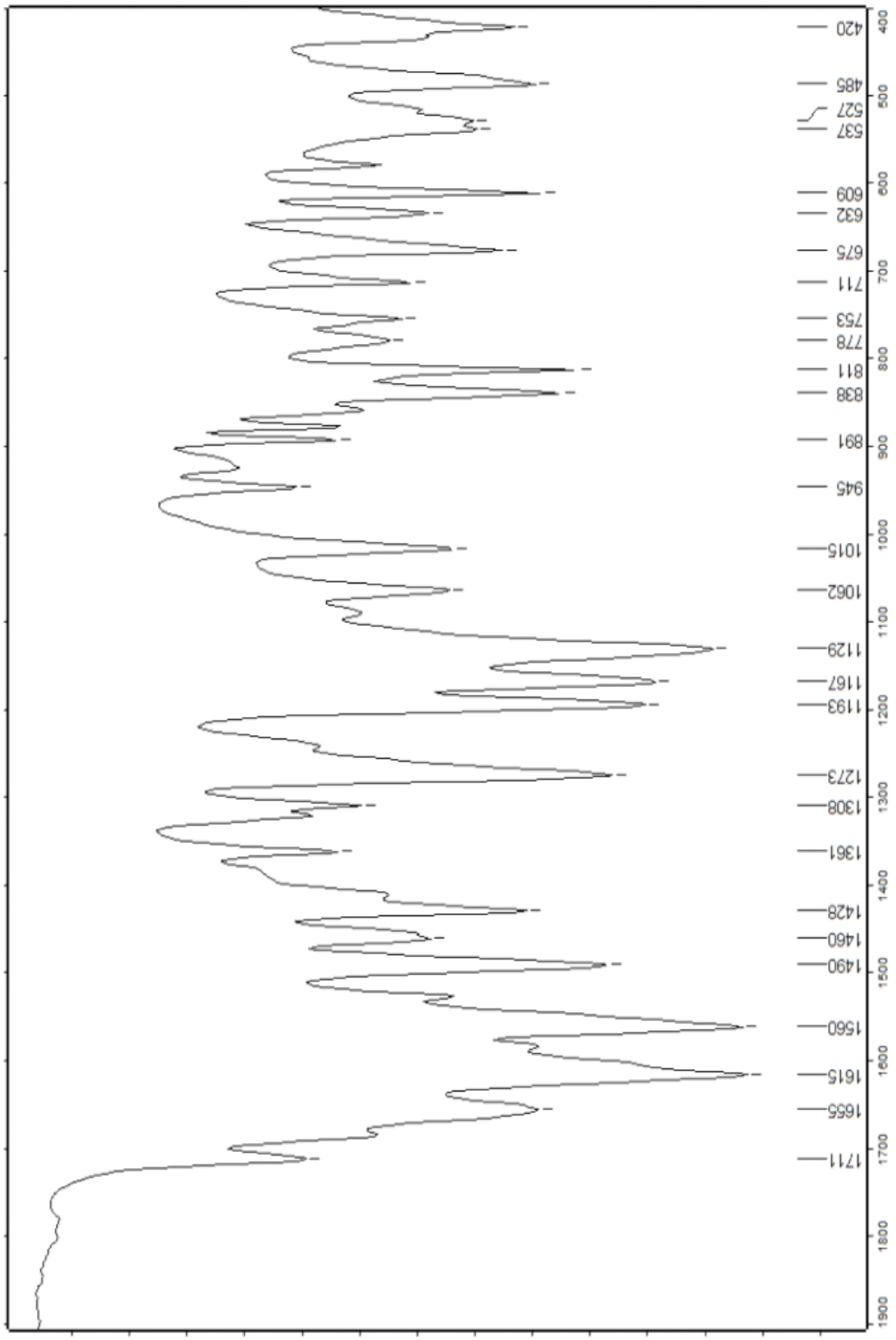

UV-Vis and **Fluorescence**:

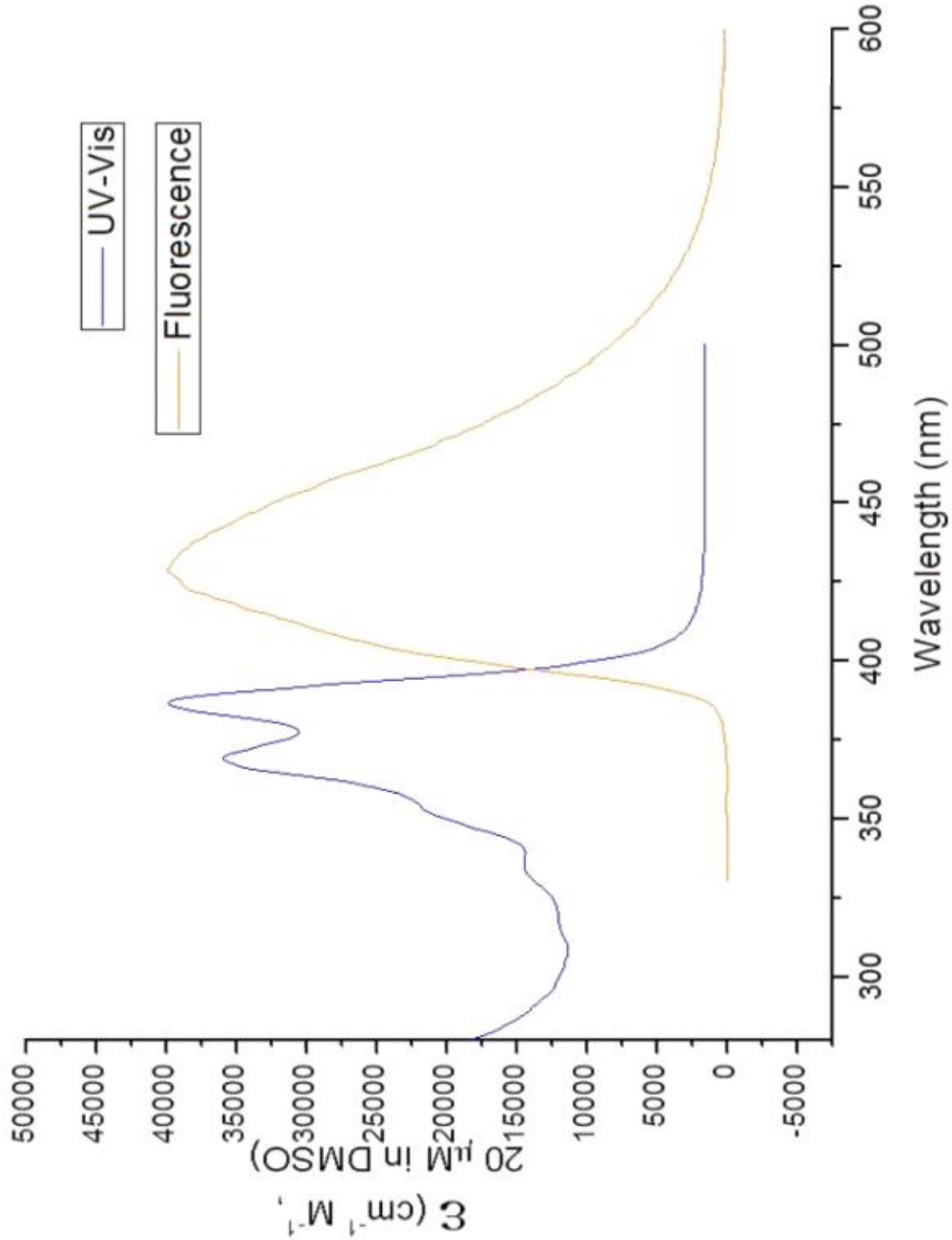

Results:

The target molecule incorporates an isocytosine motif with an organic backbone. The ideal backbone should be rigid, flat, electron-rich, and able to be modified. A rigid structure would provide more stable and strong hydrogen bonding. With the molecule being flat and conjugated, delocalization of the electron density will help with hydrogen bonding. Additionally, through initial modifications of the backbone, the final product's solubility, detection, binding affinity, and other molecular properties can be manipulated. Such compounds are heterocycles which contain electron-rich aromatic rings that can be easily functionalized. Their fluorescent properties can be utilized for detection of hydrogen bonding. Using a heterocycle as model for drug molecules is not new, as they been widely synthesized and used in the field of medicinal chemistry as a base for many drug candidates. Some of these heterocycles include quinoline, isoquinoline, and carbostyril, as shown in **Figure 3.8**. Each carbon atom of the heterocyclic ring can be functionalized to attach different substituents, which affect the property and reactivity of the heterocycles. With this assumption, different derivatives of the starting materials and intermediates were synthesized and investigated. Out of the three heterocycles mentioned, carbostyril was selected since it was not only cheaper and easier to elaborate, but also the hydrogen bonding motif of the added ring can be stabilized, as will be shown below.

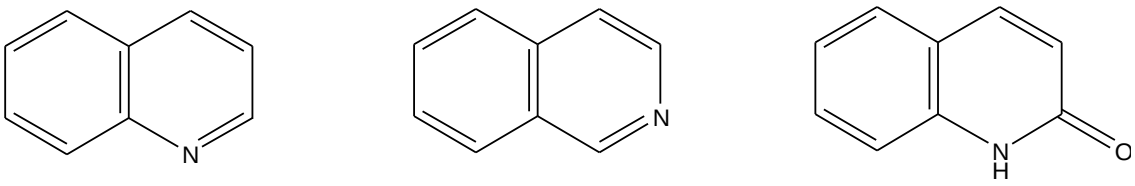

quinoline isoquinoline carbostyril

Figure 3.8: Heterocylic compounds that have been used as base cores for multiple drug candidates.

Scheme 3.13 shows the envisioned synthesis of **Target 1**, which begins with the formation of the carbostyril backbone. The end product can be very complex, as four of the substituents on the carbostyril backbone can be specifically modified. There are two ways to do this, either using starting materials with the specific substituents or modifying the intermediates between each step. As for the first strategy, a specific aniline derivative can be used to select groups R_3 and R_4, while a specific acetoacetate derivative can be used to select groups R_5 and R_6. As for the other strategy, different functionalization methods can be used to the intermediates before formation of each ring. As can be seen from the skeleton of Target 1, the NH of the right-hand ring stabilizes the carbonyl of the added ring, so as to lock in the tautomer depicted.

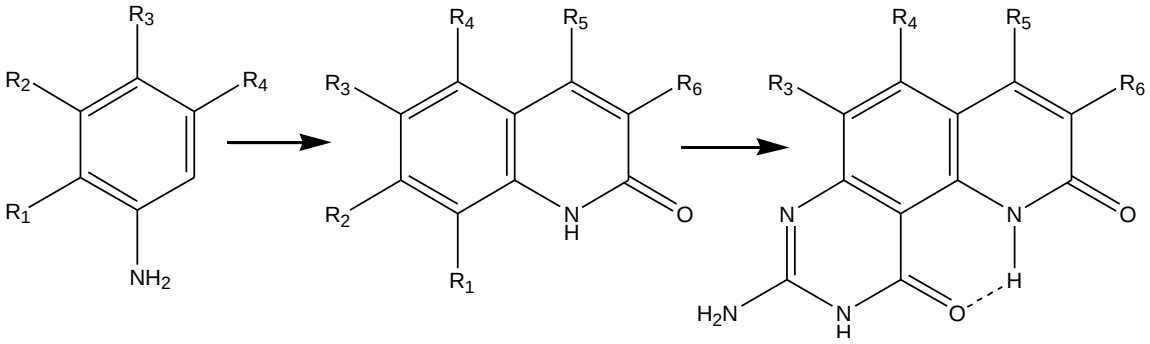

Scheme 3.13: Envisioned synthesis of the drug molecule **Target 1**.

The isocytosine region of the drug, having a D-D-A hydrogen bonding configuration, is specifically designed to hydrogen bond with a neutral cytosine, as shown in **Figure 3.9** (left). As noted above, the amide region of the carbostyril backbone can interact with the carbonyl of the isocytosine region, as shown to the right, which will restrain it from tautomerizing to the iminol form, therefore, keeping the D-D-A configuration.

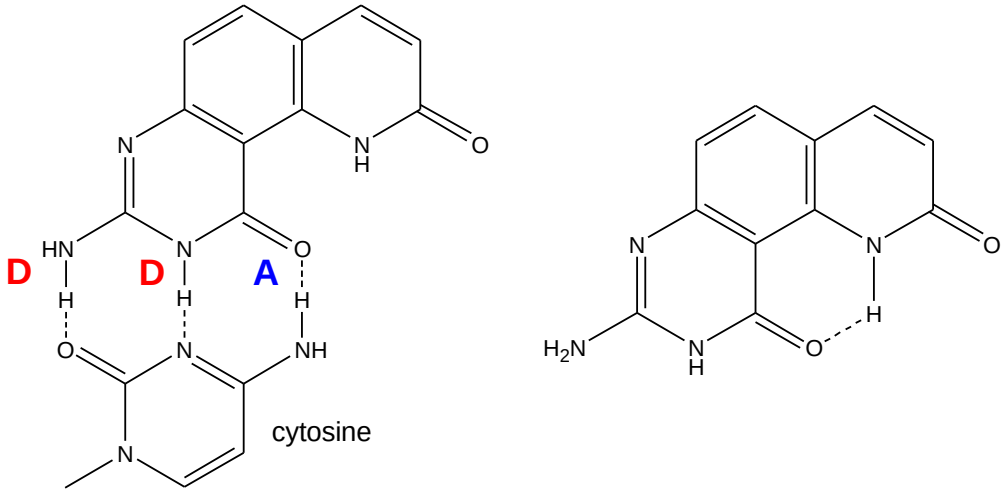

Figure 3.9: Target **1** has a D-D-A hydrogen bonding motif, which makes it able to hydrogen bond with cytosine (left). The D-D-A motif is retained by the intramolecular hydrogen bonding between the amide hydrogen of the carbostyril backbone with the carbonyl of the isocytosine (right).

The initial step for this project was to synthesize a carbostyril, without any regard for the substituent on the carbostyril, to which the isocytosine can be attached. This meant selecting a carbostyril with specific R_1 and R_2 substituents.

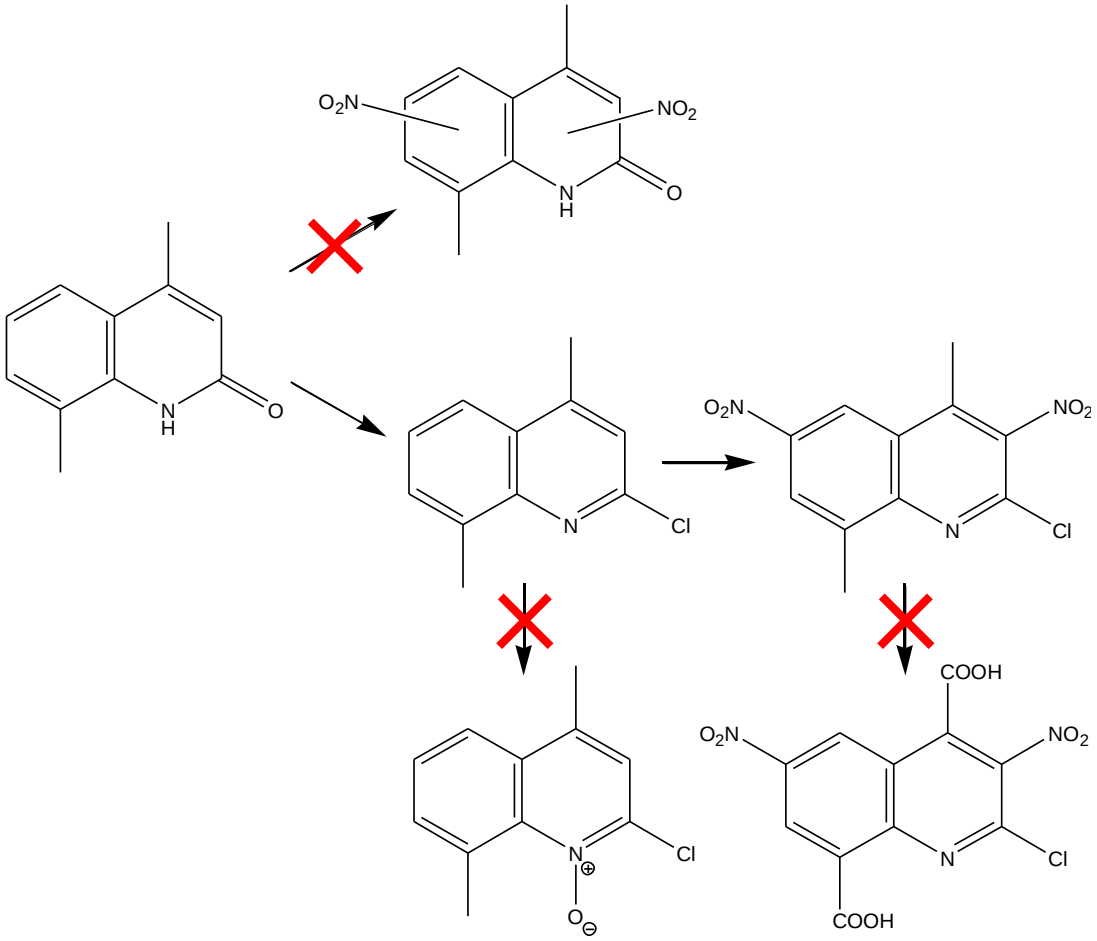

Scheme 3.14: Attempted synthetic routes taken to synthesize **Target 1** using 4,8-dimethylcarbostyril as the backbone.

Scheme 3.14 shows the synthetic route that was tried using 4,8-dimethylcarbostyril. The synthesis of 4,8-dimethylcarbostyril was done by first forming the intermediate from *o*-toluene and diketene.[23] The commercially available protected complex of diketene, 2,2,6-trimethyl-4H-1,3-dioxin-4-one, was

used instead of making diketene *in situ*. Closing the second ring to form the product required an acid catalyst and heating. Once the carbostyril backbone was formed, the next step was to functionalize certain parts of the ring. Nitration of the R_2 position followed by reduction of that nitro group would give an amine that can be used as part of the isocytosine ring. However, nitrations at the R_3, R_4, and R_6 positions can also be beneficial, as this would functionalize these positions, which opens them for later modifications. Unfortunately, reacting 4,8-dimethylcarbostyril with concentrated sulfuric acid and concentrated nitric acid gave pure starting material. Reactions using different concentrations of either the sulfuric (oleum) or nitric acid (fuming nitric acid) gave the same results. Since 4,8-dimethylcarbostyril seemed to be stable against nitration, the 2-chloro-4,8-dimethylquinoline derivative was synthesized and subjected to nitration. It may be possible that changing the electron density of the ring by substituting the carbonyl with a more electron-donating halogen may give different results upon nitration. Nitration of the 2-chloro-4,4-dimethylquinoline indeed showed that nitration on the ring occurred at the R_3 and R_6 positions but not on the R_2 position as intended. Even though the wrong positions were nitrated, the next step was taken to functionalize the methyl groups. The methyl groups can be oxidized to carboxylic acids, then esterified, and used as an intermediate for further modification. However, oxidation of 2-chloro-4,8-dimethyl-3,6-dinitroquinoline using an aerobic oxidation method only yielded starting material.

The derivative *N*-oxide-2-chloro-4,8-dimethylquinoline was also investigated to see if the *N*-oxide's electron withdrawing property might activate the R_2 position for nitration. The synthesis of *N*-oxide-2-chloro-4,8-dimethylquinoline was done by reacting 2-chloro-4,8-dimethylquinoline with hydrogen peroxide and trifluoroacetic acid as a catalyst. However, analysis of the product showed that this procedure did not give the derivative.

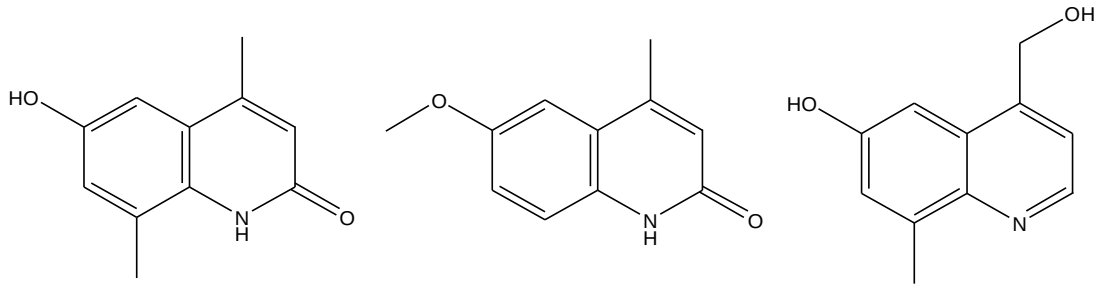

Figure 3.10: Different carbostyril or quinoline derivatives attempted as a possible backbone: 6-hydroxy-4,8-dimethylcarbostyril (left), 6-methoxy-4-methylcarbostyril (middle), and 6-hydroxy-8-methyl-4-methylhydroxyquinoline (right).

Since the pathway using 4,8-dimethylcarbostyril did not give results, synthesis of other carbostyril or quinoline backbones, shown in **Figure 3.10**, were attempted. 6-Hydroxy-4,8-dimethylcarbostyril was synthesized using the same procedure as the previous carbostyril.[23] The 4-hydroxy-2-methyl-*N*-arylacetamide intermediate was obtained by substituting *o*-toluidine with 4-amino-*m*-cresol. Unlike the previous carbostyril, this acetamide intermediate required multiple attempts and variations of the reaction conditions to get an adequate yield to move on to the next step. The cyclization of the second ring was done in the same fashion: refluxing the intermediate in concentrated sulfuric

acid. However, analysis of the crude material showed impurities in higher abundance than the desired product. Another carbostyril that was synthesized using the previous procedure was 6-methoxy-4-methylcarbostyril. Its 4-methoxy-*N*-arylacetamide intermediate was made from *p*-anisidine. Unlike the 6-hydroxy-4,8-dimethylcarbostyril, this carbostyril did not show any product when the intermediate was cyclized using refluxing concentrated sulfuric acid. 6-Hydroxy-8-methyl-4-methylhydroxyquinoline was synthesized using a different, previously published one-pot click reaction, which uses a copper catalyst and three starting materials: aniline, aldehyde, and terminal alkyne.[29] This synthesis is useful in making different varieties of quinolines by simply using different derivatives of each starting materials. However, it is limited to the extent that the functional group attached to the terminal alkyne has to be electron-withdrawing. The one-pot copper click synthesis using 4-amino-m-cresol, formaldehyde, and propargyl alcohol showed that the quinolone was not formed but stopped at the amide intermediate. The intermediate was then isolated and used as a starting material to make the reaction a two-pot synthesis instead.[30] However, even with a new set of catalyst and alkyne, the intermediate still did not give the desired quinoline product.

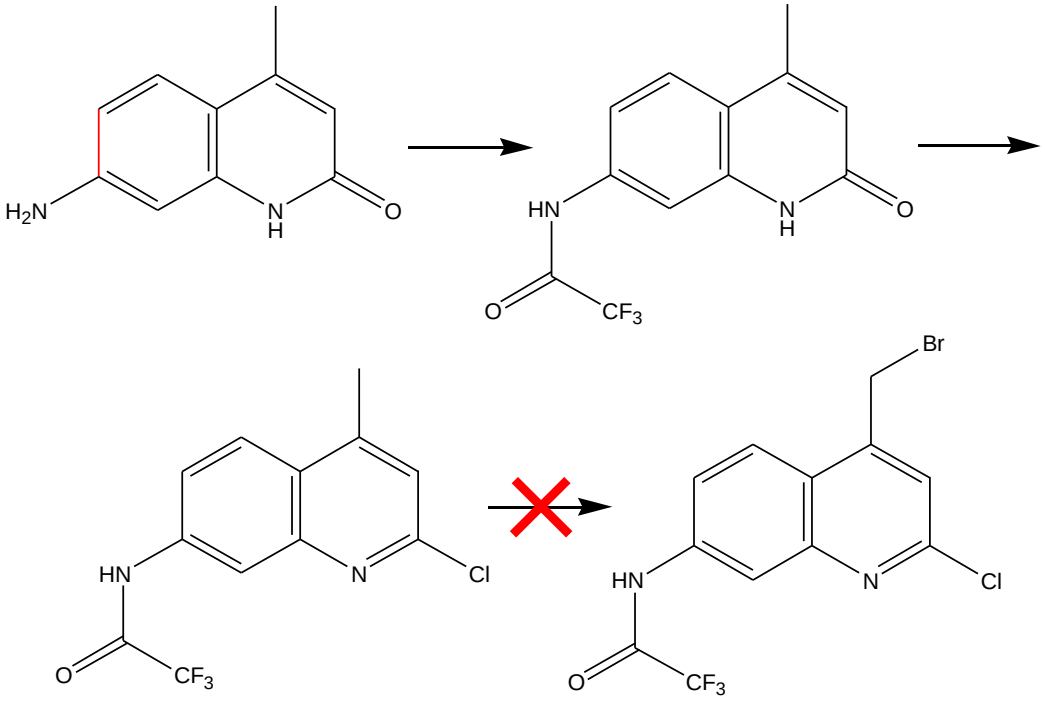

Scheme 3.15: Synthetic route to synthesize **Target 1** by using 7-amino-4-methylcarbostyril as the backbone.

Another previously published procedure for carbostyril was followed to synthesize 7-amino-4-methylcarbostyril from *m*-phenylenediamine and ethyl acetoacetate.[31] **Scheme 3.15** shows the synthesis route taken in an attempt to get **Target 1** using this carbostyril. The amine group at the 7-position can be used to be part of the isocytosine in later steps. In order to functionalize the methyl group through bromination, this amine group was protected using a trifluoroacetyl group. With the methyl group being *ortho* to the carbonyl, and thus electron deficient, this makes the methyl group less likely to be brominated through radical bromination. To solve this problem, the carbonyl was replaced with a more electron-donating halogen as done before. Using *N*-

bromosuccinimide with a radical initiator, the bromination of the methyl group was attempted. However, this reaction yielded only pure starting material.

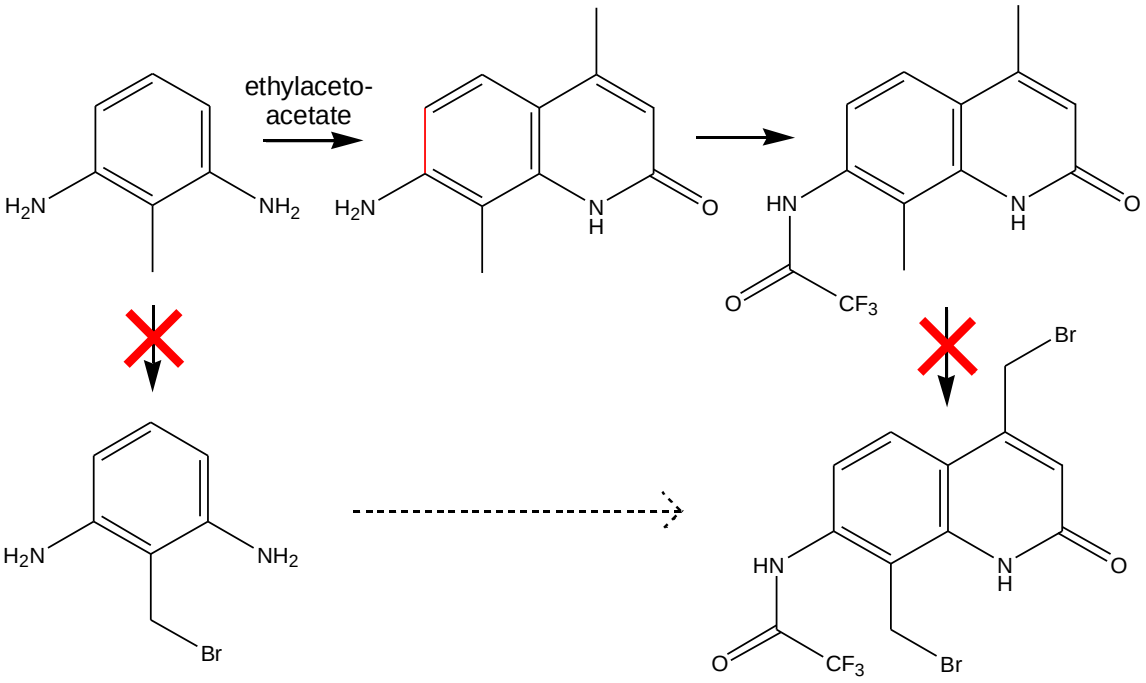

Scheme 3.16: Attempted synthetic route in hopes of synthesizing **Target 1** from using 7-amino-4-methylcarbostyril as the backbone.

Discovering that a carbostyril with an amine group at the 7-position can be prepared, 7-amino-4,8-dimethylcarbostyril was then synthesized and investigated. This carbostyril was made using a microwave method in which 2,6-diaminotoluene was reacted with ethyl acetoacetate.[33] **Scheme 3.16** shows the different pathways taken in an attempt to get **Target 1** from using 7-amino-4,8-dimethylcarbostyril as the backbone. After the formation of the carbostyril, the primary amine was protected using a trifluoroacetyl group before bromination of the methyl groups. Radical bromination using *N*-bromosuccinimide and radical initiator of the protected carbostyril showed only pure starting material. One other

way to functionalize the methyl group in the 8-position is to use 2,6-diaminobenzyl bromide. The same bromination procedure was used to brominate the methyl group of 2,6-diaminotoluene, which also showed no reaction.

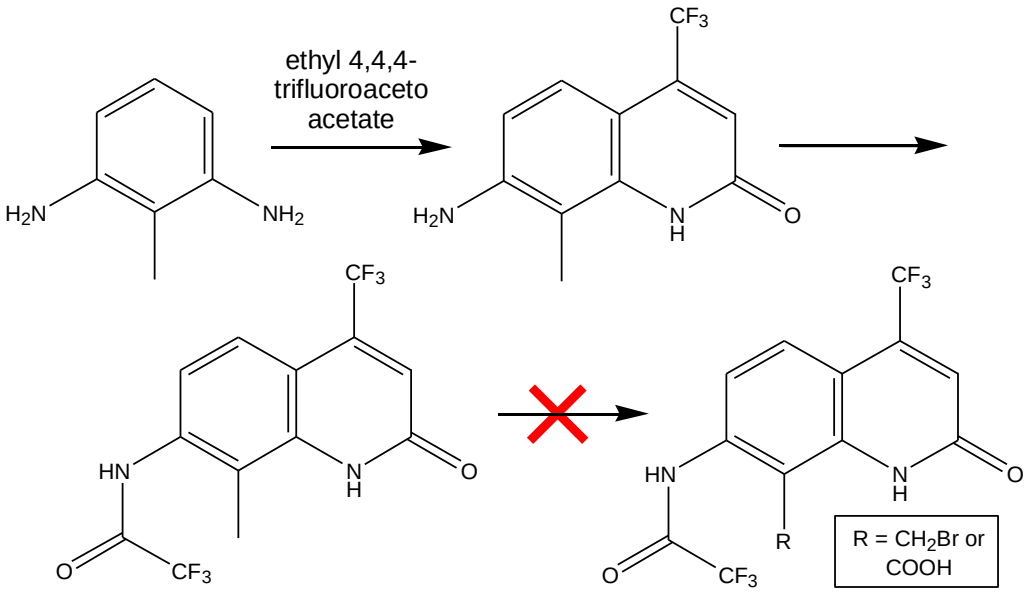

Scheme 3.17: Attempted synthetic route used in synthesis of **Target 1** from 7-amino-4-methylcarbostyril.

The microwave procedure provided different kinds of carbostyril which was considered as other candidates for the carbostyril backbone. One compound in particular was 7-amino-8-methyl-4-trifluoromethylcarbostyril, which was produced in higher yields (96% vs 40% of 7-amino-4-8-dimethylcarbostyril). This was due to the electron-withdrawing group of the trifluoromethyl group, which increases the rate of the cyclization of the ring after the acetamide intermediate was formed.[33] **Scheme 3.17** shows the synthetic pathway that was followed to get to **Target 1** using 7-amino-8-methyl-4-trifluormethylcarbostyril. Since the 7-position is already an amine, only the methyl at the 8-position needs to be

functionalized in order to form the isocytosine ring. Just as before, the primary amine was protected using trifluoroacetic anhydride and the methyl group was brominated using *N*-bromosuccinimide. Just as in previous trials, the methyl group seemed to be unreacted upon bromination. The methyl group was also subjected to oxidation, and several oxidation procedures were performed. Oxidation using catalysts/O_2, Collin's reagent, PCC, and $KMnO_4$ proved that the methyl group is indeed stable against functionalization.

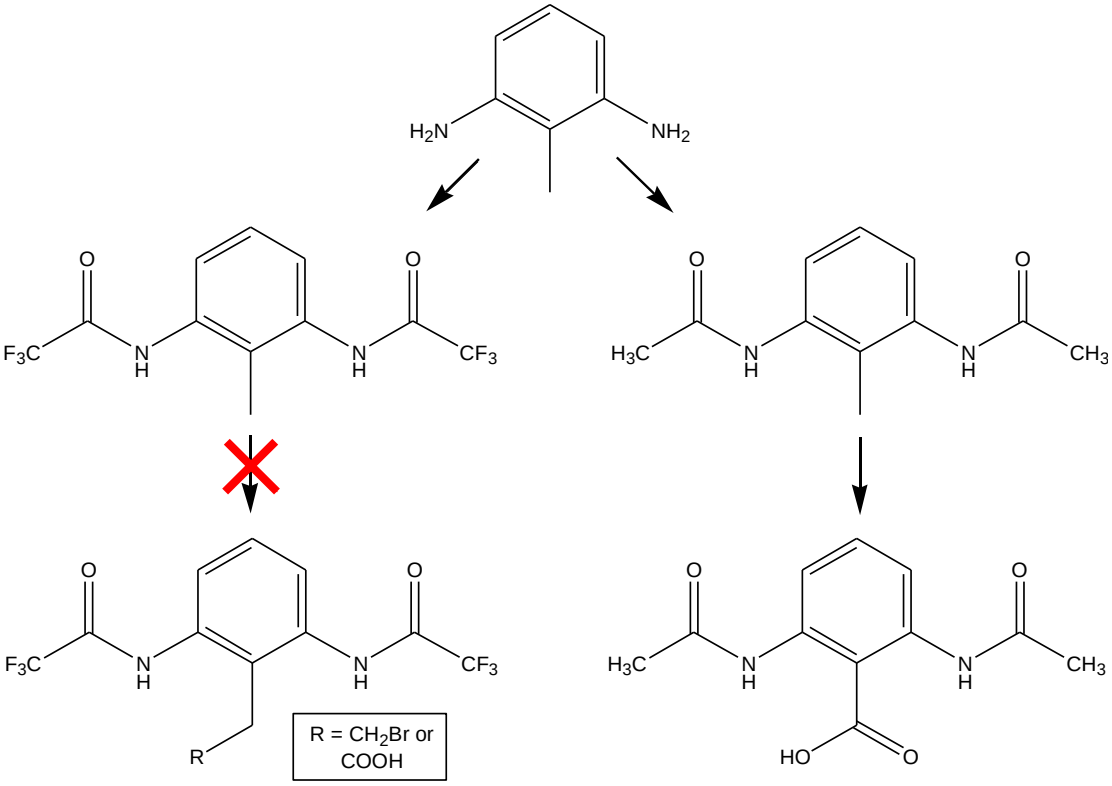

Scheme 3.18: Functionaliztion of the methyl group of the toluene prior to formation of the carbostyril.

Previous experiments showed that carbostyrils can easily be synthesized in higher yields. This led to an idea of functionalizing the methyl group of the 2,6-

diaminotoluene prior to formation of the carbostyril, as shown in **Scheme 3.18**. The two primary amines were first protected using trifluoroacetic anhydride. The methyl was then oxidized using $KMnO_4$ or brominated with *N*-bromosuccinimide, in which no product was observed for either reaction. Since the trifluoroacetamide protected compound showed no promising results, a less electron-withdrawing protecting group was chosen. The methyl group of the toluene was shown to be oxidized when an acetyl group was instead used as the protecting group. The acetate protecting groups were easily taken off by acidic conditions.

With the functionalized toluene in hand, the next step was to synthesize 7-amino-8-carboxy-4-trifluorocarbostyril. Ethyl 4,4,4-trifluoroacetoacetate was used, since it gave the highest yield of carbostyril. Analysis of the product after the reaction showed that a different molecule was formed. A new product is also a carbostyril, but the carboxyl group at the 8-position has completely vanished to give 7-amino-4-trifluoromethylcarbostyril. This was confirmed by comparing the ^{1}H NMR spectrum of the product with the literature spectrum of 7-amino-4-trifluoromethylcarbostyril.[33] It seems that decarboxylation of the carboxyl group is occurring during the microwave reaction, as shown in **Figure 3.11**. One way to prevent decarboxylation during carbostyril formation is to protect the carboxyl group by esterification.

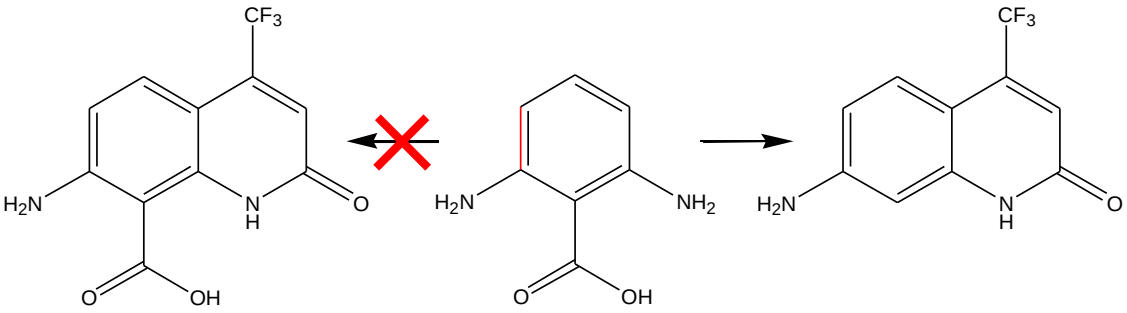

Figure 3.11: Carbostyril microwave synthesis using 2,6-diaminobenzoic acid produces 7-amino-4-trifluoromethylcarbostyril instead due to the decarboxylation of the carboxyl group during reaction.

Esterification of the carboxyl group turned out to be more difficult than anticipated. Fischer esterification, esterification using an acid chloride intermediate, esterification using methyl iodide, esterification using carbonyldiimidazole, and esterification using dimethyl carbonate showed that the carboxyl group was left untouched. Esterification was finally achieved using dimethyl sulfate. Reacting methyl 2,6-diaminobenzoate with ethyl-4,4,4-trifluoroacetoacetate gave the right compound, 7-amino-8-methyl-4-trifluoromethylcarbostyril.

With the right components on the carbostyril backbone, the next step is to form the isocytosine ring as a third ring. Just like the esterification of the 2,6-di(acetamido)benzoic acid, finding the right starting material to form the isocytosine ring proved to be more challenging than expected. Some of the procedures that were attempted were using chloroformamidine, using iodoformamidine, using thiourea, and using methylthiourea. The reaction of the carbostyril with free base guanidine finally gave some of the desired isocytosine

carbostyril compound. The final product can be synthesized by either two ways: conventional reflux for a long period of time or microwave reaction. Both these methods gave about the same yield and some impurity. Analysis of the impurity shows that it is the carboxylic acid analogue, 7-amino-8-carboxy-4-trifluoromethylcarbostyril, of the starting material.

One way that was found to isolate **Target 1** from the impurity is the formation of its trifluoroacetic acid salt. The crude material was dissolved in boiling methanol and trifluoroacetic acid was added until all the solid dissolved. After allowing the solution to evaporate on the benchtop for several days, a yellow powder was acquired. Dissolving the powder again in boiling methanol and letting the solution cool, formed a precipitate which was analyzed to be the free base of **Target 1**, leaving the impurities in the solution. During the formation of the third ring, the three aromatic hydrogens of the carbostyril backbone are unchanged, thus, the ^{1}H NMR of **Target 1** bears a similar spectrum as the carbostryil starting material. Using the ^{1}H NMR spectrum, in complement with mass spectrometry, the formation of the third ring was confirmed. ^{19}F NMR showed only a single peak, which implies that the product is the free base rather than the salt.

The ^{13}C NMR spectra of both carbostyril and **Target 1** were also recorded and comparison between the two showed the electron donating properties of the new formed third ring. This addition of the third aromatic ring, increasing conjugation and aromaticity, also showed a new absorption peak closer to the

visible region in the UV-Vis spectrum of **Target 1**. An interesting observation of the free base via negative ion mode APCI-ESI MS analysis showed that not only is the deprotonated **Target 1** present but also a dimer consisting of the deprotonated and neutral **Target 1**, as shown in **Figure 3.12**.

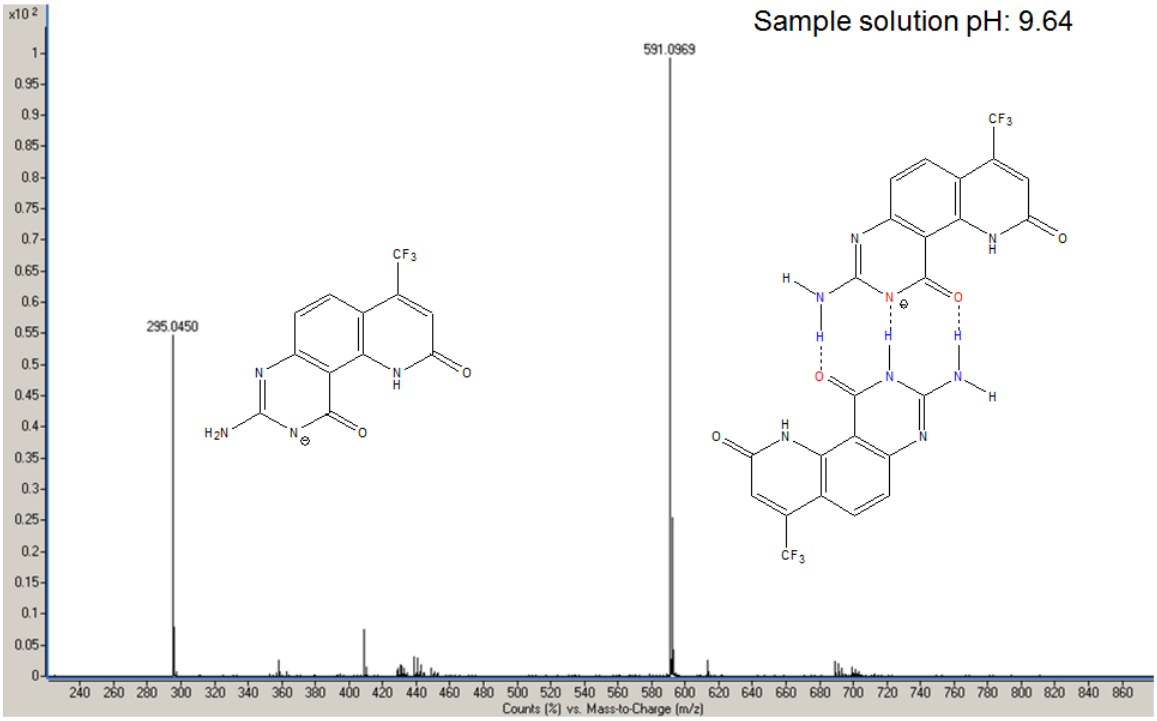

Figure 3.12: Negative ion mode ESI MS analysis of the free base **Target 1** showing not only the deprotonated compound, but also a protonated-deprotonated dimer. Deprotonation of the an amide group in **Target 1** makes it possible to form a **D**-**A**-**A** motif, which is complementary to a neutral **Target 1**'s **A**-**D**-**D** motif, forming the dimer.

The formed D-A-A motif resulting from deprotonation of one of the amine groups in **Target 1** makes it possible for the anion to form a dimer with neutral **Target 1** (which has an A-D-D motif). Other molecules, which also have an A-D-D motif, were also investigated. However, negative ion mode APCI-ESI MS

analysis of creatinine, cytosine, 1-methylcytosine, guanosine, or noraplysinopsin with **Target 1** in a basic environment did not show any formation of the complex. Calculations using DFT, shown in **Figure 3.13**, predicted that the most acidic proton in **Target 1** is the amide proton of the isocytosine ring (**Target 1** Anion 1) by 37 kcal/mol.

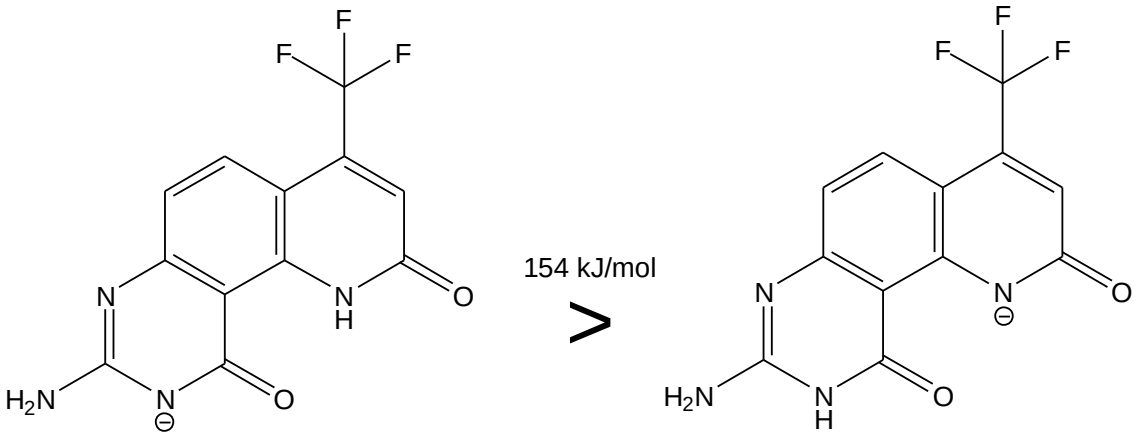

Target 1 Anion 1 **Target 1** Anion 2

Figure 3.13: DFT calculations predicted that the most acidic proton of **Target 1** is the amide proton of the carbostyril ring, showing a 84 kJ/mol energy difference between the two conjugate bases.

Even though the deprotonation of the isocytosine amide is favored, it is also possible that the amide in the carbostyril backbone can be deprotonated to form **Target 1** Anion 2. However, initial formation of **Target 1** Anion 2 does not give the Donor-Acceptor-Acceptor motif necessary for the dimer formation. Instead, tautomerization of the amide of the guanadine ring, promoted by the hydrogen bonding between the formed OH and the nitrogen anion of the

carbostyril, can form the D-A-A motif (**Target 1** Anion 4). The energies of the anions are summarized in **Table 3.1** below.

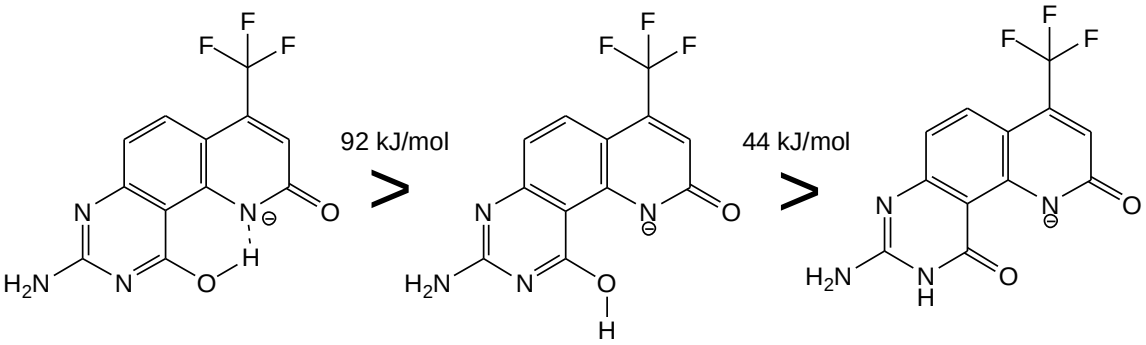

Target 1 Anion 4 **Target 1** Anion 3 **Target 1** Anion 2

Figure 3.14: Tautomerization of the amide of the third ring is influenced by the hydrogen bonding between the deprotonated amide of the carbostyril ring and the formed OH.

Table 3.1: Relative enthalpies calculated for the different conformations of **Target 1** anion (calculated at B3LYP/6-31G**, including ΔZPE).

Target 1 anion conformations	**Enthalpy** (kJ/mol at 0 Kelvin)
Target 1 Anion 1	0
Target 1 Anion 2	+ 154
Target 1 Anion 3	+ 109
Target 1 Anion 4	+ 17

Calculations on the binding of **Target 1** to itself and other molecules were performed and compared. The dimerization between neutral and anion of **Target 1**, as depicted in **Figure 3.15**, was found to be more stable by 3.88 x 10^5 kJ/mol compared to either [1-methyl-cytosine]$^+$:1-methyl-cytosine dimer or

cytosine:guanine dimer. Even though [**Target 1**]$^-$**:Target 1** dimer is more stable than [**Target 1**]$^-$:guanine dimer by just 17 kJ/mol, the formation of the latter complex is not observed in the negative ion mode APCI-ESI MS analysis.. These calculations support the preferred dimerization of **Target 1** to itself than to other base pairs, as observed in negative ion mode APCI-ESI MS analysis. It is also worth to note that calculation on the dimer consisting of **Target 1** Anion 4 converted the monomers of the dimer to the more stable **Target 1** Anion 1, as shown in Figure 3.15. The energies calculated for the binding of **Target 1** are summarized in **Table 3.2** below.

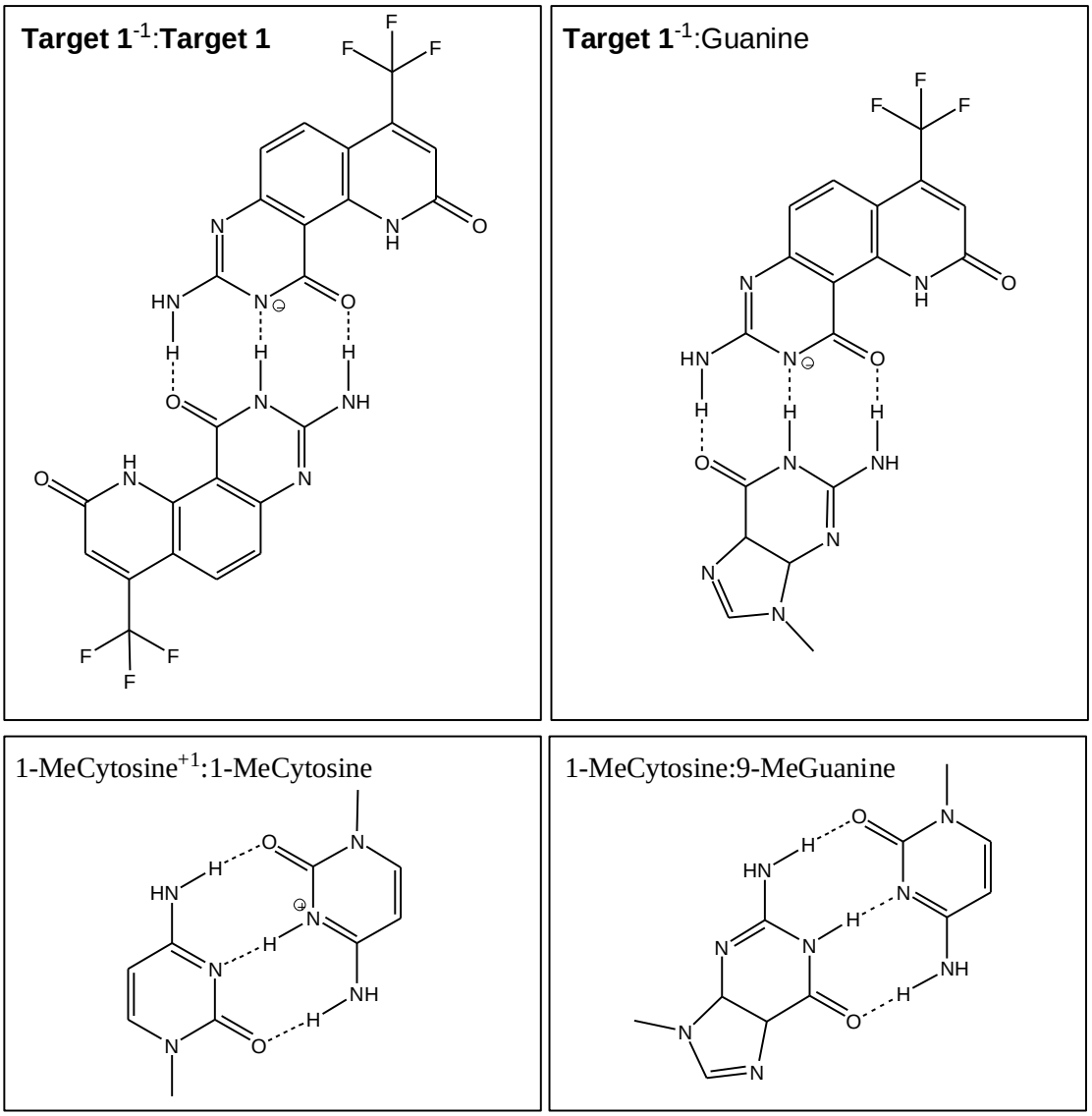

Figure 3.15: Binding affinity of heteromolecules were calculated and compared to **Target 1** dimerization.

Table 3.2: Binding enthalpies calculated for the binding of **Target 1** to different molecules (calculated at B3LYP/6-31G**, including the counterpoise estimated BSSE and ΔZPE).

Complex	**Binding Enthalpy** (kJ/mol at 0 Kelvin)
Target 1^{-1} : **Target 1**	- 166
Target 1^{-1} : Guanine	- 150
1-Methylcytosine^{+1} : 1-Methylcytosine	- 172
1-Methylcytosine : Guanine	- 96

In Vitro Cell Studies:

Having a trifluoromethyl group on the backbone gave us a chance of analyzing the binding ability of **Target 1** using ^{19}F NMR spectroscopy. One main problem with the compound was its insolubility in most solvents. The only solvents that dissolve the neutral compound were dimethylsulfoxide and dimethylformamide. If **Target 1** would be used for *in vivo* applications, the amount of DMSO or DMF has to be kept at the minimum volume.

0.22 mM samples of Target 1 were prepared by dissolving 1 mg of the compound in 30 microliters of DMSO, transferring 6 microliters of the stock, and diluting the transferred solution with a combination of methanol, water, and deuterium oxide to the proper volume. During dilution, slight cloudiness of the solution was noticed. Running NMR at such a low concentration also gave some problems as more peaks affiliated with the noise appeared. The peak associated with the impurity also became broad and decreased in intensity. The presence of the impurity in the crude sample was utilized and used as a reference. The

impurity peak became worse after addition of the DNA (Veg-F or KRAS) but was enough to use as a reference. These DNA strands have cytosine-rich regions that can form *i*-motif secondary structures as shown in **Table 3.3**. VEGF is a signal protein which stimulates angiogenesis which is important in cancer metastasis.[50] Mutation in the KRAS gene leads to development of many cancer cells.[51] By restricting the functions of VEGF protein and inhibiting a mutated KRAS protein, cancer development might be hindered or stopped. **Figure 3.16** and **Figure 3.17** show the comparisons between the ^{19}F NMR spectrum of the solution before and after the DNA was introduced. The slight downfield shift of the drug (δ +0.12 difference for Veg-F and δ +0.13 for KRAS) shows that the electron density on the trifluoromethyl group has decreased, probably due to the decreased electron density on the carbostyril backbone. This decrease of electron density in the heterocyclic ring may be attributed to hydrogen bonding happening somewhere in the ring, probably in the isocytosine region.

Table 3.3: DNA sequences of proteins of interest along with their base codes.

DNA Sequences	Base Code
VEGF promoter region*	5'-(ACCCCGCCCCCGGCCCGCCCCG-)3'
KRAS promoter region	5'-(CCTCCCCCTCTTCCCTCTTCCCACACCGCCCT-3'

*compliment to a section of the binding site for transcription factor Sp1 in the approximal promoter region of the VEGF gene[52]

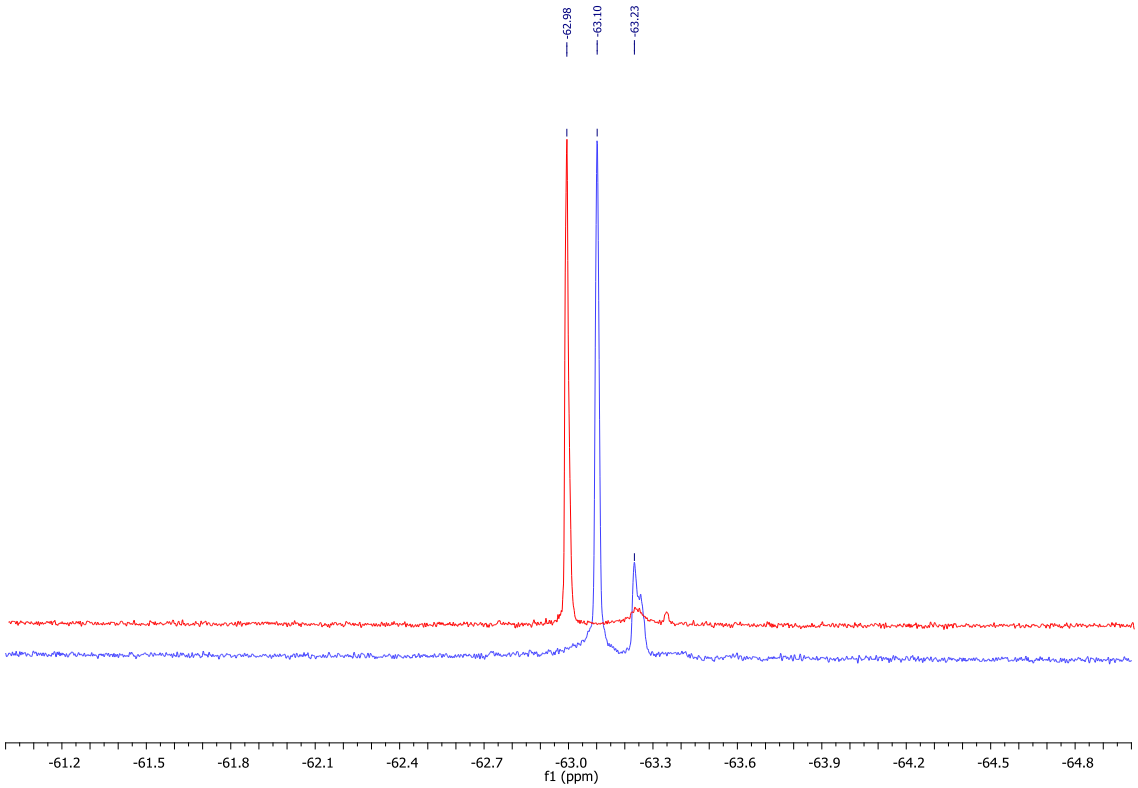

Figure 3.16: ^{19}F NMR of 221 μM drug solution before (blue spectrum) and after (red spectrum) addition of 221 μM of Veg-F DNA solution.

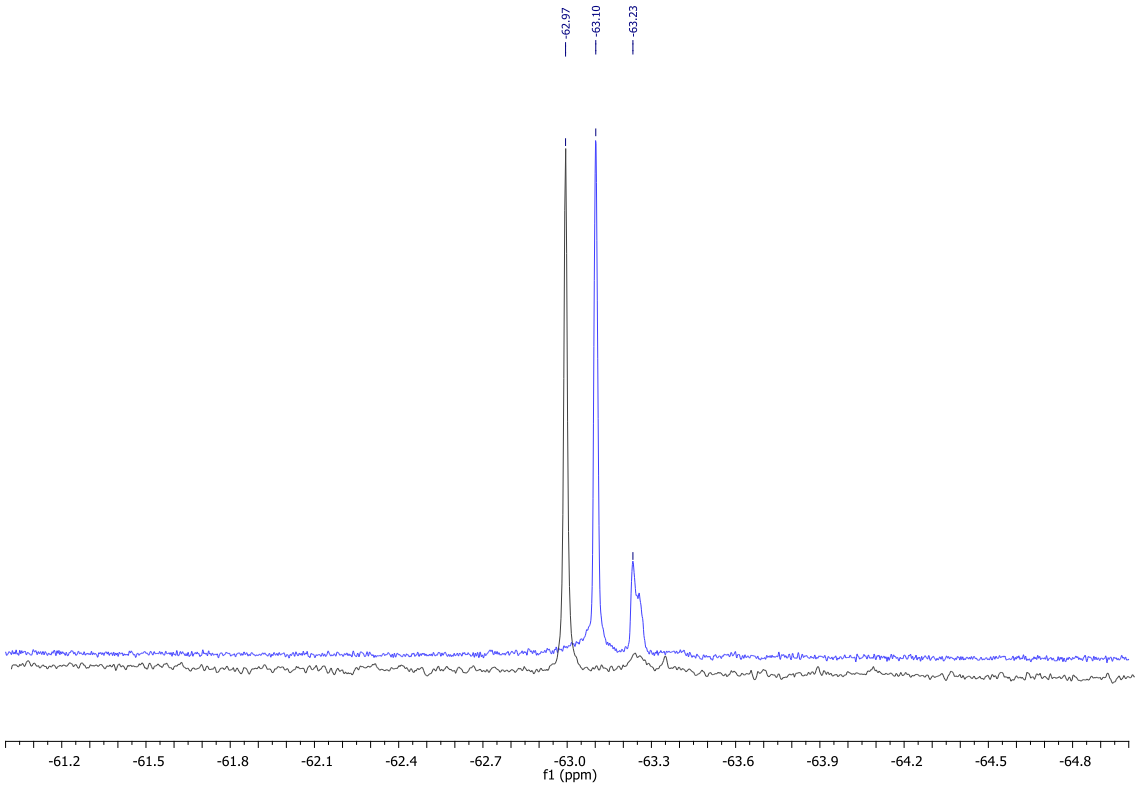

Figure 3.17: ^{19}F NMR of 221 μM drug solution before (blue spectrum) and after (gray spectrum) addition of 221 μM of KRAS DNA solution.

The potency of **Target 1** was also tested *in-vitro* with healthy cells HC11 and cancer cells 4T1, which are present in mice and humans alike. 4T1 is a tumor cell that primarily grows in the mammary gland and can spontaneously spread. Along with this, the tumor cells is also invasive and can metastasize to distant sites such as lymph nodes, blood, liver, lung, brain, and bone.[53] The availability of living mice samples in hand is what makes these cells a good starting point for *in-vitro* study. HC11 cells were used for blank reference and to see if **Target 1** can discriminate between healthy and cancer cells. Even though

the healthy cells seem to be unaffected by the drug, it seems that the drug also had no effect on the cancer cells.

Ongoing Work and AVO Studies:

Part of the ongoing work on this project is to isolate a pure compound. With a pure compound, the ^{1}H and ^{13}C NMR binding analysis can be used to further confirm that there is an interaction between **Target 1** and the DNA strand. This may also show a more promising result in the *in-vitro* studies with mice cells since the effect of the impurity is unknown. Along with mice cells, **Target 1** will also be tested with human cells. MDA-MB-231 is a cancer cell that is derived from the metastatic site in the mammary gland. A reverse preparatory HPLC, located in France, will be used to purify enough of the pure compound.

Solubility in aqueous solvent is an important property of a drug molecule. This property can be predicted using computational tools and is expressed as logS, where S is the solubility at a temperature of 20-25ºC in mol/L. Using the Chemaxon's solubility predictor[54], it was predicted that the logS value of **Target 1** in aqueous solvent at pH 7.4 to be -5.1, which falls under the solubility category of low solubility (<0.01 mg/ml). Forming the trifluoroacetic acid salt of Target 1 increases the polarity of the molecule, thus increasing the logS value to -3.85, which falls under the solubility category of moderate solubility (0.01 – 0.06 mg/ml).

As far as synthesis go, different functional groups can be attached to the 4-position of the carbostyril backbone. As shown in the Experimental section (**Scheme 3.7.4** and **3.11.4**), functionalizing this position using different methods has not been successful. Replacement of the trifluoromethyl group with a different group may improve neutral **Target 1**'s solubility in the aqueous solvent and also pave way to different modifications such as tethering two of the carbostyrils together with ethylene glycol chains.

Computational studies, using a software developed by the Marsella group, were performed on the potential of the drug. Aiden Aceves, an undergraduate student of Prof. Michael Marsella, looked over different kinds of cancerous cells and viruses to check their response to the target drug. AVO simulates a molecule's behavior in a biological environment and measures the molecule's response to each situation. Using the program, **Target 1** showed some potency towards breast cancer cells. However, **Target 1** seems to have more of an effect on the mosquito borne arboviral disease known as Japanese Encephalitis (**JE**). JE is the inflammation of the brain due to a protein known as GRIK1 (glutamate receptor, ionotropic,kainate1) and inhibiting the binding of these receptors would inhibit neurodegeneration.[55] **Target 1** showed binding to GRIK1 and showed a score of 0.8832, which is comparable Arctigenin which scored 0.7607. Arctigenin is a plant lignin and used for the treatment of JE.

Conclusion:

The discovery and their ability to inhibit cancer cells started a new study on how to probe and stabilize the secondary structure of DNA known as G-quadruplex and *i*-motif. Some ways to maintain these secondary structures included ligand binding not only on the nucleobases but also on the loop regions and on the phosphate backbone.

The path to synthesize **Target 1**, a compound that has the moiety to bind to neutral cytosine, proved to be difficult and still incomplete. In basic conditions, **Target 1** anion has shown to have a very high binding affinity to itself. DFT calculations supports this dimerization as observed in mass spectrometry. DFT calculation also predict a pretty stable binding of **Target 1** anion to guanine nucleobase, but is not observed experimentally. Furthermore, preliminary studies using ^{19}F NMR showed that **Target 1** can also interact with a DNA strand. Addition of **Target 1** with mammary cancer cells (*in vitro* studies) showed no effect on the cancer cells. Ongoing research include looking at different substituents to improve **Target 1**'s solubility on organic solvents and looking at other molecules that can bind to **Target 1**.

Using AVO, **Target 1** showed some potential not only as a cancer inhibitor but also as anti-viral agent. This is another field in which the potency of **Target 1** can be tested.

References:

1. Centers for Disease Control and Prevention, accessed 2 March 2016, <http://www.cdc.gov/nchs/fastats/leading-causes-of-death.htm>

2. American Cancer Society, accessed 2 March 2016, <http://www.cancer.org/research/cancerfactsstatistics/cancerfactsfigures2015/>

3: Hanahan, D.; Weinberg, R. A. "The Hallmarks of Cancer" *Cell*, **2000**, *100*,57-70.

4: Brooks, T. A.; Kendrick, S.; Hurley, L. "Making Sense of G-quadruplex and i-Motif Functions in Oncogene Promoters" *FEBS J.*, **2010**, *277*, 3459-3469.

5: Williams, J. S.; Kunkel, T. A. "Ribonucleotides in DNA: Origins, Repair and Consequences" *DNA Repair*, **2014**, *19*, 27-37.

6: Watson, J. D.; Crick, F. H. "Molecular Structure of Nucleic Acids; A Structure for Deoxyribose Nucleic Acid" *Nature*, **1953**, *171*, 737-738.

7: Nasiri, H. R.; Bell, N. M.; McLuckie, K. I. E.; Husby, J.; Abell, C.; Neidle, S.; Balasubramanian, S. "targeting a c-MYC G-quadruplex DNA with a Fragment Library" *Chem. Commun.*, **2014**, *50*, 1704-1707.

8: Fernando, H.; Sewitz, S.; Darot, J.; Tavare, S.; Huppert, J. L.; Balasubramanian, S. "Genome-wide Analysis of a G-quadruplex-Specific Single-Chain Antibody that Regulates Gene Expression" *Nucl. Acids. Res.*, **2009**, *37*, 6716-6722.

9: Huppert, J. L.; Balasubramanian S. "G-quadruplexes in Promoters Throughout the Human Genome" *Nucl. Acids. Res.*, **2007**, *35*, 406-413.

10: Lim, K. W.; Amrane, S.; Bouaziz, S.; Xu, W.; Mu, Y.; Patel, D. J.; Luu, K. N.; Phan, A. T. "Structure of the Human Telomere in K+ Solution: A Stable Basket-Type G-Quadruples with Only Two G-Tetrad Layers" *J. Am. Chem. Soc.*, **2009**, *131*, 4301-4309.

11: Hahn, W. C.; Stewart, S. A.; Brooks, M. W.; York, S. G.; Eaton, E.; Kurachi, A.; Beijersbergen, R. L.; Knoll, J. H. M.; Meyerson, M.; Weinberg, R. A. "Inhibition of Telomerase Limits the Growth of Human Cancer Cells" *Nature Medicine*, **1999**, *5*, 1164-1170.

12: Dexheimer, T. S.; Carey, S. S.; Zuohe, S.; Gokhale, V. M.; Hu, X.; Murata, L. B.; Maes, E. M.; Weichsel, A.; Sun, D.; Meuillet, E. J. *et al.* "NM23-H2 May Play an Indirect Role in Transcriptional Activation of *C-MYC* Gene Expression But Does Not Cleave the Nuclease Hypersensitive Element III" *Mol. Cancer Ther.*, **2009**, *8*, 1363-1377.

13: Brooks, T. A.; Hurley L. H. "The Role of Supercoiling in Transcriptional Control of MYC and its Importance in Molecular Therapeutics" *Nature Reviews Cancer*, **2009**, *9*, 849-861.

14: Yang, B.; Wu, R. R.; Berden, G.; Oomens, J.; Rodgers, M. T. "Infrared Multiple Photon Dissociation Action Spectroscopy of Proton-Bound Dimers of Cytosine and Modified Cytosines: Effects of Modifications on Gas-Phase Conformations" *J. Phys. Chem. B*, **2013**, *117*, 14191-14201.

15: Yang, B.; Rodgers, M. T. "Base-Paring Energies of Proton-Bound Heterodimers of Cytosine and Modified Cytosines: Implications for the Stability of DNA i-motif Conformations" *J. Am. Chem. Soc.,* **2014**, *136*, 282-290.

16: Kendrick, S.; Kang, H.; Alam, M. P.; Madathil, M. M.; Agrawal, P.; Gokhale, V.; Yang, D.; Hecht, S. M.; Hurley, L. H. "The Dynamic Character of the BCL2 Promoter i-Motif Provides a mechanism for Modulation of Gene Expression by Compounds That Bind Selectively to the Alternative DNA Hairpin Structure" *J. Am. Chem. Soc.*, **2014**, *136*, 4161-4171.

17: Tsai, A. G.; Engelhart, A. E.; Hatmal, M. M.; Houston, S. I.; Hud, N. V.; Haworth, I. S.; Lieber, M. R. "Conformational Variants of Duplex DNA Correlated with Cytosine-Rich Chromosomal Fragile Sites" *J. Biol. Chem.,* **2009**, *284*, 7157-7164.

18: Kendrick, S.; Akiyama, Y., Hech, S. M.; Hurley, L. H. "The *i*-Motif in the Bcl-2 P1 Promoter Forms an Unexpectedly Stable Structure With Unique 8:5:7 Loop Folding Pattern" *J. Am. Chem. Soc.*, **2009**, *131*, 17667-17676.

19: Siddiqui-Jain, A.; Grand, C. L.; Bearss, D. J.; Hurley, L. H. "Direct Evidence for G-quadruplex in a Promoter Region and its Targeting with a Small Molecule to Repress c-MYC Transcription" *PNAS*, **2002**, *99*, 11593-11598.

20: Haslam, R. J.; Koide, H. B.; Hemmings, B. A. "Pleckstrin Domain Homology" *Nature*, **1993**, *363*, 309-310.

21: Federoff, O. Y.; Rangan, A.; Chemeris, V. V.; Hurley, L. H. “Cationic Porphyrins Promote the Formation of *i*-Motif DNA and Bind Peripherally by a Nonintercalative Mechanism” *Biochemistry*, **2000**, *39*, 15083-15090.

22: Kendrick, S.; Kang, H.; Alam, M. P.; Madathil, M. M.; Agrawal, P.; Gokhale, V.; Yang, D.; Hecht, S. M.; Hurley, L. H. “The Dynamic Character of the BCL2 Promoter *i*-motif Provides a Mechanism for Modulation of Gene Expression by Compounds That Bind Slectively to the Alternative DNA Hairpin Structure” *J. Am. Chem. Soc.*, **2014**, *136*, 4161-4171.

23: Kaslow, C. E.; Summer, N. B. “Substituted Lepidines1” *J. Am. Chem. Soc.*, **1946**, *68(4)*, 644-647.

24: Malhotra, R., Narang S. C., Olah G. A. “Nitration: Methods and Mechanisms” New York: VCH Publishers, Inc., **1989**.

25: Heitbaum, M.; Froehlich, R.; Glorius, F. “Diastereoselective Hydrogenation of Substituted Quinolines to Enantiomerically Pure Decahydroquinolines” *Advanced Synthesis And Catalysis*, **2010**, *352*, 357-362.

26: Hill, M.; Taylor, F. “Nitration of 1,3,5-Trihalobenzenes” *J. Org. Chem.*, **1960**, *25 (6)*, 1037-1038.

27: Du Pont de Nemours and Co. *Chem. Abstr.*, **1941**, 5912.

28: Liotta, R. and Hoff, W. S. “Trifluoroperacetic Acid. Oxidation of Aromatic Rings” *J. Org. Chem.*, **1980**, *45*, 2887-2890.

29: Meyet, C. E.; Larsen, C. H. “One-Step Catalytic Synthesis of Alkyl-Substituted Quinolines” *J. Org. Chem.*, **2014**, *79*, 9835-9841.

30: Peshkov, V. A.; Pereshivko, O. P.; Van der Eycken, E. V. “A Walk Around the A^3-coupling” *Chem. Soc. Rev.*, **2012**, *41*, 3790-3807.

31: Woods, L. L.; Fooladi, M. M. “Nitrogen Analogs of Coumarin: 7-Amino-4-Substituted Carbostyrils” *J. Chem. Eng. Data*, **1968**, *13(3)*, 440-442.

32: Okamura, T. and Nakagawa, J. “Contribution of Intramolecular NH···O Hydrogen Bonds to Magnesium Carboxylate Bonds” *Inorg. Chem.* **2013**, *52*, 10812-10824.

33: Hashizume, H.; Ito, H.; Yamada, K.; Nagashima, H.; Kanao, M.; Tomoda, H.; Sunazuka, T.; Kumagai, H.; Omura, S. “Synthesis and Biological

Activity of New 3-Hydroxy-3-methylglutaryl Coenzyme A (HMG-CoA) Synthase Inhibitors: 2-Oxetanones with a Side Chain Mimicking the Folded Structure of 1233A" *Chem. Pharm. Bull.* **1994**, *42(3)*, 512-520.

34: Lee, H. K.; Cao, H.; Rana, T. M. "Design, Microwave-Assisted Synthesis, and Photophysical Properties of Small Molecule Organic Antennas for Luminescence Resonance Energy Transfer" *J. Comb. Chem.* **2005**, *7*, 279-284.

35: Sakaguchi, S.; Shibamoto, A.; Ishii, Y. "Remarkable Effect of Nitrogen Dioxide for N-hydroxyphthalimide-catalyzed Aerobic Oxidation of Methylquinolines" *Chem. Comm.* **2002**, 180-181.

36: Collins, J. C.; Hess, W. W.; Frank, F. J. "Dipyridine-chromium(VI) Oxide Oxidation of Alcohols in Dichloromethane" *Tetra. Lett.*, **1968**, *No. 30*, 3363-3366.

37: Corey, E. J.; William Suggs, J. "Pyridinium Chlorochromate. An Efficient Reagent for Oxidation of Primary and Secondary Alcohols to Carbonyl Compounds" *Tetra. Lett.*, **1975**, *No. 31*, 2647-2650.

38: Bogert, M. T. and Kropff, A. H. "On Some Amino and Nitroamino Derivatives of Benzoic, Metatoluic and Metaphthalic Acids" *J. Am. Chem. Soc.* **1909**, *31(7)*, 841-848.

39: Ohkata, K.; Tamura, Y,; Shetuni, B. B.; Takagi, R.; Miyanaga, W.; Kojima, S.; Paquette, L. A. "Stereoselectivity Control by Oxaspiro Rings During Diels-Alder Cycloadditions to Cross-conjugated Cyclohexadienones: The *Syn* Oxygen Phenomenon" *Journal of the American Chemical Society*, **2004**, *126*, 16783-16792.

40: Lebedev, A. V.; Lebedeva, A. B.; Sheludyakov, V. D. "Organosilicon Synthesis of Isocyanates: III. Synthesis of Aliphatic, Carbocyclic, Aromatic, and Alkylaromatic Isocyanatocatboxylic Acid Esters" *Russian Journal of General Chemistry* **2006**, *Vol. 76(7)*, 1069-1080.

41: Hoorfar, A.; Ollis, W. D.; Price, J. A.; Stephanatou, J. S.; Stoddart, J. F. "Conformational Behaviour of Medium-sized Rings. Part 11. Dianthranilides and Trianthranilides" *J. Chem. Soc. Perkin Trans. I* **1982**, 1649-1699.

42: Patent Genencor International Inc. Patent: US2002/127695 A1, **2002**.

43: Rekha, V. V.; Ramani, M. V.; Ratnamala, A; Rupakalpana, V.; Subbaraju, G. V.; Satyanarayana, C.; Rao, C. S. “A Simple, Efficient, Green, Cost Effective and Chemoselective Process for Esterification of Carboxylic Acids” *Organic Process Research & Development* **2009**, *13*, 769-773.

44: Bose, S. D.; Chary, M. V. “First Total Synthesis of (-)-Circumdatin H, a Novel Mitochondrial NADH Oxidase Inhibitor” *Synthesis* **2010**, *4*, 643-650.

45: Fabian, W. M. F.; Niederreiter, K. S.; Uray, G.; Stadlbauer, W. “Substituent Effect on Absorption and Fluorescence Spectra of Carbostyrils” *Journal of Molecular Structure*, **1999**, *477*, 209-220.

46: Patent Pharmacia and Upjohn Company LLC Patent WO2007/20502 A2, **2007**.

47: Shin, S.; Sinkeldam, R. W.; Tor, Y. “Emissive RNA Alphabet” *J. Am. Chem. Soc.* **2011**, *133 (38)*, 14912-14915.

48: Kennedy, K. J.; Simandan, T. L.; Dix, T. A. “A Facile Route to Cyclic and Acyclic Alkyl-Arginines” *Synthetic Communications*, **1998**, *28*, 741-746.

49: Patent Smithkline Beecham Intercredit B. V. US5064833 A1, **1991**.

50: Senger, D. R.; Galli, S. J.; Dvorak, A. M.; Perruzzi, C. A.; Harvey, V. S.; Dvorak, H. F. “Tumor cells secrete a vascular permeability factor that provides accumulation of ascites fluid.” *Science*, **1983**, *219*, 983-985.

51: Kranenburg, O. “The KRAS oncogene: past, present, and future.” *Biochimica et Biophysica Acta*, **1975**, *2*, 81-82.

52: Sun, D.; Liu, W.; Guo, K.; Rusche, J. J.; Ebbinghaus, S.; Gokhale, V.; Hurley, L. H. “The Proximal Promoter Region of the Human Vascular Endothelial Growth Factor Gene has a G-quadruplex Structure that can be Targeted by G-quadruplex-interactive Agents” *Molecular Cancer Therapeutics*, **2008**, *7*, 880-889.

53: Pulaski, B. A.; Ostrand-Rosenberg, S. “Mouse 4T1 breast tumor model.” *Curr Protoc Immunol*, **2001**, Chapter 20, Unit 20.2.

54: < https://www.chemaxon.com/marvin-archive/6.3.2/marvin/help/calculations/solubility.html; https://disco.chemaxon.com/apps/demos/solubility/>

55: Kalita, P. P.(**2016**) “Computational design approach to develop a novel inhibitor of GRIK1 fighting against Japanese Encephalitis” presented at 6th World Congress on Biotechnology, New Delhi, India, 2015. Germany: ResearchGate.